This electronic thesis or dissertation has been downloaded from the King's Research Portal at https://kclpure.kcl.ac.uk/portal/



Nesprin-1/-2
Roles in nuclear envelope organisation, myogenesis and dilated cardiomyopathy

Zhou, Can

Awarding institution:
King's College London

The copyright of this thesis rests with the author and no quotation from it or information derived from it may be published without proper acknowledgement.

END USER LICENCE AGREEMENT



Unless another licence is stated on the immediately following page this work is licensed

under a Creative Commons Attribution-NonCommercial-NoDerivatives 4.0 International

licence. https://creativecommons.org/licenses/by-nc-nd/4.0/

You are free to copy, distribute and transmit the work

Under the following conditions:

- Attribution: You must attribute the work in the manner specified by the author (but not in any way that suggests that they endorse you or your use of the work).
- Non Commercial: You may not use this work for commercial purposes.
- No Derivative Works - You may not alter, transform, or build upon this work.

Any of these conditions can be waived if you receive permission from the author. Your fair dealings and other rights are in no way affected by the above.

Take down policy

If you believe that this document breaches copyright please contact librarypure@kcl.ac.uk providing details, and we will remove access to the work immediately and investigate your claim.

Download date: 08. Oct. 2023

NESPRIN-1/-2: ROLES IN NUCLEAR ENVELOPE ORGANISATION, MYOGENESIS AND DILATED CARDIOMYOPATHY

PhD Thesis

Can Zhou

September 2017

Submitted for the Degree of Doctor of Philosophy from
King's College London

King's College London,
Cardiovascular Division,
School of Medicine

Supervisors: Doctor Qiuping Zhang
Professor Catherine Shanahan

Table of Contents

Declaration 6

Acknowledgements 7

Abstract 9

List of Figures 10

List of Tables 14

List of Abbreviations 15

Chapter 1: Introduction 20

1.1 Cytoskeleton network and spectrin repeat superfamily 20

1.2 Nesprins 21

1.2.1 Nesprin structure 22

1.2.2 Nesprin isoforms 27

1.3 Nuclear Envelope 32

1.3.1 Nuclear envelope structure 32

1.3.2 Nuclear envelope proteins 33

1.3.3 Nuclear lamina 35

1.4 Nesprins link the nucleoskeleton to the cytoskeleton 36

1.4.1 LINC complex structure 36

1.4.2 SUN-KASH bridge 37

1.4.3 Types of the LINC complexes 37

1.5 Nesprin and diseases 43

1.5.1 Muscle diseases: DCM and EDMD 43

1.5.2 Other muscle diseases: CMD and AMC 44

1.5.3 Neurological disease: Autosomal recessive cerebellar ataxia type 1 46

1.5.4 Other diseases: autism spectrum disorder and bipolar disorder 46

1.6 Functions of the NE-LINC complex and mechanistic basis of nesprin related diseases 52

1.6.1 Linking the nucleoskeleton to the cytoskeleton 52

1.6.2 Nuclear migration, positioning and polarisation 54

1.6.3 Mechanical signalling and mechanosensitive gene expression 56

1.7 Nesprin-1/-2 mouse models 59

1.7.1 KASH mouse model 59

1.7.2 Nesprin-1/-2 actin binding domain (ABD) KO mice 62

1.7.3 Nesprin-1 or -2 C-terminal KO mice 62

1.7.4 Specific nesprin isoform-nesprin-1α_2 KO mice 63

1.7.5 Nesprin-1 and nesprin-2 double knockout mice 64

1.7.6 Related LINC complex mouse models 65

1.8 Summary and thesis aims 71

Chapter 2: Methods and Materials 72

2.1 Patient recruitment and mutation screening 72

2.1.1 Research Subjects 72

2.1.2 Mutation analysis 72

2.2 Cell work 73

2.2.1 Cell culture 73

2.2.2 Cell passage 73

2.2.3 Isolation of neonatal rat cardiomyocytes (NRCs) 73

2.2.4 Generation of retrovirus particles 74
2.2.5 Plasmid transfection 75
2.2.6 siRNA transfection 76
2.2.7 RV infection 76
2.3 Protein techniques 77
2.3.1 Cell lysate 77
2.3.2 DC protein assay 77
2.3.3 Western blotting (WB) 77
2.3.4 Protein binding techniques 78
2.4 Microscopy work 80
2.4.1 Immunofluorescence (IF) microscopy 80
2.4.2 Histology and brightfield microscopy 81
2.5 Nucleotide techniques 82
2.5.1 RNA extraction 82
2.5.2 Reverse transcription 83
2.5.3 Quantitative polymerase chain reaction (qPCR) 83
2.5.4 Polymerase chain reaction (PCR) 84
2.5.5 Site directed mutagenesis 84
2.5.6 Agarose gel electrophoresis 85
2.5.7 Cloning 85
2.6 Animal work 89
2.6.1 Generation of a cardiac specific KASH2 Transgenic mouse model 89
2.6.2 Genotyping 89
2.6.3 Echocardiography 90
2.6.4 Transverse aortic constriction (TAC) 90
2.6.5 Harvesting of mouse heart 91
2.6.6 Whole heart perfusion and embedding 91
2.6.7 Sectioning of cryopreserved tissue 92
2.6.8 Zebrafish 92
2.7 Statistical analysis 93
2.8 Primer sequence 93
2.8.1 Primers for V5 tagged nesprin-1α_2 WT and KASH 93
2.8.2 Primers for Flag tagged nesprin-1α_2 WT 94
2.8.3 Primers for Nesprin-1α_2 mutagenesis 94
2.8.4 Primers for genotyping 94
2.8.5 Primers for qPCR 94
2.9 siRNA oligos 94
2.10 Antibodies 103
2.10.1 Primary antibodies 103
2.10.2 Secondary antibodies 103
2.11 Laboratory materials 107
2.11.1 Stock materials 107
2.11.2 Solutions 112
2.11.3 Laboratory equipment 115
2.11.4 Online tools 116
Chapter 3: Novel nesprin-1 mutants disrupted the NE-LINC complex and interfered with NE organisation 117
3.1 Introduction 117
3.1.1 Identification of three novel nesprin-1 mutants in DCM patients 118
3.2 Results 121
3.2.1 Overexpression of nesprin-1 mutants disrupted nuclear morphology 121

3.2.2 Nesprin-1 mutants reduced lamin A/C and SUN2 staining at the NE in U2OS cells 121
3.2.3 Nesprin-1 mutants reduced lamin A/C and SUN2 staining at the NE in neonatal rat cardiomyocytes 127
3.2.4 Nesprin-1 mutants disrupted the interactions between nesprin-1, lamin A/C and SUN2 within the NE complex 127
3.2.5 Nesprin-1 mutants augmented ERK activity in EDMD patients 133
3.2.6 Aberrant activation of ERK was induced in heart tissue derived from nesprin-1 KASH KO mice 137
3.2.7 Nesprin-1 mutants led to abnormal activation of ERK1/2 pathway 139
3.3 Discussion 143
3.3.1 Nesprin-1 mutations compromised structural and functional integrity of nesprin proteins 143
3.3.1.1 Mutants S8381C and N8406K 143
3.3.1.2 Mutant R8272Q 145
3.3.2 Disrupted NE-LINC complex was caused by the nesprin-1 mutants 146
3.3.3 Augmented activation of MAPK cascade was associated with disrupted NE-LINC complex 147
3.3.4 Summary 150
Chapter 4: Novel nesprin-1 mutants perturbed myogenesis 151
4.1 Introduction 151
4.1.1 Nesprin and myoblast differentiation 151
4.1.2 Nesprin interacts with microtubule motor protein kinesin-1 at the NE 153
4.2 Results 155
4.2.1 Expression levels of endogenous nesprin-1α and MRFs were upregulated during myogenesis 155
4.2.2 Generating retroviral constructs of nesprin-1α_2 WT, mutants and KASH 158
4.2.3 Infection of C2C12 myoblasts with retroviral nesprin-1α_2 WT, mutants and KASH 165
4.2.4 Nesprin-1 mutants led to defects in myotube formation 165
4.2.5 Nesprin-1 mutants led to dysregulation of MRFs 171
4.2.6 Nesprin-1α WT interacted with KLC-1/2 and nesprin-1 mutants disrupted this binding 171
4.2.7 Nesprin-1 mutants affected the binding between nesprin-1 and KLC in both myoblasts and myotubes 173
4.2.8 Depletion of KLC-1/2 affected myoblast differentiation 178
4.2.9 Generation of flag-tagged nesprin-1α_2 WT and mutant constructs for investigating the roles of nesprin-1 in cardiac cell function in zebrafish embryos 187
4.2.10 Human nesprin-1α_2 WT causes heart developmental and conduction defects in zebrafish embryos while mutants induce a less severe heart phenotype 190
4.3 Discussion 194
4.3.1 Generation of retroviral nesprin-1 WT and mutant constructs 194
4.3.2 Nesprin-1 mutations caused dysregulation of MTFs in myoblast differentiation 196
4.3.3 Nesprin-1 mutations disrupted nesprin-1/KLC interaction and myoblast fusion 199
4.3.4 Expression of nesprin-1α_2 mutants induced less severe heart defects during zebrafish heart development compared to 1α_2 WT 200
4.3.5 Summary 201
Chapter 5: Generation and characterisation of cardiac specific nesprin-2 KASH transgenic mice 202
5.1 Introduction 202
5.2 Results 206

5.2.1 Establishment of a novel cardiac specific KASH2 Tg mouse model 206
5.2.2 Characterisation of cardiac specific KASH2 Tg mouse model at basal line 210
5.2.3 Characterisation of cardiac specific KASH2 Tg mouse model under pressure overload 226
5.3 Discussion 246
5.3.1 Rationale for generation of cardiac specific nesprin-2 KASH overexpression mice 248
5.3.2 Cardiac specific nesprin-2 KASH Tg mice induced a hypertrophic response especially under the mechanical stress 249
5.3.3 csKASH-Tg mice exhibited a late onset and mild cardiac phenotype 250
5.3.4 NE-LINC complex was disrupted in csKASH-Tg mice 251
5.3.5 Functions of NE-LINC complex were perturbed in csKASH-Tg mice 252
5.3.6 Summary 254
Chapter 6: General discussion and future directions 255
6.1 Thesis summary 255
6.2 Discussion and future direction 255
6.2.1 Roles of nesprin-1/-2 in NE-LINC complex 255
6.2.2 Genotype and phenotype correlation of nesprin-1 mutations 257
6.2.3 Further characterisation of csKASH-Tg mice 260
6.3 Conclusions 262
Bibliography 263
Appendix 282
Appendix I. Clinical features of research subjects 282
Appendix II. Rare (<1%) nesprin-1 variants identified in DCM patients 283
Appendix III: Clinical description of the patients harbouring the mutations identified in this study 284
Appendix IV: List of methods and results contributed by collaborators 286
Appendix V: Novel nesprin-1 mutations associated with dilated cardiomyopathy cause nuclear envelope disruption and defects in myogenesis 287
Appendix VI: N-terminal nesprin-2 variants regulate β-catenin signalling 307

Declaration

I declare that the work undertaken in this thesis was conducted by myself, except where indicated.

Can Zhou

King's College London

Acknowledgements

I would like to extend thanks to the many people, in many countries, who so generously contributed to the work presented in this thesis. I am also grateful to King's College London and British Heart Foundation for funding my PhD research.

Special mention goes to my enthusiastic supervisor, Dr. Qiuping Zhang. My PhD has been an amazing experience and I thank Qiuping wholeheartedly, not only for her tremendous academic support, but also for her dedication and caring both in and out of work, and giving me so many wonderful opportunities.

I am also hugely appreciative to Prof. Catherine Shanahan, especially for sharing her deep expertise so willingly, and for being so dedicated to her role as my secondary supervisor. We have also bonded over failed attempts to catch Snorlaxes and Dragonites in Pokémon Go.

I am also very appreciative of the ground-breaking research on nesprin by my supervisors Qiuping and Cathy and previous colleagues: Derek Warren, Dipen Rajgor, Flavia Austore, Ash Healy, Lauren Porter and Jason Mellad, thus allowing me to write mine while standing on the shoulders of 'giants'.

I would like to acknowledge all the diverse, interesting, but above all loving individuals in my lab for making my time there enjoyable and unforgettable. Thanks to Chen Li, my former colleague who initially begun this project and guided me from the start of my research. Thanks to Andrew Cobb for his dad jokes and immature tricks, as well as critical scientific suggestions and consistent support during my PhD study. Thanks to Mengxi Sun for her sister-like warm heartedness, sharing opinions in and out of work, and her distinctive and always insightful encouragement. Special thanks to Qiuping Zhang, Andrew Cobb and Derek Warren, for their critical and patient reading of this thesis.

It was a great pleasure to know the ballet dancer Gosia Furmanik, the very talented scientist Chinyee Ho, the pole dancer Ally Santu (SUN2), the delicate graph/image artist Serena Tsakali, the quiet but smart bench partner Meredith Whitehead, the diligent histology expert Sadia Ahmad, the triathlon athlete Joanne Laycock, the multi-tasking achiever Rosie Wheeler, the angel with a smile Anne Jacob, the most organised lab manager Robert Hayward, the singer and best Santa Daniel Brayson, the serious but funny Russian secret agent Alex Kapustin, the best photographer Jayanta Bordoloi, and the RNA expert Andrew Durham. In addition,

many thanks go to my colleagues from other groups: Celio Santos, Greta Sawyer, Helena Zhang, Norman Catibog, Trusha Rajgor, Elham Zarrinpashneh, Tomofumi Misaka, Yosuki Omori, Minoru Takaoka, Ioannis Smyrnias, Min Zhang, Heloise Mongue-Din, Raj Mistry, Mat Stroud, Linfang Zeng and Zhongyi Zhang.

Thanks to my dear friends Shana De Silva, Juqian Zhang, and Xuechong Hong, for being my friends from the beginning of my PhD. Thanks for introducing me to the beauty of London and finding the perfect study-life balance. Moreover, truly thanks to my friends Yuanyuan Ye, Tingting Yu and Beiyu Wang. You are the best friends growing up with me together, always giving me the strongest spiritual support much more than you can imagine. I truly miss my friends Lvxin Chen and Qiu Zeng, I will carry on and share all the world's wonders with you.

Last, but by no means least, thanks go to my father She Zhou, my mother Liya Chen and my dearest husband Eric Liao for their unbelievable support throughout this PhD and my life in general (especially Eric for helping with the fantastic artwork and being my personal dictionary and thesaurus). They are the most important people in my world! I love you all!

To myself: during these four years, I have learnt how to think critically and I know this will benefit me during my entire life.

I would like to dedicate this thesis to my parents, Eric and myself! ☺

Abstract

Nesprins-1 and -2 are multi-isomeric scaffolding proteins. They are highly expressed in skeletal and cardiac muscle, and together with SUN (Sad1p/UNC84)-domain containing proteins and lamin A/C, forming the LInker of Nucleoskeleton and Cytoskeleton (LINC) complex at the nuclear envelope (NE). Mutations in nesprin-1/-2 have previously been identified in patients with autosomal dominant Emery–Dreifuss muscular dystrophy (EDMD) as well as dilated cardiomyopathy (DCM).

In my study, three novel rare variants (R8272Q, S8381C, N8406K) in the C-terminus of the *SYNE-1* (nesprin-1) gene were identified in 7 DCM patients by mutation screening. These mutants caused nuclear morphology defects, reduced lamin A/C and SUN2 staining at the NE and disrupted binding between nesprin-1/lamin/SUN. Nesprin-1 mutations were also associated with augmented activation of the ERK pathway *in vitro* and in hearts *in vivo*. During C2C12 myoblast differentiation, nesprin-1 protein levels increased concomitantly with kinesin light chain (KLC-1/2). GST pull-down assay showed that nesprin-1 and KCL-1/2 bind at the NE. Expression of nesprin-1 mutants in C2C12 cells caused defects in myoblast differentiation and fusion associated with dysregulation of myogenic regulatory factors and disruption of the nesprin-1 and KLC-1/2 interaction. Furthermore, expression of nesprin-1α_2 WT and mutants in zebrafish embryos caused heart developmental and conduction defects that varied in severity. In addition, a novel cardiac specific dominant negative nesprin-2 KASH (Klarsicht/ANC-1/Syne-1 homology) transgenic (Tg) mouse model was generated. Data showed overexpression of KASH domain caused disruption of NE-LINC complex and induced a hypertrophic response with activated fetal gene re-expression in Tg mice at the basal line, which was exacerbated when subjected to pathological hemodynamic stress.

These findings support roles for nesprin-1/-2 in nuclear organisation and myogenesis, which may uncover a novel mechanism whereby disruption of the NE-LINC complex may contribute to the pathogenesis of DCM.

List of Figures

Figure 1.1 Structure of giant nesprin-1 and -2 24
Figure 1.2 Ribbon representation of a single SR crystal structure 25
Figure 1.3 Schematic representation of highly conserved SRs in nesprin-1 and -2 .. 26
Figure 1.4 Nesprin isoforms derived from *SYNE-1/-2* genes 28
Figure 1.5 Nesprins form the NE-LINC complex and provide scaffolds for multiple sub-cellular compartments. 42
Figure 1.6 Nesprin-1/-2 mutations in muscle diseases 50
Figure 1.7 Overview of existing nesprin-1/-2 mouse models 67
Figure 3.1 Identification of nesprin-1 variants in DCM patients 120
Figure 3.2 Overexpression of nesprin-1 mutants caused abnormal nuclear morphology. 123
Figure 3.3 Overexpression of nesprin-1 mutants reduced NE staining of lamin A/C and SUN2 in U2OS cells. 124
Figure 3.4 Overexpression of nesprin-1 mutants reduced NE staining of lamin A/C and SUN2 in NRCs. 129
Figure 3.5 Nesprin-1 mutants affected the interaction between nesprin-1α_2 and lamin A/C or SUN2 131
Figure 3.6 Nesprin-1 mutants affected the interaction between nesprin-1α_2 and lamin A/C 132
Figure 3.7 Nesprin-1/Lamin/Emerin mutants identified in EDMD-DCM patients showed aberrant activation of ERK pathway 135
Figure 3.8 SUN2 RNA interference caused aberrant activation of ERK pathway in human lung fibroblasts 136
Figure 3.9 Nesprin-1 KASH knockout mice showed aberrant activation of ERK pathway 138
Figure 3.10 Nesprin-1 KASH augmented the ERK activities in C2C12 140
Figure 3.11 Nesprin-1 mutants caused aberrant activation of ERK pathway in C2C12 myoblasts 141
Figure 3.12 Nesprin-1 mutants caused aberrant activation of ELK pathway in H9C2 cells 142

Figure 3.13 Computer models showed the structure of nesprin-1 giant SR72 and the localisations of mutations within this region 144
Figure 4.1 Nesprin-1 mutations were identified and localised at the binding region with microtubule motor protein KLC-1/2 154
Figure 4.2 C2C12 myoblasts formed the myotubes within 6 days 156
Figure 4.3 Protein expression levels of nesprin-1α and MRFs were upregulated during C2C12 myoblast differentiation 157
Figure 4.4 mRNA expression levels of MRFs were upregulated during C2C12 myoblast differentiation 159
Figure 4.5 V5-tagged nesprin-1α_2 and KASH1 were amplified by PCR 160
Figure 4.6 Strategy of generating retroviral nesprin-1α_2 WT and mutants' constructs 162
Figure 4.7 Generation of V5-tagged nesprin-1α_2 WT, mutants and KASH constructs using pGEM T-easy vectors 163
Figure 4.8 Generation of V5-tagged nesprin-1α_2 WT, mutants and KASH constructs using retroviral vectors 164
Figure 4.9 C2C12 myoblasts were highly infected with retroviral nesprin-1α_2 WT, mutants and KASH1 167
Figure 4.10 Exogenous nesprin-1 WT/mutants/KASH1 localised at the NE in C2C12 myoblasts. 168
Figure 4.11 Nesprin-1 mutants led to fewer myotube formation 169
Figure 4.12 Nesprin-1 mutants caused defects in myoblast differentiation 170
Figure 4.13 Nesprin-1 mutants caused dysregulation of MRFs during differentiation. 172
..... 174
Figure 4.14 Nesprin-1α_2 localised at the ONM 174
Figure 4.15 Nesprin-1α WT interacted with KLC-1/2 and nesprin-1 mutants disrupted this binding 175
Figure 4.16 Endogenous KLC-1/2 increased during differentiation process 176
Figure 4.17 Defects in nesprin-1 and KLC-1/2 interaction 177
Figure 4.18 Overexpression of DN KASH1 mis-localised KLC-1/2 from the NE . 179
Figure 4.19 The localisation of siRNA oligos targeted to different regions of KLC-1/2 genes 180

Figure 4.20 WB showed KLC-1/2 was knocked down in myoblasts and myotubes by using multiple siRNA oligos 181
Figure 4.21 IF showed KLC-1/2 was knocked down in myoblasts and myotubes by using siRNA oligos 182
Figure 4.22 Endogenous nesprin-1α remained at the NE upon KLC-1/2 knockdown in myoblasts 183
Figure 4.23 Knockdown of KLC-1/2 caused defects in myoblast fusion and differentiation (I) 184
Figure 4.24 Knockdown of KLC-1/2 caused defects in myoblast fusion and differentiation (II) 185
Figure 4.25 IF showed knockdown of KLC-1/2 caused defects in myoblast fusion and differentiation 186
Figure 4.26 Generation of flag-tagged nesprin-1α_2 WT and mutants constructs using pcDNA3.1(-) vectors 188
Figure 4.27 Human nesprin-1α_2 WT induced dilated atrial chamber and reduced heart rate 191
Figure 4.28 Expression of MYL7 indicated the dilated heart in zebrafish overexpressing human nesprin-1α_2 WT 192
Figure 4.29 Human nesprin-1α_2 WT induced heart development defects while mutants induced a less severe heart phenotype in zebrafish embryos 193
Figure 4.30 Overexpression of flag/V5-tagged nesprin-1α_2 in C2C12 cells 195
Figure 4.31 Expression level of V5-tagged nesprin-1α_2 and GFP was positively correlated 197
Figure 5.1 Overexpression of EGFP-KASH2 result in NE-LINC complex disruption 204
Figure 5.2 Breeding strategy of cardiac specific KASH2 Tg mice 205
Figure 5.3 Transgenic mice were born at the expected Mendelian ratios 207
Figure 5.4 GFP-KASH was cardiac specifically expressed 208
Figure 5.5 csKASH-Tg mice developed normally up to 1 year 212
Figure 5.6 Echocardiography showed an increased LV wall thickness in csKASH-Tg mice 213
Figure 5.7 Echocardiography showed the cardiac hypertrophic response was induced in csKASH-Tg mice 214

Figure 5.8 HE staining showed an increased LV wall thickness in csKASH-Tg mouse hearts 219
Figure 5.9 Myocardial fibrosis was observed in csKASH-Tg mice 220
Figure 5.10 Size of cardiomyocytes was increased in csKASH-Tg mice 221
Figure 5.11 Cardiomyocyte nuclear morphology was altered in csKASH-Tg mice 222
Figure 5.12 Hypertrophic and fibrotic genes were expressed in csKASH-Tg mouse hearts 224
Figure 5.13 Endogenous NE-LINC complex components were mis-localised from NE in csKASH-Tg mice 225
Figure 5.14 qPCR showed SUN1 was increased in csKASH-Tg mice 228
Figure 5.15 WB showed unchanged protein levels of NE-LINC complex components 229
Figure 5.16 Echocardiographic images of the aorta in TAC mice 231
Figure 5.17 Heart mass was increased by pressure overload in both FLctrl and csKASH-Tg mice 232
Figure 5.18 Echocardiography showed reduced heart contraction after TAC surgery 234
Figure 5.19 Echocardiography showed severe cardiac structural and functional changes in csKASH-Tg TAC mice 236
Figure 5.20 Massive myocardial fibrosis was present in csKASH-Tg TAC mice .. 239
Figure 5.21 Upregulated expression of hypertrophic and fibrotic genes in csKASH-Tg TAC mouse hearts 240
Figure 5.22 qPCR showed SUN2 was reduced in FLctrl TAC mice and lamin A/C was increased in csKASH-Tg TAC mice 241
Figure 5.23 WB showed no significant changes of expression levels of NE-LINC complex components in csKASH-Tg after TAC 243
Figure 5.24 Mechanosensitive genes were altered in csKASH-Tg mice under the pressure overload 245
Figure 6.1 Working model for the roles of nesprin-1/-2 256
Figure 6.2 Working model for nesprin-1/-2 mutants 259

List of Tables

Table 1.1 Summary of the tissue specific nesprin-1/-2 variants 30
Table 1.2 Types of LINC complexes 40
Table 1.3 Nesprin mutations and associated diseases 48
Table 1.4 Nesprin-1 mutations in muscle diseases 49
Table 1.5 Nesprin-1/-2 mutations in muscle and CNS diseases 51
Table 1.6 Nesprin-1/-2 mouse models 68
Table 2.1 Primers used for V5 tagged nesprin-1α_2 WT and KASH 96
Table 2.2 Primers used for Flag tagged nesprin-1α_2 WT 97
Table 2.3 Primers used for nesprin-1α_2 mutagenesis 98
Table 2.4 Primers for genotyping 99
Table 2.5 Primers for qPCR 100
Table 2.6 siRNA oligos 102
Table 2.7 Primary antibodies 104
Table 2.8 Secondary antibodies for WB 105
Table 2.9 Secondary antibodies for IF 106
Table 5.1 Echocardiographic analysis showed a cardiac hypertrophic response 216
was induced in csKASH-Tg mice at 52 weeks 216
Table 5.2 Characterisation of cardiac phenotype and cellular changes in csKASH-Tg
mice 247

List of Abbreviations

ABD	Actin Binding Domain
AD	Adaptive Domain
AMC	Arthrogryposis Multiplex Congenita
AP-1	Activating Protein 1
ARCA1	Autosomal Recessive Cerebellar Ataxia Type 1
ASD	Autism Spectrum Disorder
BAF	Barrier to Auto-Integration Factor
BD	Bipolar Disorder
BPAG1	Bullous Pemphigoid Antigen 1
BPM	Beats Per Minute
BRCA2	Breast Cancer Susceptibility Gene 2
BSA	Bovine Serum Albumin
BW	Body Weight
CD	Conduction Defects (heart)
C. elegans	*Caenorhabditis elegans*
c-FOS	c-Fos Proto-Oncogene, AP-1 Transcription Factor Subunit
CH domain	Calponin-Homology domain
CMD	Congenital Muscular Dystrophy
CMs	Cardiomyocytes
CMT	Charcot-Marie-Tooth syndrome
CNS	Central Nervous System
csKASH-Tg	cardiac specific Transgenic KASH2
DAPI	4', 6'-Diamidino-2-Pheylindoledihydrochloride
DCM	Dilated Cardiomyopathy
DiH_2O	Deionized Water
DKO	Double Knockout
DMD	Duchenne Muscular Dystrophy
DMEM	Dulbecco's Modified Eagle's Medium
DN	Dominant Negative

DN KASH1	Dominant Negative nesprin-1 KASH
DN KASH2	Dominant Negative nesprin-2 KASH
ECG	Electrocardiogram
ECM	Extracellular Matrix
EDMD	Emery-Dreifuss Muscular Dystrophy
EF	Ejection Fraction
ER	Endoplasmic Reticulum
ERK1/2	Extracellular signal-Regulated Kinase 1/2
ES	Enzyme Solution
ESV	left ventricular End-Systolic Volume
FACS	Fluorescence-Activated Cell Sorting
FBS	Fetal Bovine Serum
FLctrl	FLoxed control
GST pull-down	Glutathione S-Transferase pull-down
HDFs	Human Dermal Fibroblasts
HEK 293T	Human Embryonic Kidney cells 293T
HF	Heart Failure
HFpEF	Heart Failure with preserved Ejection Fraction
HFrEF	Heart Failure with reduced Ejection Fraction
HGPS	Hutchinson-Gilford Progeria Syndrome
HLFs	Human Lung Fibroblasts
HP-1	Heterochromatin Protein-1
hpf	hours post-fertilization
HRP	Horseradish Peroxidase
HS	Horse Serum
HW	Heart Weight
IF	Immunofluorescence
IFs	Intermediate Filaments
INM	Inner Nuclear Membrane
IP	Immunoprecipitation
IVSd	Interventricular Septum (diastole)

IVSs	Interventricular Septum (systole)
JNK	c-Jun NH2-terminal Kinase
KHC	Kinesin Heavy Chain
KLC	Kinesin Light Chain
KO	Knockout
LAPs	Lamin Associated Polypeptides
LINC	LInker of Nucleoskeleton and Cytoskeleton
LRMP	Lymphoid-Restricted Membrane Protein
LV	Left Ventricle
LVIDd	Left Ventricular Internal Diameter (diastole)
LVIDs	Left Ventricular Internal Diameter (systole)
LVPWd	Left Ventricular Posterior Wall (diastole)
LVPWs	Left Ventricular Posterior Wall (systole)
M199	Medium 199
MACF	Microtubule-Actin Cross-linking Factor
mAKAP	muscle A-Kinase Anchoring Protein
MAPK	Mitogen-Activated Protein Kinase
MCK	Muscle Creatine Kinase
MEFs	Mouse Embryonic Fibroblasts
MHC	Myosin Heavy Chain
MKL1	Megakaryoblastic Leukaemia 1
MKS	Meckel Syndrome
MLC2V	Ventricular Myosin Light Chain 2
M-MLV RT	Moloney Murine Leukaemia Virus Reverse Transcriptase
MRFs	Myogenic Regulatory Factors
MTOC	Microtubule-Organizing Centre
Myf5	Myogenic factor 5
MYL7	Myosin Light chain polypeptide 7
MyoD	Myoblast determination protein
NE	Nuclear Envelope
NF-κB	Nuclear Factor kappa-light-chain-enhancer of activated B cells

NMJ	Neuromuscular Junction
NPC	Nuclear Pore Complex
NRCs	Neonatal Rat Cardiomyocytes
OCT compound	Optimal Cutting Temperature compound
ON	Overnight
ONM	Outer Nuclear Membrane
ORF	Open Reading Frame
PBS	Phosphate Buffered Saline
PCM-1	Pericentriolar Material 1 protein
PCR	Polymerase Chain Reaction
pELK1	phosphorylated Ets-like transcription factor 1
pERK	phosphorylated Extracellular signal Regulated Kinase
PFA	Paraformaldehyde
PIC	Protease Inhibitor Cocktail
PML NBs	Promyelocytic Leukaemia protein Nuclear Bodies
PNS	Perinuclear Space
PSG	Penicillin-Streptomycin-L-Glutamine
qPCR	quantitative Polymerase Chain Reaction
RA	Right Atrium
RLC	Regulatory myosin Light Chain
RPM	Revolutions Per Minute
RT	Room Temperature
RVs	Retroviruses
siRNA	small interfering RNA
SR	Spectrin Repeat
SRF	Serum Response Factor
SUN	Sad1/UNC-84
SV	Stroke Volume
TAC	Transverse Aortic Constriction
TA muscle	Tibialis Anterior muscle
TAN line	Transmembrane Actin-associated Nuclear line

tERK	total Extracellular signal-Regulated Kinase
Tg	Transgenic
TGF-β	Transforming Growth Factor beta
TL	Tibia Length
U2OS	Human Osteosarcoma
VSMC	Vascular Smooth Muscle Cell
WB	Western Blotting
WISH	Whole-mount *In Situ* Hybridization
WT	Wild Type
YAP	Yes-Associated Protein

Chapter 1: Introduction

Nesprins (nuclear envelope spectrin repeat proteins), are multi-isomeric scaffolding proteins [1]. They localise at the nuclear envelope (NE) and interact with SUN domain proteins to form the LINC (LInker of Nucleoskeleton and Cytoskeleton) complex. The LINC complex provides a stable physical connection between the nucleus and the cytoskeleton, and also participates in mechanotransduction via transmitting the cellular mechanical force to the nucleus [2]. To date, nesprin-1 and nesprin-2 mutations have been identified in Emery-Dreifuss muscular dystrophy (EDMD) and Dilated Cardiomyopathy (DCM) patients [3, 4]. In this chapter, I will comprehensively review the current research on nesprin proteins, in particular nesprin-1 and -2, including their structural properties, roles in the LINC complex, and discuss any potential mechanisms linking these mutations to muscle specific disorders.

1.1 Cytoskeleton network and spectrin repeat superfamily

The cell is the basic unit for structure and function in all living organisms. In eukaryotic cells, the cellular architecture is maintained by the cytoskeleton network that connects the nucleus to the extracellular matrix (ECM). Three major cytoskeleton network components are: microfilaments (Filamentous-actin, F-actin), intermediate filaments (IFs) and microtubules, which vary in size and stiffness, all work together with their associated proteins to build stable interconnected scaffolds. The cytoskeleton network plays important roles in regulating cell shapes and migration, transporting intracellular cargo and resisting deformation [5].

An important family of proteins that connect cytoskeletal elements, cell membrane, and the nucleus are the spectrin repeat (SR) containing proteins [6, 7]. This superfamily is characterised by multiple arranged SRs arranged in tandem to form the coiled-coil rod domain. In addition, the majority of these proteins contain the N-terminal calponin-homology domain (CH) which binds to F-actin, and the featured C-terminal protein-binding motif that binds to microtubules, IFs and the nuclear membrane [8]. To date, a growing list of proteins have been identified as members of this superfamily, which include α-actinin, spectrins, dystrophin/utrophin,

spectraplakins/plakins and nesprins. Those proteins can be characterised by various SRs and C-terminal unique structural domains, with different and specific functions.

1.2 Nesprins

Nesprins, the latest identified SR containing proteins, are a novel family of multi-isomeric scaffolding proteins [1]. To date, six genes (*SYNE-1, -2, -3, -4, LRMP and KASH5*) have been identified encoding nesprins-1, -2, -3, -4, Lymphoid-restricted membrane protein (LRMP) and KASH5, localizing on chromosome 6q25, 14q23.2, 14q.32.13, 19q13.12, 19q10 and 12q12.1 respectively [1, 9-12].

Full length human nesprin-1 and nesprin-2 are giant SR proteins with molecular masses of ~1000kDa and ~800kDa respectively, which are the second and third largest known proteins. Nesprin-1, also known as synaptic nuclear envelope-1 (SYNE-1) [13], and myocyte nuclear envelope protein-1 (Myne-1) [14], was identified in searching of vascular smooth muscle cell (VSMC) differentiation markers using differential cDNA screening of rat VSMCs [15]. A 10kb transcript of rat nesprin-1 (1RA1), was highly expressed in differentiated aortic VSMCs compared to cultured undifferentiated VSMCs [1]. Nesprin-2 was identified in the same differential cDNA screening, sharing 64% homology with nesprin-1 [1]. Other research groups reported nesprin-2 as SYNE-2 [13], and nucleus and actin connecting element (NUANCE) [16] that was identified via yeast two-hybrid or screening the human EST database using the peptide sequence of known α-actinin-related proteins as a query. My research is mainly focused on nesprin-1 and -2.

Nesprin-3 was first isolated from a yeast two-hybrid screen using the actin binding domain of plectin-1C as bait, with a molecular mass of 110kDa and around 22-25% homology with the same region in both mouse and human nesprin-1 and nesprin-2 [9]. Nesprin-4 was identified via a BLAST search using the human nesprin-2 transmembrane domain as probe; however, this protein showed lower similarity (26%-36% identical) to nesprin-1/-2/-3 at the protein level. It is a relatively small isoform with a molecular mass of 42kDa [10]. LRMP was originally identified in B and T cells, localised to the endoplasmic reticulum (ER) membrane via the C-terminal KASH homology domain [11, 17, 18]. LRMP was also expressed in a subset of taste receptor cells in mammals [19], and rich in zebrafish zygotes [18]. KASH5, also

known as Ccdc155, with a molecular weight of 72kDa, was identified using a BLAST search with LRMP. It was highly expressed in testes, and is a meiosis-specific KASH domain protein [12, 20].

1.2.1 Nesprin structure

The typical structure of giant nesprin-1 and -2 consists of three major parts: A C-terminal Klarsicht/ANC-1/Syne Homology (KASH) domain that is targeted to the NE, an N-terminal paired Calponin Homology (CH) domain that binds to the actin cytoskeleton, and a central domain containing multiple SRs that link the CH and KASH domains and provide the elasticity needed for protein-protein interactions [21]. Of note, there is a highly conserved adaptive domain (AD) at the C-terminus of nesprin-1 and -2, between SR71-SR72 of nesprin-1 and SR53-SR54 of nesprin-2 respectively [22, 23]. The AD region has relatively little secondary structure, but it significantly stabilises multiple SRs by increasing their overall helicity, thermal stability and cooperativity of folding [23] (Figure 1.1).

1.2.1.1 Klarsicht/ANC-1/Syne Homology (KASH) domain

Nesprin-1 and -2 show the NE targeting property which relies on the C-terminal transmembrane KASH domain. The KASH-domain family includes Kms1 in *Schizosaccharomyces pombe*, Interaptin in *Dictyostelium discoideum*, ANC-1, UNC-83 and ZYG-12 in *Caenorhabditis elegans* (*c. elegans*) as well as Klarsicht and MSP-300 (muscle-specific protein 300) in *Drosophila melanogaster* [24-26]. KASH domain proteins are type-II transmembrane proteins that contain a single transmembrane segment, followed by an evolutionarily conserved sequence, then a short luminal tail that extends into the perinuclear space (PNS) [26]. The KASH domain tails terminate with a PPPX motif (this motif is very conserved in mammals where X is variable residue), and interacts with luminal Sad1p-UNC84 (SUN) domain proteins [26, 27]

1.2.1.2 Spectrin repeat (SR) rod domain

A single SR contains three bundled antiparallel α-helices (helix A, B and C) separated by two loop regions (called loop AB and BC) (Figure 1.2). SRs link to each other via a helix region (the 'linker') which connects the last helix of one repeat with the first helix of the next [28, 29]. Multiple consecutive SRs are arranged in tandem and localise between N- and C-terminal domains. This rod domain not only serves as a simple spacer, it is also involved in the formation of the tertiary/quaternary structure, interacting with other molecules, and potentially contribute to protein elasticity and structural flexibility [7, 29].

The central rod domain of nesprins comprises of numerous SRs that tightly link the N-terminus to the C-terminus. Full length nesprin-1 is formed of 74 SRs, whereas nesprin-2 is formed of 56 SRs. Nesprin-1 and -2 are both typical SRs fold with a high proportion of α-helical structure [29].

Evolutionary conservation of amino acid positions in nesprins reveals both nesprin-1 and -2 have a very high similarity in their sequences, and good stability in the temperature and denaturation studies [29]. The most conserved SRs are the nesprin-1 SR69-SR71 and nesprin-2 SR51-SR53. Interestingly, these SRs are both the 3rd to the 6th SRs counting backwards from nesprin-1 and nesprin-2 respectively, indicating this structure may have some critical function in nesprin proteins. The nesprin-1 SR69-SR71 (red coloured SRs) are more conserved than nesprin-2 SR51-SR53 (pink coloured SRs). This difference results in the distinct electrostatic surface and hydrophobic/hydrophilic properties, divergent potential binding sites for the interaction partners and different flexibility/elasticity (Figure 1.3) [29].

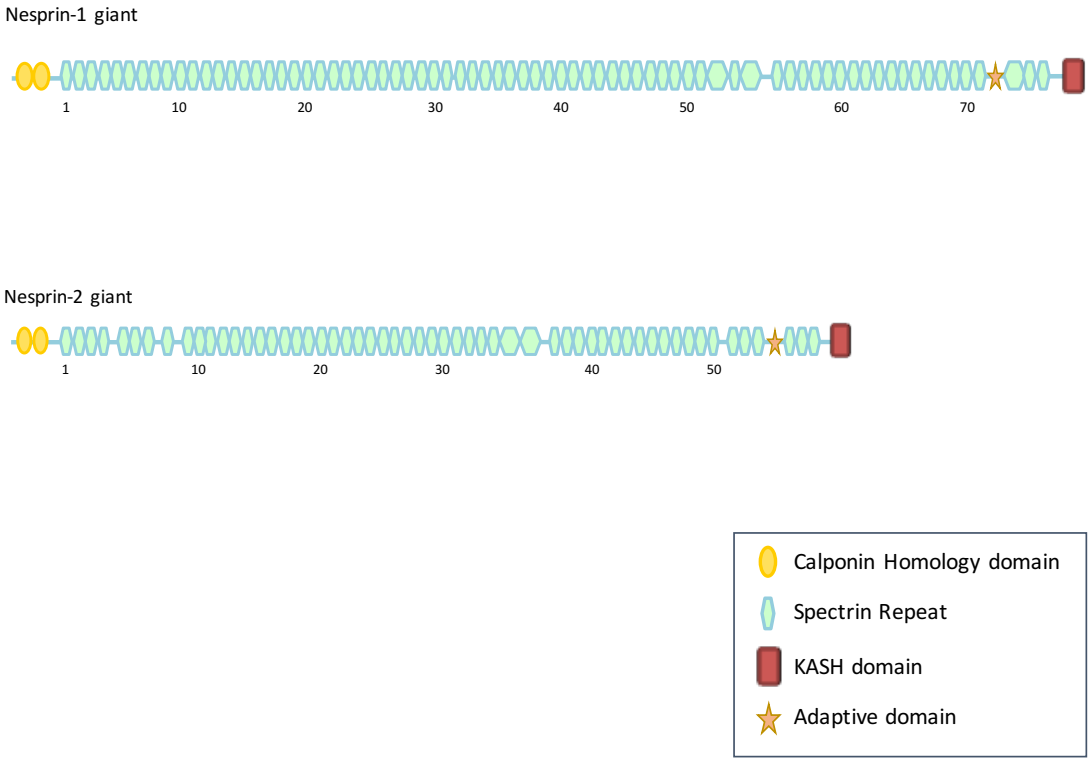


Figure 1.1 Structure of giant nesprin-1 and -2

The giant nesprin-1 and -2 consist of three major parts: C-terminal Klarsicht/ANC-1/Syne Homology (KASH) domain targeting to the NE; N-terminal paired Calponin Homology (CH) domains binding to the actin cytoskeleton; whilst multiple SRs in the central, linking the CH and KASH domains, which maintain elastic properties and mediate protein-protein interactions. Noteworthy, an unstructured region named as adaptive domain (AD) localises at the C-terminus and helps to stabilise the multiple SRs.

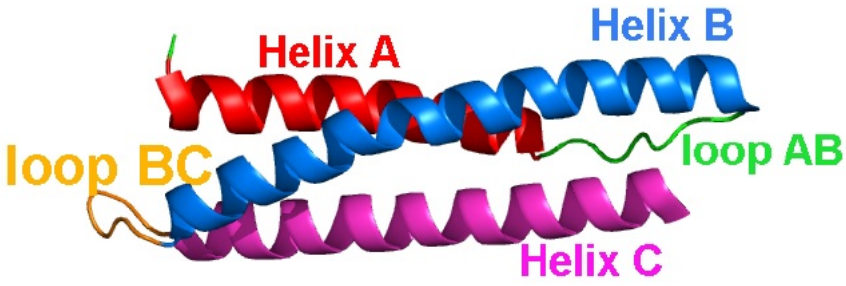


Figure 1.2 Ribbon representation of a single SR crystal structure

Representation of the crystal structure of a single unit SR from chicken brain α-spectrin, which consists of three bundle α-helices (helix A/B/C) in an antiparallel manner, and separated by two loop regions (loop AB/BC). The SR unit comprises the majority of the nesprin backbone. Image adapted from Autore, *et al*. 2013 [29].

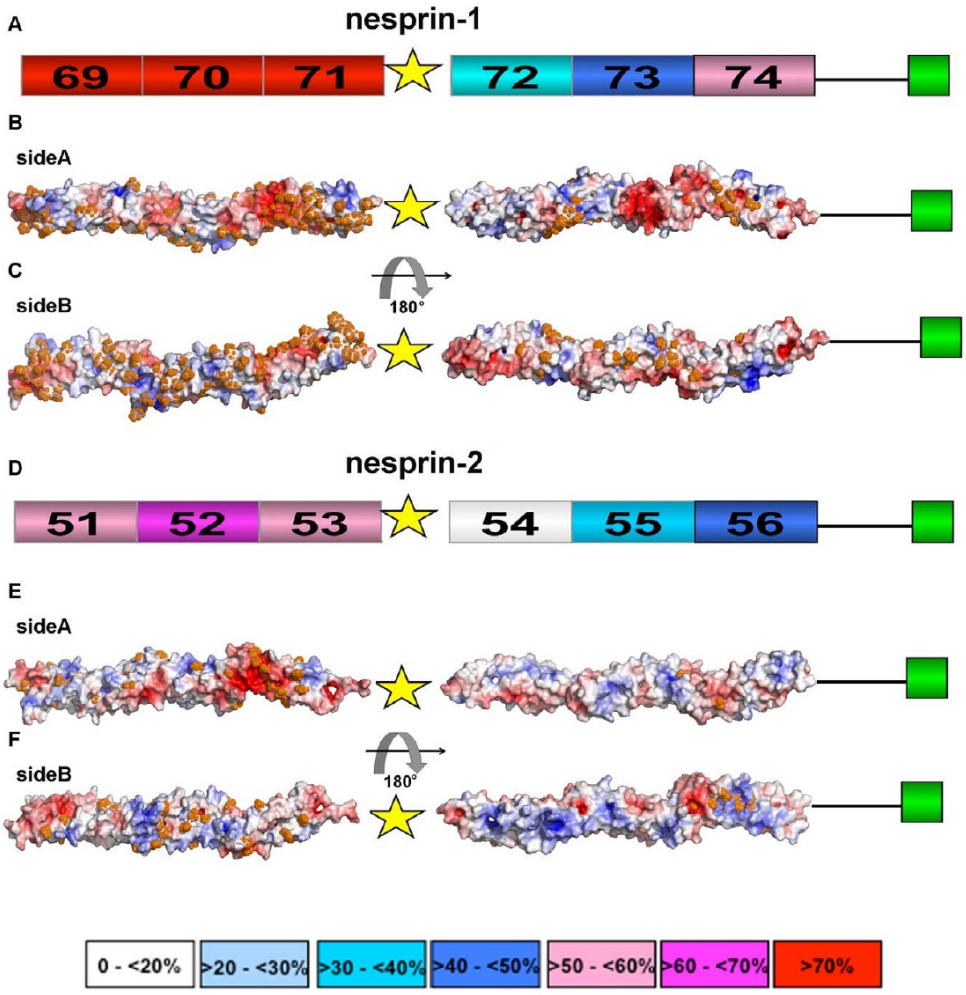


Figure 1.3 Schematic representation of highly conserved SRs in nesprin-1 and -2

The most conserved SRs are SR69-SR71 and SR51-SR53 in nesprin-1 and -2 respectively. The colour code indicates the different evolutionary conservation of amino acids in nesprin-1 SR69-SR74 (A) and nesprin-2 SR51-SR56 (D). Panels B-C and E-F represent the electrostatic potential surfaces (side A and side B) of nesprin-1 SR69-SR74 and nesprin-2 SR51-SR56. Blue – positive charge potential; red – negative charge potential. The yellow star represents the adaptive domain. Image adapted from Autore, *et al*. 2013 [29].

1.2.1.3 Calponin Homology domain

CH domain was first identified in the Calponin protein, which is a calcium-binding protein presents in smooth muscle with a single CH domain [30]. The compact globular CH domain comprises of four α-helices in roughly parallel orientation. Each α-helix is 11-18 residues in length, linked by the other three helices to form the sandwich-like structure [31]. Nesprin-1 and -2 contain two CH domains (CH1 and CH2) at the N-terminus in the juxtaposition, functioning as the actin-binding domain (ABD). A single CH2 domain is not able to bind to actin filaments, but it acts as a CH1 enhancer to strengthen the binding with F-actin [32, 33].

1.2.2 Nesprin isoforms

SYNE-1 and *SYNE-2* genes consist of 146 and 116 exons respectively. Within such long genes, there are multiple different starting and termination sites as well as alternative splicing allowing them to generate numerous isoforms (Figure 1.4).

1.2.2.1 Giant nesprin-1 and nesprin-2

Giant nesprin-1 and nesprin-2 localise at the outer nuclear membrane (ONM) via the C-terminal KASH transmembrane domain, and connect the NE to the actin cytoskeleton through the N-terminal CH domains. Nesprin-1 and nesprin-2 giant isoforms make up 80% of the total nesprin mRNA in 20 different human tissues. But they were less in cardiac muscle (63%), skeletal muscle (66%) and the spleen (56%), suggesting those tissues have a higher proportion of shorter isoforms that may be required for tissue-specific functions. The mRNA level of giant nesprin-2 is greater than giant nesprin-1 in the majority of human tissues and cell lines, except in brain and VSMCs with 81% and 92% of nesprin-1 respectively.

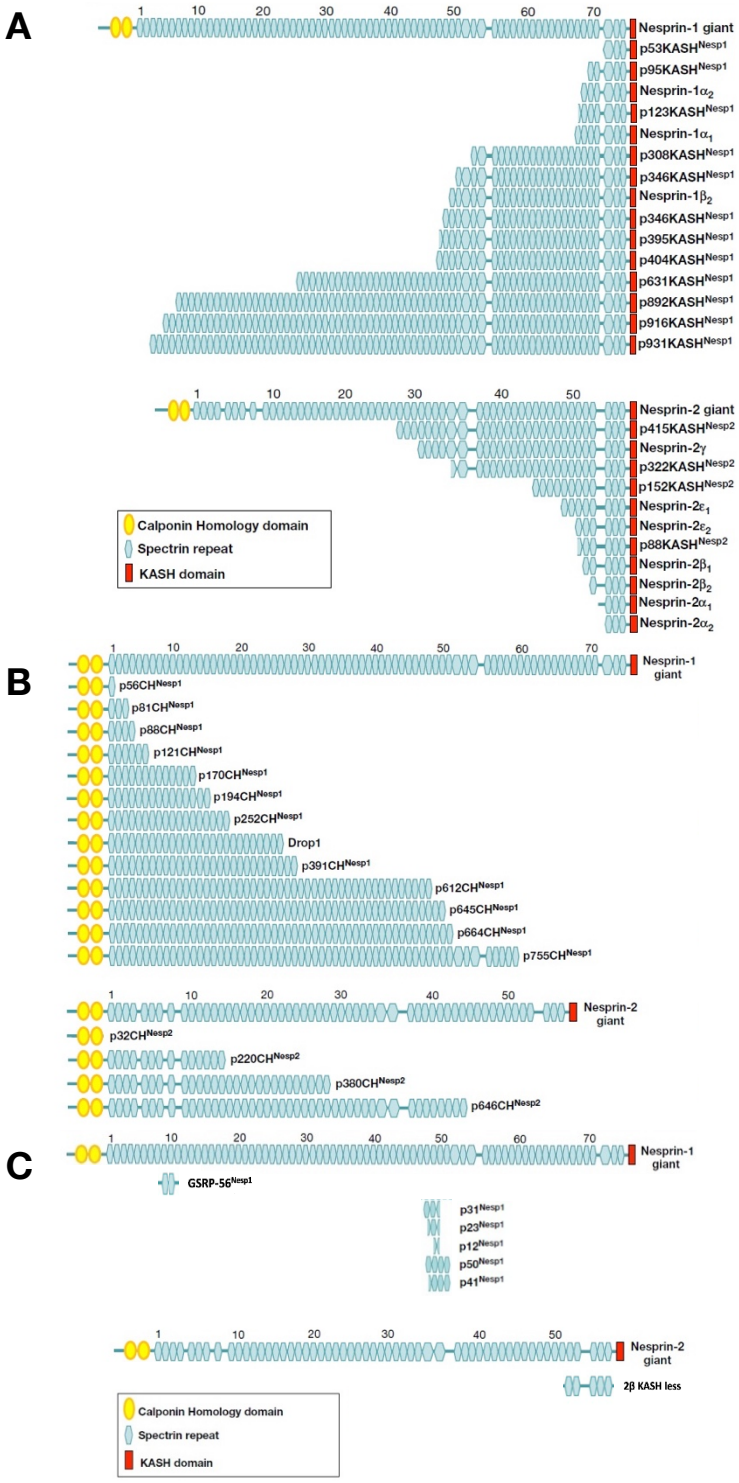


Figure 1.4 Nesprin isoforms derived from *SYNE-1/-2* genes

By combining the identified 5′UTRs and 3′UTRs with the nesprin-1 giant and nesprin-2 giant, different nesprin-1/-2 variants with or without KASH/CH domains can be created. A: Potential nesprin-1/-2 KASH domain isoforms; B: Potential nesprin-1/-2 CH domain isoforms; C: Potential SR only nesprin-1/-2 isoforms (Image adapted and modified from Rajgor and Shanahan 2013 [21]).

1.2.2.2 Nesprin isoforms with KASH domain

The KASH domains between nesprin-1 and nesprin-2 are highly homologous to each other with the difference of only 10 out of the total 60 amino acids. To date, by alternative combinations of identified 5'UTR with the 3'UTR of the giant nesprin-1 and nesprin-2, 16 nesprin-1 and 12 nesprin-2 KASH containing isoforms can theoretically be generated (Figure 1.4A). These nesprin KASH isoforms exhibit varied tissue specific patterns [34]. In muscle, nesprin-1α_2 and nesprin-2α_1 are highly expressed in both heart and skeletal muscle, accounting for 30% of the total mRNA of nesprin-1/-2; nesprin-2β is only highly expressed in skeletal muscle, whilst nesprin-2ε_2 is heart specific. In other tissues: nesprin-1β is highly expressed in spleen; nesprin-2α_2 is mainly present in the kidney; nesprin-2ε_1 is found in early embryonic cells; and nesprin-2γ is present at a low level in all tissues [1, 35, 36] (Table 1.1).

There is evidence that shows nesprin isoforms are dynamically regulated during different cellular activities. In human myoblasts, expression level of nesprin-1α_2 is very low, whereas it is massively up-regulated around 50-fold after differentiation [37]. *In vivo*, during the transition from immature to mature muscle fibers, nesprin-2 KASH isoforms partly replaces nesprin-1 KASH isoforms at the NE, and short isoform nesprin-1α_2 becomes more dominant [38].

1.2.2.3 Nesprin KASH less isoforms with CH domains

Hypothetically combining 5'UTR with the alternative 3'UTR of the giant nesprin-1 and nesprin-2, 14 nesprin-1 and 5 nesprin-2 CH domains containing and KASH less isoforms can be generated (Figure 1.4B). The fully cloned nesprin-1 P56CH is formed by paired CH domains and the first SR of nesprin-1. It is ubiquitously expressed, but exhibits tissue specific localisation. In primary human dermal fibroblasts (HDFs), it interacts with F-actin and focal adhesion, while in U2OS cells, it surprisingly localise to the nucleolus, and interacts with nuclear actin [34].

Table 1.1 Summary of the tissue specific nesprin-1/-2 variants

Variants		**Tissue**
Nesprin-1	Nesprin-1α_2	Heart and skeletal muscle
	Nesprin-1β_1	Spleen
Nesprin-2	Nesprin-2α_1	Heart and skeletal muscle
	Nesprin-2α_2	Kidney
	Nesprin-2β	Skeletal muscle
	Nesprin-2ε_1	Embryonic cells
	Nesprin-2ε_2	Heart

During ciliogenesis, a 250kDa and a 150kDa nesprin-2 CH domain containing isoforms can interact with Meckel syndrome (MKS) proteins through the SRs near N-terminus at the cell periphery, and bind with F-actin via the CH domains. The connections between nesprin-2 CH isoforms with microtubule and actin cytoskeleton form the cellular scaffolds to regulate centrosome migration [39]. Loss of MKS protein causes a dramatic remodelling of the actin cytoskeleton, aberrant localisation of nesprin-2 isoforms to actin stress-fibers and activation of RhoA signalling [39]. These findings further highlight that nesprin CH domain isoforms display a non-NE targeted localisation, interact with cytoskeletal elements, and play roles in centrosome migration and early ciliogenesis.

1.2.2.4 Spectrin repeat only nesprin isoforms

To date, more alternative 5'UTR and 3'UTR for KASH less isoforms have been identified in *SYNE-1* rather than *SYNE-2*, implying nesprin-1 has the potential to generate more SR only isoforms than nesprin-2 (Figure 1.4C).

Nesprin-1 SR containing protein, named Golgi-localized SR-containing protein-56 (GSRP-56), plays a role in maintenance of the Golgi structure [40]. Recently, nesprin-1 p50, a 50kDa isoform with 4 SRs, has been identified from the *SYNE-1* gene. Nesprin-1 p50 is widely expressed and localises to the processing bodies, acting as a microtubule-associated scaffold protein, and participating in miRNA-mediated silencing [41].

Nesprin-2β KASH less isoform has been detected in the VSMCs. This 75kDa nesprin-2 isoform tethers the extracellular signal-regulated kinase 1/2 (ERK1/2) at the promyelocytic leukaemia proteinnuclear bodies to form the nuclear complex and serves to regulate nuclear signalling. Interference of nesprin-2 function results in sustained ERK1/2 signalling which eventually promotes the VSMC proliferation [42]. These findings demonstrate that nesprin SR isoform can act like a novel intra-nuclear scaffold, involved in cell signalling regulation and cell cycle progression.

1.2.2.5 Nesprin KASH or KASH less isoforms

Nesprins are multi-isoform proteins, and many antibodies are generated against different regions. Thus, the nesprin antibodies are more likely to detect a group of

isoforms containing that regions rather than a single isoform. Using the nesprin-2 antibody that targets SRs towards the C-terminus, nesprin-2 KASH isoform like nesprin-2β, nesprin-2γ and other potential nesprin-2 KASH-less isoforms can be detected. Immunofluorescence (IF) showed weak NE and nuclear staining, in contrast with a strong sarcomere staining in both C2C12 myotube and human skeletal muscle [35]. The staining is particularly abundant over the Z-line and A/I junction, indicating those isoforms may function in sarcoplasmic reticulum and muscle contraction [35]. While the KASH domain isoforms targeted to the NE, the KASH less isoforms could potentially form the sarcomeric network in skeletal muscle [35]. In future, further work is required to fully characterise these nesprin isoforms and reveal their specific functions.

1.3 Nuclear Envelope

In eukaryotic cells, the nucleus is the most featured organelle that contains the genetic material and determines cell fate. Like the capital city standing in the crucial part of the cell, the nucleus is well guarded by the walls of the nuclear envelope, reinforced by the underneath intermediate filaments– nuclear lamina [43].

1.3.1 Nuclear envelope structure

The NE consists of two lipid membranes and nuclear pore complex (NPC). In mammalian cells, the outer nuclear membrane (ONM) and the inner nuclear membrane (INM) are separated by a ~50nm wide lumen called perinuclear space (PNS) [44, 45]. These two nuclear membranes are perforated by NPCs, which help to facilitate the molecular trafficking between the cytoplasmic and nuclear compartments. The transport is bidirectional, allowing the movement of molecules [46]. Proteins which are required for nuclear functions are synthesized in the cytoplasm and imported into the nucleus, whereas much of the RNA synthesized in the nucleus is transported to the cytoplasm [47]. The ONM is continuous with the endoplasmic reticulum (ER). It has been shown that there are abundant ribosomes presents at the ONM as well as the ER [44]. In addition, the INM consists of a wide range of transmembrane proteins that interact underneath nuclear lamina. Proteomics studies suggested that more than 70

different INM transmembrane proteins from several species have been identified. Some of these proteins present in a tissue-specific manner, which suggest the NE will recruit their specialised components to form the cell-type/function associated NE complex [48-50].

1.3.2 Nuclear envelope proteins

Among the wide range of INM transmembrane proteins, emerin and SUN proteins have been extensively characterised and are closely related to my research.

1.3.2.1 Emerin

Emerin is encoded by the *EMD* gene located on the X-chromosome. It is 254 amino acid long and consists of a 220 amino acid N-terminal nucleoplasmic domain, followed with a 23-amino acid C-terminal transmembrane domain and a small 11 amino acid luminal tail [51, 52]. Emerin, along with other INM transmembrane proteins like lamin associated polypeptides (LAPs) and MAN1 are founding members of the LEM-domain proteins [53]. LEM-domain comprised of 40 amino acids (residues 4-40 at emerin N-terminal), is conserved in prokaryotic and eukaryotes. This domain can directly bind to a conserved chromatin protein named barrier to auto-integration factor (BAF), which has essential roles in higher-order chromatin structure, nuclear assembly, and gene regulation [54]. Emerin is synthesized in the cytoplasm and then diffused from the ER to the nucleus [55]. During integration into the INM, emerin is retained through binding to the nuclear lamina. Deletion of lamin binding sites in emerin (residues 107–175) cause cytosolic aggregation of emerin [56]. In mice, embryonic fibroblasts (MEFs) lacking A-type lamins exhibited, emerin with more diffusional mobility, and this can be rescued by restoring the A-type lamins [57].

Emerin is ubiquitously expressed and predominately localise at the NE in skeletal muscle and heart [53, 58-60]. It has at least 14 binding partners including nesprin, nuclear lamina, Sad1/UNC-84 (SUN), BAF and chromatin-silencing enzyme HDAC3 (histone deacetylase 3) [61-65]. Notably, emerin binds to the small nesprin isoforms nesprin-1α and nesprin-2β within the same region as lamin A/C [66]. Evidence shows emerin relies on nesprin-1 and -2 for its proper NE targeting. Overexpressing or knocking down nesprin-1α mis-localises emerin from the INM in

U2OS and HDFs [3]. Overexpression of nesprin-2β mutants reduces emerin from the NE in HDFs [3]. These various partners of emerin suggests it is a critical component among the INM transmembrane proteins and is involved in the NE structure, chromatin integrity, gene regulation and cell signalling [67].

1.3.2.2 SUN

Sad1/UNC-84 (SUN) domain proteins were initially characterised from the *Schizosaccharomyces pombe* Sad1 protein and *Caenorhabditis elegans* UNC-84 protein [68, 69]. SUN domain proteins are conserved across eukaryotes including fungi, plants and animals [69-71]. So far, five SUN domain proteins have been identified in mammals. In addition to the wide expressed SUN1 and SUN2, SUN3, SUN4 (also known as SPAG4) and SUN5 are limited to the testes, and function in sperm development [72-75].

SUN1 and SUN2 have many common features. They are both INM transmembrane proteins; They are both comprised of the N-terminal nucleoplasmic domain, which can interact with nuclear lamina; a single transmembrane domain targets it to the INM; then two coiled-coiled regions that aid in dimerization or multimerization in PNS; followed with a highly conserved SUN domain at the C-terminal and can bind with nesprin [76-78]. SUN1 is the largest SUN protein in this family with a molecular mass ~90kDa, while SUN2 is slightly smaller with a molecular mass ~80kDa. Due to the alternative splicing site at the N-terminal of *SUN1* gene, it results in 7 different SUN1 variants [79]. Structure analysis speculated these SUN1 variants contain different hydrophobic motifs at the N-terminal and these may affect the dynamic properties of this molecule [80]. For SUN2, there was no literature reporting any potential variants, suggesting it may be more conserved in all cell types.

With loss of both SUN1 and SUN2, mice die at birth, which is likely due to a nuclear migration defect during the central nervous system (CNS) development [81]. Interestingly, depletion of either SUN1 or SUN2 in mice exhibit different phenotypes. SUN1 null mice are deaf with reduced rod cell number and thinner outer nuclear layer in the retina compared with SUN2 null mice [82, 83]. Disruption of SUN1 in mice also perturbs telomere attachment to the NE, leading to inefficient homologous chromatin pairing and synapse formation during mammalian gametogenesis [84]. SUN1 and SUN2 are both rich in the heart and skeletal muscles [85]. Recently mutations in SUN1

and SUN2 have been reported in human muscular dystrophies, affecting the cardiac and skeletal muscle. Myoblasts or fibroblasts derived from these patients displayed the changed expression level of nesprin-2, lamin A/C and emerin, as well as altered binding [86, 87].

1.3.3 Nuclear lamina

1.3.3.1 Structure and isoforms of nuclear lamins

The nuclear lamina is the meshwork comprised of type V intermediate filaments that link the NE and nucleoskeleton. Many ~3.5 nm thick filaments form a complex meshwork at the nuclear periphery, underneath NPCs and these display a pattern of sparsely and densely packed regions [88]. Each lamin features a central α-helical rod domain flanked by a small head (10-20 amino acids) and a carboxyl-terminal tail (200-300 amino acids) which contains a nuclear localisation signal, and an immunoglobulin (Ig)-like β fold domain and a CAAX motif (C: cysteine, A: an aliphatic amino acid, X: a variable amino acid, usually a methionine) [89, 90].

Nuclear lamins are divided into two classes, A-type and B-type. Lamin A/C and lamin B1, B2 are the major isoforms representing A-/B-type lamins respectively [91-94]. All nucleated cells express at least one B-type lamin at all stage of development [95]. Whereas A-type lamins are absent during early pre- and post-implantation embryonic stages and in embryonic stem (ES) cells. It starts to appear during tissue development [96].

1.3.3.2 A-type lamins

Prelamin A, the precursor of lamin A undergoes a series of post-translational modifications to become mature lamin A with removal of the modified C-terminal 15 amino acids via enzyme FACE1 (ZMPSTE24) [97, 98]. Abnormal accumulation of prelamin A results in the premature ageing disorder Hutchinson–Gilford progeria syndrome (HGPS) [99]. Notably lamin C does not undergo extensive post-translational modifications. In mammals, lamin A/C is highly dynamic and undergoes re-modelling throughout development. Protein levels of lamin A/C correlates with tissue elasticity and lamin A/C is 30-fold higher in stiff tissue relative to soft tissue [100]. Enhanced

lamin A/C in a stiff tissue such as muscle, heart, or bone will tend to impede rapid nuclear distension during the high stresses and/or stress fluctuations, to stabilise the chromosome territories or chromatin-lamina interactions [100].

Lamin A/C has numerous diverse interaction proteins. At least 54 binding partners and more than 100 indirect interactions have been identified using various proteomics-based studies [101, 102]. In general, lamin A/C binding partners can be categorized into three groups: chromatin-associated proteins including heterochromatin protein-1 (HP-1), H2A-H2B histone dimer and BAF [103-105]; NE transmembrane proteins such as nesprin, SUN, emerin, LAP2 [35, 77, 106, 107]; and signalling molecules and transcription factors like Phosphorylated-Retinoblastoma (pRb), extracellular signal-regulated kinase 1/2 (ERK1/2), c-Fos Proto-Oncogene, AP-1 Transcription Factor Subunit (c-fos), Sterol response element binding protein-1 (SREBP1) [108-110]. Those multiple binding molecules indicate the 'hub' role of lamin A/C in maintaining chromatin structure, gene regulation and cell signalling.

1.4 Nesprins link the nucleoskeleton to the cytoskeleton

The nucleus is the most crucial part of a cell. However, it is not isolated and is connected to the cytoplasm, cell membrane and extracellular matrix (ECM) via the 'bridge' crossing the NE. The cytoskeleton network was discovered to be specifically anchored at the NE by different types of LINC (linker the nucleoskeleton and cytoskeleton) complexes. These act as 'bridges' to maintain the NE structural integrity, regulate nuclear migration and positioning, sense the mechanotransduction and participate in gene regulation [2, 111-113].

1.4.1 LINC complex structure

The larger nesprin isoforms localise at the ONM, and directly bind to the cytoskeleton network including actin filaments, microtubule-dependent motors and plectin through their N-terminal domain [9, 10, 25, 114], whilst the C-terminal KASH transmembrane domain expands into the PNS and binds with SUN domain proteins embedded in the INM [78, 115]. This forms the LINC complex that links the

nucleoskeleton to the cytoskeleton. In addition, the nucleoplasmic domains of SUN proteins bind with INM transmembrane proteins, including small nesprin isoforms (nesprin-1α, nesprin-2β), emerin and nuclear lamina (lamin A/C), forming the NE complex which integrates with LINC complex to scaffold the entire cell [1, 35, 63] (Figure 1.5).

1.4.2 SUN-KASH bridge

The central part of the LINC complex is formed by the interaction of the KASH domain and SUN domain at the PNS. Recently, a significant insight into this SUN-KASH bridge has provided us with more details of this fundamental structure [78, 115]. The crystal structure of SUN-KASH demonstrated that a trimeric SUN domain has the capacity to bind three KASH peptides. There are three key points of interaction between SUN and KASH domains. Firstly, SUN proteins assemble into trimers. The two adjacent SUN domains form a deep groove acting like KASH binding pocket. Thus, a trimeric SUN domain is sufficient to bind with three KASH domains. Secondly, at the KASH domain, the C-terminal forms several contacting points with the SUN domain. Meanwhile, the hydrophobic residues on the KASH domain bind to a structure called the KASH-lid across two neighbouring SUN domains. Thirdly, a highly conserved cysteine at the KASH domain forms a disulphide bond covalently linking SUN and KASH, further enhancing this binding. These findings explain how this SUN-KASH bridge can form a high-order complex and serve as the fundamental core that can resist the substantial forces that are required for nuclear movement and chromosome rearrangements [78, 115, 116].

1.4.3 Types of the LINC complexes

1.4.3.1 Nesprin-1/-2 associated LINC complexes

One of the most characterised LINC complexes is the actin associated nesprin-1/-2-SUN LINC complex (Table 1.2, Figure 1.5). Not only acting to physically couple the cytoplasm and nucleus, the actin LINC complex also defines the mechanical properties as propagating the long-distance force through cytoplasm (F-actin) - NE (nesprin-1/-2 to SUN1/2) - nucleus (lamin A/C) in the cell [117]. In fibroblasts, this

linker specially formed with nesprin-2 is called the transmembrane actin-associated nuclear line (TAN line) [118, 119]. Disruption of this LINC complex using: depolymerized F-actin, inhibition of F-actin associated Rho kinase, overexpression of exogenous dominant negative (DN) KASH, or deletion of nesprin-2 giant results in altered nuclear shape, shrinking and mis-positioning of nuclei [118, 120, 121].

Another nesprin-1 and -2 associated LINC complex is the microtubule LINC complex (Table 1.2, Figure 1.5). Nesprin-1 and -2 interact with dynein/dynactin and kinesin-1 to link the nucleus with centrosomes, regulate the nuclear migration and positioning in skeletal muscle, retina and brain during development. Perturbing this LINC complex result in the nuclear aggregation or mis-localisation, which is similar to the phenotype, observed in human disease [83, 114, 122-124].

1.4.3.2 Other nesprin associated LINC complexes

In addition to nesprin-1 and -2, four other nesprins including nesprin-3, -4, LRMP and KASH5 have been shown to participate with the microtubule LINC complex (Table 1.2, Figure 1.5). Nesprin-3 can associate with the microtubule motor protein bullous pemphigoid antigen 1 (BPAG1), microtubule–actin cross-linking factor (MACF) and breast cancer susceptibility gene 2 (BRCA2), to regulate centrosome polarisation and nuclear migration especially under fluid shear stress [125, 126]. Nesprin-4, LRMP and KASH5 interact with either kinesin-1, dynein or dynactin to participate in numerous cell activities such as nuclear migration and localisation, centrosome-nucleus movement during spermatogenesis and fertilization [10, 12, 20, 82, 127, 128].

Furthermore, nesprin-3 associates with plectin to form IFs LINC complex [9] (Table 1.2, Figure 1.5). It connects the nucleus to the hemidesmosomes at the cell surface, which can help the firm attachment of the basal epithelial cells to the underneath basement [129, 130]. Overexpression or depletion of nesprin-3 results in mis-positioned plectin both *in vitro* and *in vivo* [9, 131-133], emphasizing the central role of nesprin-3 in recruiting plectin to the NE and maintaining the integrity of IFs LINC complex.

1.4.3.3 Interaction between different LINC complexes

The actin, microtubule and IFs associated LINC complex have been shown to form united LINCs (Table 1.2, Figure 1.5). Evidence shows that F-actin connects with microtubules through microtubule–actin cross-linking factor (MACF), whilst interacting with IFs through the plectin protein [134]. Multiple nesprin isoforms also contribute to this network. For example, the nesprin-1/-2 ABD domain has similar binding properties to nesprin-3 SRs [121]. In addition, nesprin-3 directly links to plectin and IFs. This intricate interaction of LINC complexes links the whole cytoskeleton, KASH-SUN and nucleus tightly together, to maintain nuclear morphology, movement and transmission mechanical forces.

Table 1.2 Types of LINC complexes

Type	Cytoplasmic factor	KASH domain	SUN domain	Functions
Actin LINC complex	Actin filament	Nesprin-1 Nesprin-2	SUN1 SUN2	Nuclear size/morphology [121, 135, 136] Synaptic and non-synaptic nuclear anchorage in muscle fibers [81, 135, 137, 138] TAN-line: nuclear migration and positioning in fibroblast [118, 119]
IFs LINC complex	Plectin	Nesprin-3	SUN1 SUN2	Cell morphology and cytoskeleton organisation [9, 125, 131-133]
Microtubule LINC complex	Dynein Dynactin Kinesin-1 (kif5b)	Nesprin-1 Nesprin-2	SUN1 SUN2	Centrosome-Nucleus Coupling [123] Nuclear migration in skeletal muscle, retinal and brain [83, 114, 122-124]
	Kinesin-2 (kif3b)	Nesprin-1	nd	Facilitate the accumulation of membrane vesicles during cytokinesis [139]
	BPAG1 MACF BRCA2	Nesprin-3	SUN1 SUN2	Nuclear positioning [9, 126] Centrosome polarisation and cell migration in endothelial cells [125]

Type	Cytoplasmic factor	KASH domain	SUN domain	Functions
Microtubule LINC complex	Kinesin-1 (KLC-1/-2 and kif5b)	Nesprin-4	SUN1 SUN2	Cell morphology [10] Nuclear positioning in the outer hair cells of the cochlea [82]
	Dynein Dynactin	LRMP	SUN	Nucleus-centrosome attachment and pronuclear congression during fertilization [18]
	Dynein Dynactin	KASH5	SUN1	Meiotic chromosome movement [12, 20, 127, 128]
nd: not defined				

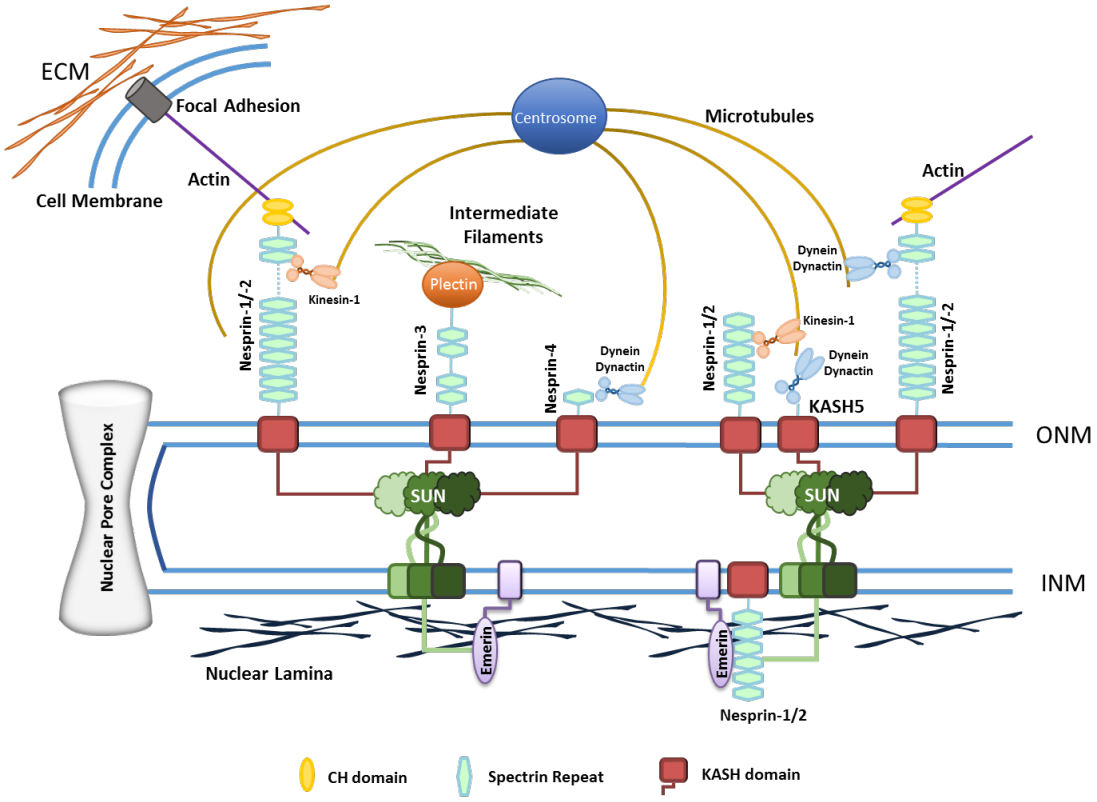


Figure 1.5 Nesprins form the NE-LINC complex and provide scaffolds for multiple sub-cellular compartments.

At the ONM, nesprin interact directly or indirectly with all three major cytoskeleton network to form the LINC complex. F-actin (nesprin-1/-2), microtubule (nesprin-1/-2/-3/-4/KASH5 via dynein/dynactin and kinesin-1) and intermediate filaments (IFs) (nesprin-3 via plectin). At the INM, small nesprin-1/-2 isoforms targeted to the NE through KASH domain, and interact with emerin, SUN and lamin A/C through their SRs at the nucleoplasmic side, forming the NE complex. The NE-LINC complex links the nucleoskeleton to the cytoskeleton and maintains the cellular structure and stability.

1.5 Nesprin and diseases

A number of human diseases are associated with mutations in genes coding for NE proteins. Mutations in lamin A/C are involved in a wide spectrum of diseases referred as laminopathies [140], which include the dilated cardiomyopathy (DCM) and Emery-Dreifuss muscular dystrophy (EDMD). In addition, emerin mutations also have been reported to cause EDMD [52, 53, 58].

DCM is characterised by dilatation and impaired contraction of the left or both ventricles, and is an important cause of heart failure and sudden cardiac death, particularly in the young. The genetic causes of DCM are extremely complicated and over 50 genes have been implicated, many of them encoding components of the cytoskeleton and NE [141, 142]. Mutations in the *LMNA* gene, encoding protein lamin A/C, account for 5% of familial DCM patients [143].

EDMD manifests with skeletal muscle wasting with a distinctive humeroperoneal distribution early in the course of the disease and later extends to the proximal limb girdle musculature. Cardiac involvement is another feature of EDMD including heart conduction defects (CD) and DCM. Although CD and DCM always develop later in the patients' life, they are the main cause of death [144-147]. There are two forms of EDMD, including autosomal dominant and X-linked. The AD-EDMD has been linked to lamin A/C mutations, whereas the X-linked are associated with mutations in emerin [52, 145]. EDMD or EDMD-like phenotypes have variable penetrance and phenotypic heterogeneity, suggesting the mutations in presently unknown modifier genes may contribute to the variable phenotypic expression of the disease [106, 148]. Interestingly, *LMNA* and *EMD* mutations only account for 40% of EDMD [149, 150], indicating other structurally or functionally related genes may be involved. Evidence has shown both lamin A/C and emerin associate with nesprin and SUN to form the NE-LINC complex. Therefore, mutations in nesprin and SUN could be potential candidates that result in laminopathies.

1.5.1 Muscle diseases: DCM and EDMD

Reports have demonstrated the mutations in nesprin-1 and -2 have been implicated in DCM and EDMD, and SUN1 and SUN2 in EDMD, strengthening the

hypothesis that the NE-LINC complex and its associated NE components contribute to EDMD and DCM [3, 4, 87, 151, 152] (Table 1.3, Table 1.4 and Figure 1.6).

Missense nesprin-1 R8212H mutation was identified at the C-terminal of nesprin-1 in a 26-year old male patient who underwent a heart transplant. This patient had enlarged left ventricular with severe systolic dysfunction and without any skeletal muscle defects. HDFs derived from this individual showed strong staining of nesprin-1 and lamin A/C at the NE, which mimics the findings from EDMD-DCM caused by lamin A/C mutations, indicating that the R8212H nesprin-1 mutation perturbs the LINC complex, which is crucial to maintaining the cardiomyocytes (CMs) function in hearts [4, 60].

Furthermore, C-terminal mutations in nesprin-1 (R8095H, V8387L, E8461K) and in nesprin-2 (T6211M) and two other N-terminal mutations in nesprin-1 (G2297R and N108S) were reported from small kindred families with EDMD and EDMD-like phenotypes respectively [3, 151, 152]. The C-terminal regions where these mutations were localised were equivalent to the skeletal muscle and heart specific isoforms nesprin-1α_2 and nesprin-2β. Importantly this is also the binding region for lamin A/C and emerin [3]. The clinical phenotypes were variable, ranging from almost asymptomatic moderately increased creatinine kinase levels to muscular dystrophy combined with severe DCM. Notably, the most severe case was a 26-year old male individual harbouring a double heterozygote for nesprin-1 V8387L and nesprin-2 T6211M, who required a heart transplant. At subcellular level, the changes occurred in both HDFs and skeletal muscle, include nuclear morphology defects (convoluted nuclei, micronuclei, giant and fragmented nuclei), mis-localisation of endogenous nesprin, emerin, lamin A/C, disrupted nesprin/emerin/lamin bindings and reduced differentiation ability [3]. Knockdown of nesprin-1 in U2OS cells exhibited a separation of the INM from the ONM, suggesting uncoupling the LINC complex, which is similar to the phenotypes in muscle tissue from *LMNA* null mice or other fibroblast from Duchenne muscular dystrophy (DMD) or EDMD/Charcot-Marie-Tooth syndrome (CMT) [2, 3, 153, 154].

1.5.2 Other muscle diseases: CMD and AMC

In addition to DCM and EDMD, nesprins also involved in other muscular dystrophies (Table 1.3, Table 1.4 and Figure 1.6). A nesprin-1 mutation E7854X from

congenital muscular dystrophy (CMD), which results in a premature stop codon to delete the KASH domain, were examined using the isolated patient myoblasts [155]. The patient displayed clinic symptoms including adducted thumbs, mental retardation and cerebellar hypoplasia. Myotube formation showed the nuclei aggregation accompanied with reduced protein levels of both nesprin-1 giant and muscle specific isoform nesprin-1α_2 in the patient cells [37].

Two other nonsense nesprin-1 mutations are linked to arthrogryposis multiplex congenita (AMC), with the clinic symptoms such as muscular hypotonia associated with delayed motor development and persistent contractures of interphalangeal joints [156, 157]. The mutations H8105Vfs*8 and R8746X either delete or have a premature stop codon on KASH domain, causing deficiency of nesprin-1 KASH domain containing isoforms in HDFs from these patients [156]. Loss of KASH function also leads to multiple invaginations of the NE, detachment of INM and ONM, and abnormal condensation of chromatin structure in the muscle fibers; all of which are similar to the subcellular changes in EDMD patients [3, 157].

Taken together, the muscle diseases affecting the heart (DCM) and skeletal muscle (EDMD/CMD/AMC) can be caused by mutations in either of the NE-LINC complex proteins nesprin-1/-2, lamin A/C, emerin and SUN, and they have divergent phenotypes. How these ubiquitously expressed proteins lead to muscle specific disease is still not clear. However, the evidence shows they all link together to form the NE-LINC complex, which is particularly important in muscle as it is subject to mechanical strain.

Meanwhile, nesprin-1/-2 isoforms are expressed in a tissue specific manner. For example, in human myoblasts, the giant nesprin-1 was present and nesprin-1α_2 was merely undetectable. During myogenesis, nesprin-1α_2 was massively upregulated accompanied with 2-time increased nesprin-1 giant [37]. *In vitro* differentiation models showed that both nesprin-1 and nesprin-2 isoforms may re-localise from the NE in C2C12 myoblasts to the sarcomere of myotubes during skeletal muscle and CM differentiation [35, 158]. *In vivo*, during the transition from immature to mature muscle fibers, nesprin-2 giant partly replaces nesprin-1 giant at the NE, and short isoform nesprin-1α_2 becomes dominant [38]. These findings indicate that nesprin-1/-2 muscle specific isoforms may help to contribute to these mechanistic processes especially in the heart and skeletal muscle.

1.5.3 Neurological disease: Autosomal recessive cerebellar ataxia type 1

Nesprin-1 mutations have been identified in French-Canadian and Japanese populations who were diagnosed with autosomal recessive cerebellar ataxia type 1 (ARCA1) [159-162]. ARCA1 is characterised by progressive problems with cerebellar dysarthria, limb and gait ataxia and diffuse cerebellar atrophy, and may be accompanied with motor neuron impairment which mimics juvenile-onset amyotrophic lateral sclerosis (ALS) [161, 163] (Table 1.3).

These mutations scatter along the *SYNE-1* gene and the majority are homozygous non-sense mutations [159-162]. The premature stop codon or frame-shift caused by mutations result in many truncated nesprin-1 variants lacking SRs and KASH domain or absence of nesprin-1 due to nonsense-mediated decay of mutant mRNA [162, 164]. Recently, a nesprin-1 giant KASH less isoform was identified specifically expressed in the cerebellum. Its involvement in vesicular trafficking and structural organisation of dendritic membrane, emphasises that intact nesprin-1 transcripts is functionally important for cerebellum and neurons [165].

1.5.4 Other diseases: autism spectrum disorder and bipolar disorder

SYNE-1 mutation was implicated as a candidate for autism disorder (ASD) by the presence of a de novo single nucleotide variant (Y282C) in an ASD patient [166] (Table 1.3). This finding was substantiated by the homozygous missense nesprin-1 mutation L3206M found in one family. Neuronal ChIPseq and RNAseq data demonstrated one transcriptional start site localised just upstream of this mutation, suggesting nesprin-1 L3206M mutation may be implicated in ASD via their neuronal activity-dependent roles in regulating synaptic strength [167]. Other genome-wide association studies reported nesprin-1 was associated with both bipolar disorder (BD) and major depression [168] (Table 1.3).

In summary: the two major diseases related to nesprin-1/-2 mutations affect either muscle tendons or the CNS system (Table 1.5). The homozygous nonsense mutations identified in ARCA1 or heterozygous missense mutations identified in EDMD-DCM lead to reduced or absent nesprin-1/-2 expression or dysfunction of

nesprin-1/-2 proteins. The loss or gain of nesprin protein function, affects the NE-LINC complex, leading to either structural disruption or gene dysregulation. Subcellular changes occur such as altered nuclear morphologies, defects in microtubule regulated nuclear positioning in muscle tendon or vesicle trafficking in CNS, which are linked to the structural disruption hypothesis [3, 122, 165]. In addition to the cellular structural changes, abnormal heterochromatin is another main feature caused by nesprin mutations [3, 4], indicating the perturbed gene transcription and cell signalling which are linked to the gene dysregulation hypothesis. However, both are not mutually exclusive, which are potentially underlying molecular mechanisms of these diseases and all linked to one key point- importance of the integrity of LINC complex.

Table 1.3 Nesprin mutations and associated diseases

Gene	Encoded proteins	Disease	Phenotype	Ref
SYNE-1	Nesprin-1	DCM	Left ventricle dilation and systolic dysfunction, underwent heart transplant.	[4, 122]
SYNE-1 *SYNE-2*	Nesprin-1 Nesprin-2	EDMD-DCM	Genetically heterogeneous neuromuscular disorder associated with early contractures, slowly progressive skeletal muscle wasting and weakness, CD, DCM.	[3, 151, 152]
SYNE-1	Nesprin-1	CMD	Adducted thumbs, mental retardation, cerebellar hypoplasia and cataracts.	[155]
SYNE-1	Nesprin-1	AMC	Muscular hypotonia associated with delayed motor development and persistent contractures of interphalangeal joints.	[156, 157]
SYNE-1	Nesprin-1	ARCA1	Progressed cerebellar dysarthria, limb and gait ataxia and diffuse cerebellar atrophy, may accompanying motor neuron impairment which mimics juvenile-onset amyotrophic lateral sclerosis (ALS)	[159-162]
SYNE-1	Nesprin-1	ASD	Communication deficits, abnormal social interests, and restricted and repetitive behaviour.	[166, 167]
SYNE-1	Nesprin-1	BD	Mental disorder mixed with depression and elevated mood.	[168]

DCM: dilated cardiomyopathy; EDMD: Emery-Dreifuss muscular dystrophy; CD: conduction defect; CMD: congenital muscular dystrophy; AMC: arthrogryposis multiplex congenita; ARCA1: autosomal recessive cerebellar ataxia type 1; ASD: autism disorder; BD: bipolar disorder.

Table 1.4 Nesprin-1 mutations in muscle diseases

Disease	***SYNE-1* gene mutation**	**Amino acid substitution in nesprin-1 giant**	**Ref.**
DCM	25237G>A	R8212H	[4]
	25417G>A	R8272Q	[122]
	25743A>T	S8381C	
	25820C>A	N8406K	
	25468A>G	Y8289C	[169]
EDMD-DCM	25983G>A	E8461K	[3]
	25761G>A	V8387L	
	24886G>A	R8095H	
	6889A>G	G2297R	[151]
	323C>T	N108S	[152]
	29A>G	5'UTR ($1\alpha_2$)	[3]
	525G>A	5'UTR ($2\alpha_2$)	
CMD	23560 G>T	E7854X	[155]
AMC	24313-2A>G	H8105Vfs*8	[156]
	24577C>T	R8193*	[170]
	26236C>T	R8746X	[157]
fs: frame shift; ins: insert; X: stop codon.			

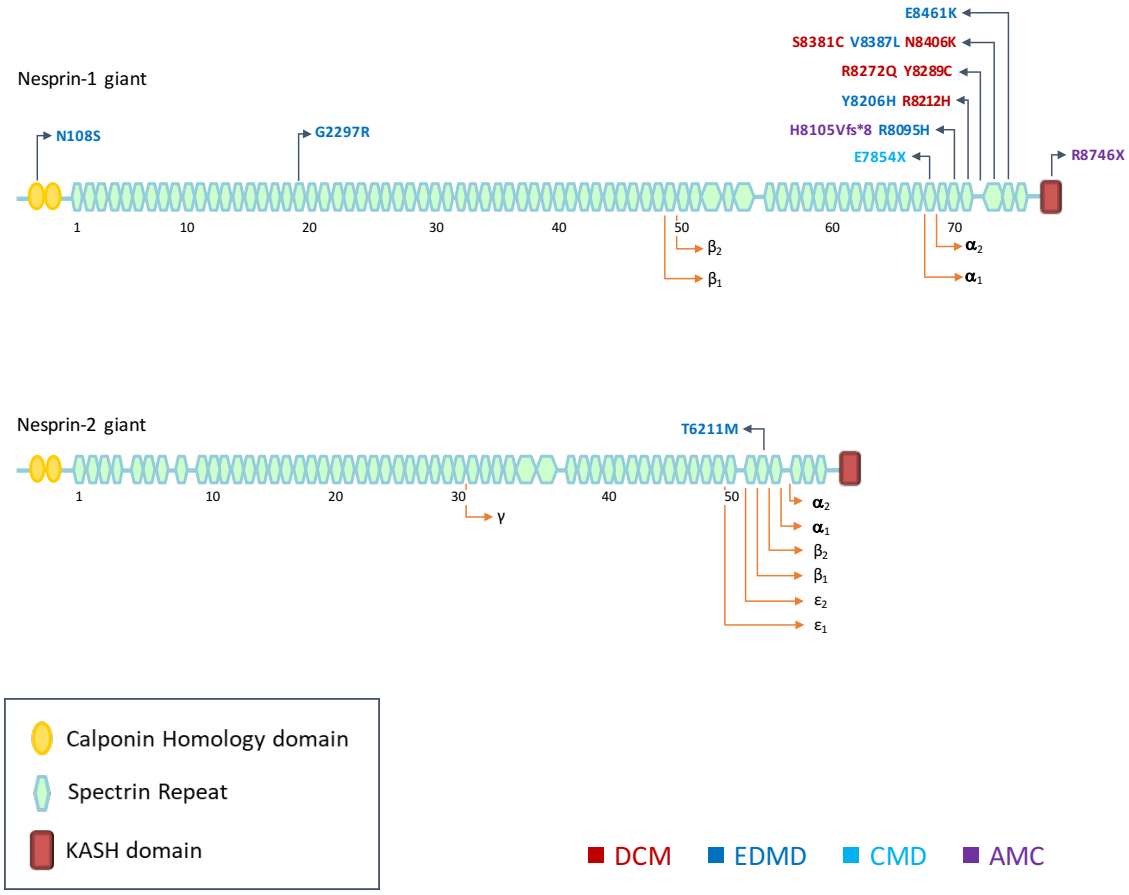


Figure 1.6 Nesprin-1/-2 mutations in muscle diseases

The nesprin-1/-2 KASH containing isoforms are labelled on the *SYNE-1* and *SYNE-2* genes. Reported nesprin-1/-2 associated human muscle diseases (DCM - red, EDMD - dark blue, CMD - light blue and AMC - violet) are labelled on this schematic.

Table 1.5 Nesprin-1/-2 mutations in muscle and CNS diseases

Category	**DCM/EDMD/CMD/AMC**	**ARCA1**
Affected tissue	Heart and skeletal muscle	CNS: cerebellum
Mutation localisation	Mainly at the C-terminal hot spot regions (corresponding to muscle specific isoform nesprin-1α_2 or nesprin-2β)	Scattered along nesprin-1
Mutation types	Heterozygous	Homozygous
	Missense mutation	Nonsense mutation
Effects on nesprin proteins expression and functions	Dysfunction of nesprin proteins, loss or gain of functions	Reduced or absent nesprin proteins, loss of functions

1.6 Functions of the NE-LINC complex and mechanistic basis of nesprin related diseases

The NE-LINC complex, a multi-protein structure, provides a physical connection from inside of nucleus to the cytoskeleton and plasma membrane and through to the outside of cells, the ECM, and adjacent cell connections. Their multiple functions have been fully characterised as three major parts: 1) directly coupling the nucleoskeleton with the cytoskeleton to maintain the structural integrity and propagate force transmission within a cell; 2) regulating nuclear migration, positioning and polarisation; 3) maintaining genome stability and modulating mechanical signalling and expression of mechanosensitive gene.

1.6.1 Linking the nucleoskeleton to the cytoskeleton

The fundamental function of the NE-LINC complex is as a physical linker that scaffolds the nucleus and cytoskeleton. The structural integrity is directly related to nuclear morphology and force transmission.

1.6.1.1 Maintaining nuclear size and morphology

Nuclear size varies greatly among different cell types and organisms, with a relatively regular spherical or ovoid morphology [171]. Nuclear size and shape are largely controlled by LINC complex and its associated components including nuclear lamins and chromatin [172, 173].

In vertebrates, deletion of nesprin-1 in endothelial cells or nesprin-2 in epithelial cells results in increased nuclear size and heavily misshaped nuclear morphology [136, 174]. Overexpression of nesprin-2 ABD or KASH domain also lead to nuclear expansion [136], indicating their important roles in nuclear size/integrity maintenance. Conversely, nuclear compaction was observed by overexpression of nesprin-2 mini (containing the ABD and KASH domain, but lacking the massive nesprin-2 giant SRs), and was exacerbated upon nesprin-3 co-expression. The potential explanation is the mini nesprin-2 isoform dislodges the endogenous giant nesprin isoforms from the NE and re-organizes a new but tighter (because of its drastically shorter SRs) nesprin-1/-2/-3 belt that normally encapsulate the NE [121]. Furthermore, the SUN1/2-KASH

forms a 45nm length bridge to support spacing in the PNS in mammalian cells. Down-regulation of SUN1, SUN2 or nesprin-1 causes the nuclear envelope lumen to expand, suggesting that the LINC complex controls parallel organisation of the ONM and the INM [2, 116].

Alongside nesprin, other components related to LINC complex can also alter the nuclear size and morphology. Depolymerization of F-actin shrinks the nuclei, while depolymerization of microtubules increases nuclear size. Disruption of both F-actin and microtubules leads to smaller nuclear size, indicating that nuclear connections with the actin cytoskeleton may be dominant in regulating nuclear size [121, 175]. In addition, cells with abnormal shaped nuclei are associated with diseases caused by defective lamina [146]. Similarly, fibroblast derived from muscle dystrophy patients carrying either nesprin-1 or nesprin-2 mutations exhibited a convoluted appearance accompanied by chromatin re-organisation [3].

All together, these findings illustrate that nuclear shape and morphology are the net outcome of complex intrinsic and extrinsic interactions that requires integral LINC complex and nuclear lamina.

1.6.1.2 Force transmission

The LINC complex is essential for transmission of ECM mechanical stimulus across the cytoskeleton to the nucleus [112, 176]. The direct mechanical connection between the cell membrane and nucleus was demonstrated via applying tensional forces on the cell surface adhesion receptor integrin, that resulted in reoriented cytoskeletal filaments, distorted nuclei and re-distributed nucleoli along the axis of the applied tension field in bovine capillary endothelial cells [177].

Recently, studies focusing on the LINC complex provide more evidence about the force transmission. Disruption of LINC complex by overexpression of KASH1, KASH2 or KASH3 in Swiss 3T3 fibroblasts (Immortal MEFs) resulted in significantly reduced elasticity and increased deformation of the cytoplasm that was measured by ballistic intracellular nanorheology. Importantly, these changes were comparable to MEFs derived from lamin A/C null mice, which displayed the EDMD-DCM phenotype. These data strongly suggested the involvement of LINC complexes in maintaining cellular force transmission and mechanical stiffness [178]. Furthermore, knocking down nesprin-1 in endothelial cells exhibited increased nuclear allowance

for deformation under uniaxial pulling stretching on one side of the culture dish, indicating increased nuclear strain (deformation) was caused by disconnection of sustainable force transmission from F-actin through nesprin to the nucleus [179]. Another new approach using biophysical assays was used to detect force transmission via precisely applied strain to the cytoskeleton within a cell. Overexpression of nesprin-1 KASH or nesprin-2α disrupted the LINC complex, impaired propagation of intracellular forces, leading to fewer nuclear and cytoskeletal displacement, reduced nuclear deformation and discontinuous and fragmented F-actin and IFs at perinuclear regions [112].

Due to the different cell types, employment of different methods to disrupt the LINC complex and different force application methods, studies have shown that disturbed LINC complex can either increase [179] or reduce nuclear deformation [112]. However, they all suggested the disruption of LINC complex would result in impaired propagation of intracellular forces, caused abnormal nuclear deformation and disturbed organisation of the perinuclear cytoskeleton networks. In future, 3-D culture and 3-D strains are needed to more accurately mimic the *in vivo* environment, and reveal force transmission through the LINC complex especially in tissues subjected to mechanical strain.

1.6.2 Nuclear migration, positioning and polarisation

1.6.2.1 Nuclear migration and positioning

Nuclear positioning within a cell is dependent on cell type, stage of the cell cycle, migratory state and differentiation status. The LINC complex has been revealed as a primary exert force on the nucleus via connections to the NE to maintain the position of the nucleus and its movements during cell migration and differentiation [180, 181].

The initial models to study nuclear migration and positioning were in lower organisms such as *C. elegans* and Drosophila melanogaster. Most of adult *C. elegans* are covered with four large hypodermal syncytia containing more than 100 nuclei in total. ANC-1, the orthologous nesprin-1/-2, interacts with SUN protein ortholog, UNC-84, to tether the nucleus to the cytoskeleton and evenly space and anchor them in body wall muscle [182, 183]. In ANC-1 or UNC-84 mutated *C. elegans*, nuclei float freely in the cytoplasm, often grouped in large clusters [69, 184].

Similarly, in mammals, deletion or overexpression of the nesprin-1 KASH domain in mice abolishes synaptic nuclei aggregation and disrupts even spacing of non-synaptic nuclei in skeletal muscle [137, 138]. Furthermore, these mis-positioned nuclei are a common feature in muscle fibers derived from EDMD patients carrying nesprin-1/-2 mutations, as well as myotubes formed by myoblasts derived from EDMD patients carrying SUN1/2 mutations [3, 87]. These findings suggest that cytoskeleton dependent nuclear positioning is a contributing factor to muscle disease.

Indeed, recent data have uncovered more underlying molecular mechanisms responsible for myonuclear positioning. Studies from *C. elegans* revealed that UNC-83 and UNC-84 form the LINC complex and recruit the microtubule motor protein kinesin-1 and dynein to the NE that are needed to drive bidirectional movements during nuclear migration [185, 186]. Further studies in mammalian cells confirmed the C-terminal region of nesprin-2 mediates myonuclear positioning by attaching the microtubule network to the NE during embryonic muscle development [187, 188]. These interactions occur via the microtubule motor proteins, dynein and kinesin-1, the latter being a heterotetramer of two kinesins heavy chain (KHC) subunits -Kif5A, Kif5B, or Kif5C- and two KLC-1/2 subunits. Nesprin-2 was shown to interact with KLC-1/2 at the ONM via a newly identified four-residue tryptophan-acidic (W-acidic) "LEWD" binding motif within an adaptive domain (AD) at its C-terminus, which is present in all muscle-specific isoforms [22, 23, 114]. Disruption of the LINC complex with a DN nesprin-2 KASH impaired kinesin-1 association with the NE and induced nuclear aggregation in myotubes [114]. As both nesprin-1 and -2 are highly conserved in this C-terminal region, it is likely that nesprin-1 may also mediate the nesprin/KLC interaction via the "LEWD" binding motif but so far this has not been tested.

In addition to muscle cells, precise nuclear movement is also crucial for other organ development. For example, depletion SUN1/2 or nesprin-2 not only affects neurogenesis and neuronal migration during brain development, but also abolishes photoreceptor cells migration, which is the critical step for retina development [83, 123].

1.6.2.2 Nuclear polarisation

Besides the nuclear bipolar dynamic movement is driven by microtubule motor proteins dynein/dynactin and kinesin-1, nuclei possess self-rotation ability which can

facilitate their motility through the complex and crowded cellular environment of developing cells, allowing for proper migration and positioning [189]. In fibroblasts, nuclear polarity can be observed under stretch induced cytoskeletal re-arrangement. However, overexpression of DN SUN1 or nesprin-2 abolished this re-orientation, due to loss of actin associated LINC complex [190]. Depletion of nesprin-2 in C2C12 myoblasts, interferes with the orientation of centrosomes, which failed to adopt specific positions relative to the nucleus and perturbed efficient myotube formation [191]. Similar results can be seen during depolymerization of the actin cytoskeleton, the rearward movement of the nucleus is perturbed during wound-induced fibroblast and astrocyte polarisation [192, 193]. Taken together, these studies indicate the LINC complex is a powerful toolbox to modulate the proper nuclear migration, positioning and cell polarisation.

1.6.3 Mechanical signalling and mechanosensitive gene expression

LINC complex mediated force transmission initiates mechanotransduction events, directly contributing to the cell's ability to adapt to its mechanical environment by triggering force-induced changes in nuclear structures, downstream signalling and gene expression.

1.6.3.1 Mechanotransductive signalling

The process of mechanotransduction is initiated by a mechanical force passing through sub-cellular structures whose conformations change in response to mechanical stress, resulting in activation of biochemical signalling pathways and gene expression [117]. The LINC complex and its associated proteins engage in a wide network of intermolecular interactions that affect numerous mechanical signal pathways, including mitogen-activated protein kinase (MAPK), Wnt-β-catenin, nuclear factor kappa-light-chain-enhancer of activated B cells (NF-κB), transforming growth factor beta (TGF-β) and Notch signalling pathway [194-199].

Muscle restricted laminopathies associated with mutations in the LINC complex (lamin A/C, emerin, nesprin, SUN) are EDMD and DCM [3, 53, 87, 153]. The initial mouse model that recapitulates LINC complex associated EDMD and DCM has been

generated with lamin A/C or emerin mutants. Analysis of genome-wide expression profiles in hearts from the *LMNA*^{H222P} and *EMD*-/- mouse models, showed statistically significant differences in expression of genes in the MAPK pathways [194, 195]. MAPK signalling has essential roles in cell proliferation, differentiation, survival, and death [200, 201]. ERK1/2 and c-Jun NH2-terminal kinase (JNK) are the well-characterised branches of the MAPKs. In response to stimuli, JNK and ERK1/2 become phosphorylated and activate their translocation from the cytoplasm to the nucleus, to regulate transcription and cell cycle progression [201-203].

In *LMNA*^{H222P} mouse hearts, pERK1/2 and pJNK are induced in CMs, which then activate a series of downstream target genes, including bcl-2, Elk1, junD and c-Jun. Transcription factors encoded by these genes can in turn regulate the expression of additional genes, including those encoding proteins involved in sarcomere structure, cardiomyofiber organisation and other aspects of heart function [194, 204, 205]. Augmented ERK activation is further observed in other cell lines such as COS7 and HeLa which were transfected with *LMNA*^{H222P}, as well as in ex-vivo fibroblasts from EDMD/DCM patients carrying lamin A/C mutations [194, 206]. Using ERK inhibitors, the EDMD and DCM phenotype is rescued in *LMNA*^{H222P} mice, which further supports the important role of ERK1/2 in the pathogenesis of LINC complex related muscle disease [207-209]. Apart from those data, there is evidence showing that nesprin-2 directly interacts with ERK1/2 via their SRs and recruits them to promyelocytic leukaemia protein nuclear bodies (PML NBs) to regulate the cell cycle and DNA damage response in VSMCs [42, 210].

1.6.3.2 Mechanosensitive gene expression

The cells response to mechanical strain can be measured by the expression of mechanosensitive genes egr-1 and iex-1 [211, 212]. The MEFs from *LMNA* or *EMD* null mice both showed irregularly shaped nuclei and heterochromatin, with attenuated mechanical induction of egr-1 and iex-1 in 2 hours and 4 hours of strain [153, 213, 214]. Moreover, the altered mechanosensitive genes were evaluated in nesprin-1/-2 knockout (KO) mice. CMs isolated from those mice presented with blunted mechanosensitive response with impaired activation of egr-1, iex-1, c-fos, c-jun [85]. Those data underscore the critical role of integral LINC complex in mechanotransduction and gene regulation.

1.6.3.3 Nuclear stiffness

Tissue elasticity is quite varied. For example, fat is soft and bone is very stiff. This difference will provide opposite stress environments for cells. Mouse proteomic analyses reveals the expression levels of lamin A/C scaled with tissue elasticity. Human mesenchymal stem cells on soft matrix differentiate into fat cells enhanced by low lamin A/C, while on the stiff matrix differentiate into bone enhanced by high lamin A/C. Lamin B did not show any significant change during this process. Altered nuclear stiffness regulated by shifted lamin A/C levels helps to stabilise the nucleus and protect chromatin from excessive strain, in order to preserve chromatin organisation and nuclear function [100].

How the nucleus responds to mechanical stress was further investigated by using isolated single nuclei with removal of all cytoskeletons. Using magnetic tweezers to apply force on nesprin-1, nuclear stiffening was induced through recruitment of lamin A/C, indicating the reinforcement of the physical connection between lamin A/C and the LINC complex will help nucleus to sustain induced tension [215]. This theory is further confirmed in fibroblasts from HGPS patients carrying lamin A/C mutations. The nucleus is stiffened through the accumulation of a mutant lamin A/C. Cells became trapped in the close spacing in 3-D environment with increased nuclear stiffness, reduced force generation and decreased nuclear deformability, which both lead to reduced cellular motility [216]. This pattern is also evident in culturing myoblasts from muscular dystrophy patients carrying either nesprin-1 or lamin A/C mutations on the hydrogel that has a similar stiffness to the physiological muscle. These mutated cells both showed reduced nucleus thickness and plasticity, in term of increased actin cytoskeleton assembly and traction force, indicating the impaired muscle cell function [217]. The cell signalling molecules involved in regulation of nuclear and ECM elasticity and stiffness include Yes-associated protein (YAP)- Hippo pathway, megakaryoblastic leukaemia 1 (MKL1)-serum response factor (SRF) pathway and vitamin A/retinoic acid (RA) pathway [100, 215, 218-220]. Increasing amounts of studies implicate that applied force or environment stress can directly induce nuclear stiffness changes via regulating mechanical signalling. In particular, lamin A/C and the LINC complex play central roles in adaptation of cells to their mechanical environment.

Taken together: the evidence shows that in an intact cell, the LINC complex mediates nuclei responses to mechanical transduction. Any disruption in structural integrity of cytoskeleton components in the cytoplasm, SUN-KASH interaction at the NE, lamin A/C and emerin at the INM may result in dramatic or subtle changes in mechanical force propagation from the ECM to the nucleus. Those changes can affect nuclear size and morphology, cause defects in nuclear migration, positioning and/or polarisation, as well as led to dysregulation of mechanical signalling and gene expression among different cell types.

1.7 Nesprin-1/-2 mouse models

To further understand to the roles of nesprins in the LINC complex and nesprin related diseases, total 13 nesprin mouse lines have been generated to model the muscular and neurological disorders caused by *SYNE-1/-2* mutations (Figure 1.7 & Table 1.6).

1.7.1 KASH mouse model

1.7.1.1 KASH1 mice

There is one transgenic (Tg) KASH1 and two KO KASH1 established mouse lines that exhibit altered skeletal muscle, heart and CNS phenotypes [4, 137, 138, 221].

The Tg KASH1 mice and the first nesprin mouse line was focused on the functions of nesprin in muscles. It was generated by expressing nesprin-1 C-terminal 344 amino acid including the last SR and KASH domain under the muscle creatine kinase (MCK) promoter [137, 222] (Figure 1.7 & Table 1.6). The transgene behaves like a DN KASH1 domain to displace endogenous nesprin-1 (and/or nesprin-2, as they share a highly homologous sequence of KASH domain) from the NE in the skeletal muscle and heart. There are no overt symptoms reported from this model [137]. However, in the skeletal muscle fibers, synaptic nuclei fail to aggregate at the neuromuscular junction (NMJ) in these transgenic mice. Introducing DN KASH1 in the mature muscle at postnatal day 20 (P20) reduced the synaptic nuclei and increased presynaptic nuclei [137]. Notably, the function of NMJ and mitochondria localisation are not affected.

Furthermore, the KASH1 KO mouse model displays a similar phenotype. These mice were generated by deletion of the last exon of *SYNE-1*, resulting in removal of KASH1 domain [138] (Figure 1.7 & Table 1.6). The NMJ phenotype is more severe than that in DN KASH1 mice, with an almost complete loss of synaptic nuclei [138]. The difference may be caused by the low level of endogenous nesprin-1 still present in the DN KASH1 mice, which is sufficient to migrate myonuclei at the NMJ, but is not sufficient to anchor them when the muscle underwent contractions. In KASH1 KO mice, both migration and anchorage processes are abolished due to complete loss of nesprin-1. In addition, the non-synaptic nuclei formed clusters and arrays in KASH1 KO homozygotes, while the heterozygotes still maintained evenly distributed myonuclei along the muscle fibers [138].

The functions of nesprin-1 in heart are characterised in another global KASH1 KO mouse model [4, 221]. This model was generated via deletion of the last exon of *SYNE-1* through inserted LoxP sites, leading to remove of the last two exons including KASH domain (Figure 1.7 & Table 1.6). Approximately 50% homozygous KASH1 KO pups die at or near birth due to un-inflated lungs causing respiratory failure. Survived litters exhibit EDMD and cardiomyopathy-like phenotypes including hind limb weakness, abnormal gaits, kyphoscoliosis, muscle pathology and conduction defect (CD) and heart failure with the increased age. The CD in atria is noted earlier than in ventricle; when the mice show both atria and ventricle CD, heart failure is evidenced by a reduction of fractional shortening. Those changes in heart mimic patients with DCM and conduction system disease. Isolated CMs display elongated nuclear shape with large invaginations of the NE, and reduced total amount of heterochromatin. The LINC complex components lamin A/C, emerin, SUN2 still localise at the NE, while immunoprecipitation (IP) reveals interaction between nesprin-1 and SUN2 is abolished, suggesting the disrupted SUN-KASH LINC complex in this model could be the trigger of pathological process in heart. Of note, unexpected insertion of an extra 61 amino acids occurs during KASH1 deletion, although this sequence is not homologous to any known proteins. Therefore, it is not clear that the EDMD and DCM like phenotypes in those mice are resulted from the additional 61 amino acids or the disruption the LINC complex via deletion of KASH domain. In addition, muscle biopsies from these KASH1 KO mice displayed similar changes: central nuclei with decreased fiber size in soleus muscle compared with the arranged nuclei under the sarcolemma in the WT [221]. These findings are consistent

with the observations in muscle from EDMD and DCM patients; further strengthening the evidence that nesprin-1 is indispensable in proper anchoring of synaptic and non-synaptic nuclei and maintaining proper skeletal muscle functions.

In addition to muscle system, deletion of KASH1 affect the CNS [138]. The phrenic nerves display longer branches at innervation sites, suggesting the mis-localised muscular synaptic nuclei may contribute to maintenance of the innervation sites by strengthening the communication between muscle-nerve contacts.

1.7.1.2 KASH2 mice

Similar to the DN KASH1 mice, the DN KASH2 mice is established by overexpression C-terminal 183 amino acids KASH containing domain of *SYNE-2* under the MCK promoter [138] (Figure 1.7). The phenotype of DN KASH2 mice is similar to the DN KASH1 mice, including expelling the synaptic nuclei from under the NMJ to the peripheral region, without perturbing the non-synaptic nuclei in the muscle fibers [137, 138]. The nesprin-1 and -2 has high homology KASH domains, therefore expression either KASH1 or KASH2 domain may have a similar dominant negative effect to the nesprin-1 and -2 proteins.

In contrast to DN KASH2 mice, the KASH2 KO mice display major defects in the development of CNS rather than skeletal muscle or heart [83, 123, 138]. Targeted deletion of the last two exons of *SYNE-2* gene, generated nesprin-2 KASH KO mice [138] (Figure 1.7). No defects in the synaptic and non-synaptic nuclei in the myofibers were observed from this model. Comparing the phenotypes among the four KASH1 or 2 mouse models, it suggests that nesprin-1 may play a more dominant role in nuclei migration and anchorage in the muscle than nesprin-2 [137, 138].

The following studies using the same KASH2 KO mice focus on brain development. KASH2 KO mice exhibit a smaller cerebellum, disrupted laminary structure and pyramidal cell layer, and impaired working memory and abnormally active responses to a new environment, which are similar to the cerebellum changes in ARCA1 patients [123]. Combining these data with another CNS defects mouse model via depletion of SUN1/2, the underlying mechanisms are revealed: nesprin-2 interacts with SUN1/2 at the NE to form the LINC complex, which connects to the centrosome via microtubule motor proteins dynein/dynactin and kinesin-1, to mediate the neuronal migration. Uncoupling the LINC complex through either KO SUN or KASH2, will

abolish the centrosome-nucleus mediated nuclear migration during neurogenesis, causing CNS development defects [123].

1.7.2 Nesprin-1/-2 actin binding domain (ABD) KO mice

Nesprin-2 ABD is knocked out by deletion of the 2nd - 4th exon of the *SYNE-2* gene encoded first CH domain [136] (Figure 1.7 & Table 1.6). These mice are well developed and have no skeletal muscle or heart defects. However, the epidermis from these mice was thicker, which is caused by the increased epithelial nuclear size. Isolated primary dermal fibroblasts and keratinocytes from KO mice show heavily misshaped nuclei with unevenly distributed emerin, which is similar to nuclear deformations characteristic of laminopathies.

Different from the nesprin-2 CH KO mice, nesprin-1 CH KO mice were generated by floxed the 9th exon, which encodes for the second CH domain of nesprin-1 (Figure 1.7 & Table 1.6). These mice showed normal expression levels and localisations of NE-LINC complex protein, without any phenotypes [124]. The different phenotypes could arise due to the distinct functions of two CH domains. The second CH domain is not able to bind with the actin cytoskeleton, but it acts as a CH1 enhancer to strengthen binding with F-actin [32, 33]. Therefore, functional ABD is still partially retained in nesprin-1 CH KO as it is only knocked out the second CH domain, while the function of ABD is completely abolished in nesprin-2 CH KO mice via knocking down the first CH domain.

1.7.3 Nesprin-1 or -2 C-terminal KO mice

This was the first global nesprin-1 KO mice model. It was established by floxed deletion of the 16th exon of *SYNE*-1 and resulted in a premature stop codon at the 13th exon (counted backward from the last exon) [135] (Figure 1.7 & Table 1.6). This transgenic mouse theoretically will be ablated of all nesprin-1 isoforms containing the C-terminal SR region with or without KASH domain, which include nesprin-1α_1, nesprin-1α_2 and nesprin-1β. These nesprin-1 KO mice litters exhibited over 60% lethality due to the insufficient feeding caused by muscle weakness. Survived pups were marked by growth retardation and increased variability in body weight at the first three months [135]. In skeletal muscle: nesprin-1 KO mice showed normal fiber size,

but with an excessive number of centrally located nuclei, which is also reported in the nesprin-1 KASH KO mice [135, 138]. Nuclear positioning and anchorage is defective in the KO mice, and nuclei deformation failed in response to mechanical stress, indicating the nesprin-1 forms the critical link to anchor the nuclei to muscle fibers.

Heart function is specifically characterised by breeding nesprin-1 KO with mice carrying cardiac promoter Nkx2.5Cre (Figure 1.7 & Table 1.6). Littermates survived over 1 year with normal heart functions [85]. Protein levels of NE-LINC complex components lamin A/C, emerin and lamin B1/B2 were unchanged, except the upregulation of SUN1, signifying the perturbed LINC complex in CMs [135]. Furthermore, the isolated CMs showed irregular nuclear shape including decreased nuclear circularity, increased nuclear area/length/perimeter, as well as reduced nuclear distance. These changes lead to the failed response of neonatal CMs to the mechanical stress and dysregulated biomechanical gene like egr-1 and iex-1 [85]. Additionally, the irregular nuclear morphology and the reduction of biomechanical genes were also observed in nesprin-2 global KO mice [85]. Nesprin-2 KO mice were generated by floxed deletion of the 7th exon of *SYNE-2* (counted backward from the last exon), which theoretically deletes all the known nesprin-2 isoforms including the muscle specific isoforms nesprin-2α_1, nesprin-2β and nesprin-2ε_2 [85] (Figure 1.7 & Table 1.6). The two nesprin-1/-2 C-terminal KO mouse models gave insights into the roles of nesprins, particularly in maintaining intact mechanotransduction and gene regulation in hearts.

1.7.4 Specific nesprin isoform-nesprin-1α_2 KO mice

Global nesprin-1α_2 KO mice were generated by floxed the first unique exon of nesprin-1α_2, then crossed with Sox2Cre delete mice twice to obtain the homozygous KO mice (Figure 1.7 & Table 1.6). The lethality is much higher than any other nesprin mouse models. Only 2 out of 17 littermates survived at weaning (P21). Extraction E18.5 embryos were showed, the nesprin-1α_2 KO embryos remained cyanotic and died within 5 minutes while the WT turned pink and started to breathe. Those findings strongly indicate the nesprin-1α_2 is indispensable for embryonic development.

The two surviving KO mice were small with reduced body weight, and developed kyphosis after P21, indicating EDMD-like skeletal muscle dysfunction. The skeletal muscle was analysed using the samples isolated from embryonic day 18.5

(E18.5). In those nesprin-1α_2 null mice, nuclei clustering is the most striking defect seen from the tibialis anterior (TA) muscle, which is akin to other nesprin-1 mouse models [4, 135, 138, 221]. The LINC complex shows subtle changes with decreased SUN1 expression level and diffused localisation away from the NE to the cytoplasm. However, surprisingly, the microtubule motor protein kinesin-1 including the subunits KLC-1/-2 and kif5b were displaced from the NE [124], revealing that the nesprin-1α_2 is critical to recruiting kinesin-1 to the NE and form the nucleus-microtubule network to ensure the proper nuclear migration and positioning in muscle fibers.

In this mouse model, cardiac dysfunction is not observed in the nesprin-1α_2 KO embryos. Due to the limited number of surviving individuals, the role of nesprin-1α_2 in heart development is required for further study.

1.7.5 Nesprin-1 and nesprin-2 double knockout mice

1.7.5.1 KASH1 and KASH2 double knockout

KASH1 and KASH2 double knockout (DKO) mice were generated by breeding the KASH1 KO mice (deletion of the last exon of *SYNE-1*) with the KASH2 KO mice (deletion of the last two exons of *SYNE-2*) [123, 138] (Figure 1.7). Homozygous DKO littermates were born alive but died within 20 minutes due to respiratory failure caused by unexpanded lungs. The muscle fibers from DKO mice exhibit the completely eliminated synaptic nuclei in NMJ [138]. Further analysis showed a much smaller brain at E18.5 with impaired laminar structure. Neuron from DKO lost their migration ability due to the detachment with the centrosome [123]. Although the reason of lethality is still not clear, the essential function of LINC complex in neuron migration have been confirmed and is indispensable for neurogenesis.

1.7.5.2 Nesprin-1 and nesprin-2 C-terminal double knockout

This nesprin DKO mouse line was generated with cardiac specific nesprin-1 deletion and global nesprin-2 deletion mice described in 1.7.3 [85] (Figure 1.7 & Table 1.6). The DKO mice did not have any significant lethality over 1 year, but display early onset cardiomyopathy, which is similar to patients with DCM [85]. The left ventricle wall was thinner and fractional shortening was decreased from 10 weeks and

deteriorated over time. The fetal gene ANP, βMHC and fibrotic genes procollagen 1α1, 3α1 were all increased, indicating heart failure and fibrosis. Histology also revealed massive fibrosis that started from 10 weeks and TUNEL staining revealed increased apoptosis in CMs from 5 weeks [85].

The CMs from nesprin-1/-2 DKO have dramatic nuclear deformation compared with either KO nesprin-1 or -2, including an increased nuclear area/length/perimeter; deceased nuclear circularity and distance; with dense heterochromatin defects. Biochemical stimulation of CMs led to attenuated response of biomechanical genes such as egr-1, iex-1, c-jun, c-fos and c-myc. Of note, NE-LINC complex associated proteins, lamin A/C, emerin were mis-localised from the NE with unchanged expression level, indicating the ablation of nesprins compromise the NE complex. All these sub-cellular changes are aggravated in hearts from DKO mice comparing with knockout either nesprin-1 or -2.

Together, this model demonstrated that nesprin-1 and -2 are essential for CM function. They localise at the NE, forming the NE-LINC complex to maintain CM morphology, positioning, mechanotransduction and gene expression under the biomechanical load. This provides us with insight into pathology of the cardiomyopathy caused by disrupted NE-LINC complex that resulted from nesprin mutations.

1.7.6 Related LINC complex mouse models

Lamin A/C and emerin are the first two mutations associated with the LINC complex to cause laminopathies including the EDMD and DCM [143, 149]. Various mouse models with knock in or KO *LMNA* mutants have been established and investigated for over twenty years. Those mouse mutants develop the human like EDMD and DCM phenotype, which is similar to the muscle disease caused by nesprin-1/-2 mutations [223]. Therefore, the findings from those *LMNA* mutation models may provide the insights into the common mechanisms underlying EDMD and DCM.

To date, *LMNA* mutant mice have been shown to have early postnatal lethality, EDMD, CD, and DCM [223]. The CMs derived from $LMNA^{H222P}$ mice (identified in EDMD patients) and $LMNA^{N195K}$ (identified in DCM patients) showed structural disruption: these mutations resulted in extremely disorganized and fragile nuclei, with elongated nuclear shape, deep indentation of nuclear membrane and condensed

heterochromatin [224, 225]. The myofibers exhibited a wider variation of size, more atrophic and regeneration fibers with internal nuclei [208].

Also, abnormal mechanotransduction was evident and gene regulation was perturbed: analysis of genome-wide expression profiles in $LMNA^{H222P}$ hearts showed activation of the MAPK including ERK and JNK, as well as in the skeletal muscle [194]. It was found ERK or JNK inhibitors could reduce fibrosis, promote the heart function, increase the skeletal strength and successfully rescue the DCM and EDMD phenotype in $LMNA^{H222P}$ mice. Therefore, specific targeted MAPK caused by the abnormal mechanotransduction could be a potential therapy for LINC complex associated laminopathies [207-209, 226-228]. In addition to these findings, the MEFs from *LMNA* or *EMD* null mice both showed attenuated mechanotransductive gene like egr-1 and iex-1 response [213]. The *LMNA* null heterozygous had a blunted cardiac hypertrophy response to the hemodynamic pressure overload due to the impaired mechanosensitive gene egr-1 [229].

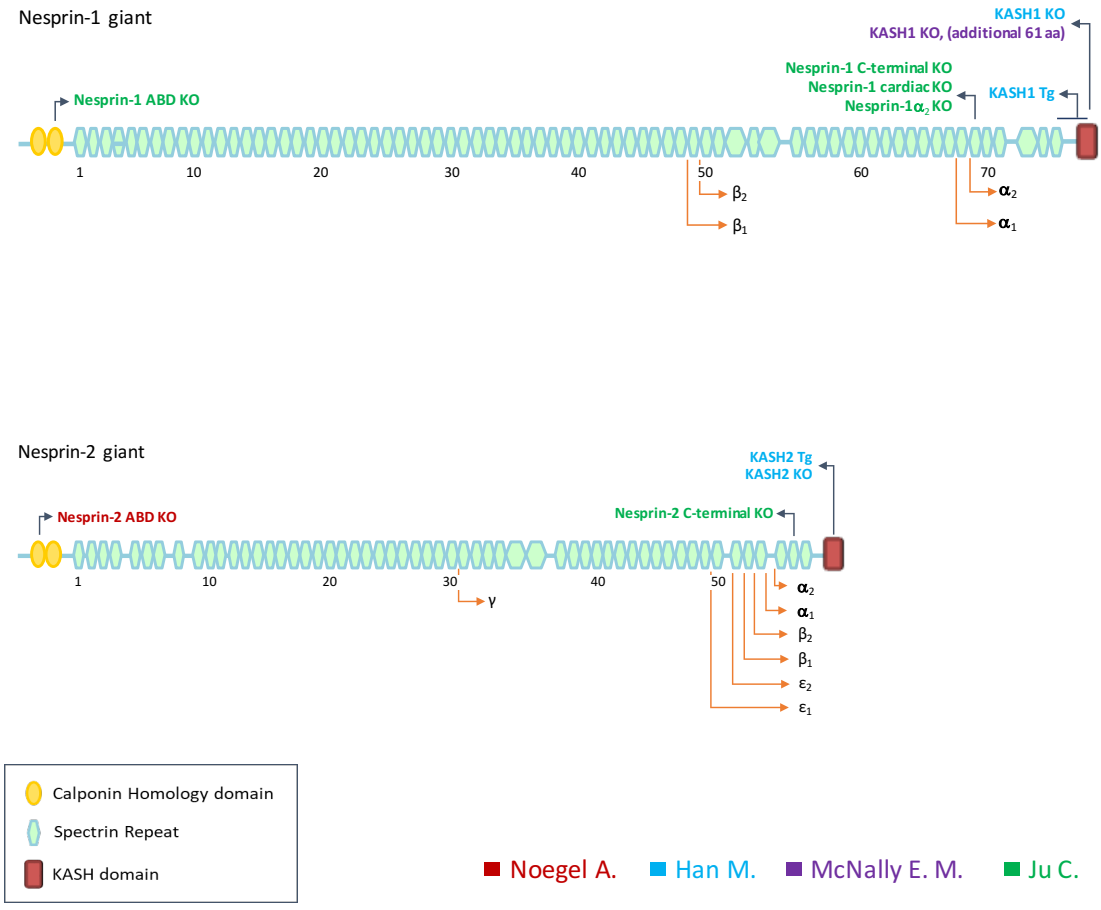


Figure 1.7 Overview of existing nesprin-1/-2 mouse models

Various nesprin-1/-2 mouse models were generated via targeting to different regions of *SYNE-1* and *SYNE-2* genes. The colours indicate the research group who generated the models (Red – Noegel A. [136]; Blue - Han M. [3, 137]; Violet - McNally, E. M. [4, 221]; Green - Ju C. [85, 124, 135]. Double KASH KO mice were generated via breeding the KASH1 KO with KASH1 KO (Han group). Double nesprin-1/-2 KO were generated via breading nesprin-1 cardiac KO with nesprin-2 global KO (Ju group). KO: knockout, Tg: transgenic; aa: amino acid.

Mice	Target protein	Method	Phenotype	Ref.
SYNE-1 KO	Nesprin-1	Crossed the *SYNE-1* KO mice [135] with *Nkx2.5*Cre to conditionally knockout *SYNE-1* in heart.	No overt defects in cardiac structure and function.	[85]
SYNE-1 CH KO	Nesprin-1	Floxed exon 9F, encoding for the latter CH domain in *SYNE-1*, and crossed with *Sox2*Cre deleter mice to ablate expression of nesprin-1 CH domain containing isoforms globally.	Survived up to 18 months; no overt skeletal muscle or cardiac phenotypes.	[124]
Nesprin-1α_2 KO **(s, m)**	Nesprin-1α_2	Floxed the first exon that was unique to nesprin-1α_2, then crossed with *Sox2*Cre deleter mice to ablate expression of nesprin-1α_2 globally.	12% litters survived, nuclei were mis-positioned in anterior muscle due to loss the interaction between nesprin-1α_2 and microtubule motor protein kinesin-1; no cardiac dysfunction.	[124]
SYNE-2 DN KASH **(s, m)**	Nesprin-2	Overexpressed 183 amino acids KASH containing domain of *SYNE-2* under the MCK promoter	In muscle fibers, synaptic nuclei failed to aggregate at the NMJ, but with even spaced non-synaptic nuclei along the muscle fibers; no cardiac related phenotype reported.	[138]
SYNE-2 KASH KO **(m)**	Nesprin-2	Targeted deletion of the last two exons of *SYNE-2* including KASH domain	Defects in photoreceptor cell migration in retina, thinner out nuclear layer, electrophysiological dysfunction; defects in learning and memory; no skeletal muscle or cardiac phenotypes reported.	[83, 123, 138]

Mice	Target protein	Method	Phenotype	Ref.
SYNE-2 KO	Nesprin-2	Floxed deletion of the 7th exon of *SYNE-2* (counted backward from the last exon), targeted to delete all nesprin-2 isoforms containing the C-terminal SR region with or without KASH domain.	Survived up to 18 months; no overt skeletal muscle or cardiac phenotypes.	[85]
SYNE-2 CH KO	Nesprin-2	Targeted deletion of the 2nd-4th exons of *SYNE-2* gene encoding the first CH domain.	In skin: thicker epidermis, epithelial nuclear size increased and heavily misshaped; No reported skeletal muscle or cardiac phenotypes.	[136]
SYNE-1 *SYNE-2* KASH KO **(s, m)**	Nesprin-1 Nesprin-2	Crossed the KASH1 KO mice (deletion of the last exon of *SYNE-1*) with KASH2 KO mice (deletion of the last two exons of *SYNE-2*).	Newborn litters failed to breathe and died shortly after born. The synaptic-nuclei number reduced in the NMJ, but not the essential account for the lethality.	[123, 138]
SYNE-1 *SYNE-2* KO **(c, m)**	Nesprin-1 Nesprin-2	Crossed the cardiac specific nesprin-1 KO mice [135] with the global nesprin-2 deletion mice [85].	Heart: reduced LV wall thickness and systolic function, mis-positioned nuclei in myocardium, dense heterochromatin in CMs; no skeletal muscle related phenotype reported.	[85]
C: cardiac phenotype; S: skeletal muscle phenotype; M: mis-positioned nuclei DN: dominant negative; KO: knockout				

1.8 Summary and thesis aims

Nesprins are the multi-isomeric scaffolding proteins [1]. They localise at the ONM, interact with SUN domain proteins via C-terminal KASH domain at PNS, bind with the actin cytoskeleton via N-terminal CH domains [2]; meanwhile, nesprins interact with lamin A/C, emerin and SUN1/2 at the INM, thus forming the NE-LINC complex [35]. The major functions of NE-LINC complex includes: physical linker and force transmitter of the nucleoskeleton and cytoskeleton; roles in nuclear migration, positioning and polarisation; and regulation of mechanical signalling and mechanosensitive genes [21, 176, 230].

Mutations in NE-LINC complex proteins nesprin-1/-2, lamin A/C, emerin and SUN1/2 have been identified in EDMD and DCM patients [3, 4, 52, 86, 87, 122, 145]. Both *in vitro* and *in vivo* studies focused on these mutations have revealed two NE-LINC complex mechanisms underlying these muscle diseases. Firstly, the structural integrity hypothesis is that mutations in the NE-LINC complex will increase nuclear deformation and affect the localisation and interaction of the NE-LINC complex components. This will then uncouple the nucleoskeleton from the cytoskeleton, perturb the mechanical force propagated from the ECM to the nucleus and increase its susceptibility to stress. The second hypothesis relates to cell signalling/gene dysregulation and that disruption of NE-LINC complex would not only impair mechanical cell signalling and mechanosensitive gene expression, but also have a direct effect on the chromatin structure and impact on gene transcription. These two hypotheses are not mutually exclusive and both contribute to pathogenesis of EDMD and DCM.

In this thesis, I focused on investigating the roles of nesprin-1/-2 and its associated NE-LINC complex in the heart. In collaboration with a lab in China, 218 DCM patients were screened for *SYNE-1* and *SYNE-2* gene mutations and three novel rare variants (R8272Q, S8381C, N8406K) were identified at the C-terminus of the *SYNE-1* gene from 7 DCM patients. I aimed to use these variants to:

1. Determine the effect of nesprin-1 mutants at the NE-LINC complex *in vitro*;
2. Investigate if nesprin-1 mutants affect the myogenesis *in vitro*;
3. Generate the cardiac specific nesprin mutant mouse model to elucidate the potential pathogenic mechanisms of nesprin-associated cardiomyopathy.

Chapter 2: Methods and Materials

2.1 Patient recruitment and mutation screening

2.1.1 Research Subjects

The study cohort consisted of 218 unrelated individuals with DCM and 210 healthy controls, collected from the West China Hospital, Sichuan University, China. All blood materials of the patients and controls included in this study were taken with informed consent for DNA analysis and approval of the local ethics board. The clinical characteristic of the patients and controls were summarized in Appendix 1-3. Most of DCM patients were men and had significantly larger left ventricular (LV) chamber and lower left ventricular ejection fraction (LVEF) when compared with the ethnic and age-control samples.

2.1.2 Mutation analysis

Primer pairs were designed across the intron/exon boundaries and untranslated regions of nesprin-1α_1 and 1α_2, nesprin-2α_1, 2 α_2, 2β, 2ε_1 and 2ε_2, i.e., the smaller INM localised isoforms of nesprin-1 and nesprin-2 shown to bind emerin and lamin and be either highly or specifically expressed in muscle tissue. 180 oligonucleotide primers from intronic sequences for 88 exons were designed using the program Primer3Input (primer3_www.cgi v 0.2) and used previously [3]. Mutation screening was performed using the PCR-based mutation detection technique DHPLC (WAVE 4500B system, Transgenomic). Appropriate DHPLC conditions for running temperatures and buffer gradients were established for each individual exon. This method and associated experiments were carried out by our collaborator in Sichuan University.

2.2 Cell work

2.2.1 Cell culture

All cell lines were cultured in a humidified incubator with 5% CO_2 at 37^{o}C. Immortal cell lines human osteosarcoma (U2OS), C2C12 mouse skeletal myoblast, H9C2 rat cardiac myoblast, human embryonic kidney 293T cells (HEK 293T) and primary cell lines Human Lung Fibroblasts (HLFs), Human Dermal Fibroblasts (HDFs) were cultured in Dulbecco's modified Eagle's medium (DMEM) supplemented with 10% heat inactivated fetal bovine serum (FBS), 10units/ml penicillin, 10μg/ml streptomycin and 200μM L-Glutamine (PSG).

To induce the formation of myotubes, C2C12 were grown to 80-90% confluency and then incubated with DMEM containing 2% horse serum (HS), 1% PSG. Cells were observed daily for the formation of myotubes, the characteristics of which include a distinct change in morphology from rounded to spindle like cells and the presence of multiple nuclei within the cells.

2.2.2 Cell passage

All the cells were passaged when at 60-80% confluency, except C2C12 which were passaged at 60% confluency to prevent terminal differentiation. The culture medium was removed, followed by 1 time wash with phosphate buffered saline (PBS). Then cells were incubated in an appropriate volume (to cover the whole surface of culture flask) of trypsin-EDTA solution for 2-3 minutes in the incubator at 37°C until cells detached from the flask surface. U2OS were split 1:6, C2C12 and HEK 293T 1:10, H9C2 1:4, HDFs 1:3 in fresh culture medium and allowed to adhere.

2.2.3 Isolation of neonatal rat cardiomyocytes (NRCs)

1- or 2- day old Sprague-Dawley rat pups (10-12 rat pups in total) were anesthetized, then the abdomens were sterilized with an antiseptic solution. The beating hearts were surgically removed and immediately placed into ice-cold ADS to stop beating and general cleaning (removal of blood). Then heart tissue was minced with small scissors or a razor blade to less than 1mm^3 pieces. Minced hearts were

transferred into a 50ml falcon tube with a wide-mouth transfer pipette. After removing the supernatant, the heart tissue was subjected to a serious enzymatic digestion. The enzyme solution (ES) contained type II collagenase (57.5 U/mL) and pancreatin (1.5 mg/mL) in ADS buffer was filter sterilized before use.

First digestion: 5ml of ES was pipetted into tissue and shaken for 5 minutes at 37°C at 220rpm (revolutions per minute). 1st digestion supernatant was discarded due to presence of excess endothelial cells and blood. 2nd digestion: Another 5ml of ES was added and shaken for 25 minutes under the same conditions. Supernatant was transferred into in a clean 15ml falcon tube with 3ml non-heat inactivated FBS which stopped the enzyme reaction. Cells were centrifuged at 400g/660rpm at room temperature (RT) for 5 minutes. Pellets were re-suspended in 4 ml FBS, then incubated in a humidified incubator with 5% CO_2 at 37°C with a loose lid. 3rd and 4th digestion: repeat steps as 2nd digestion until all the tissue adequately digested. Next, the cells in the incubator were transferred into a 50ml falcon tube through a pre-rinsed cell strainer and centrifuged 5 minutes at 400g/660rpm. Then the pellet was re-suspended with 10ml plating media. All the cells were plated in a 10cm petri-dish, and kept in incubator for 1 hour until all fibroblasts had adhered to the dish. Following this, the supernatant containing NRCs was counted on a haemocytometer, and then an appropriate number of cells were plated on 35mm petri-dishes which were pre-coated with 1% gelatin for 4 hours at 37°C. These were left for 24 hours until NRCs had attached to the dishes.

2.2.4 Generation of retrovirus particles

RV were packaged in HEK 293T cells, at 70-80% confluency in a 10cm Petri dish (split $3x10^6$ cells/dish 24 hours in advance). 1st day: fresh 6ml DMEM with 10% FBS (without antibiotics) was changed 1 hour before transfection. Transfection mix was prepared with 4µg plasmid of interest, 4µg DNA RV helper (from Prof. Peter Zammit lab, King's College London) and 1,800µl opti-mem serum reduced medium with flick-mix. After 5 minutes incubation at RT, 6µl Lipofectamine Plus reagent was added and incubated for another 5 minutes. Then 24µl Lipofectamine LTX was added, mixed, and incubated for another 30 minutes. Mixture was added drop-wise to HEK 293T cells. 2nd day: 10ml fresh DMEM medium with 10% FBS and 2% L-Glutamine

was replaced. 3rd day: 48 hours after the transfection, the same medium as 2nd day was replaced but volume was reduced to only 6ml.

RV particles were collected three times at different time points. 1st collection: 12 hours after last medium changed, which contained the RV at a high titre. All 6ml of medium was collected into a 15ml Falcon tube, followed by passing viral supernatant through a 0.45μm filter into a fresh 15ml Falcon tube. Then RVs were aliquoted into 1.5ml Eppendorf tubes and immediately frozen at -80°C. 2nd collection: 6ml of fresh culture medium was added to the cells and collected following the previous steps. 3rd collection: repeated as previous. Lastly, the HEK 293T cells were discharged with detergent treatment as they could not be reused.

2.2.5 Plasmid transfection

2.2.5.1 Use of FuGENE HD Transfection Reagent

Cells (excluding NRCs) were counted and plated out at ～50% confluency the day prior to transfection. The culture medium was changed into DMEM containing 10% FBS without PSG. For a 24-well plate: one well was transfected with 0.75μg of plasmid which was mixed with 37.5μl opti-mem reduced serum medium and 2.5μl FuGENE® HD Transfection Reagent. Before adding to the cells, the transfection mixture was vortexed thoroughly and incubated at room temperature for 15 minutes while transfection complexes assembled, then was added drop by drop to the culture medium. Transfected cells were cultured for 24-48 hours before fixation or harvesting.

2.2.5.2 Use of Escort III Transfection Reagent

One 35mm petri-dish of NRC was transfected with 1μg of plasmid which was mixed with 100μl Medium 199 (M199) and 4μl Escort III Transfection Reagent. The transfection mixture was vortexed thoroughly and incubated at RT for 15 minutes while transfection complexes assembled. NRCs were washed two times with M199, then 0.8ml NRC transfection medium was added. Finally, transfection complex was added drop by drop to NRCs and swirled gently. NRCs were incubated for 6 hours before replacing with regular maintenance medium. Transfected cells were cultured for 36 hours before fixation.

2.2.6 siRNA transfection

Small interfering RNA (siRNA) transfection complex was prepared at the initial step. For a T25 flask: 2.5µl RNA (20µM) was added into 1ml opti-mem and then mixed with 50µl HiPerFect Transfection Reagent. The transfection mix was mixed thoroughly and incubate for 10 minutes to form the transfection complexes. Cells were trypsinised, counted and added to the transfection mix in a final volume of 5ml ($2*10^5$/T25 for C2C12, $7* 10^5$/T25 for human lung fibroblast) with the siRNA mix in T25 flask. Cells were left to adhere and grow for a set time. In C2C12 differentiation, siRNA transfection medium was replaced every two days, mixing with the differentiation medium, until the terminal time point. Of note, two control groups were performed together in each experiment. One was MOCK control in which the cells were subjected to the transfection medium only in the absence of siRNA oligos. The other control was using Allstars Negative Control siRNA, which had no homology to any known mammalian gene.

2.2.7 RV infection

The RV only infects actively proliferating cells. The cell density is not an issue, as long as the cells have enough space to proliferate. The RV has to be defrosted on ice and used straight away. Before infection, C2C12 cells medium was changed to minimum volume (1.5ml fresh culture medium for T25) 1 hour in advance. Polybrene infection reagent was added to the RV aliquot at a final concentration of 4µg/ml. Then drop-wise the RV mix was added to C2C12. After 4 hours infection, 3ml fresh culture medium was added to one T25. Cells were then cultured for 48 hours before the next experimental step.

2.3 Protein techniques

2.3.1 Cell lysate

Adherent cells were put on ice and washed three times with ice-cold PBS. Proper amount of IP buffer-1 with 2µl/ml protease inhibitor cocktail (PIC) was used to harvest cells by using cell scrapers. Cell lysates were transferred to a pre-cooled 1.5ml Eppendorf and sonicated for 10 seconds at 4^{o}C to break the cell membrane and NE to release all the proteins. Cell debris was pelleted by centrifugation at 12,100g speed for 10 minutes at 4^{o}C. Clear supernatant was transferred to a fresh tube and the pellet was discarded.

2.3.2 DC protein assay

The protein concentration was measured by Bio-Rad DC Protein Assay. Standard curve was made by the serial dilution of 1.54mg/ml BSA in a 96-well plate. 5µl of cell lysis and standard were incubated with 25µl of Bio-Rad DC Assay Reagent A for 5 minutes at RT to allow the reaction between protein and copper in an alkaline medium. Then, 200µl Bio-Rad DC Assay Reagent B (Folin reagent) was mixed to promote the reduction-oxidation reaction of the protein-copper complex and that produced a blue colour which can be measured at 710nm. The protein concentration was calculated according to the ratio to the standard proteins.

2.3.3 Western blotting (WB)

Gel preparation: SDS-PAGE consists of stacking gel and resolving gel. They can separate the proteins based on the difference of their molecular weight [231]. Different concentrations (8%-15%) of resolving gel was made according to the various size of proteins of interest, whereas the stacking gel was always 4%.

Sample preparation: Protein lysate was diluted into the same concentration by mixing with 4*sample loading buffer and deionized water (DiH_2O). Then proteins were denatured via boiling at 95^{o}C for 10 minutes.

Protein separation by gel electrophoresis: equal amount of protein sample was loaded to each well, along with the molecular weight marker. Polymerised gel was submerged into running buffer and ran at 120 volts for 90 minutes.

Transferring the protein from the gel to membrane: Protein was transferred from the gel to the PVDF membrane with 0.45μm pore size. The PVDF membrane was activated in 100% methanol for 15 seconds in advance. The gel, membrane and filter paper were sufficiently pre-soaked in the transfer buffer. Then, the gel was packed in the 'transfer sandwich' structure (filter paper-PVDF membrane-gel-filter paper) and placed horizontally between two plate electrodes in a semi-dry transfer apparatus, ran at 25 volts for 1 hour. After transfer, the gel was stained with Coomassie blue to check the efficiency of the transfer.

Antibody incubation and detection: The membrane with immobilized proteins were blocked in 5% skimmed milk powder (Marvel) in TBST at RT for 1 hour, followed by incubation with the primary antibody which was diluted into the blocking buffer according to the manufacturer's recommended ratio at 4^{o}C overnight (ON). The next day, membrane was washed with 3 x 5 minutes in TBST, then subjected to the horseradish peroxidase (HRP) conjugated secondary antibody which was diluted in the blocking buffer at RT for 1 hour. The excess secondary antibody was removed by washing 3 x 10 minutes in TBST. Finally, protein bands were detected by ECL chemiluminescent development onto X-ray films. X-ray films were scanned and saved as 300bp TIFF format image and the density of WB bands were analysed using ImageJ software (1.48V).

Stripping and reprobing: the used membrane was stripped with stripping buffer at RT for 30 minutes, followed by re-blocking, primary antibody targeting to the protein of interest, secondary antibody addition and development.

2.3.4 Protein binding techniques

2.3.4.1 GST pull-down

Glutathione S-Transferase (GST) fused proteins encoded by pGEX vectors were transformed into *E. coli* strain BL21. Single colonies were cultured in 5ml of LB broth containing ampicillin antibiotics at 37^{o}C/220rpm ON. Next day, 5ml of bacteria containing GST fusion proteins or GST alone was amplified in 100ml of LB broth for

2 hours at 37°C, followed by addition of 0.2mM isopropyl-1-thio-β-d-galactopyranoside (IPTG) to further induce expression of GST fused proteins for another 2 hours at 30°C. Bacteria was centrifuged at 4000g for 45 minutes at 4°C. The pellet was re-suspended was in 5ml ice-cold PBS with PIC, followed by a 10 seconds sonication.

500µl 10% Triton (in PBS) was added in the lysate as a non-ionic surfactant to further lyse the bacteria. After 10 minutes rotation and 30 minutes 4000g centrifugation, the debris pellet was removed and supernatant containing GST fused protein was purified by incubating with GST beads for 1 hour at 4°C. The expression of recombinant beads-proteins was confirmed by SDS-PAGE and coomassie blue staining. In addition, cell lysate was acquired as protocol described in Section 2.3.1. Briefly, 200µg extracts from U2OS or C2C12 myoblasts/myotubes were incubated with 50µl beads with constant rotation for 16 hours at 4°C. Bound proteins were washed and eluted into sample buffer, followed by WB. In particular, to investigate the interaction between nesprin-1 and its NE binding partners, protein lysates from Myc-SUN2 transfected (for SUN binding) and untransfected U2OS cells (for lamin A/C and emerin binding), C2C12 myoblast and myotubes (for KLC-1/2 interaction) were harvested and subjected to pull down using either GST-WT or mutant nesprin-1α_2 SR1-6 beads (GST-nesprin-1α_2 R8272Q, S8381C, N8406K were previously generated in our lab, GST-nesprin-1α_2 LEAA was generated by our collaborator Dr. Sue Shackleton from Leicester University). To further confirm the bindings, U2OS cells were transfected with either GFP-nesprin-1α_2 WT or mutants, protein lysates were harvested and subjected to pull-down using either GST-lamin A (amino acids 356-665) or GST-emerin (amino acids 1-176).

2.3.4.2 Co-immunoprecipitation (Co-IP) assays

U2OS cells were transfected using GFP-nesprin-1α_2 WT/mutants with HA-KLC-1/2 WT/ mutant respectively, harvested about 24 hours later and kept in IP buffer-2 with protease inhibitor cocktail on ice for 30 minutes, followed by 10 seconds sonication and centrifugation at 8,300g for 10 minutes. 500µg of protein was pre-cleared with Protein A and/or G sepharose beads for 1 hour at 4°C. Beads were removed by centrifugation and 2.5µg primary antibody was added to lysates and left rotating at 4°C for 16 hours ON. Next day, A/G sepharose beads were then added to

reactions rotating at 4°C. After 2 hours incubation, the formed beads-antibody-protein complexes were pelleted by centrifugation. The supernatant was discarded, and pellets were washed 3 times with IP-PIC buffer and re-suspended in sample buffer, heated at 95°C for 10 minutes and analysed by WB as described in Section 2.3.3.

2.4 Microscopy work

2.4.1 Immunofluorescence (IF) microscopy

Cells grown on coverslips in 24-well plates or 30mm petri dishes were washed three times with ice-cold PBS, then fixed and permeabilized with different reagents according to different experimental aims and various primary antibodies. In general, there were two fixation and permeabilization methods used in this study: 1) Fixed by pre-warmed 4% paraformaldehyde (PFA) for 10 minutes at RT, washed 3 x PBS, then permeabilized with either 0.0001% Digitonin or 0.5% NP-40 for 3 minutes at RT; 2) Fixed and permeabilized with pre-cold methanol - acetone fixative at -20°C for 10 minutes. Then, all cells were washed 3 x 5 minutes in PBS, and the water repelling circle was drawn along the inner petri dish to reduce the quantity of reagents used for IF. Samples were blocked in 3% bovine serum albumin (BSA) solution or 5% goat serum for 1 hour at RT, then directly subjected to the primary antibodies diluted in the same blocking buffer ON at 4°C. The following day, excess primary antibodies were washed off with three changes of PBS for 5 minutes each time. Then the cells were incubated with appropriate secondary antibodies diluted in the same blocking buffer for 1 hour at RT followed by another 3 x 10 minutes in PBS. Samples were then stained with 4',6'-Diamidino-2-Pheylindoledihydrochloride (DAPI), followed by three washes with PBS (each time 5 minutes). For the last step, each coverslip, petri dish or slide was mounted with the appropriate size of cover glass on the top using Mowiol mounting media.

Confocal images were captured using a Leica SP5 laser scanning confocal microscope. All confocal images were taken with 63X oil immersion objective lenses. Laser power (5-8%), gain and offset were adjusted accordingly to ensure image acquisition efficiently and avoid image saturation and sample bleaching. Z-stacks were taken throughout the height of samples and restored using Leica confocal software (LAS AF Lite.). 'Analyse particles' function in ImageJ (1.48V) was used to measure

circularity of cell nuclei, with circularity values given between 0 and 1 (values closer to 1 being more circular in shape) [232]. Cell membrane of individual CM was manually drawn and the cell size were quantified under 'measurement' function in ImageJ (1.48V).

2.4.2 Histology and brightfield microscopy

2.4.2.1 Haematoxylin and Eosin staining

Frozen heart tissue sections were removed from -80°C and dried in RT for 30-60 minutes. Sections were fixed with pre-warmed 4% PFA at RT for 10 minutes. After three washes with DiH_2O, the samples were subjected to 1% Aqueous Eosin for 10 seconds for cytoplasmic staining, then washed again with running tap water for 5 minutes. The sections were again emerged in Harris' haematoxylin solution for 30 seconds to stain the nucleus, and the excessive staining was removed under running tap water for 5 minutes. Finally, the slides were dehydrated and cleared in successively higher concentration of ethanol and absolute xylene respectively. Coverslips were mounted using DPX and allowed to dry overnight.

2.4.2.2 Masson's trichrome staining

Frozen heart tissue sections were removed from -80°C and dried at RT for 30-60 minutes. The samples were fixed with pre-cold acetone at 4°C for 15 minutes. Then, the protocol from the Masson's trichrome staining kit was followed. First, samples were further fixed in Bouin's solution at RT ON to improve the staining quality. Next day, excess picric acid was removed from the slides under running tap water for 5 minutes. Then all the samples were subjected to Weigert's iron haematoxylin working solution for 10 minutes to stain the nucleus with black colour. Next, Biebrich scarlet - acid Fuchsin solution (5 minutes) stained all acidophilic tissue elements such as cytoplasm, muscle, and collagen with red colour, followed by using phosphotungstic - phosphomolybdic acid solution (10 minutes) to diffuse the collagen colour while retaining the cytoplasmic and muscle red colour. Application of aniline blue (5 minutes) stained the collagen with blue colour, after which, 1% acetic acid (1 minute) was applied to differentiate the tissue sections. Finally, the slides were dehydrated and

cleared in successively higher concentrations of ethanol and absolute xylene respectively. Coverslips were mounted using DPX and allowed to dry overnight.

2.4.2.3 Brightfield microscopy

Images of histology tissues were obtained under brightfield microscopy (Leica ICC50 W Microscope). All images were taken with 4-/10- X objective lenses and saved as TIFF format. The intensity of illuminator and obtain gain were adjusted according to selected objective lens and different histological stainings.

2.5 Nucleotide techniques

2.5.1 RNA extraction

Cells grown in T25 flasks were washed three time with ice-cold PBS, and scraped together with 1ml of RNA STAT-60, then transferred into 1.5ml Eppendorfs. Heart tissues were homogenized by Lysis Beads in 1ml of RNA STAT-60 and suspensions were transferred to 1.5ml Eppendorfs. Samples were stored on ice for 5 minutes for complete dissociation of nucleoprotein complexes. Next, 200µl of chloroform was added to each reaction and shook vigorously for 15 seconds. After 2-3 minutes standing at RT, all samples were centrifuged at 12,000g for 15 minutes at 4°C. There were two phases presented in the tube: a lower red phenol chloroform phase containing DNA and proteins, while the upper colourless aqueous phase (60% of total volume) contained the RNA. The aqueous phase was carefully transferred to a fresh tube with 500µl of isopropanol. RNA precipitation occurred within 30 minutes and this was pelleted by centrifugation at 12,000g for 10 minutes at 4°C. The RNA white pellet was washed with 1ml of 70% pre-chilled ethanol solution (in diethylpyrocarbonate (DEPC) treated water) and centrifuged at 7,500g for 5 minutes at 4°C. The RNA pellet was briefly dried in the air and re-suspended in 50µl (for cell) or 100µl (for tissue) DEPC treated water. The RNA concentration was measured by Nano drop and stored in -80°C.

2.5.2 Reverse transcription

2µg of RNA was used for reverse transcription. This process consists of three steps. 1ST step: RNA, 0.5µl Oligo dT primer, 0.5µl Oligo Random primer, 1µl dNTP were mixed and heated at 65°C for 5 minutes to melt the secondary structure within the RNA template, then cooled down immediately to 4°C to prevent secondary structure from reforming. 2nd step: 5µl 5X reaction buffer, 1µl of RNasin ribonuclease inhibitor, DEPC treated water (added to equal final volume of 24µl) were added to step 1 mix, and incubated at 37°C for 3 minutes to allow the efficiently binding of primers and RNA template, then cooled down to 4°C. 3rd step: 1µl Moloney Murine Leukemia Virus Reverse Transcriptase (M-MLV RT) was added after 2nd step and heated in a thermocycler to 25°C for 10 min, 37°C for 50 min and cooled to 4°C. The synthesized cDNA was finally diluted to 200µl total volume with DEPC treated water with a resulting concentration of 10ng/µl.

2.5.3 Quantitative polymerase chain reaction (qPCR)

qPCR is a very sensitive and reliable method to quantify RNA expression level. It is based on detection and quantification of fluorescence emitted from a reporter molecule during each cycle of PCR process [233, 234].

qPCR reaction was performed in a 20µl reaction which consisted of 10µl 2*Sybr green qPCR master mix, 1µl of Forward primer (5µmol), 1µl of Reverse primer (5µmol), 2µl of cDNA template (10ng/µl), and 6µl DEPC treated water. Prior to qPCR, designed primers had been examined using Taq polymerase based PCR to ensure the amplified product was unique with the right size. Reactions were performed on RotorgGene-3000 by Corbett. Initial step was denaturation of the template at 94°C for 8 and half minutes, then followed with 35-40 combined cycles of 94°C for 15 seconds (denaturation) and 60°C for 1 minute (annealing and extension). The threshold of significant and specific amplification starting points was manually set as 0.5. The cycle threshold (Ct) for each gene was obtained according to the threshold. ΔCt was calculated by the difference between $\Delta Ct_{\text{target gene}}$ and $\Delta Ct_{\text{internal control gene}}$, while ΔΔCt was calculated by the difference between $\Delta Ct_{\text{treated sample}}$ and $\Delta Ct_{\text{control sample}}$. qPCR primers used for this study are described in 2.8.5.

2.5.4 Polymerase chain reaction (PCR)

PCR is a simple and widely used technique to amplify a specific DNA fragment from a template plasmid or a complex pool of DNA [235].

For generating nesprin-1α constructs, GC-RICH PCR kit was used for more efficient and accurate amplification. PCR reaction was composed of two mixes. Mix 1 (35µl) consisted of 19µl PCR grade water, 2µl dNTP mix, 2µl Forward primer (5µmol), 2µl Reverse primer (5µmol), 5µl GC-RICH resolution solution and 5µl template (10ng/µl). Mix 2 (15µl) consisted of 4µl PCR grade water, 10µ GC-RICH reaction buffer and 1µl GC-RICH enzyme mix (Taq DNA polymerase and proofreading polymerase). Then the total content of PCR reaction (50µl) was mixed in a thin-walled PCR tube and the reaction was carried out in a thermocycler by utilizing the following conditions: Initial denaturation 95°C for 3 minutes, denaturation 95°C for 30 seconds*, annealing 60°C for 1 minute*, extension 72°C for 1 minute per kb*, (*repeated for 30-40 cycles) and final extension 72°C for 10 minutes and held at 4°C.

For the rest of PCR reactions, the DNA fragment was amplified with Tag polymerase. Each reaction (20µl) was composed of 10µl 2*GoTaq green master mix, 2µl template (10ng/µl), 0.5µl Forward primer (5µmol), 0.5µl Reverse primer (5µmol), 7µl DiH_2O. The cycling parameters were same as GC-RICH reaction.

After amplification, PCR products were mixed with 6× DNA loading buffer and separated by 1% agarose gel electrophoresis. Then PCR products were visualized by UV detection before being purified.

2.5.5 Site directed mutagenesis

In vitro site-directed mutagenesis is achieved by using the QuikChange Site-Directed Mutagenesis Kit which allows site-specific mutation in any double-stranded DNA plasmid. This works by using a designed pair of complementary primers with a mutation. During PCR cycles, these primers anneal to the template DNA, replicating the plasmid DNA with the mutation [236]. The paired synthetic oligonucleotide primers were designed to be between 25 and 45 bases in length, with a melting temperature (Tm) of ≥78°C. PfuUltra high-fidelity (HF) DNA polymerase was utilized to ensure the precise extension of mutation containing strand without primer displacement. The total volume of each reaction was 50µl consisting of 5µl

10*reaction buffer, 1µl plasmid template (50ng/µl), 1.25µl Forward primer (100ng/µl), 1.25µl Reverse primer (100ng/µl), 1µl dNTP mix, 3µl Quicksolution, 37.5µl DiH_2O and 1µl PfuUltra HF DNA polymerase. Cycling parameters were: Initial denaturation 95°C for 3 minutes, denaturation 95°C for 30 seconds*, annealing 55°C for 1 minute*, extension 68°C for 1 minute per kb*, (*repeated for 18 cycles) and final extension 68°C for 20 minutes and held at 4°C. After the temperature cycling, the PCR products were treated with endonuclease Dpn I (target sequence: 5′-Gm6ATC-3′, for methylated and hemimethylated DNA) which was used to digest the parental DNA template and select the mutation containing DNA. The template plasmid was isolated from *E. coli* which was dam methylated and susceptible to Dpn I digestion. The vector DNA containing the desired mutations was transformed into XL1-Blue super-competent cells and isolated for DNA sequencing.

2.5.6 Agarose gel electrophoresis

PCR products were mixed with 6*DNA loading dye and separated by 1-2% TAE agarose gel electrophoresis. According to the size of PCR products, the 1kb or 100bp DNA ladder was used. Electrophoresis was performed at 120 volts for 30-50 minutes until the separation of bands were adequate. The PCR products were bound by the fluorescent dsDNA stain Nancy-520 and thus could be visualized via UV transillumination.

2.5.7 Cloning

DNA sequence of interest were either amplified from the template plasmid by PCR or isolated from the plasmid by restriction enzyme digestion.

2.5.7.1 Agarose gel extraction

The PCR product separated by agarose gel electrophoresis was cut under the UV transillumination and extracted by QIAquick Gel Extraction Kit. Briefly, the Buffer QG was added 3 volumes to 1 volume of gel weight and incubated at 50°C until the gel slice was completely dissolved (around 10 minutes). Then 1 gel volume of isopropanol was added to form the DNA participate. The sample was gone through the

provided collection tube and DNA was bound to the filter. After wash with 750µl Buffer PE, the DNA was eluted into a clean Eppendorf with 15µl DiH_2O at maximum centrifuge speed. The final step can be repeated twice to increase the final concentration. The DNA concentration was measured by Nano drop and then used for the ligation step.

2.5.7.2 Restriction enzyme digestion

2µg DNA plasmid was digested with 10-20 unit of each restriction enzyme. The reaction buffer for more than two enzymes were chosen according to the tool of 'double digest finder' online to ensure the most efficient digestion process. In general, digestion was performed in a 37°C water bath for 2-3 hours. For cloning, at the end, the digested vector was treated with 1µl of Antarctic Phosphatase (AnP) at 37°C for 30 minutes, and heat-inactivated at 80°C for 2 minutes. This step could dephosphorylate of 5′ and 3′ ends of DNA phosphomonoesters and prevented re-ligation of linearized plasmid DNA. The digested products could be purified by agarose gel electrophoresis and gel extraction as described in Sections 2.5.6 and 2.5.7.1.

2.5.7.3 DNA ligation

For sequencing and cloning purposes, the PCR product or digested DNA fragment of interest was ligated directly into the pGEM T-easy vector. The pre-linearized pGEM T-easy vector contains 3′-T overhangs at the insertion site to provide a compatible overhang for the ligation products. The α-peptide coding region for β-galactosidase is inactivated by the inserted fragment and can be used to identify the blue (un-inserted) / white (inserted) colonies on the plates. The insert/vector molar ratios were ideally to be 3:1, 6:1 or 9:1. Ligation was carried out in a final 10µl volume: 5µl 2*ligation buffer (or 1µl 10*ligation buffer), 1µl pGEM T-easy vector (50ng/µl), 1µl T4 DNA Ligase (3 Weiss units/µl), Xµl insert, DiH_2O to a final volume of 10µl. The reaction was incubated longer at 4°C ON to increase the number of transformants.

For the constructs using retroviral vector MIG, mammalian expression pcDNA3.1(-): The MIGplus vector was a kind gift from Prof. Peter Zammit [237], which was modified from the retroviral backbone pMSCV-puro (Clontech, Mountain

View, CA), in which the puromycin selection gene was replaced with eGFP to create pMSCV–IRES–eGFP, served as the RV control vector and eGFP as a reporter for retroviral infection. pcDNA3.1(-) vector was purchased from Invitrogen. These vectors were linearized by restriction enzyme digestion with EcoRI and NotI, and ligated with DNA fragment nesprin-1α_2 WT and mutant (amino acids 1-977, equivalent to nesprin-1 giant 7875-8796) which were digested from the pGEM T-easy vector with the same enzymes. The ligation method was the same as pGEM T-easy vector.

2.5.7.4 Transformation

Different competent cells were chosen for different experiment targeting. In general, GST fused constructs were transformed into BL21, the site directed mutagenesis constructs were transformed into XL1-Blue, others were chosen either DH5α or JM109. Briefly, 30-50µl competent cells were thawed on ice, and incubated with 2µl plasmid for 30 minutes. The following heat shock step was dependent on the accurate temperature and time. Heat shock occurs in a calcium rich environment to counteract the electrostatic repulsion between the plasmid and bacteria cellular membrane. A sudden increased temperature creates pores in the bacteria cell membrane and allow the plasmid DNA to enter. No mixing or shaking was allowed during the heat shock. BL21 needed exactly 30 seconds in the 42°C water bath, XL1-Blue required 45 seconds at 42°C, whereas DH5α and JM109 needed 20 seconds at 42°C. After heat shock, the tubes were immediately placed on ice for 2 minutes. The 300µl pre-warmed S.O.C medium was added into the tubes and left to shake in a 37°C incubator at 200-220rpm for 1 hour. The bacteria were plated out onto LB agar plates with appropriate antibiotics. X-gal and IPTG were added together when blue/white selection was needed. The plate was incubated at 37°C ON to allow colonies to grow.

2.5.7.5 LB broth medium and LB agar plates

LB broth medium was used for bacteria culture. It was made by mixing 20g LB powder and 1L DiH_2O. The relevant antibiotics (20µg/ml Kanamycin, 150µg/ml Ampicillin) were supplied after LB broth had cooled down post-autoclave.

LB agar was made by dissolving 35g LB Agar powder with 1L DiH_2O. This mixture was autoclaved for purification. When solution cooled to 55°C, the relevant antibiotics (20µg/ml Kanamycin, 150µg/ml Ampicillin) were added and mixed well. Then this mixture was poured into petri dishes.

Either LB broth or LB Agar plates could be stored for 1 month in darkness at 4°C.

2.5.7.6 Plasmid isolation

For obtaining small yields of purified plasmid: Individual round and white colonies were selected and cultured in 5 ml of LB broth (with appropriate antibiotic) at 37°C, 200-220rpm ON. 3ml of the culture was used for plasmid isolation using the Promega Pure Yield Plasmid Miniprep System. Briefly, the bacteria were pelleted by centrifugation at 12,300g for 1 minute. Then the pellets were completely re-suspended in 600µl DiH_2O, lysed in added 100µl Cell Lysis Buffer and the reaction was stopped by adding 350µl of cold (4°C) Neutralization Solution. The mixture was centrifuged at 12,300g for 3 minutes at RT and the supernatant was transferred to a Pure Yield minicolumn. The plasmid was captured onto a minicolumn and washed with 200µl Endotoxin Removal Wash and 400µl Column Wash Solution. For the last step, the plasmid was eluted by incubating the minicolumn with 15-30µl of DiH_2O for 1 minute. The eluted plasmid was collected in a clean 1.5ml Eppendorf tube by centrifugation at 12,300g for 1 minute.

For isolating large amounts of plasmid: a single colony was picked from the plate and cultured in 5ml of LB broth (with appropriate antibiotic) at 37°C, 200-220rpm for 8 hours. 1ml of starter culture was diluted into 200ml selective LB broth medium at 37°C for vigorous shaking (200-220rpm) ON. Next day, bacteria cells were harvested by centrifugation at 4,000g for 45 minutes at 4°C. Plasmids were isolated using the Qiagen Endofree Plasmid Maxiprep kit according to the manufacturer's instructions. First, the bacteria were lysed in 10ml of lysis buffer, which was then neutralized by the addition of 10ml of neutralization solution. Subsequently, the plasmid was separated from cell debris by passing the mixture through a filtered syringe and then was incubated with 2.5ml of endotoxin removal buffer for 20 minutes on ice. Next, the plasmid was eluted in 15ml of elution buffer and precipitated with 10.5ml isopropanol followed by centrifugation as 4,000 g for 1 hour at 4°C. The DNA was washed again

in an ethanol-containing wash buffer and re-pelleted by centrifugation at 4,000 g for 30 minutes at 4°C. Finally, the pellet was air dried and re-suspended in 200µl of DiH_2O.

The DNA concentration was measured by Nano drop and stored at -20°C. In addition, the bacteria glycerol stock can be made by mixing 700µl bacteria solution and 300µl 70% glycerol (autoclaved) and stored in -80°C for long-term storage.

2.6 Animal work

2.6.1 Generation of a cardiac specific KASH2 Transgenic mouse model

All the mice used in this study were C57BL/6 strain. The original Transgenic (Tg) KASH mouse strain (CAG-LacZ-V5/EGFP-KASH2) was generated by our collaborator Dr. Didier Hodzic in Washington University [238, 239]. The Tg KASH mouse harbours a genetic construct consisting of an open reading frame (ORF) encoding mouse nesprin-2 KASH domain fused to EGFP (EGFP-KASH2) cloned downstream of a Lox-flanked ORF encoding β-galactosidase fused to a V5 epitope (LacZ-V5) with a flanked STOP codon at the end. Myosin light chain 2 ventricular (MLC2V) is a muscle regulatory myosin light chain isoform which is the earliest ventricular-restricted marker presented at E8 during mammalian cardiogenesis [14]. MLC2V involved in maintaining the cardiac contractility and ventricular chamber morphogenesis [15, 16]. By breeding MLC2V Cre mice [17] with Tg KASH mice, Cre recombinase-mediated somatic excision of the LacZ/V5 ORF and STOP codon, and allowed activation of transcription of EGFP-KASH2 specifically in CMs under the MLC2V promotor.

2.6.2 Genotyping

The new born mouse litters were genotyped after weaning. Ear biopsies were acquired. DNA was prepared by boiling the samples in 300µl 50mM NaOH at 95°C for 10 minutes followed by vortexing and addition of 25µl Tris at pH 8.0. The reactions were left at 4°C ON and used as template for next day PCR which was described in Section 2.5.4. The specific primers designed for *in vivo* study were listed in Table 2.4.

Identification of offspring was achieved by performing three separate PCRs: one to identify expression of the transgene GFP-KASH2 and one to identify Cre recombinase, GAPDH served as internal control. Mice positive for both GFP-KASH2 and Cre were named as csKASH-Tg, while mice only positive for GFP-KASH2 were referred as FLctrl.

2.6.3 Echocardiography

Echocardiography is a quick, reliable and non-invasive measurement of cardiac function, which can assess the size and shape of the heart, blood flow and systolic and diastolic functions in murine models [240]. In this study, the heart function was accessed using the Vevo 2100 ultrasound system (Visualsonics, Toronto, Canada) equipped with a high-frequency (30 MHz) linear array transducer. Mice were examined at week 15, 30, 52. Briefly, mice were given a quick anaesthesia induced by 5% isoflurane/95% oxygen, then were maintained under the 1.5% isoflurane/98.5% oxygen level. Mice were placed supine on an electrical heating pad (37°C), and the physiological parameters were monitored. Continual ECG was obtained via limb electrodes and heart rate were >450 beats per minute (bpm) while respiratory rate was ~100 breaths per minute for the duration of the study. The chest hair was removed by applying hair removal cream. The echocardiographic study was performed predominantly in parasternal and suprasternal notch long-axis. All views were digitally stored in cine loops consisting of 300 frames. Subsequent analysis was performed off-line on a Vevo 2100 software (version 1.4.0) workstation.

2.6.4 Transverse aortic constriction (TAC)

Transverse aortic constriction (TAC) in the mouse is a widely used experimental model for pressure overload induced cardiac hypertrophy and heart failure [241]. The TAC procedure was performed by a professional experienced technician in collaboration with Prof. Ajay Shah's lab (King's College London). Briefly, the aorta was well exposed after dissecting the muscle surrounding the trachea. The aortic binding used a 6-0 nylon suture ligature to tie around the transverse aorta tightly against a 27-gauge needle. The binding site was positioned at the bifurcation of the left common carotid and innominate arteries. For Sham, the aorta was exposed and touched

by surgical instrument as previous steps, without any binding. All the mice were monitored post-surgery every day and abnormal behaviours were recorded. The termination point was two weeks after surgery.

2.6.5 Harvesting of mouse heart

Mice were quickly and deeply anaesthetised with 5% isoflurane/95% oxygen. The unconscious mice were removed from the chamber and it was ensured that they were fully anaesthetised via absence of pedal reflex prior to dissection. Mice were placed supine and all limbs were taped. The xiphoid was lifted to allow a cut through the abdominal muscle just caudal to the rib cage. Then the visualized diaphragm was cut away from the ribs and the extended lateral cutting was along the lower curve of the rib cage on both side. The chest cavity was open and lifted by the Mosquito forceps via holding the xiphoid. Prior to harvesting, the beating heart was stopped at diastole via injecting 300µl salt solution containing 5% KCL directly to the heart chamber. Then, the heart was disconnected from the aorta roots and placed in ice-cold PBS. Cotton buds were used to press the heart to remove extra blood from the chamber. The extra connective and fatty tissue around the heart was carefully removed, and the whole heart was weighed. Both right and left atrium as well as right ventricle were removed and weighed, the rest left ventricle was weighed and dissected from the middle of long axis. The part close to heart base was embedded with Optimal cutting temperature compound (OCT compound) on the disc cork, and gradually frozen by placing it above the liquid nitrogen. The other part toward the apex, was cut from the short axis into two equal parts for WB and RNA analyses respectively. These two parts were sealed in the tubes and immediately frozen using liquid nitrogen. The tibia was dissected out and cleaned of all soft tissue. The length was determined using a micrometer. Meanwhile, the tail biopsy (around 5mm) was cut to further confirm the genotyping. The frozen tissue was well preserved at -80°C.

2.6.6 Whole heart perfusion and embedding

The mice chest cavity was open as described in Section 2.6.5 and the heart beating was stopped at the diastole. A tiny hole was incised with scissors at the right atrium (RA). 5ml of ice-cold PBS was injected from the apex of LV via a 27-gauge

needle to remove the blood inside of the chambers (The PBS flowed out from the RA). The heart was pale, indicating efficient removal of blood. Then another 5ml ice-cold 4% PFA was injected from the same site at the LV for fixation. The soft tissue was removed and whole heart was merged into 4% PFA for ON fixation at 4°C. Next day, hearts were rinsed in PBS and dehydrated in successively higher concentration of sucrose solutions from 10% to 20%. The heart was embedded by the OCT compound, slowly frozen on the dry ice and stored at -80°C.

2.6.7 Sectioning of cryopreserved tissue

Heart tissue was removed from storage at -80°C and allowed to equilibrate in the cryostat chamber temperature (-20°C) for approximately 30 minutes. The disc cork connected to the tissue was mounted onto the stage of a cryostat with OCT compounds. The stage temperature was set to -22°C while the knife was set to 2 degrees above. The frozen tissue was sectioned into 8μm thick and mounted onto high quality Superfrost slides. The sections were air-dried in the RT for 30-60 minutes and stored at -80°C.

2.6.8 Zebrafish

The nesprin-1α_2 WT and mutants in mammalian expression vectors were generated as methods described in PCR, site directed mutagenesis and cloning. This part of work was completed by me. However, the methods described below and associated experiments during zebrafish embryos developments were performed by our collaborators in Sichuan University.

2.6.8.1 Zebrafish Embryos

WT embryos from AB strain were used. Embryos were obtained by natural matings and cultured in embryo medium [242]. Staging of the embryos was carried out as described by Kimmel et al [243]. Ethical approval was obtained from the Animal Care and Use Committee of Sichuan University.

2.6.8.2 *In vitro* synthesis of mRNA and microinjection

Capped GFP and nesprin mRNAs were synthesized using mMESSAGE mMACHINE® Kit (Ambion); Synthetic capped mRNAs were injected into single-cell embryos. Injection dose (60mg) was an optimised amount received by a single embryo.

2.6.8.3 Zebrafish whole-mount *in situ* hybridization

Whole-mount *in situ* hybridization was carried out as previously described [244, 245]. After linearization by appropriate restriction enzymes, antisense RNAs for *in situ* hybridization were synthesized using DIG RNA Labelling Kit (SP6/T7) (Roche) and purified by MEGAclear (Ambion). Signal area of whole-mount *in situ* hybridization was measured by software ImageJ (1.48V).

2.7 Statistical analysis

Cell counts for statistical analysis were performed on n= 100-200 cells/n=10 confocal microscope fields (63x magnification) for each control and experimental group. All the results were verified in at least 3 independent experiments. The data were analysed using GraphPad Prism software by the Student's t-tests, One way or Two-way analysis of variance (ANOVA) with Dunnett's multiple comparison test or Turkey's post-test for two independent groups or multiple comparisons, respectively. The values are expressed as mean ± standard error of mean (SEM). The p-values<0.05 were considered statistically significant.

2.8 Primer sequence

2.8.1 Primers for V5 tagged nesprin-1α_2 WT and KASH

Primers were designed to amplify V5 tagged nesprin-1α_2 WT and KASH and cloned into MIG retroviral vector. V5 sequence was at the N-terminal of these translated proteins. Primers used for V5 tag nesprin-1α_2 WT and KASH are shown in Table 2.1.

2.8.2 Primers for Flag tagged nesprin-1α$_2$ WT

Primers were designed for amplified Flag tagged nesprin-1α$_2$ WT and cloned into mammalian pcDNA3.1(-) vector. Flag sequence was at the N-terminal of the nesprin-1α$_2$ WT. Primers used for Flag tag nesprin-1α$_2$ WT are shown in Table 2.2.

2.8.3 Primers for Nesprin-1α$_2$ mutagenesis

Primers for site directed mutagenesis were designed to be between 25 and 45 bases in length with the mutated site in the central region of the primers. Primers used for nesprin-1α$_2$ mutants R8272Q, S8381C, N8406K are shown in Table 2.3.

2.8.4 Primers for genotyping

Primers for genotyping the cardiac specific KASH2 overexpression transgenic mice were shown in Table 2.4. Primers for GFP-KASH2 were obtained from the mice strain's original creator Dr. Didier Hodzic in Washington University, while the primers for Cre and GAPDH were from the colleague Dr. Daniel Brayson (King's collage London).

2.8.5 Primers for qPCR

Primers sequence for myogenic regulatory factors were from our collaborator Prof. Peter Zammit (King's collage London). Primers sequence for NE-LINC complex associated proteins and mechanosensitive genes were from Prof. Ju Chen (University of California San Diego). Other primers were designed via the online tool 'Primer3Input Program'. Primers used for qPCR are listed in Table 2.5.

2.9 siRNA oligos

siRNA oligos of KLC-1/-2 group A were obtained from a paper authored by Dr. Holzbaur [114]. siRNA oligos of KLC-1/-2 group B/C were purchased from Qiagen.

siRNA oligos of SUN2 was from colleague Dr. Derek Warren. siRNA oligos used in this thesis are listed in Table 2.6.

Table 2.1 Primers used for V5 tagged nesprin-1α$_2$ WT and KASH

	Forward primer (5' to 3')	**Reverse primer (5' to 3')**
V5 nesprin-1α$_2$ WT	ATA GCG GCC GCC ACC ATG GGA AAG CCT ATT CCT AAT CCT CTT CTA GGT CTA GAT TCT ACT GGC GGA GGC GTG GTG GCG GAG GAC	TAT AGA ATT CTC AGA GTG GAG GAG GGC CAT TC
V5 nesprin-1 KASH	ATA GCG GCC GCC ACC ATG GGA AAG CCT ATT CCT AAT CCT CTT CTA GGT CTA GAT TCT ACT GGC GGA GGC CGC GGC TTC CTG TTCA	

Table 2.2 Primers used for Flag tagged nesprin-1α$_2$ WT

	Forward primer (5' to 3')	**Reverse primer (5' to 3')**
Flag nesprin-1α$_2$ WT	ATA GCG GCC GCC ACC ATG GAC TAC AAA GAC GAT GAC GAC AAG GGC GGA GGC GTG GTG GCG GAG GAC CTG	TAT AGA ATT CTC AGA GTG GAG GAG GGC CAT TC

Table 2.3 Primers used for nesprin-1α$_2$ mutagenesis

	Forward primer (5' to 3')	Reverse primer (5' to 3')
R8272Q	CGG TCA GGA CAA GAC ACC CCA	TGG GGT GTC TTG TCC TGA CCG
S8381C	GCT GGG CGA ATG CTG TAG CAG TAT AGA	TCT ATA CTG CTA CAG CAT TCG CCC AGC
N8406K	CTG GCT TTG TTA AAC TGC ATA GTA CCG	CGG TAC TAT GCA GTT TAA CAA AGC CAG

Table 2.4 Primers for genotyping

	Forward primer (5’ to 3’)	Reverse primer (5’ to 3’)
GFP-KASH	GGA GTT CGT GAC CGC CGC CGG GAT CAC TCT CAG	TTT AAA CGG GCC CCC TAG GTG GGA GGT GGC
Cre	TGC CAG GAT CAG GGT TAA AG	CCC GGC AAA ACA GGT AGT TA
GAPDH	CCT AGA CAA AAT GGT GAA GG	GAC TCC ACG ACA TAC TCA GC

Table 2.5 Primers for qPCR

	Forward primer (5' to 3')	Reverse primer (5' to 3')
Myogenin	TGT TTG TAA AGC TGC CGT CTG A	CCT GCC TGT TCC CGG TAT C
MHC	AGA GCT GAC GTG CCT CAA TG	ATG CCT CTT CTT GCC CTT GT
MyoD	GCC GCC TGA GCA AAG TGA ATG	CAG CGG TCC AGG TGC GTA GAA G
V5	ATA TCC TCG TTC GAC CCC GCC	TCA TTA AGC TTT CTC TGT ATT TCT TCC GAG
GFP	GGT CGA GCT GGA CGG CGA CGT AAA	CAC CAG GGT GTC GCC CTC GAA CTT
Nesprin-1α_2	TCC TCA TCC AGG AAG GAC TG	CAA CCA GCG TCT CCT TTA GC
KASH1	TCC TGC TGC TGC TTA TTG GAC TCA	TCC TCT TAC TGC CTG CAC TTG TGT
KASH2	TCC TTC CTC TCA AGG GTG ATC AGG	AGA AGG ATC GGG CAA AGT TGT TGG
Nesprin-2 CH domain	AGC AGT TGC CTC GGG ATA AAG GAT	AGG CCA AGG ATA ATG GAC GGG TTT
Lamin A/C	CCT TCG CAT CAC TGA GTC TG	AGT CCC CCT CCT TCT TGG T
Emerin	TTG GGC CCT GTC TGT AGG	TAG GAG AAT GAA GAA GAT GAC GAG T
SUN1	ATG GAA CAC ATT CCA AAG ACA CTA T	GAG CTC TAC TAT CTG GAA GGC TTG
SUN2	CAC TCG CTA CTC TCA GGA TGA TAA	TAG GAC TCT CGA ACC ACA GAC TC
ANP	GAT AGA TGA AGG CAG GAA GCC GC	AGG ATT GGA GCC CAG AGT GGA CTA GG

BNP	TGT TTC TGC TTT TCC TTT ATC TGT C	CTC CGA CTT TTC TCT TAT CAG CTC
αMHC	CTG CTG GAG AGG TTA TTC C TCG	GGA AGA GTG AGC GGC GCA TCA AGG
βMHC	TGC AAA GGC TCC AGG TCT GAG GGC	GCC AAC ACC AAC CTG TCC AAG TTC
Procollagen1α_1	TCA CCA AAC TCA GAA GAT GTA GGA	GAC CAG GAG GAC CAG GAA G
Procollagen3α_1	ACA GCA GTC CAA CGT AGA TGA AT	TCA CAG ATT ATG TCA TCG CAA AG
egr-1	CCT ATG AGC ACC TGA CCA CA	TCG TTT GGC TGG GAT AAC TC
iex-1	TTA TAG GGT CGG TAA GAC AGA GTT G	GAC GGA GTG TTA CCC CTA ATC TTA T
c-myc	ATG CCC CTC AAC GTG AAC TTC	GTC GCA GAT GAA ATA GGG CTG
c-jun	TTC CTC CAG TCC GAG AGC G	TGA GAA GGT CCG AGT TCT TGG
c-fos	AGC CCC TGT GTA CTC CCG TG	GCC TTG CCT TCT CTG ACT GC
18S	CCC AGT AAG TGC GGG TAC TAA	GGT TTA GTG AGG CCC TCG G
GAPDH	CGT GCC GCC TGG AGA A	CCC TCA GAT GCC TGC TTC AC

Table 2.6 siRNA oligos

	Sequence (5' to 3')
KLC-1A	GAG TAT GGC GGC TGG TAT A
KLC-1B	CAG AGA GTG GCT GAA GTG CTA
KLC-1C	AGG GAT CAG AAC AAG TAT AAA
KLC-2A	TGT AGA AAT AAA GAC GAT
KLC-2B	CAG CTG GTA CAA AGC CTG TAA
KLC-2C	AAA GAC GAT TTG AAT CTG AAA
SUN2	CCT GAG GGC CTT CGA CAA A

2.10 Antibodies

2.10.1 Primary antibodies

All the primary antibodies used in this thesis were obtained from different manufacturers. The catalogue numbers and the dilution information for both WB and IF are listed in Table 2.7.

2.10.2 Secondary antibodies

The secondary antibodies used in this thesis were obtained from different manufacturers. The catalogue numbers and the dilution information for WB and IF are listed in Table 2.8 and 2.9 individually.

Table 2.7 Primary antibodies

	Catalogue number	WB	IF
β-actin	A5316, Sigma	1:10,000	-
α-actinin	A7811, Sigma	-	1:500
α-tubulin	Ab5266, Abcam	1:1000	-
emerin	NCL-EMERIN, Novocastra	1:200	1:40
GAPDH	SC-25778, Santa Cruz	1:1000	-
GFP	Ab290, Abcam	1:1000	-
GFP	Ab13970, Abcam	-	1:1000
HA	Ab1424, Abcam	For Co-IP	
KLC-1/2	63-90, gift from Prof. S. Brady	1:500	1:100
Lamin A/C	2320S, Cell signalling	1:1000	1:100
Nesprin-1 (C-terminal region of nesprin-1 giant)	MANNES1A	-	1:2
	MANNES1E	1:10	-
Myogenin	SC-576, Santa Cruz	1:200	-
MHC	A4.1025, Alexis Corporation	1:1000	1:150
pELK	9181, Cell signalling	1:1000	-
pERK	4370, Cell signalling	1:1000	1:100
SUN1	Gift from Prof. S. Shackleton	1:1000	-
SUN2	Ab124916, Abcam	1:1000	-
SUN2	Gift from Prof. S. Shackleton	-	1:100
tERK	9120, Cell signalling	1:1000	-
V5	R96025, Invitrogen	1:500	1:100

Table 2.8 Secondary antibodies for WB

HRP-conjugated secondary antibodies	Catalogue number	Dilution
Amersham ECL Mouse IgG, HRP-linked whole Ab (from sheep)	NA931, GE	1:3000
Amersham ECL Rabbit IgG, HRP-linked whole Ab (from donkey)	NA934, GE	1:3000

Table 2.9 Secondary antibodies for IF

HRP-conjugated secondary antibodies	Catalogue number	Dilution
Goat anti-Chicken IgY (H+L), Alexa Fluor 488	A11039, Invitrogen	1:500
Goat anti-Mouse IgG (H+L), Alexa Fluor 488	A11001, Invitrogen	1:300
Goat anti-Rabbit IgG (H+L), Alexa Fluor 488	A11008, Invitrogen	1:300
Goat anti-Mouse IgG (H+L), Alexa Fluor 546	A11030, Invitrogen	1:300
Goat anti-Rabbit IgG (H+L), Alexa Fluor 546	A11035, Invitrogen	1:300
Goat anti-Mouse IgG (H+L), Alexa Fluor 647	A21236, Invitrogen	1:500

2.11 Laboratory materials

2.11.1 Stock materials

100bp DNA ladder	Biolab	N3231L
1kb DNA ladder	Biolab	N3232L
4-(2-Hydroxyethyl) piperazine-1-ethanesulfonic acid, N-(2-Hydroxyethyl) piperazine-N′-(2-ethanesulfonic acid) HEPES	Sigma	H3375-25G
Acetone	Sigma	439126
Acrylamide/Bis solution 30%	Bio-Rad	161-0158
Agarose	Sigma	A5093
AllStars Negative Control siRNA	QIAGEN	SI03650318
Amersham ECL Mouse IgG, HRP-linked whole Ab (from sheep)	GE	NA931
Amersham ECL Rabbit IgG, HRP-linked whole Ab (from donkey)	GE	NA934
Ammonium Persulfate	Bio-Rad	161-0700
Ampicillin sodium salt	Sigma	A0166
Antarctic Phosphatase	Biolab	M0289
Bio-Rad DC Protein Assay Reagent A & B	Bio-Rad	5000113 & 5000114
BioSafe^{TM} Coomassie Stain	Bio-Rad	161-0787
Bovine serum albumin	Sigma	A4503
Cell Scraper 24cm/30cm	TPP	99002/99003
Cell strainer 40μm	BD Falcon	352340
Chloroform	Sigma	288306-1L
Collagenase type II	Lorne labs/Worthington	LS004176
DABCO (1,4-Diazabicyclo [2.2.2] octane)	Sigma	D2522

DAPI (4',6'-Diamidino-2-Pheylindoledihydrochloride)	Sigma	D9542
Deionized H_2O (DiH_2O) 18.2Ω	Millipore purification system	
DEPC (diethylpyrocarbonate) treated water	Invitrogen	750023
DH5α™ Competent Cells	Invitrogen	18265017
Digitonin	Sigma	D141
Disc cork for Cryostat use 20mm diameter x 3mm depth	ThermoFisher	12688566
dNTP mix	Eurogentec	NU-0010-10
DPX Mounting Media	Merck	10197905000
Dried Skimmed Milk	Marvel	
Dulbecco's Modified Eagle's Medium (DMEM)	Sigma	D5671
ECL™ Prime Western Blotting System	GE Healthcare	RPN2232
EcoRI enzyme	Biolab	R0101S
Eosin	Raymond A Lamb	Lamb/100d
Escort III Transfection Reagent	Sigma	L3037-1ML
Ethanol (CH_3CH_2OH, EtOH)	Fisher	10428671
Ethylenediaminetetraacetic acid disodium salt dehydrate (EDTA)	Sigma	E5134
Fetal Bovine Serum - heat inactivated FBS	ThermoFisher	16140071
Fetal Bovine Serum - non-heat inactivated FBS	Sigma	F7524-500ML
FlexiTube GeneSolution for Klc1	QIAGEN	GS16593
FlexiTube GeneSolution for Klc2	QIAGEN	GS16594
FuGENE® HD Transfection Reagent	Promega	E2311
Fujifilm Corporation™ RX NIF Sheet X-ray Film	Fuji	12715325
GC-RICH PCR System	Roche	12140306001
Gel loading dye, Purple (6X)	Biolab	B7024S
Gelatin 2%	Sigma	G1393-100ML
Glacial acetic acid	Sigma	537020

Glucose	Sigma	G8270
Glutathione Sepharose 4B beads	GE	17075601
Glycerol	Fisher Scientific	BPE229-1
Glycerol	Sigma	G5561
Goat serum blocking solution	Vector	S1000
GoTaq® Green Master Mix	Promega	M7122
Harris' Haematoxylin	Raymond A Lamb	Lamb/230d
HiPerFect Transfection Reagent	Qiagen	301707
Horse Serum (HS)	Sigma	H1270
Isopropanol (C_3H_8O)	Sigma	19516
Isopropyl-1-thio-β-d-galactopyranoside (IPTG)	Sigma	I1284-5ML
JM109 Competent Cells	Promega	L2001
Kanamycin disulphate salt	Sigma	K1876
L-Glutamine 200mM	Sigma	G7513-20ML
L-Glutamine-Penicillin-Streptomycin solution (PSG)	Sigma	G1146
LB Agar	Sigma	L2897
LB Broth	Sigma	L3022
Lipofectamine™ LTX Reagent with PLUS™ Reagent	ThermoFisher	15338100
M-MLV Reverse Transcriptase	Promega	M1701
M199 medium	Sigma	M4530
Magnesium sulphate ($MgSO_4$)	Sigma	M7506-500G
Masson's trichrome staining kit	Polysciences	25088-100
Methanol (CH_3OH, MeoH)	Fisher	10428671
Millex-HV Syringe Filter, 0.45µm/0.22µm	Millipore	SLHV033RS/ SLGP033RS
Mowiol 4-88	Calbiochem	475904
Nancy-520	Sigma	1494
Nonidet P-40 (NP-40) Alternative	Calbiochem	492016

NotI enzyme	Biolab	R1089S
Oligo (dT) 15 primer	Promega	C1101
Opti-MEM® I Reduced Serum Medium	ThermoFisher	1158021
Optimal cutting temperature compound (OCT compound)	VWR International	720-1731
Pancreatin from porcine pancreas	Sigma	P3293-25G
Paraformaldehyde (PFA)	Sigma	P6148
pGEM T-easy vector system II	Promega	A1380
Phosphate buffered saline (PBS)	Sigma	D8537
Phosphate Buffered Saline (PBS) Tablets	Oxoid	BR0014G
Polybrene Infection/Transfection reagent	Millipore	TR-1003-G
Potassium Chloride	Sigma	P9333-500G
Precision Plus Protein™ All Blue Prestained Protein Standards	Bio-Rad	1610373
Protease Inhibitor Cocktail	Sigma	P8340
Protein A-Sepharose® 4B	Sigma	P9424-5ML
Protein G-Sepharose® 4B	Sigma	P3296-5ML
PureYield™ Plasmid Miniprep System	Promega	A1222
PVDF membrane with 0.45µm pore size	Millipore	IPVH00010
QIAquick Gel Extraction Kit	QIAGEN	28706
QuikChange® Site-Directed Mutagenesis Kit	Stratagene	200518
Random primer	Promega	C1181
Recombinant RNasin® Ribonuclease Inhibitor	Promega	N2511
Restore™ Western Blot Stripping Buffer	ThermoFisher	21059
RNA STAT-60	Amsbio	CS-110
S.O.C. Medium	Invitrogen	15544034
Sodium Chloride (NaCl)	Sigma	S7653
Sodium dodecyl sulphate solution (SDS) 20% in H_2O	Sigma	5030
Sodium Hydroxide (NaOH)	Sigma	S8045

Sodium phosphate monobasic (NaH_2PO_4)	Sigma	S8282-500G
Sucrose	Sigma	839
Superfrost Slides white	VWM	48311-601
Sybr green qPCR master mix	Eurogentec	RT-SY2X-03+NRWOUB
TEMED	Bio-Rad	492016
Tris base	Sigma	10708976001
Triton-X 100	Sigma	X100
Trypsin 1×-EDTA solution	Sigma	T3924
Tween-20	VMR	437082
X-gal solution	ThermoFisher	R0941
XL1-Blue Competent Cells	Agilent Technologies	200249
XmnI enzyme	Biolab	R1094S
Xylenes	Sigma	534056

2.11.2 Solutions

4', 6'-Diamidino-2-Pheylindoledihydrochloride (DAPI) solution	1µl DAPI, 10ml PBS
ADS buffer	116mmol/L NaCl, 20mmol/L HEPES, 0.8mmol/L NaH_2PO_4, 5.6mmol/L glucose, 5.4mmol/L KCl, 0.8mmol/L $MgSO_4$, pH=7.35, filtered
Agarose gel 1-2% (100ml)	1-2g agarose, 100ml 1× TAE, boiled, add 5µl Nancy-520
APS (w/v) 10% (1ml):	10mg Ammonium persulfate, 1ml DiH_2O
Bovine serum albumin (BSA) 3% (50ml)	1.5g BSA, 50ml PBS
Ethanol 70% for RNA wash (50ml)	35ml Ethanol, 15ml DEPC treated water
Goat serum blocking solution 5% (50ml)	2.5ml Goat serum, 47.5ml PBS
IP buffer-1:	10mM Tris pH=7.4, 150mM NaCl, 1mM EDTA, 1% Triton
IP buffer-2	10mM Tris pH=7.4, 50mM NaCl, 5mM EDTA, 1% Triton
LB Broth (medium)	20g LB Broth, 1L DiH_2O, sterile
Methanol - Acetone fixative (100ml)	50ml Methanol, 50ml Acetone
Mowiol Mounting medium	2.4g Mowiol 4-88, 6g Glycerol, 6ml DiH_2O, mix and rotation ON; 12ml 200mM Tris pH=8.5, stir at 50°C until dissolved, then add 2.5% DABCO
NP-40 (100ml) 0.5%:	500µl NP-40, 100ml PBS

NRC Enzyme solution (ES) (25ml)	20.5mg Collagenase, 15mg Pancreatin, 25ml ASD buffer, filtered
NRC Maintenance medium (500ml)	DMEM 375ml, M199 100ml, HS 10ml, PSG 5ml, L-glutamine (200mM) 10ml
NRC Plating medium (500ml)	DMEM 337.5ml, M199 82.5ml, HS 50ml, FBS 25ml, PSG 5ml
NRC Transfection medium (100ml)	73ml ASD, 21ml M199, 4ml HS, 2ml 200mM L-Glutamine
PFA 4% (50ml)	2g paraformaldehyde, 50ml PBS
Potassium Chloride (KCL) 5% (50ml)	2.5g KCL, 50ml PBS, through a 0.22µm syringe filter
Resolving PAGE gel 8% (~ 15ml):	7ml DiH_2O, 3.75ml 1.5M Tris pH=8.8, 4ml 30% acrylamide, 150µl 10% SDS, 200µl 10% APS, 8.5µl TEMED
Resolving PAGE gel 10% (~ 15ml):	6ml DiH_2O, 3.75ml 1.5M Tris pH=8.8, 5ml 30% acrylamide, 150µl 10% SDS, 200µl 10% APS, 8.5µl TEMED
Resolving PAGE gel 12% (~ 15ml):	5ml DiH_2O, 3.75ml 1.5M Tris pH=8.8, 6ml 30% acrylamide, 150µl 10% SDS, 200µl 10% APS, 8.5µl TEMED
Resolving PAGE gel 15% (~ 15ml):	3.5ml DiH_2O, 3.75ml 1.5M Tris pH=8.8, 7.5ml 30% acrylamide, 150µl 10% SDS, 200µl 10% APS, 8.5µl TEMED
Running buffer 10 X (500 ml)	72.2 g Glycine, 15.15g Trizma, 10ml 20% SDS, DiH_2O to 500ml
Sample loading buffer (4×)	40% Glycerol, 240mM Tris/HCl pH=6.8, 8% SDS, 0.04% bromophenol blue, 5% β-mercaptoethanol
Sodium Hydroxide (NaOH) 200mM (500ml)	4g NaOH, 500ml DiH_2O

Sodium Hydroxide (NaOH) 50mM (500ml)	1g NaOH, 500ml DiH_2O
Stacking PAGE gel 4% (~ 10ml):	6ml DiH_2O, 2.5ml 0.5M Tris pH=6.8, 100µl 10% SDS, 1.7ml 30% acrylamide, 200µl 10% APS, 8.5µl TEMED
Sucrose 10% (50ml):	5g Sucrose, 50ml DiH_2O
Sucrose 30% (50ml):	15g Sucrose, 50ml DiH_2O
Transfer buffer 10× (500ml):	72.2g Glycine, 15.15g Tris, DiH_2O to 500ml
Transfer buffer 1× (500ml):	50ml 10× Transfer buffer, 100ml Methanol, 350ml DiH_2O
Tris-acetate-EDTA (TAE) Buffer 50X (1000 ml):	242g Tris, 57.1ml glacial acetic acid, 18.6g EDTA, 943ml DiH_2O
Tris-Buffered Saline (TBS) 10× pH 8.0 (1000ml):	24.5g Tris, 175g NaCl, DiH_2O to 1000ml
TBS-T (500ml) 1×:	50ml 10X TBS, 1.5ml Tween-20, DiH_2O to 500ml
Triton 10% (50ml):	5ml Triton, 45ml PBS
Western blocking buffer (100ml):	5g Dried skimmed milk, 100ml 1× TBS-T

2.11.3 Laboratory equipment

Branson Sonifier 150D

Clifton Water Bath 95825

Corbett RotorGene-3000 qPCR Machine

ThermoFisher CryoStar NX70

Eppendorf Centrifuge 5415R Microcentrifuge

FastPrep® Lysis Beads & Matrix Tubes for Sample Disruption

Bio-Rad Horizontal Electrophoresis Chamber

InforsHT Ecotron Bacterial Shaker

InforsHT Ecotron Incubator Shaker

Leica ICC50 W Microscope

Leica SP5 Confocal Microscope

NanoDrop ND-1000

Eppendorf Mastercycler® Pro

Olympus CKX41 Inverted Microscope

Bio-Rad PowerPac™ HC High-Current Power Supply

Bertin Instruments Precellys®24 Homogenizer

Bio-Rad Protein Electrophoresis Chamber / Vertical

Rodwell Phoenix 40E Autoclaves PHX40

Tecan Genios Pro Fluorescence

Thermo Scientific HERAcell 150 Incubator

Thermo Scientific Heraeus Multifuge 3SR^{+} Centrifuge

Trans-Blot® SD Semi-Dry Transfer Cell, Bio-Rad

UVP Bio Spectrum AC Imaging System

Visualsonics Vevo 2100 Ultrasound System

2.11.4 Online tools

DNA Sequence Reverse and Complement

http://www.cellbiol.com/scripts/complement/dna_sequence_reverse_complement.php

DNA Sequencing Service

https://www.sourcebioscience.com/services/genomics/sanger-sequencing-service/

DNA Translator

http://www.fr33.net/translator.php

FuGENE HD Transfection database

https://www.promega.com/techserv/tools/FugeneHdTool/

IDT Primer Quest

https://www.idtdna.com/PrimerQuest/Home/Index

Mutation Taster

http://www.mutationtaster.org/

NCBI Nucleotide/protein Blast

https://blast.ncbi.nlm.nih.gov/Blast.cgi

Polyphen-2

http://genetics.bwh.harvard.edu/pph2/

Primer3Input Program

http://bioinfo.ut.ee/primer3/

Restriction Enzyme Double Digestion Finder

https://www.neb.com/tools-and-resources/interactive-tools/double-digest-finder

SIFT

http://sift.jcvi.org/

Chapter 3: Novel nesprin-1 mutants disrupted the NE-LINC complex and interfered with NE organisation

3.1 Introduction

The giant nesprin-1 and -2 isoforms bind to actin cytoskeleton via paired N-terminal CH domains, and are targeted to the ONM via a C-terminal KASH domain. The KASH domain interacts with the SUN domain of INM proteins SUN1/2 forming the SUN-KASH bridge that spans the PNS. Meanwhile, SUN1/2 bind to lamin A/C via their N-terminal nucleoplasmic domains, thus providing a physical connection between the nucleus and actin cytoskeleton [2, 27, 77]. The small nesprin-1 and -2 isoforms that have a truncated N-terminal but share SRs in common with the C-terminal regions of the giant proteins also localise at the INM where they bind to emerin, lamin A/C and SUN1/2, forming the NE complex [35]. These small isoforms, in particular, nesprin-1α_2 and nesprin-2α_1, are highly expressed in cardiac and skeletal muscle [1, 36]. The NE-LINC complex maintains the cellular structure and nuclear morphology, regulates the nuclear migration and positioning, propagates the mechanical force and participates in cell signalling and gene transcription [111, 112, 127, 176].

Mutations in the C-terminal region of the *SYNE-1/-2* (nesprin-1 and -2) have been identified in EDMD patients with DCM from small kindred families. HDFs derived from EDMD patients display defects in nuclear morphology, loss of NE integrity and mis-localisation of NE-LINC complex proteins lamin A/C, emerin and SUN2, as well as the altered binding between nesprin and those proteins [3]. A missense mutation in the C-terminal region of nesprin-1 was identified in a DCM patient, which resulted in the increased expressions of nesprin-1 and lamin A/C, indicating a perturbation of the LINC complex [4], suggesting these mutations are likely to play a key role in muscle-specific laminopathies.

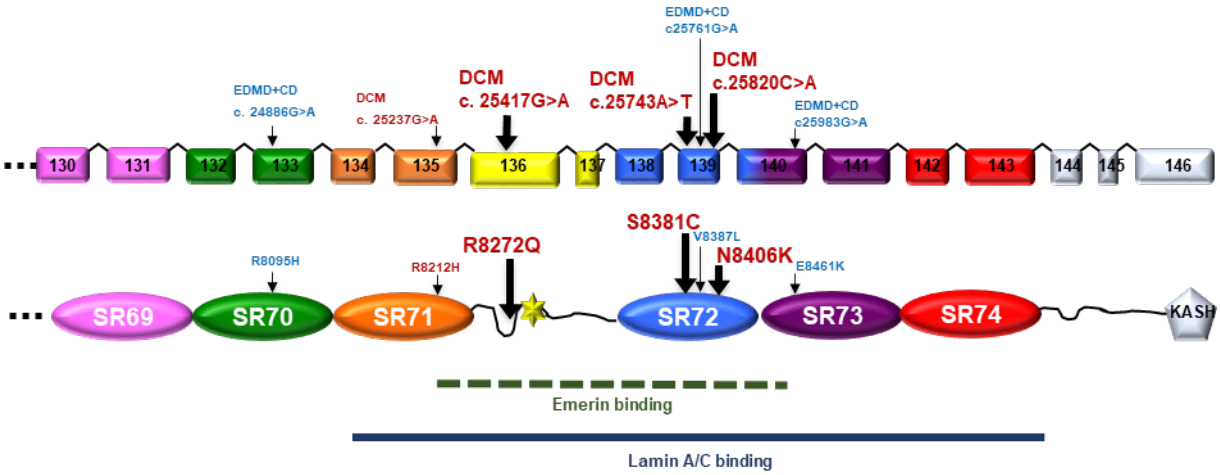
3.1.1 Identification of three novel nesprin-1 mutants in DCM patients

In order to study the roles of nesprin-1/-2 in cardiac disease, in collaboration with a lab in China, we recently screened the *SYNE-1* and *SYNE-2* genes in 218 sporadic DCM patients and 210 ethnically matched controls (Appendix I). 23 exons for nesprin-1 corresponding to nesprin-1α_1 and 1α_2 and 16 exons for nesprin-2 corresponding to isoforms nesprin-2α, 2β and 2ε were screened. This screening strategy was based on high and specific expression of these isoforms in cardiac and skeletal muscle as well as mapping of the lamin A/C, emerin and SUN1/2 binding sites to domains within these isoforms [36, 61, 66]. Twelve single nucleotide polymorphisms (SNPs)/variants in *SYNE-1* were identified, which included intronic sequence variations (n=2), synonymous (n=5) and non-synonymous, amino acid exchanges (n=5). Eight of the variants were not present in 420 control alleles of an ethnically matched reference population (Appendix II). None of nesprin-2 SNPs/variants were identified in the region screened. Interestingly, three of the identified nesprin-1 mutations were unique DNA variants, which resulted in R8272Q, S8381C, N8406K amino acid exchanges in the C-terminus of nesprin-1 giant as well as within the muscle specific isoform nesprin-1α_2 (equivalent to nesprin-1 giant 7875-8796), and identified in 7 unrelated DCM patients (Figure 3.1A, Appendix III). The amino acids changed by these missense mutations were in regions that were evolutionarily well conserved and within the mapped emerin and lamin A/C binding domains [22] (Figure 3.1). The rarity of these variants and their conservation and positioning suggest they may be causative for DCM in the patients examined. An ExAC database search revealed that population frequencies for the R8272Q allele were 0.0002145 (26/121204). Further *in silico* functional analyses showed that all three variants were predicted to cause significant functional impairment for nesprin-1 (Polyphen-2: possibly damaging, SIFT: damaging and Mutation Taster: disease causing).

In this chapter, I will focus on investigating if these three novel nesprin-1 mutations cause any impact on the structural and functional integrity of the NE-LINC complex:

1) Any nuclear morphology changes caused by these nesprin-1 mutations;
2) Any changes of NE-LINC complex components including their localisation at the NE and interactions with nesprin-1;
3) Any defects in mechanical signalling caused by any structural changes in the NE-LINC complex identified in Aim 2.

A.



B.

	R8272Q	S8381C	N8406K
Human nesprin-1	ERSGRDTPASVDSIPLEWDHDYD	MKLLGECSSSIDSV	LPGFVNLHSTETQT
Mouse nesprin-1	ERSGRDTPASVDSIPLEWDHDYD	MKLLGECSSSIDSV	FPGFVNLNSTETQT
Chick nesprin-1	ERSGRDTPASVDSIPLEWDHDYD	MKLLGECSSSIDSV	LSGLINLNSTETQT
Frog nesprin-1	ERSGRDTPASVDSIPLEWDHDYD	MKLLGECRESIDTV	ISGFINLNSTESQS
ZFish nesprin-1	ERSGRDTPASVDSIPLEWDHDYD	MKLLEECRGSIDAV	ISGFVNPNSSESQT

Figure 3.1 Identification of nesprin-1 variants in DCM patients

Mutation screening in *SYNE-1* and *-2* genes was performed in 218 DCM patients and 210 healthy controls, and identified 7 patients harbouring three novel nesprin-1 mutations (R8272Q, S8381C, N8406K, coloured in red and bold) in the C-terminus of nesprin-1 giant (A), equivalent to nesprin-1α_2, within an evolutionally conserved region containing the lamin A/C and emerin binding domains (A, B). Previously identified nesprin-1 mutants in DCM (R8212H, in red) [4] and EDMD-CD patients (R8095H, V8387L and E8461K, in blue) [3] were also shown (A).

3.2 Results

3.2.1 Overexpression of nesprin-1 mutants disrupted nuclear morphology

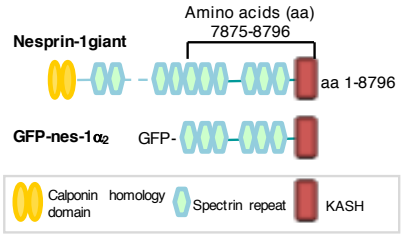
A defective nuclear morphology is a common feature observed in muscular tissue or HDFs derived from EDMD/DCM patients carrying by lamin A/C, emerin or nesprin-1/-2 mutants [3, 246, 247]. Therefore, the impact of the three nesprin-1 mutations on nuclear morphology was our first objective. We previously generated GFP tagged WT and mutant R8272Q, S8381C, N8406K constructs in the context of muscle specific isoform nesprin-1α_2 (amino acid 1-977), which is equivalent to nesprin-1 giant SR69-74 with KASH domain (nesprin-1 giant 7875-8796) where these mutations identified/localised (Figure 3.2A). U2OS cells were transfected with those plasmids and the nuclei were visualised using DAPI staining. Either exogenous nesprin-1α_2 WT or mutants were present at the NE, whilst GFP-only distributed through the cell (Figure 3.2B). In contract to the normal ovoid or spheroid morphology seen in the majority of control cells, abnormalities in nuclear morphology were seen following overexpression of the three novel nesprin-1α_2 mutants, especially in S8381C (Figure 3.2B & 3.2C). These analyses were based on counting cell circularity in more than 100 transfected nuclei in each experiment and in total three individual experiments were performed.

3.2.2 Nesprin-1 mutants reduced lamin A/C and SUN2 staining at the NE in U2OS cells

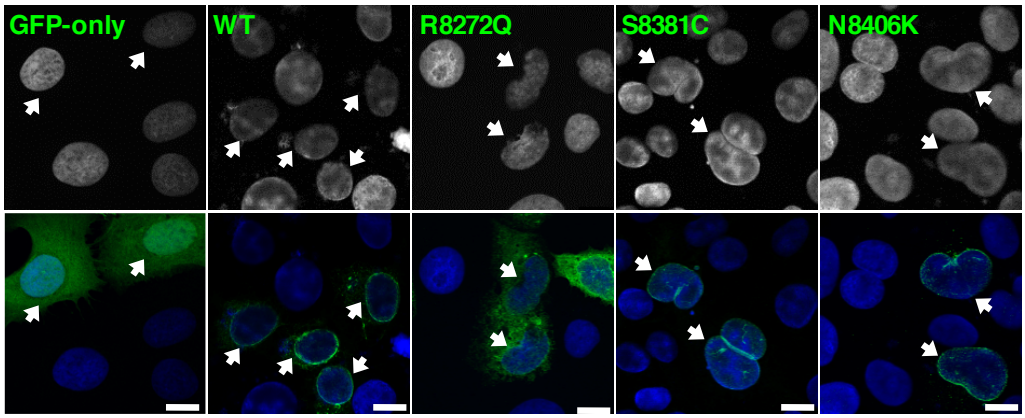
Previous experiments showed the mis-localisation of NE binding partners lamin A/C, emerin and SUN2 caused by the nesprin-1 and -2 mutations in HDFs derived from EDMD patients [3]. Thus, we set out to investigate whether these three mutations affected the localisation of nesprin binding partners lamin A/C, emerin and SUN2 at the NE. Initial experiment and quantification were done in U2OS cells. IF staining showed that lamin A/C was dramatically reduced or absent from the NE in cells that expressed exogenous mutants, especially S8381C (Figure 3.3A & 3.3C), while all three mutants caused weaker staining of SUN2 at the NE, when compared with WT

nesprin-1α_2 (Figure 3.3B & 3.3C). In addition, emerin was mis-localised by both WT and mutants when compared with GFP alone (Figure 3.3C).

A.



B.



C.

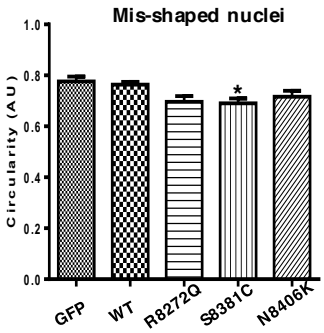


Figure 3.2 Overexpression of nesprin-1 mutants caused abnormal nuclear morphology.

GFP-tagged nesprin-1α_2 WT and mutants are shown schematically (A). The full length of this isoform is 977 amino acids, equivalent to amino acids 7875-8796 in nesprin-1 Giant. U2OS cells were transfected with either GFP-nesprin-1α_2 WT or mutants. IF staining showed overexpression of mutants, especially S8381C, led to abnormalities in nuclear morphology (B, arrowed). The misshapen nuclei were measured by circularity. Graphical representation of the frequency of misshapen nuclei caused by all three mutants (C). At least 100 transfected nuclei were counted in more than three individual experiments and the results were analysed by Student's t-tests, shown as mean±SEM. (*: $P<0.05$ compared with WT). Scale bar=12.5µm.

A.

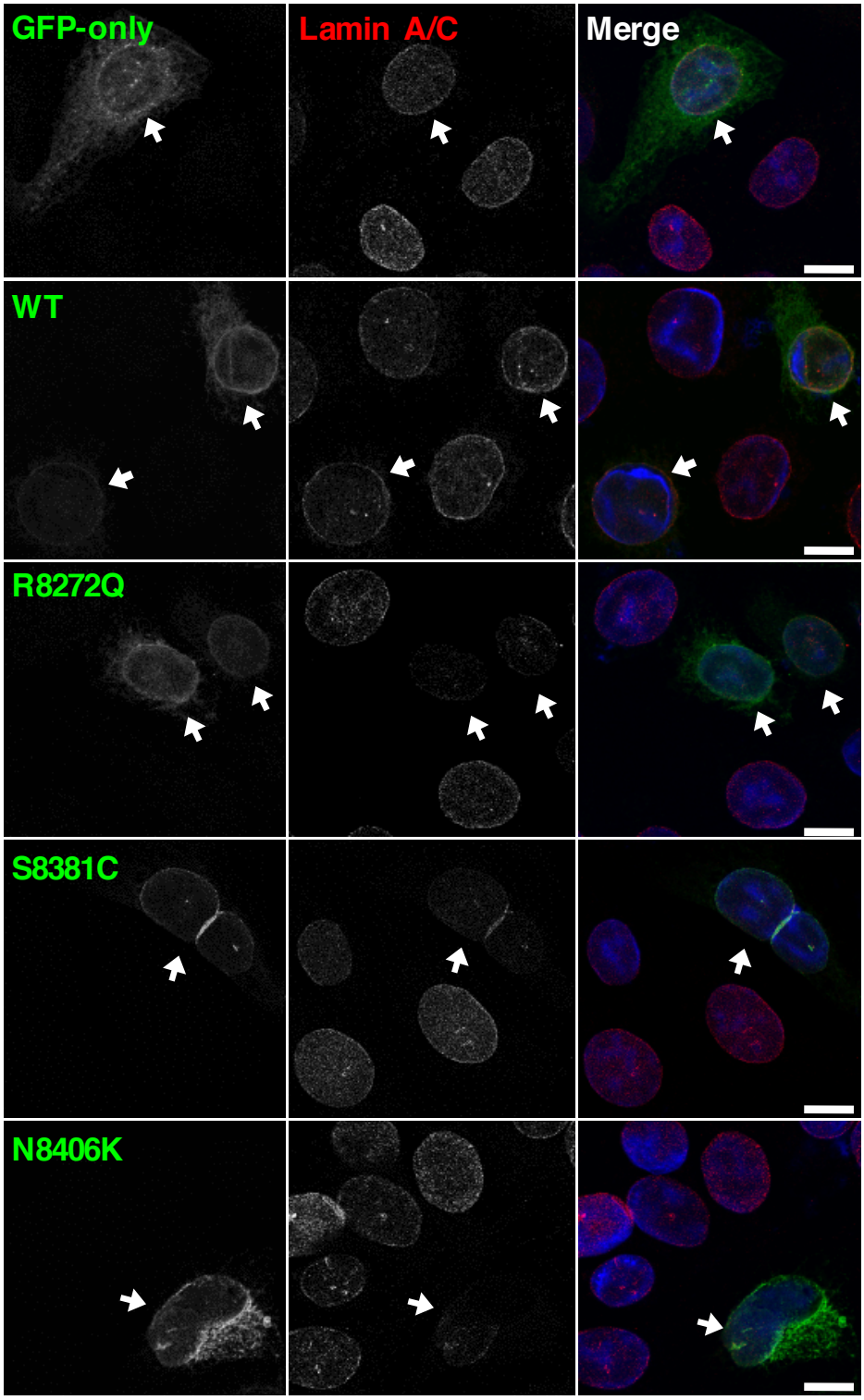


Figure 3.3 Overexpression of nesprin-1 mutants reduced NE staining of lamin A/C and SUN2 in U2OS cells.

IF showed exogenous expression of GFP tagged mutants, especially S8381C, caused weaker staining of lamin A/C at the NE (A, arrowed). Scale bar=12.5μm.

B.

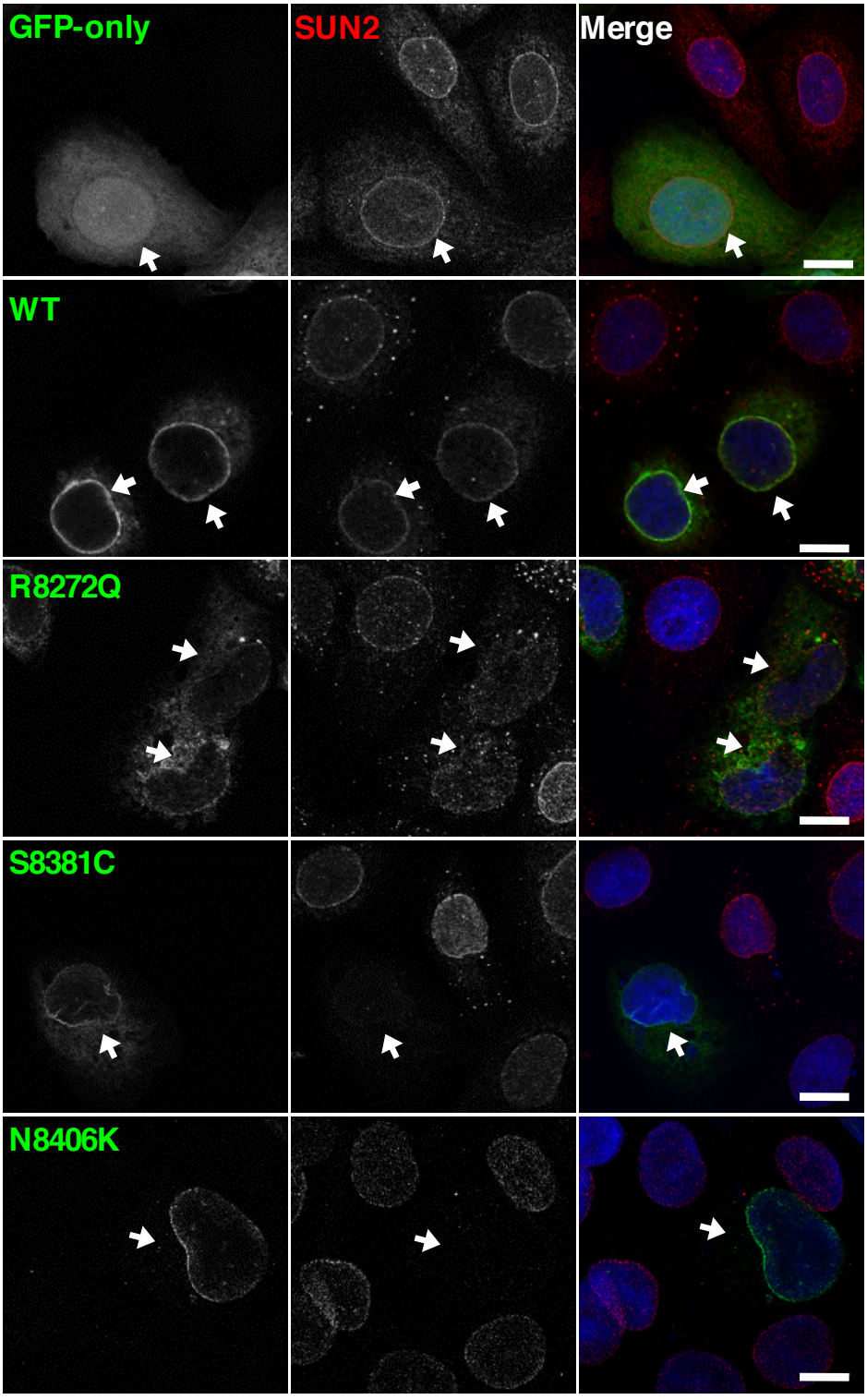


Figure 3.3 Overexpression of nesprin-1 mutants reduced NE staining of lamin A/C and SUN2 in U2OS cells.

All three mutants caused weaker staining of SUN2 at the NE (B, arrowed) when compared with a WT nesprin-1α_2 in U2OS cells. Scale bar=12.5μm.

C.

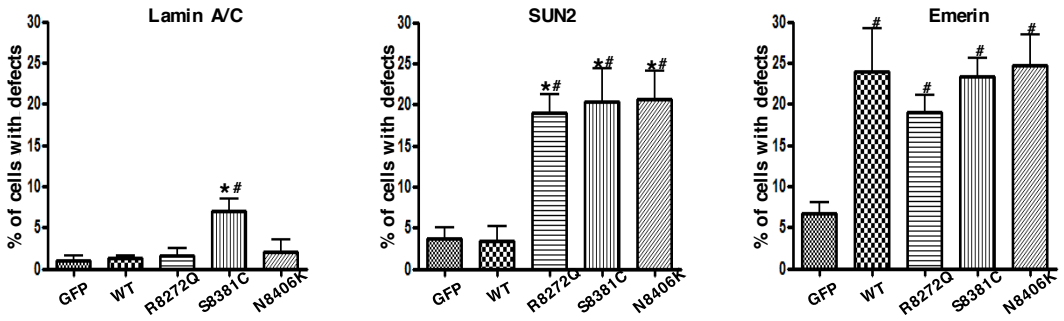


Figure 3.3 Overexpression of nesprin-1 mutants reduced NE staining of lamin A/C and SUN2 in U2OS cells.

Mis-localisation of lamin A/C, SUN2 and emerin in the transfected cells was quantified by comparing the NE staining in non-transfected cells on the same slide. Graphical representation of the frequency of defects in lamin A/C, SUN2, and emerin at the NE caused by all three mutants (C). At least 100 transfected nuclei were counted in each experiment and three individual experiments in total were performed. The results were analysed by one-way ANOVA, shown as mean±SEM (*: $P<0.05$ compared with WT; #: $P<0.05$ compared with GFP only). (Statistical analysis was done by Chen Li, King's College London.)

3.2.3 Nesprin-1 mutants reduced lamin A/C and SUN2 staining at the NE in neonatal rat cardiomyocytes

As these mutations were originally identified from DCM patients, we further confirmed their effects on neonatal rat cardiomyocytes (NRCs). NRCs were isolated from the neonatal rat hearts and stained with α-actinin as the sarcomeric marker to distinguish CMs from the potentially mixed fibroblasts. The same GFP tagged nesprin-1α_2 WT and mutants were transfected in NRCs. IF staining showed that both lamin A/C and SUN2 staining was present continuously at the NE in the CMs that overexpressed either GFP alone or nesprin-1α_2 WT, while in the cells transfected with all three mutants, lamin A/C (Figure 3.4A) and SUN2 (Figure 3.4B) was reduced or absent at the NE, indicating nesprin-1 mutants affected the localisation of their NE binding partners.

3.2.4 Nesprin-1 mutants disrupted the interactions between nesprin-1, lamin A/C and SUN2 within the NE complex

To investigate whether these mutants affected the bindings between nesprin-1 and its NE binding partners, GST pull-down assays were performed. GST-tagged WT and mutant nesprin-1α_2 constructs lacking the KASH domain (equivalent to nesprin-1 giant amino acids 7875-8662) were previously generated in our lab (Figure 3.5A). GST tagged nesprin-1 WT and mutants conjugated to sepharose beads were mixed with equal amount of protein lysates from untransfected U2OS cells (for lamin and emerin binding) or transfected cells with Myc-SUN2 (full length). All three mutants had significantly reduced binding to lamin A/C and SUN2, but not emerin when compared with WT nesprin-1α_2 (Figure 3.5B & 3.5C).

Furthermore, a reverse GST pull-down was also performed to confirm their binding. Protein lysates from U2OS cells transfected with either GFP-nesprin-1α_2 WT or each of three mutants were subjected to pull-down using either GST-lamin A (amino acids 356-665, containing nesprin-1/2 binding domain) or GST-emerin (amino acids 1-176, lacking the TM domain). The results confirmed all three mutants had significantly reduced binding to lamin A (Figure 3.6B), but not emerin (Figure 3.6A). Taken

together, these data indicated that these nesprin-1 mutations in the $1\alpha_2$ region cause disruption of the lamin A/C, SUN2 and nesprin-1 complex at the INM.

A.

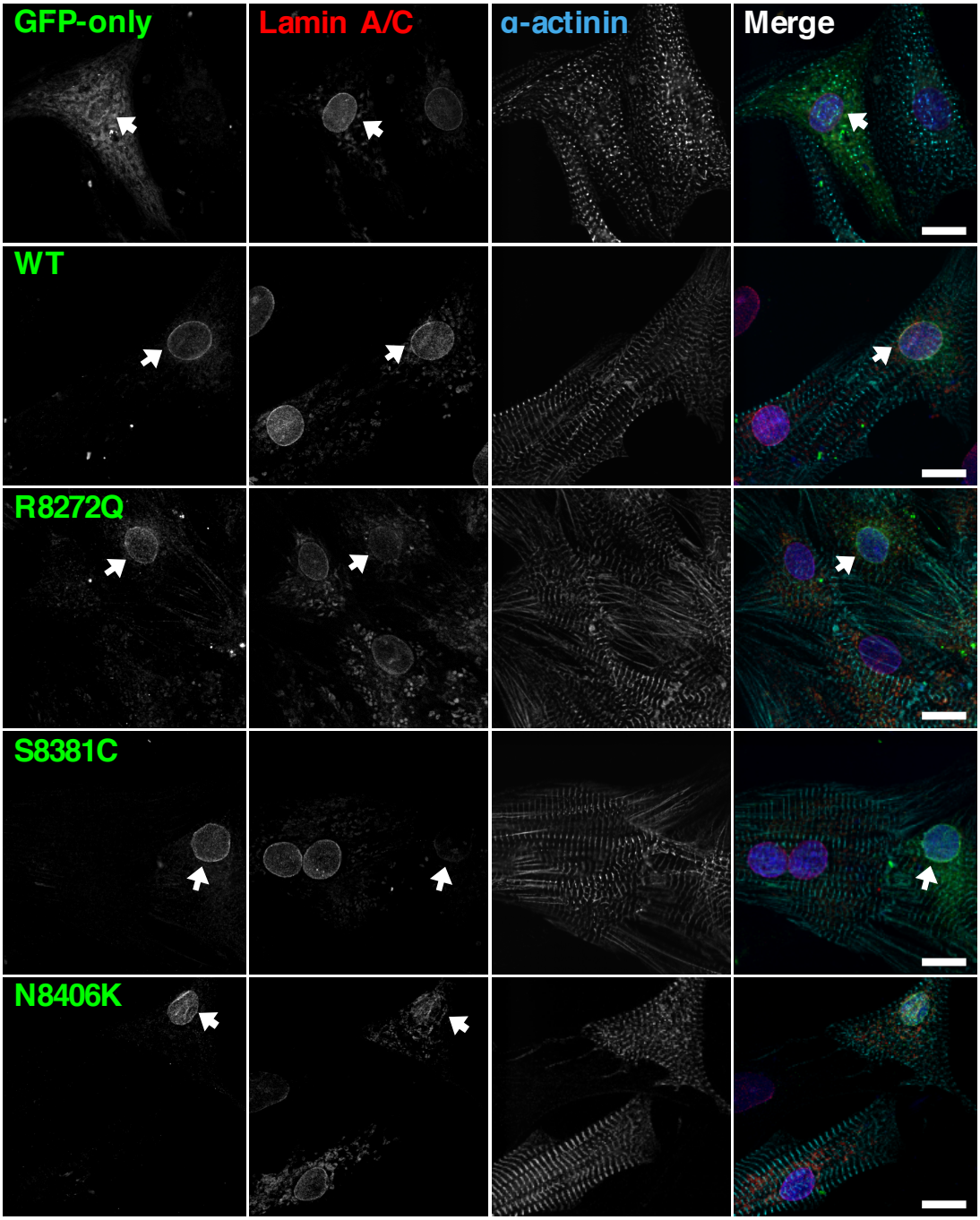


Figure 3.4 Overexpression of nesprin-1 mutants reduced NE staining of lamin A/C and SUN2 in NRCs.

IF showed lamin A/C (A) staining was reduced at the NE in the NRCs transfected with three mutants compared with nesprin-1α_2 WT and GFP only. Scale bar=15μm.

B.

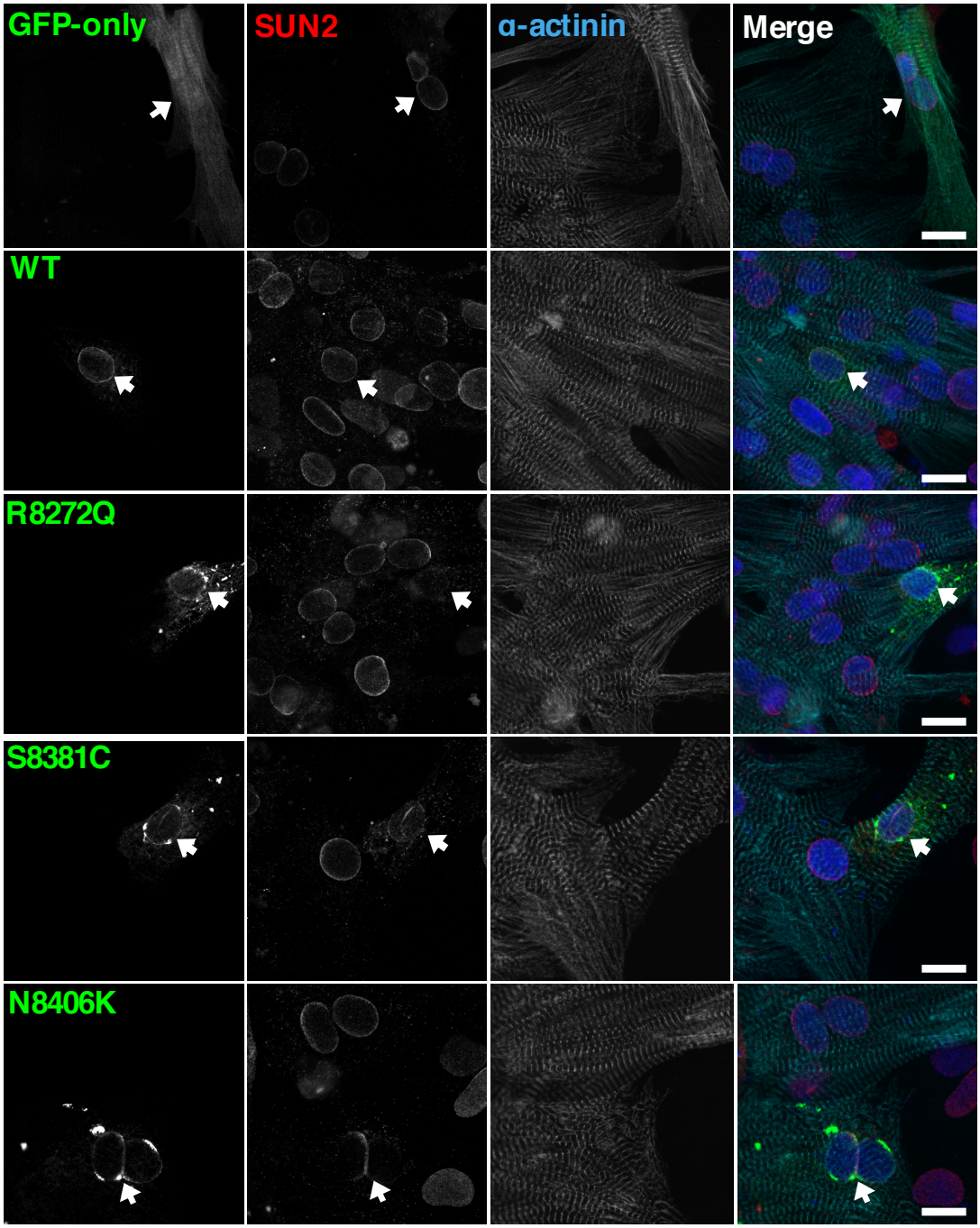


Figure 3.4 Overexpression of nesprin-1 mutants reduced NE staining of lamin A/C and SUN2 in NRCs.

IF showed SUN2 (B) staining was reduced at the NE in the NRCs transfected with three mutants compared with nesprin-1α_2 WT and GFP only. Scale bar=15μm.

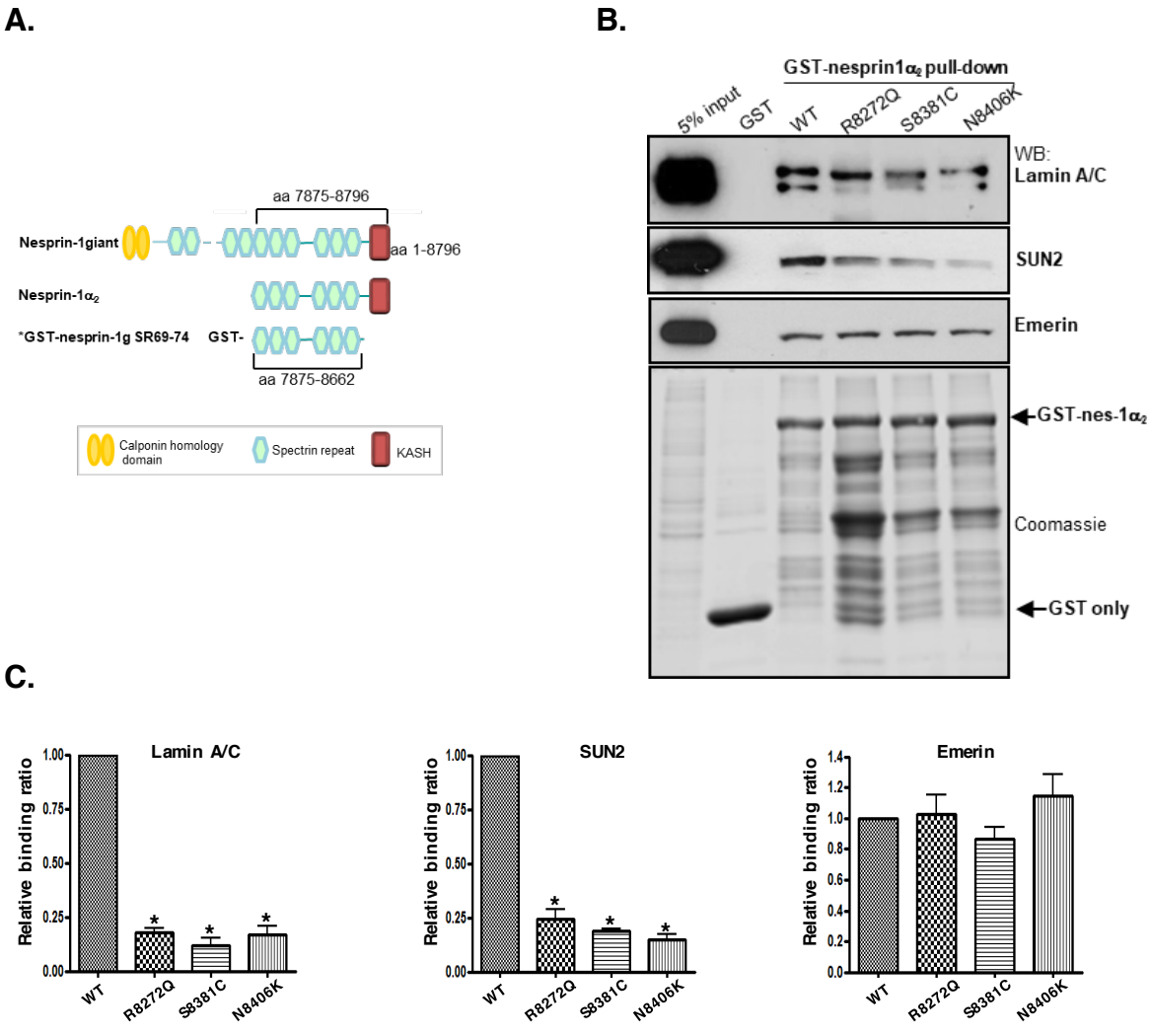
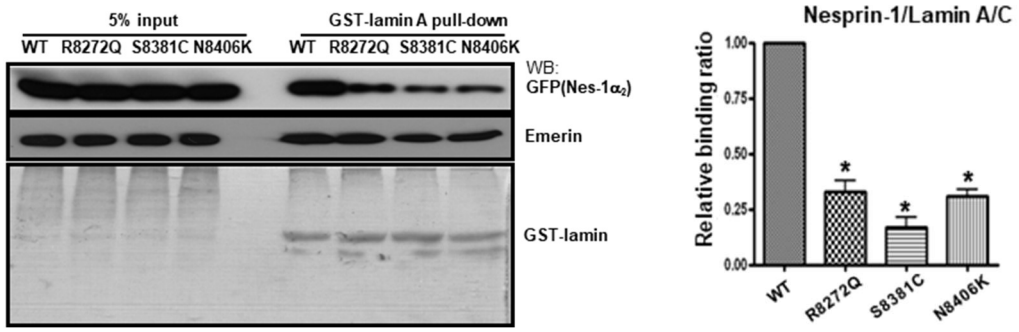


Figure 3.5 Nesprin-1 mutants affected the interaction between nesprin-1α$_2$ and lamin A/C or SUN2

GST-tagged WT nesprin-1α$_2$ SR1-6 (equivalent to nesprin-1 giant SR 69-74) and mutants were previously generated and shown schematically (A left panel, labelled with *), which constructs consisted of 837 amino acids, lacking KASH domain, equivalent to amino acids 7875-8662 of nespin-1 giant. GST pull-down using either GST-WT or mutant nesprin-1 beads showed all three mutants affected binding between nesprin-1 and lamin A/C or SUN2, but not emerin (A, B). The binding for each mutant was quantified by densitometry with respect to the input material and expressed as a ratio of the value obtained for WT protein. Three independent experiments were performed shown as mean±SEM, *P<0.05 using one-way ANOVA analysis. Coomassie blue staining gel also showed equal amount of GST-nesprin 1α$_2$ WT and mutants beads used. (The bindings experiments between nesprin with emerin and SUN2 were done by Chen Li, King's College London.)

A.



B.

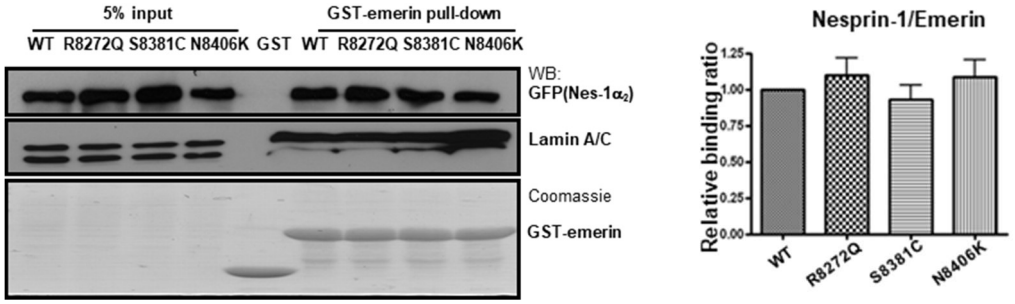


Figure 3.6 Nesprin-1 mutants affected the interaction between nesprin-1α2 and lamin A/C

Reverse GST pull-down by transfecting either GFP-nesprin-1α2 WT or each mutant and using either GST-lamin A (amino acids 356-665) (A) or GST-emerin (amino acids 1-176) beads (B). The binding for each mutant was quantified by densitometry with respect to the input material and expressed as a ratio of the value obtained for WT protein. Three independent experiments were performed shown as mean±SEM, *P<0.05 using one-way ANOVA analysis. Coomassie blue staining gel also showed equal amount of GST-lamin or emerin beads used. (This experiment was done by Chen Li, King's College London.)

3.2.5 Nesprin-1 mutants augmented ERK activity in EDMD patients

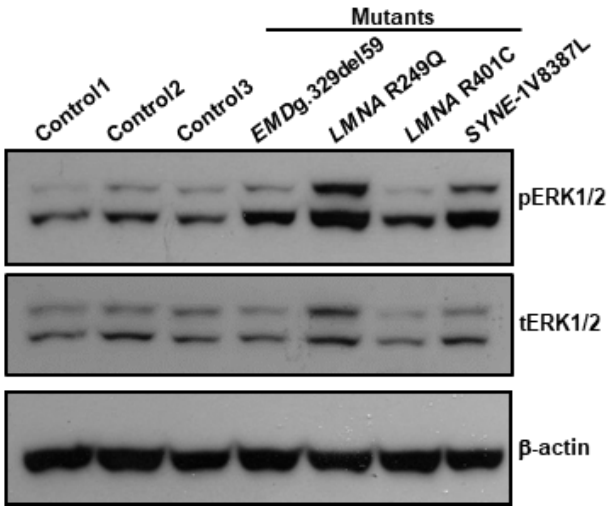
LMNA^{H222P} knock-in and *EMD* KO mouse models exhibited EDMD and DCM phenotypes [194, 195], which is similar to the muscle disorder caused by nesprin-1 and -2 mutations [3]. Analysis of genome-wide expression profiles in hearts from these mice revealed statistically significant differences in expression of genes in the MAPK cascades, including ERK and JNK. The hyperactivation of ERK and JNK can be rescued by using ERK and JNK inhibitors [207-209, 227, 228].

Up to date, there has been no evidence showing nesprin-1/-2 mutations' involvement in the augmentation of MAPK kinase in muscle disease. As we did not have access to the DCM patient samples, we started to examine if there were any changes of ERK pathway using the HDFs derived from EDMD patients carrying either nesprin-1, lamin A/C or emerin mutations. The control HDFs were derived from the healthy donors without any muscle defects. These cells were cultured and harvested at passage numbers restricted to between 11 and 14, to reduce the culture artefact caused by different passage numbers. Immunoblotting showed an increase of ERK1/2 in all the EDMD patients compared with other 3 individual controls (Figure 3.7A). The ratio of phosphorylated ERK1/2 to the total ERK1/2 was around 2-3 fold higher in EDMD patients compared to controls which was quantified with ImageJ through three individual experiments (Figure 3.7B).

In addition, we investigated if there were any changes in ERK pathway signalling when one of the major components of the LINK complex, SUN2 was depleted. IF showed endogenous nesprin-1 was mis-localised from the NE upon SUN2 siRNA knock down in human lung fibroblasts (HLFs), indicating SUN2 is indispensable for nesprin-1 to target to the NE. Meanwhile, IF staining also showed both nesprin-1 and SUN2 were present in mitochondria like organelle in cytoplasm, whereas depletion of SUN2 showed some changes of SUN2 and nesprin-1 staining on this structure (Figure 3.8A). Moreover, our preliminary WB data showed the SUN2 depletion was able to induce an increased trend of ERK1/2 phosphorylation (Figure 3.8B). However, further experiments are required to confirm the aberrant ERK pathway caused by SUN2 interference.

In summary, these data showed the aberrant activation of ERK1/2 could be caused by mutations in genes encoding NE-LINC complex components.

A.



B.

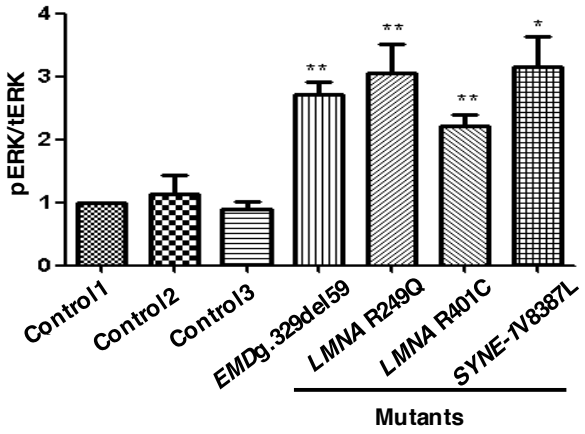
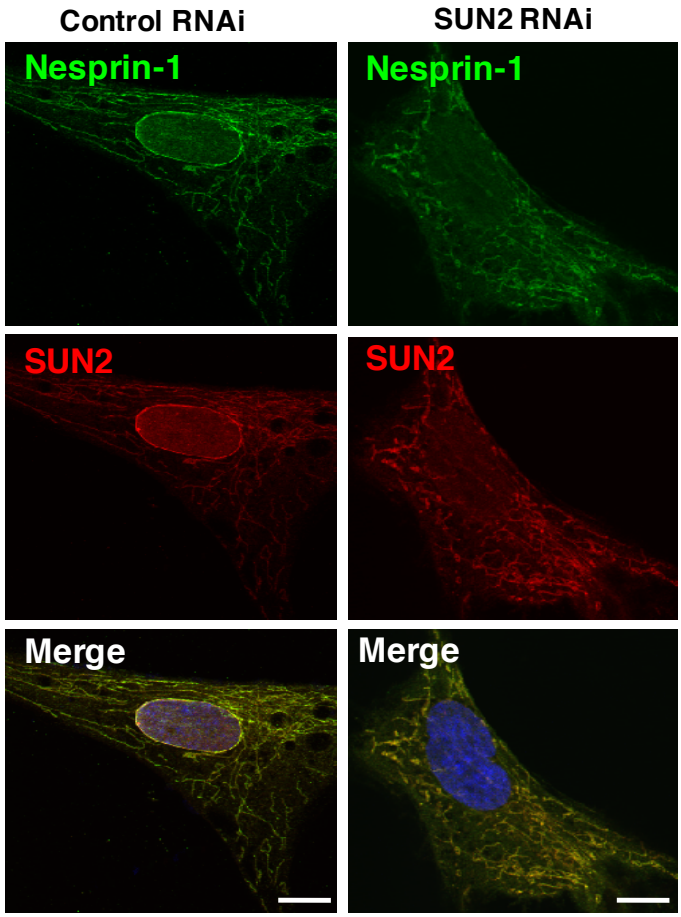


Figure 3.7 Nesprin-1/Lamin/Emerin mutants identified in EDMD-DCM patients showed aberrant activation of ERK pathway

WB showed that aberrant activation of pERK was observed in human dermal fibroblasts derived from EDMD-DCM patients carrying nesprin-1 (V8387L), lamin A/C (R249Q and R401C) and emerin (329del59) mutations. Three independent experiments were performed shown as mean±SEM, *P<0.05 using one-way ANOVA analysis.

A.



B.

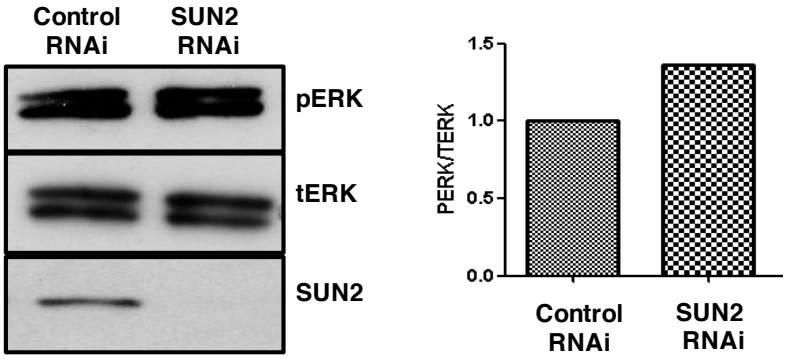


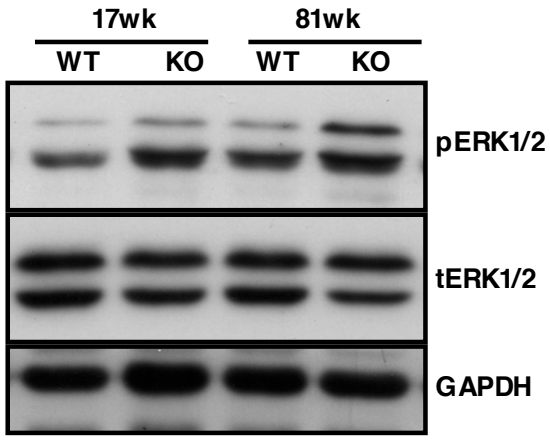
Figure 3.8 SUN2 RNA interference caused aberrant activation of ERK pathway in human lung fibroblasts

IF showed knocking down SUN2 led to mis-localised endogenous nesprin-1 at the NE in HLFs (A). WB demonstrated SUN2 was efficiently depleted and ERK pathway was preliminarily shown to be activated upon depletion of SUN2 when compared with the control RNAi. n=1. Scale bar=15μm.

3.2.6 Aberrant activation of ERK was induced in heart tissue derived from nesprin-1 KASH KO mice

The nesprin-1 KASH KO mouse model was generated by Prof. Elizabeth McNally in Northwestern University [221]. Litters exhibited EDMD phenotypes at the early stage (<32 weeks), and cardiomyopathy associated with CD at late stage (>52 weeks). Isolated CMs showed elongated nuclear shape with large invaginations of the NE, and reduced total amount of heterochromatin. The LINC complex components lamin A/C, emerin and SUN2 still localised at the NE, while IP revealed interaction between nesprin-1 and SUN2 were abolished, suggesting the SUN-KASH LINC complex was disrupted in this model [4, 221]. To further investigate if nesprin-1 defects lead to an aberrant activation of ERK in nesprin-1 KASH KO mice, heart tissue from WT and KASH1 KO mice at early stage (17 week) and late stage (81 week) were subjected to WB. The protein lysates demonstrated ERK signalling was significantly increased in nesprin-1 KASH KO mouse hearts compared to WT in both early stage (<32 weeks) and late stage (>52 weeks) (Figure 3.9A). Quantification by densitometry of the ratio of pERK to tERK revealed the KO group raised 2.5- and 3-fold higher than WT in early and late group respectively (Figure 3.9B). Of note, ERK activation was exacerbated over time, especially in the KO group (Figure 3.9). The findings in KASH KO mouse hearts further enhanced the hypothesis that the aberrant activation of ERK involved in cardiomyopathy and was induced by nesprin-1 mutants.

A.



B.

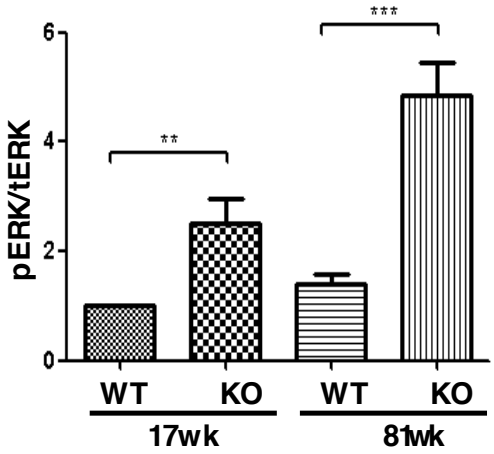


Figure 3.9 Nesprin-1 KASH knockout mice showed aberrant activation of ERK pathway

WB showed that augmented pERK activity in the nesprin-1 KASH KO mouse hearts compared to WT mouse hearts that were both collected at 17 and 81 weeks. Three independent experiments were performed shown as mean±SEM, *P<0.05 using Student's t-tests.

3.2.7 Nesprin-1 mutants led to abnormal activation of ERK1/2 pathway

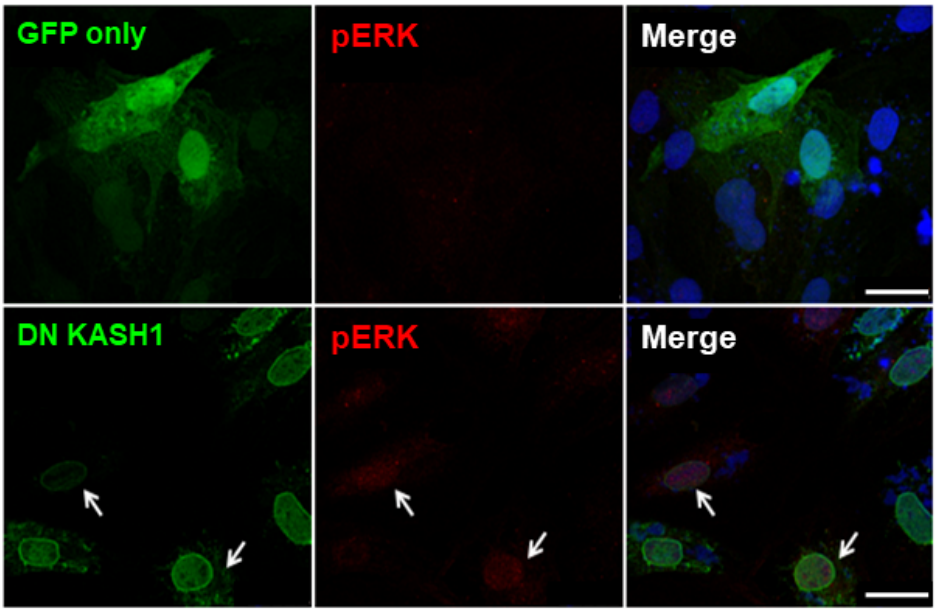
To determine whether these three novel nesprin-1 mutants could also induce aberrant activation of ERK1/2 pathway, GFP-nesprin-1α_2 WT and mutants, as well as a dominant negative nesprin-1 KASH (DN KASH1), which has previously been shown to localise to the NE and displace endogenous nesprin-1 and cause NE defects, were transiently transfected into C2C12 [2, 112].

Firstly, ERK activation was investigated in the C2C12 cells transfected with DN KASH1. IF showed more intense and predominant nuclear fluorescence signal of phosphorylated ERK1/2 in myoblasts that overexpressed DN KASH1 than the GFP only (Figure 3.10A). The augmented activation of ERK was further confirmed by the immunoblotting (Figure 3.10B).

Next, WT and nesprin-1α_2 mutants were all transfected in the C2C12 cells. Immunoblotting against the pERK and tERK demonstrated that the ERK activation was not altered in cells transfected with nesprin-1α_2 WT compared with GFP only, suggesting the nesprin-1α_2 WT does not perturb the ERK pathway in muscle cells. However, the activation of ERK was detected from the cells expressing exogenous DN KASH1 or three mutants when compared with nesprin-1α_2 WT (Figure 3.11).

Furthermore, phosphorylated Ets-like transcription factor 1 (pELK1), a downstream target of ERK1/2, was examined in H9C2 cardiac myoblasts. Consistently, overexpression of the GFP tagged-nesprin-1 mutants and DN KASH1 increased the expression of pERK1/2 and pELK1 compared with GFP alone or WT nesprin-1α_2, revealing that the MAPK cascades including ERK and downstream ELK were activated by these three novel nesprin-1α_2 mutations (Figure 3.12).

A.



B.

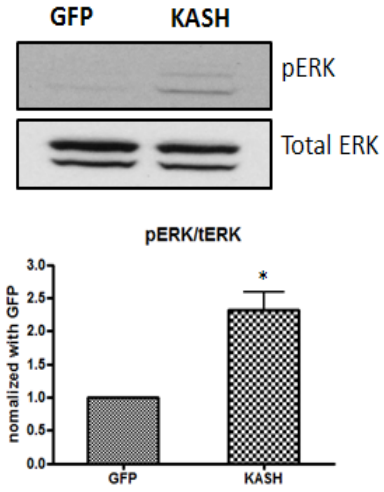
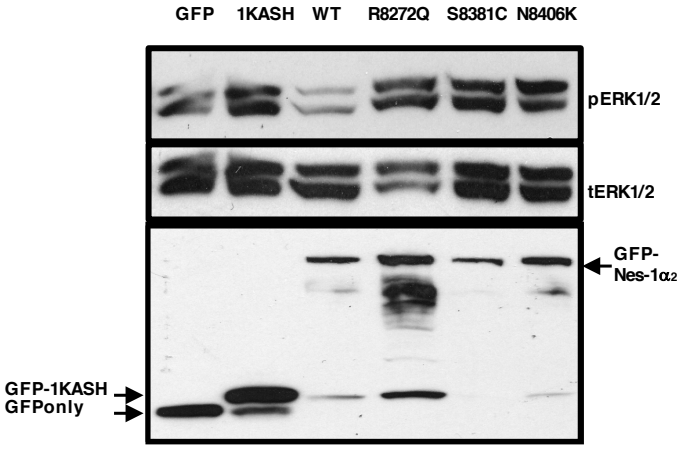


Figure 3.10 Nesprin-1 KASH augmented the ERK activities in C2C12

IF showed more intense pERK staining was presented inside of the nucleus in the C2C12 myoblasts transfected with DN KASH1 compared with the cells transfected with GFP only, suggesting the hyperactivation of pERK (A). The increased protein level of pERK was also substantiated by WB (B). Three independent experiments were performed shown as mean±SEM, *P<0.05 using Student's t-tests. (This experiment was done by Chen Li, King's College London.). Scale bar=25μm.

A.



B.

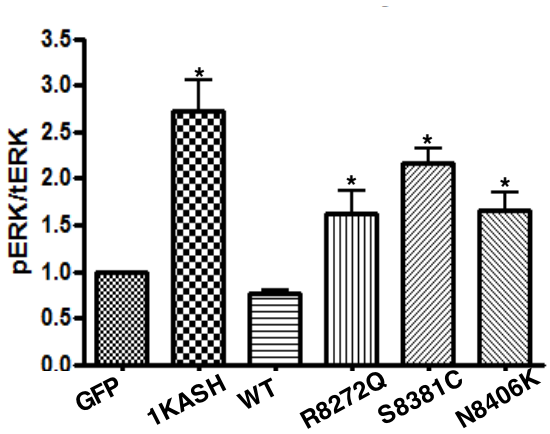


Figure 3.11 Nesprin-1 mutants caused aberrant activation of ERK pathway in C2C12 myoblasts

WB showed overexpression of all three nesprin-1 mutants and dominant negative KASH1 led to augmented pERK activity compared with WT nesprin-1. GFP empty vector was used for negative control and a dominant negative KASH1 construct as a positive control. Three independent experiments were performed shown as mean±SEM, *P<0.05 using one-way ANOVA analysis.

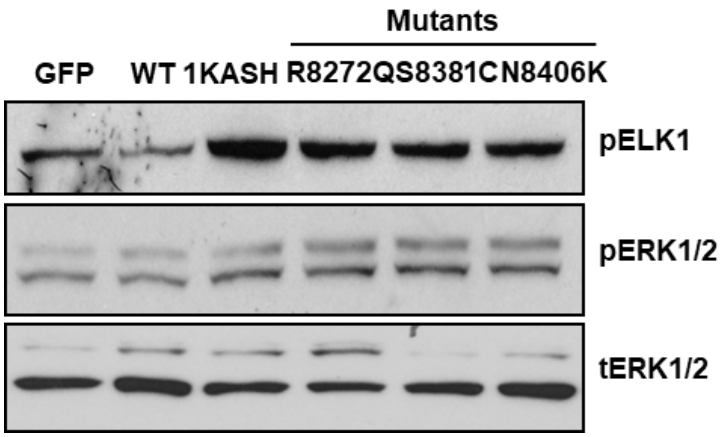


Figure 3.12 Nesprin-1 mutants caused aberrant activation of ELK pathway in H9C2 cells

Overexpression of three nesprin-1 mutants led to increased pERK1/2 and pELK1 activities in H9C2 cells (n=1). (This experiment was done by Chen Li, King's College London.)

3.3 Discussion

In this study, three novel *SYNE-1* missense mutations (R8272Q, S8381C and N8406K) were identified in DCM patients. Overexpression of the GFP tagged nesprin-1α_2 WT and mutants, the nuclear morphology was perturbed in the cells transfected with the nesprin-1α_2 mutant. Binding partners lamin A/C and SUN2 were also mis-localised from the NE, and GST pull-down indicated the binding affinity between nesprin-1α_2 and lamin A/C, SUN2 was reduced by nesprin-1 mutants. This part of data suggested the nesprin-1α_2 mutations (R8272Q, S8381C and N8406K) caused NE-LINC complex disruption. In addition, the disrupted LINC complex induced by the three novel nesprin-1α_2 mutations also caused hyperactivation of MAPK cascades (ERK1/2), indicating perturbed mechanotransduction.

3.3.1 Nesprin-1 mutations compromised structural and functional integrity of nesprin proteins

The three novel missense mutations (R8272Q, S8381C and N8406K) identified in DCM patients in this study resided within the unique adaptive domain (AD) region and the SR72 at the C-terminus of the nesprin-1 protein [22, 23] (Figure 3.1A). The SR72 and AD are extremely well conserved [23, 29]. It would therefore be reasonable to postulate that changes in these regions would not only impact the local structure, but also the function of the region.

3.3.1.1 Mutants S8381C and N8406K

The S8381C and N8406K mutations localised within SR72 on nesprin-1 giant, both are regions where uniform structure is not only critical but also conserved [23]. A serine was replaced with a cysteine in S8381C at the loop of α-helix structure (Figure 3.13). Serine is a hydroxyl-containing neutral polar residue, while cysteine is sulphur-containing non-polar hydrophobic residue [248]. Thus the cysteine may form the new hydrophobic core of the SR [6], leading to a completely disrupted secondary α-helix structure.

In N8406K, an asparagine was replaced with a lysine at the α-helix (Figure 3.13). Asparagine is a neutral polar residue and uncharged, whereas lysine is a basic polar

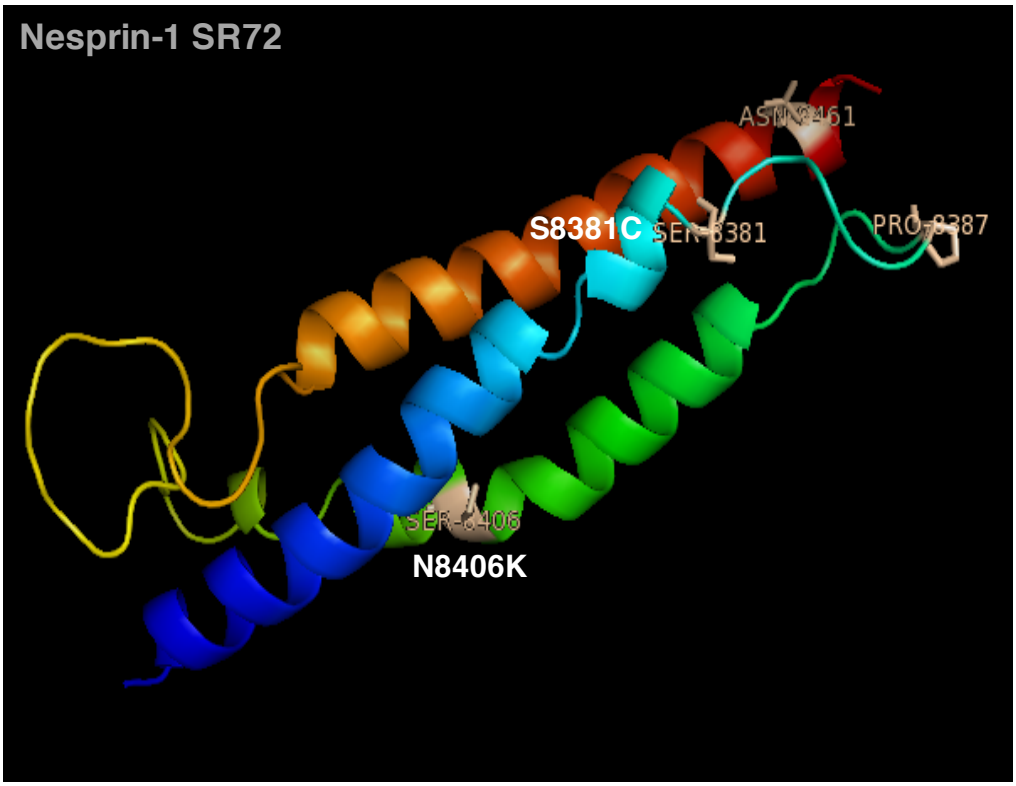


Figure 3.13 Computer models showed the structure of nesprin-1 giant SR72 and the localisations of mutations within this region

Two nesprin-1α_2 mutations localised at the SR72 of nesprin-1 giant, equivalent to the SR4 in the nesprin-1α_2 isoform. The S8381C localised at the loop at the adjacent of the two α-helices, while the N8406K localised at the α-helix (The Ribbon representation of nesprin-1 giant SR72 was generated using Modeller 9v2 and nesprin-1 mutations were labelled according to their positions in the predicted SR by Yueping Ou, King's College London.).

residue with positive charge [248]. They are functionally similar as polar residues, but charged lysine is more likely to participate in hydrogen bonding, thus changing the conformation of secondary α-helix structure.

These exchanges of amino acids may lead to a severe disruption of secondary structure, and ultimately tertiary structure in nesprin proteins. Another alternate possibility is that the mutations, ultimately disrupting SR structure, have a knock-on effect on AD structure. As the AD can adapt its conformation to suit adjacent structures, the convolution of SR72 in nesprin-1 may lead to an altered AD structure [23]. This may affect the ability of nesprin-1 to maintain structural integrity to the nucleus via both ONM and INM isoforms and impact the ability of nesprin-1 to bind either emerin or lamin A/C. Comparing the S8381C and N8406K mutations, the serine to cysteine mutant (S8381C) has more dramatic changes in amino acid properties compared to the asparagine to lysine mutant (N8406K). This may help to explain the more convoluted nuclear morphology and severe impacts on their binding partners lamin A/C, as well as augmented ERK pathway observed in S8381C mutation.

3.3.1.2 Mutant R8272Q

The R8272Q mutation localised within an AD region [22, 23, 29]. The central domain has relatively little secondary structure, but strongly stabilised SRs within and/or among nesprin isoforms by increasing their overall helicity, stability and cooperativity of folding [23]. In R8272Q, an arginine was replaced with a glutamine. Arginine is a strongly basic polar residue and suitable for binding to molecules with many negative charges on its surface, while the glutamine is a neutral polar residue [248]. The mutations in the AD region may not have the same structural implications as if they were in an SR. However, the AD is able to stabilise the SRs and the whole nesprin-1 structure. Therefore, the R8272Q mutation may disrupt the AD regulation of nesprin-1 structural conformation and dimerization, and impact the function of this protein.

The R8272Q mutation may have a more direct consequence on a nesprin binding partner KLC-1/2 [114]. Nesprin-2 has shown to bind with microtubule motor protein KLC-1/2 though a 'LEWD' at the AD region [114]. As nesprin-1 and -2 are highly homologous at this region, R8272Q localises just several amino acids upstream this binding motif [114]. Therefore, KLC-1/2 binding is likely to be negatively affected by nesprin-1 mutations especially R8272Q. We will further discuss the impact of the interaction between nesprin-1 mutations and KLC-1/2, as well as their functions in regulating nuclear migration and positioning in next chapter.

3.3.2 Disrupted NE-LINC complex was caused by the nesprin-1 mutants

Mutations in the *LMNA* gene, encoding A-type lamins, cause a number of different tissue specific laminopathies, including the muscle specific disorder: DCM and EDMD [249]. The molecular pathogenesis of these diseases is unknown but in some cases, may be related to disruption of the NE-LINC complex. Mice lacking A-type lamins display phenotypes that are reminiscent of human muscular dystrophies and cardiomyopathies [250]. CMs derived from homozygous *LMNA* KO mice are characterised with grossly misshapen cell nuclei with clumping of peripheral heterochromatin, disorganised nesprin-1α and actin filaments, suggested a structurally weakened NE [250, 251]. MEFs from *LMNA* null mice were subjected to mechanical strain, and showed the increased nuclear deformation, defective mechanotransduction, and impaired viability due to lose of the intact NE-LINC complex [214]. Mutations in both nesprins and SUN1/2 have also been implicated in EDMD-DCM, whereby mutants cause abnormal localisation of the LINC complex proteins including lamin, emerin and SUN, and disrupted nesprin/lamin/emerin/SUN interactions, leading to defects in nuclear morphology and nuclear-cytoskeletal coupling [3, 4, 86, 87]. Furthermore, the disruption of endogenous LINC complexes by recombinant DN KASH constructs of nesprins -1, -2 and -3 also causes a significant loss of mechanical stiffness [2, 112, 178].

The three nesprin-1 mutations (R8272Q, S8381C and N8406K) identified in this study has altered protein structural properties, changed the associations between nesprin SRs and lamin A/C at the INM (for nesprin-1α_2) or SUN proteins at the ONM

(for nesprin-1α_2 and -1 giant isoforms), leading to nuclear deformation and uncoupled NE-LINC complex.

Interestingly, the R8272Q mutant was able to bind lamin A at comparable levels to the WT nesprin-1, in contrast to weak binding to lamin C. Our current understanding of the interactions between nesprins and lamin A and lamin C remains incomplete. HDFs from limb-girdle muscular dystrophy patients carrying homozygous *LMNA* mutants Y259X which led to absence of both lamin A and lamin C. In those cells, nesprin-1α exhibited aberrant localisation in the ER, however it can be restored to the NE by transfection either lamin A or lamin C [252]. Another study showed in normal skin where lamin A/C is differentially expressed, strong nesprin-2 expression was found in all epidermal layers, including the basal layer where only lamin C is present, indicating that nesprin was able to localise properly dependent on lamin C protein only [253]. Altered ratios of lamin A to lamin C has been shown in some types of laminopathies [254], the dynamic and aberrant binding of nesprin-1 with lamin A or lamin C requires further investigation.

We did not observe a defect in binding between nesprin-1 mutants and emerin, which is consistent with the notion that mutations in emerin are primarily associated with EDMD rather than DCM. Moreover, the nesprin-1α can bind tightly the emerin, and the binding affinity is relatively much higher than the binding with lamin A/C [61]. Overexpression exogenous nesprin-1α_2, including WT, may dislodge endogenous nesprin from the NE with tightly bounded emerin together or the excessive overexpression of nesprin in the cytoplasm may compete for binding with the emerin [35]. Therefore, either exogenous nesprin-1α_2 WT or mutants, will result in mis-localisation of emerin.

The data above support possible involvement of LINC complex disruption in the pathogenesis of DCM. Future studies on structure/flexibility of the SRs that are predominantly present in the muscle-specific nesprin isoforms will be required to confirm this hypothesis.

3.3.3 Augmented activation of MAPK cascade was associated with disrupted NE-LINC complex

Several studies on *LMNA*^{H222P} knock-in mice have indicated activation of MAPKs in the development of DCM and EDMD [224]. In *LMNA*^{H222P} mice, pERK1/2

and pJNK are induced and activate a series of downstream target genes, including bcl-2, Elk1, junD and c-Jun in CMs from the mouse hearts as well as skeletal muscle tissue [194]. Transcription factors encoded by these genes can in turn regulate the expression of additional genes, including those encoding proteins involved in sarcomere structure, cardiomyofibre organisation and other aspects of heart function [194, 204, 205]. The aberrant ERK activity is further proved in other cell lines such as COS7 and HeLa which were transfected with *LMNA*^{H222P}, or depletion of lamin A/C in C2C12 and Hela cells, as well as in *ex vivo* fibroblasts from EDMD/DCM patients carrying lamin A/C mutations [194, 206, 255]. Using MAPKs inhibitor, fibrosis can be reduced, heart function restored, increased the skeletal strength, and successfully rescue the DCM and EDMD phenotypes in *LMNA*^{H222P} mice [207-209]. Those findings indicate that the activation of MAPK signalling could be a cornerstone in the development of DCM.

Our data showed that enhanced pERK activity is also observed from fibroblasts derived from EDMD-DCM patients, the heart tissue derived from nesprin-1 KASH KO mice, and nesprin-1 mutants transfected C2C12 and H9C2 cells, suggesting that nesprin and lamin A/C function through a similar pathway and trigger up-regulation of ERK. Moreover, the hyperactivation of pERK was exacerbated with the increased age in nesprin-1 KASH KO mouse hearts, while the clinical cardiomyopathies symptoms were deteriorating [4], indicating the dynamic changes of the ERK pathway is associated with the severity of cardiomyopathies.

In addition, there is evidence highlighting that nesprin-2 directly interacts with ERK1/2 via their SRs and recruit them to PML NBs to regulate the cell cycle and DNA damage response in VSMCs [42, 210]. Evidence also suggests that lamin A/C have an altered biochemical interaction with ERK1/2 to regulate the activator protein 1 (AP-1), which is a transcription factor that regulates gene expression and key cellular processes [109, 256]. Thus, future work will examine how NE proteins regulate ERK activity potentially via influencing interactions between A-type lamins, NE proteins and components of MAPK cascades, as well as nuclear translocation of activated MAPKs.

Of note, there is an interesting finding in addition to augmented ERK activities in HLFs with deletion of SUN2: IF staining showed endogenous nesprin-1 and SUN2 localise at mitochondria like organelle in cytoplasm and deletion of SUN2 may led to perturbed structure of this organelle. However, it still need to be further investigated by using Mito Tracker to show if the structural integrity of mitochondria is affected.

Moreover, this finding is in agreement with previous studies that ANC-1 (the ortholog of nesprin in *C. elegans*) and Uth1p and Sun4p (the ortholog of SUN protein in *Saccharomyces cerevisiae*) both localise at mitochondria whereas ANC-1 mutants display defective mitochondrial positioning [182, 257]. Further experiments are needed to characterise: 1) if endogenous SUN2 also localise at mitochondria in mammalian cells similar to endogenous nesprin-1 [3]; 2) the dysfunction of LINC complex on the structure and function of mitochondria, especially in muscle cells.

3.3.4 Summary

Novel nesprin-1 mutations identified from the DCM patients have a significant impact on nuclear structural integrity and lead to augmented cell signalling:

1) Structural disruption: alteration of nuclear morphology, mis-localisation of its NE-LINC complex binding partners lamin A/C and SUN2 and reduction of their interactions, leading to disrupted NE-LINC complex *in vitro*;
2) Aberrant cell signalling: augmented ERK activation caused by nesprin-1 mutants *in vitro* and *ex vivo* which may be cause by the direct impact of NE structural disruption or impaired mechanotransduction;
3) Nesprin-1 was previously identified as a VSMCs differentiation marker [15], and evidence has shown it participates in muscle cell differentiation [35, 37, 190]. Therefore, the effects of nesprin-1 mutations on nuclear migration/position and gene regulation during myogenesis will be further characterised in the next chapter.

Chapter 4: Novel nesprin-1 mutants perturbed myogenesis

4.1 Introduction

Nesprin-1 was first identified as a VSMC differentiation maker. A 2.1kb cDNA clone, (1RA1) was identified from the differentiated rat aortic VSMCs, which further helped to identify the human ortholog of 1RA1, which was renamed as nesprin-1 [1]. The identification of nesprins indicated that they are tightly related to the differentiation process.

Nesprins generate multiple isoforms by extensive alternative initiation, termination and splicing. Those isoforms contain different numbers of SRs, vary in size and are with or without KASH domains and CH domains. They exhibit tissue specific expression profiles [34]. For example, in muscles, nesprin-1α_2 and nesprin-2α_1 are highly expressed in both heart and skeletal muscle, nesprin-2β is only highly expressed in skeletal muscle, whilst nesprin-2ε_2 is heart specific [34]. Nesprin-1 is shown to be concentrated in synaptic nuclei postnatally in the NMJ. It remains synaptically enriched following muscle fibre degeneration and/or regeneration, and presents at high levels in the central nuclei of dystrophic myotubes [13]. In addition, nesprin-1α can bind to muscle A-kinase anchoring protein (mAKAP) to control the Ca^{2+} release channel of the sarcoplasmic reticulum within CMs [258]. The data suggests essential roles of nesprins in muscle differentiation and function.

4.1.1 Nesprin and myoblast differentiation

In normal conditions, muscle cell differentiation involves a series of steps: myoblasts enter a quiescent phase where myoblast fusion starts; myotubes are created by fused myoblasts, in which nuclei are positioned at regular intervals; then, the myotubes undergo a phenotypic change, characterised by myofibril assembly [259, 260]. The differentiation process also requires the sequential activation of myogenic regulatory factors (MRFs), such as Myogenic factor 5 (Myf5), Myoblast determination protein (MyoD), myogenin and MRF4. During development, up-regulation of MyoD and/or Myf5 drives myogenic cells to become myoblasts. Proliferating myoblasts withdraw from the cell cycle to become terminally differentiated myocytes that

express myogenin and MRF4, and subsequently muscle-specific genes such as myosin heavy chain (MHC) and the muscle creatine kinase (MCK) [260-262].

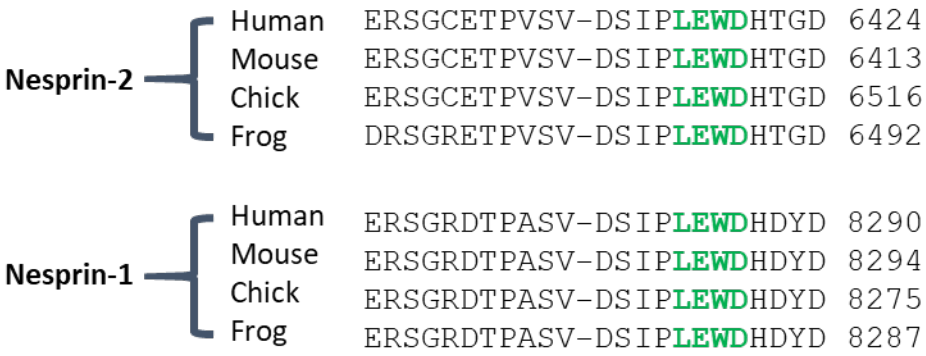
The dynamic change of small and giant nesprin isoforms has been shown to be involved in muscle differentiation. In human myoblasts, the expression of giant nesprin-1 is present and nesprin-1α_2 is relatively very low. During myogenesis, nesprin-1α_2 is massively upregulated and this is accompanied with a two-fold increase in nesprin-1 giant [37]. *In vitro* differentiation models, nesprin-2 isoforms have been shown to re-localise from the NE of C2C12 myoblasts to the sarcomere of myotubes [35]. Knocking down nesprin-1 prevents the mouse embryonic stem cells from differentiating into CMs [158]. *In vivo*, during the transition from immature to mature muscle fibres, nesprin-2 giant partly replaces nesprin-1 giant at the NE and short isoform nesprin-1α_2 becomes dominant [38].

The LINC complex associated EDMD and DCM disorders have been implicated with the defects of myogenesis. The *LMNA* R453W mutation from EDMD patients is shown to severely impair C2C12 myoblast differentiation with a reduction of myogenin expression [263, 264]. Myoblasts from EDMD carrying compound heterozygous SUN1 mutations exhibit accelerated differentiation, both in terms of the total numbers of myotubes and the numbers of nuclei per myotube [87]. In another case, myoblasts from the EDMD patients carrying nesprin-1 or -2 mutations show the impaired differentiation with less well defined sarcomeric structures and diffusely distributed nesprin-1 and -2 [3]. In summary, those mutations from EDMD carrying either nesprin, lamin A/C or SUN perturb muscle differentiation, indicating the NE-LINC complex plays an important role in myogenesis. Malfunction in the NE-LINC complex caused by overexpressed DN KASH2 or DN SUN1 perturbed C2C12 differentiation with dysregulated the MRFs such as MyoD, myogenin and MHC [190]. Those data further support that the NE-LINC complex participates in mechanotransduction and gene regulation during muscle differentiation. More studies regarding to the underlying mechanism are required to help us to understand the pathogenesis of muscular dystrophies.

4.1.2 Nesprin interacts with microtubule motor protein kinesin-1 at the NE

Mis-positioned myonuclei are not only a symptom of muscle disease but also are a direct cause. In healthy and mature muscle fibres, myonuclei are spaced throughout the periphery of the muscle fibre with even distance between nuclei. However, in diseased muscles, the nuclei are often clustered within the centre of the muscle cell [265]. NE-LINC complex has been discovered to participate in nuclear movement via connecting the NE to the microtubule to maintain the position of the nucleus and to move it during cell activities such as the cell migration and differentiation [180, 181]. Indeed, recent data have shown that the C-terminal region of nesprin-2 mediates myonuclear positioning by attaching the microtubule network to the NE during embryonic muscle development and cell migration [114]. These interactions occur via the microtubule motor proteins, dynein and kinesin, the latter being a heterotetramer of two KHC subunits -Kif5A, Kif5B, or Kif5C- and two KLC-1/2 subunits. Nesprin-2 is shown to interact with KLC-1/2 at the ONM via a newly identified four-residue tryptophan-acidic (W-acidic) "LEWD" binding motif within an adaptive domain (AD) at its C-terminus, which is present in all muscle-specific isoforms [22, 23, 114]. Disruption of the LINC complex with a dominant-negative nesprin-2 KASH impairs the recruitment of kinesin-1 to the NE and induces nuclear aggregation in myotubes [188]. As both nesprin-1 and -2 are highly conserved in this C-terminal region, it is likely that nesprin-1 may also mediate the nesprin/KLC interaction via the "LEWD" binding motif but so far this has not been tested. The three novel nesprin-1 mutations localised near the "LEWD" binding region, notably R8272Q which was only 11 amino acids upstream of the binding motif (Figure 4.1)

A.



B.

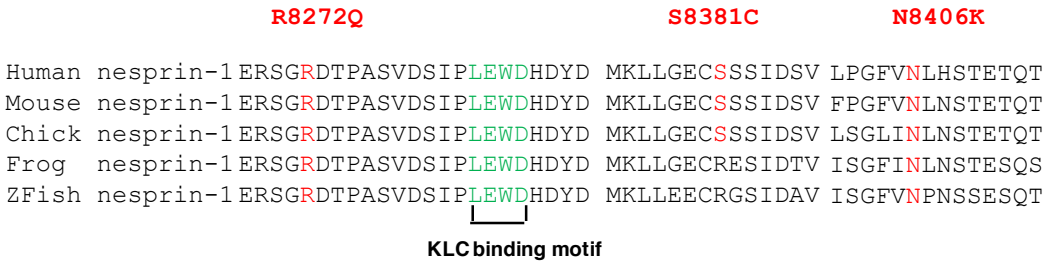


Figure 4.1 Nesprin-1 mutations were identified and localised at the binding region with microtubule motor protein KLC-1/2

Nesprin-1 and -2 are highly homologous at the "LEWD" binding motif, which suggests that nesprin-1 may interact with microtubule motor protein kinesin-1 through the same binding region as shown in nesprin-2 (A). All three mutants were close to the KLC binding motif ("LEWD"), especially R8272Q (B).

In this chapter, I will set up to investigate:

1) If nesprin-1 mutants perturb the nuclear migration and compromise the differentiation process in C2C12 mouse myoblast differentiation model *in vitro*;
2) The mechanism of nesprin-1 in regulating nuclear distribution: If nesprin-1α_2 WT binds with microtubule motor protein KLC-1/2 and if novel nesprin-1 mutations perturb their binding;
3) Investigate the effect of nesprin-1 mutants during cardiac development in zebrafish embryos *in vivo*.

4.2 Results

4.2.1 Expression levels of endogenous nesprin-1α and MRFs were upregulated during myogenesis

The C2C12 mouse myoblast cell line is a reliable immortal one, which has the capacity to form myotubes and has been widely used as a model of skeletal muscle development [266]. C2C12 myoblasts were cultured in the flask until they reached 90% confluency, then were induced to differentiate with low serum differentiation medium. Small and short myotubes can be seen by day 2 and the number and size of myotubes quickly increased during the process. By day 6, the multi-nucleated myotubes were well formed over the whole culture dish (Figure 4.2).

Using this model, firstly, the expression level of endogenous nesprin-1, MRFs (MyoD and myogenin), as well as the skeletal muscle marker MHC during the myoblast differentiation were examined. The differentiated muscle cells were collected from days 0, 2, 4 and 6 and extracted cell lysates were subjected to immunoblotting. WB showed that endogenous expression levels of nesprin-1α (including both 1α1 and 1α_2) increased from day 2, followed by a rapid increase from day 2 to day 4, then gradually reached the highest level at day 6 (Figure 4.3). Myogenin, which was upregulated in differentiated myocytes, peaked at day 2 and then decreased when myocytes started to fuse together (Figure 4.3). MHC, a typical marker of terminally differentiated muscle cells, initially increased at day 2, and reached a 7-fold high at day 6 (Figure 4.3).

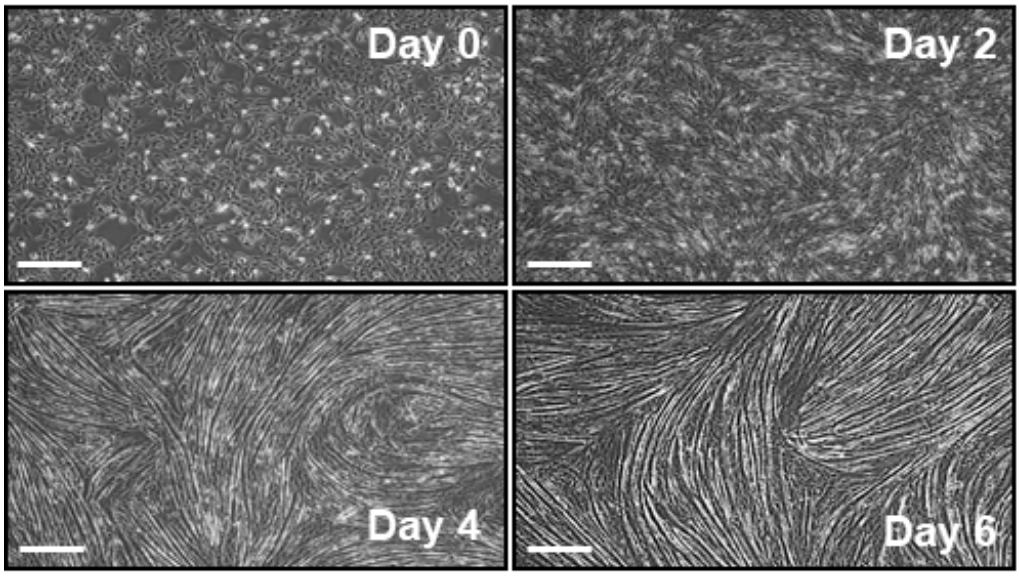
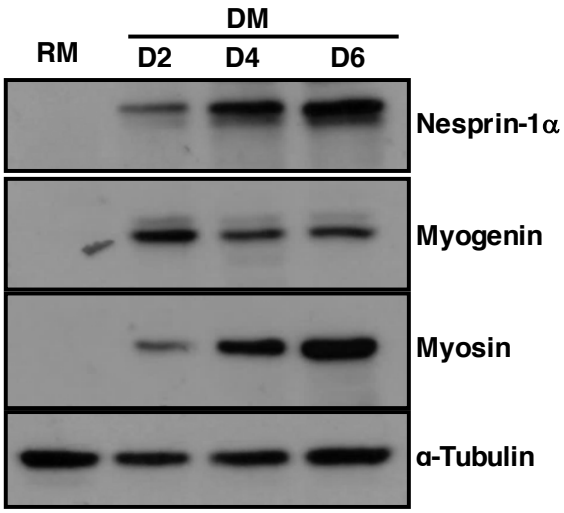


Figure 4.2 C2C12 myoblasts formed the myotubes within 6 days

Myoblasts were grown on the uncoated flask with the normal culture medium until they reach 90% confluency. Then they were stimulated with a low serum medium to initialise the differentiation. The myotubes started to form from day 2 and were well formed at day 6. Scale bar=200μm.

A.



B.

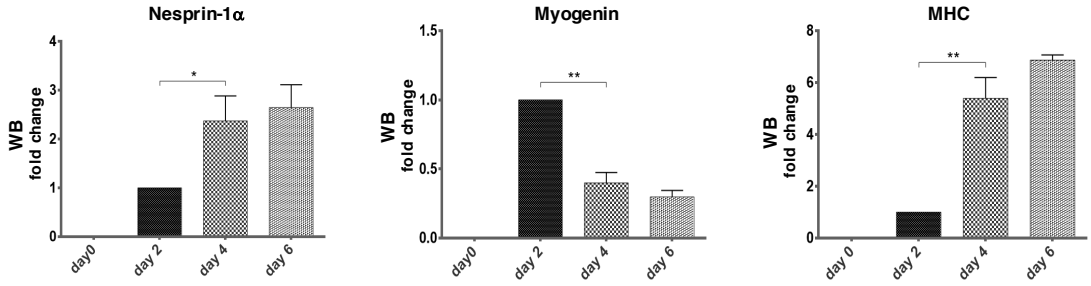


Figure 4.3 Protein expression levels of nesprin-1α and MRFs were upregulated during C2C12 myoblast differentiation

Protein lysates were collected at different differentiation time points. WB showed endogenous expression levels of nesprin-1, myogenin and MHC increased during myotube formation (A, B). The nesprin-1α protein level was highest at day 6, whereas myogenin was highest at day 2, and MHC was detected from day 2 and increased until day 6. Three independent experiments were performed shown as mean±SEM, *P<0.05 using Student's t-tests.

RNA levels of MRFs were evaluated by qPCR. MyoD level was highest at day 2, and reduced to basal level at day 6 (Figure 4.4); Myogenin rapidly increased at the day 2, then reduced until day 6 (Figure 4.4); MHC kept increasing from day 2, and was massively upregulated until the termination time point day 6 (Figure 4.4).

Both WB and qPCR indicated the C2C12 muscle differentiation model was successfully generated under these experiment conditions. The myogenesis process can be monitored through the individual MRF such as MyoD, myogenin and MHC at each time points. In order to investigate whether the nesprin-1 mutants affect myogenesis, the optimised time points were chosen as following: day 2 for MyoD and myogenin, and day 6 for MHC at early and late differentiation respectively for investigation in further experiments.

4.2.2 Generating retroviral constructs of nesprin-1α_2 WT, mutants and KASH

To investigate whether the novel nesprin-1 mutants could disrupt muscle cell differentiation, we generated retroviral constructs of nesprin-1α_2 WT, mutants and DN KASH1 to achieve the high transduction efficiency and stable expression of nesprin-1 in C2C12 cells. The strategy of generating retroviral constructs was following three major steps.

First, V5-tagged nesprin-1α_2 WT was amplified from the previously generated 'GFP-nesprin-1α_2 WT' construct, by using a V5 tagged forward primer containing NotI site from 5' end of nesprin-1α_2 and a reverse primer containing EcoRI site targeted to 3' end of nesprin-1α_2 (Figure 4.5A); V5-nesprin-1 KASH was amplified by using another V5 tagged forward primer containing NotI site that started from the beginning of KASH domain and a reverse primer as same as the one for WT (Figure 4.5B).

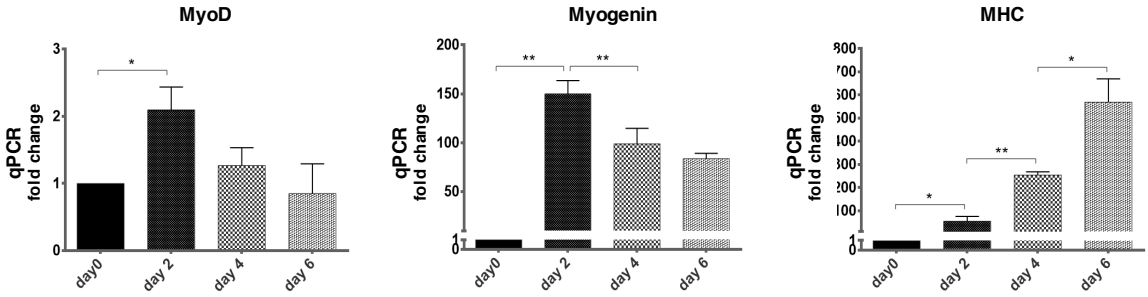


Figure 4.4 mRNA expression levels of MRFs were upregulated during C2C12 myoblast differentiation

qPCR showed endogenous expression levels of MyoD, myogenin and myosin increased during myotube formation. MyoD and myogenin peaked at day 2; MHC was detected from day 2 and increased until day 6. Three independent experiments were performed shown as mean±SEM, *P<0.05 using Student's t-tests.

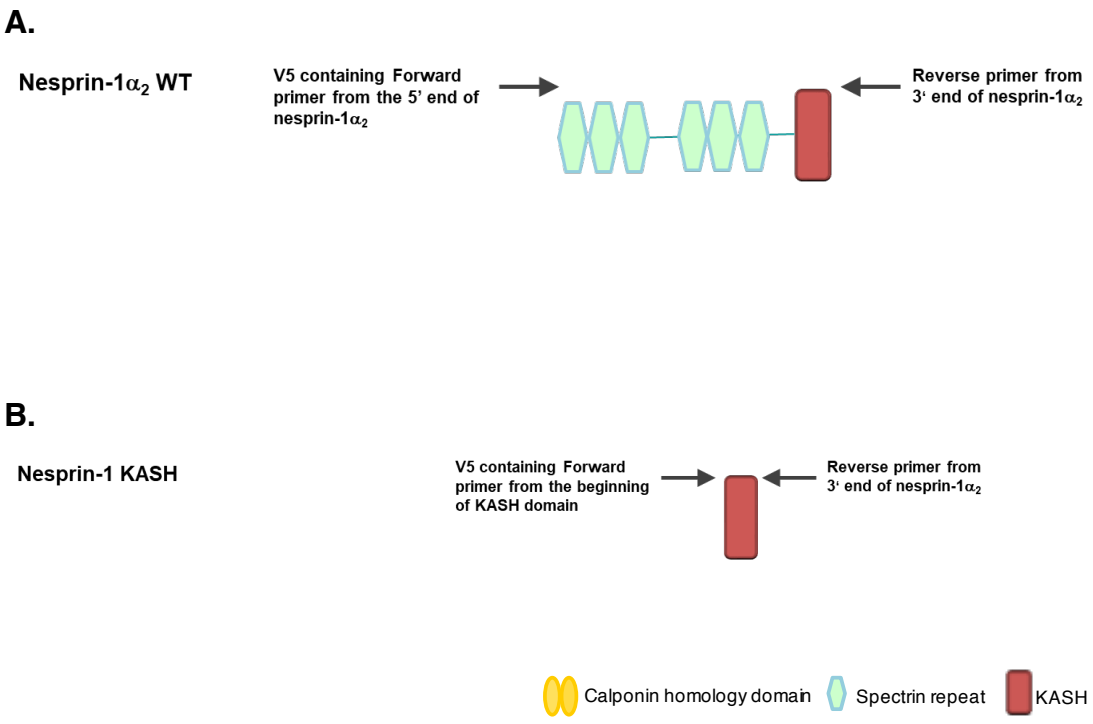


Figure 4.5 V5-tagged nesprin-1α$_2$ and KASH1 were amplified by PCR

V5-tagged nesprin-1α$_2$ WT was amplified from the previously generated 'GFP-nesprin-1α$_2$ WT' construct, via using V5 tagged forward primer from 5' end of nesprin-1α$_2$ and a reverse primer targeted to 3' end of nesprin-1α$_2$ (A); V5-tagged nesprin-1 KASH was amplified by using another V5 tagged forward primer that started from the KASH domain and the same reverse primer as WT (B).

Following this, the amplified PCR products were inserted into pGEM T-easy vectors (Figure 4.6 A-C). The T-easy vector has 'A' and 'T' overhangs, which is the best backbone to readily ligate with PCR products with an extra 'T' or 'A'. Mutants R8272Q, S8381C and N8406K were generated by site directed mutagenesis using the V5-nesprin-1α_2 WT as a template. The successful ligations and colony growth were confirmed by unique restriction enzyme digestion. There were three clear bands present on the agarose gel representing V5-nesprin-1α_2 WT and mutants (digested by NotI, EcoRI and XmnI) (Figure 4.7A). Two clear bands that estimated sizes indicated V5-nesprin-1 KASH and T-easy vector on the gel (digested by NotI and EcoRI) (Figure 4.7B). All the constructs in T-easy vectors were subjected to DNA sequencing for confirmation.

Finally, V5-tagged nesprin-1α_2 WT, mutants (R8272Q, S8381C and N8406K) and KASH in T-easy vector were digested using the restriction enzyme (Figure 4.6D). The right size bands corresponding to nesprin-1α_2 WT, mutants and KASH were extracted from the agarose gel, then ligated with retroviral MIG vectors (A gift from Prof. Peter Zammit's lab, King's College London [237]) (Figure 4.6E). The MIG vector was modified from the retroviral backbone pMSCV-puro (Clontech, Mountain View, CA), in which the puromycin selection gene was replaced with eGFP to create pMSCV–IRES–eGFP. This served as the retroviral control vector and eGFP as a reporter for retroviral infection. The insertion site of nesprin-1 fragments was just before IRES, to form pMSCV-nesprin-IRES-eGFP, thus V5-tagged nesprin-1α_2 WT/mutants/KASH and GFP would be expressed under the same promotor as independent proteins due to the 'IRES' sequence. The successful insertions were confirmed by restriction enzyme digestion using unique enzymes NotI and EcoRI. MIG vector was shown on the gel with 6000bp size, while V5-nesprin-1α_2 and mutants were shown with the 3000bp (Figure 4.8A & 4.8B) and KASH was around 300bp (Figure 4.8C). All the constructs were subjected to DNA sequencing for further confirmation.

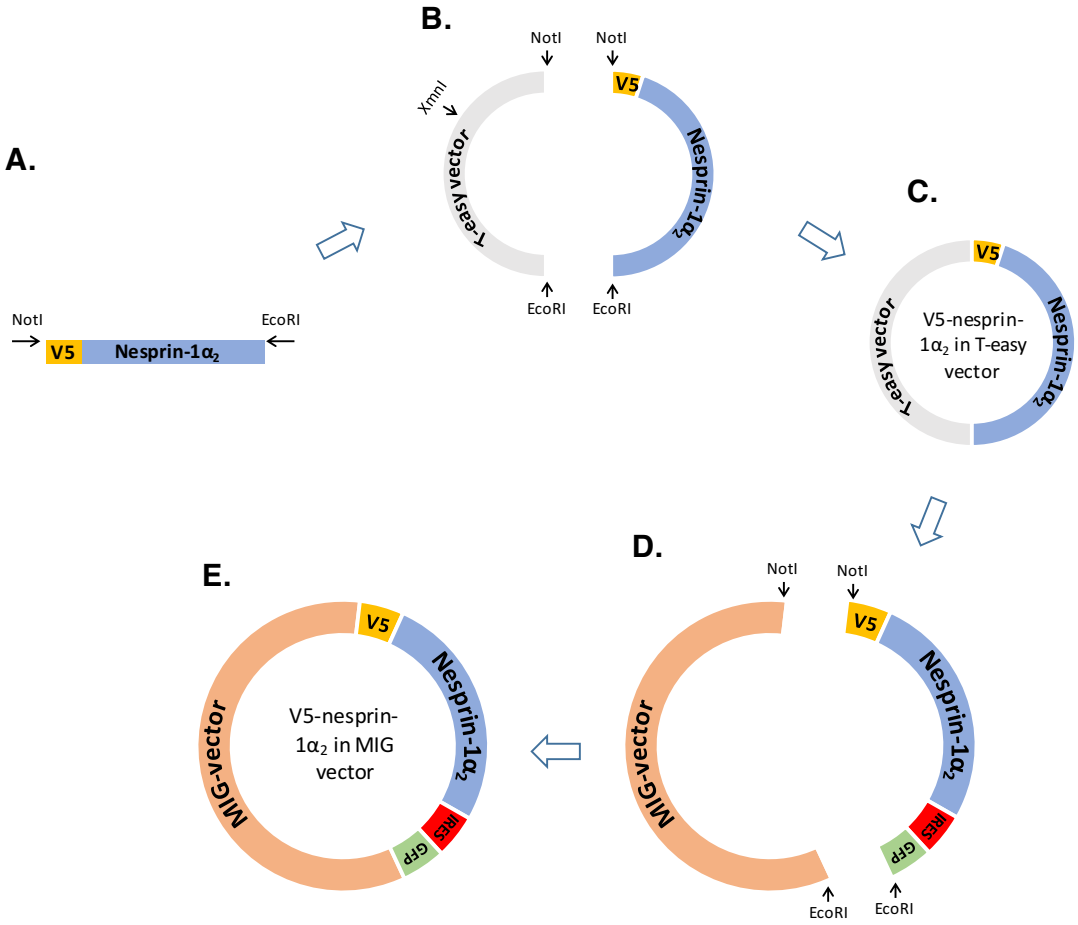


Figure 4.6 Strategy of generating retroviral nesprin-1α$_2$ WT and mutants' constructs

V5-tagged nesprin-1α$_2$ WT and KASH domain were amplified (A), then inserted into pGEM T-easy vectors by A/T overhang (B, C). Mutants were generated by the site directed mutagenesis using the V5-nesprin-1α$_2$ as a template. The V5-nesprin-1α$_2$ WT/mutants/KASH were extracted from the T-easy vectors by restriction enzyme digestion (NotI, EcoRI and XmnI for V5-nesprin-1α$_2$ WT/mutants, NotI & EcoRI for V5-nesprin-1α$_2$ KASH) (D), then ligated with retroviral MIG vectors (E).

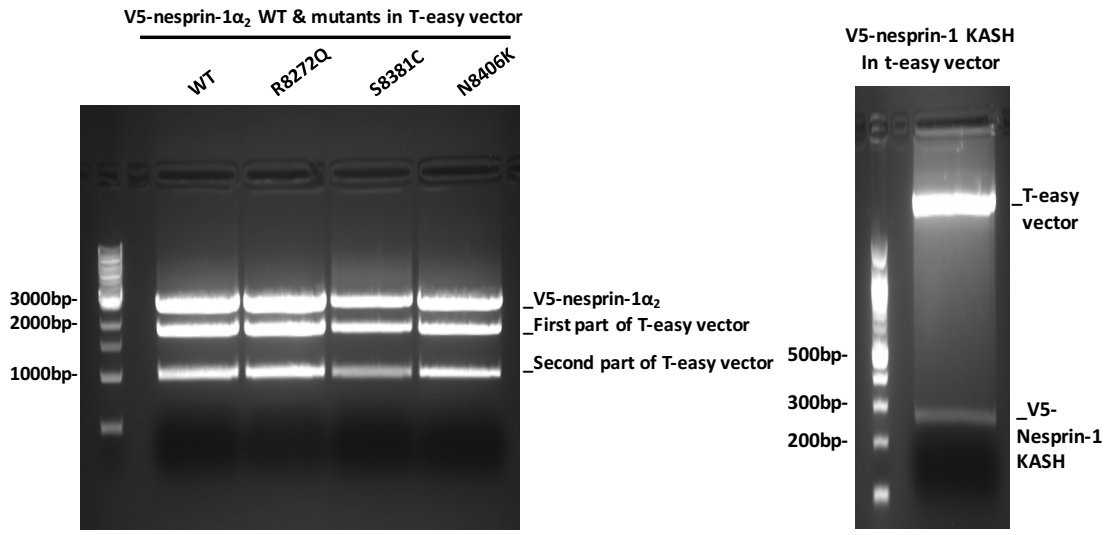


Figure 4.7 Generation of V5-tagged nesprin-1α$_2$ WT, mutants and KASH constructs using pGEM T-easy vectors

V5-tagged nesprin-1α$_2$ WT was amplified from the previously generated 'GFP-nesprin-1α$_2$ WT' construct, by using V5 tagged forward primer containing NotI site from 5' end of nesprin-1α$_2$ and a reverse primer containing EcoRI site targeted to the 3' end of nesprin-1α$_2$; V5-nesprin-1 KASH was amplified, by using another V5 tagged forward primer containing NotI site which started from the KASH domain and a reverse primer same as the one for WT, then were inserted into pGEM T-easy vectors. Mutants were generated by site directed mutagenesis using the V5-nesprin-1α$_2$ WT as a template. Successful ligations were confirmed by unique restriction enzyme digestion (NotI, EcoRI and XmnI for V5-nesprin-1α$_2$ WT/mutants, NotI & EcoRI for V5-nesprin-1α$_2$ KASH). There were three clear bands present on the agarose gel, in which the 3000bp band represented the V5-nesprin-1α$_2$ WT and mutants (A). Two clear bands in which the 300bp represented the V5-nesprin-1 KASH (B). All the constructs were subjected to DNA sequencing.

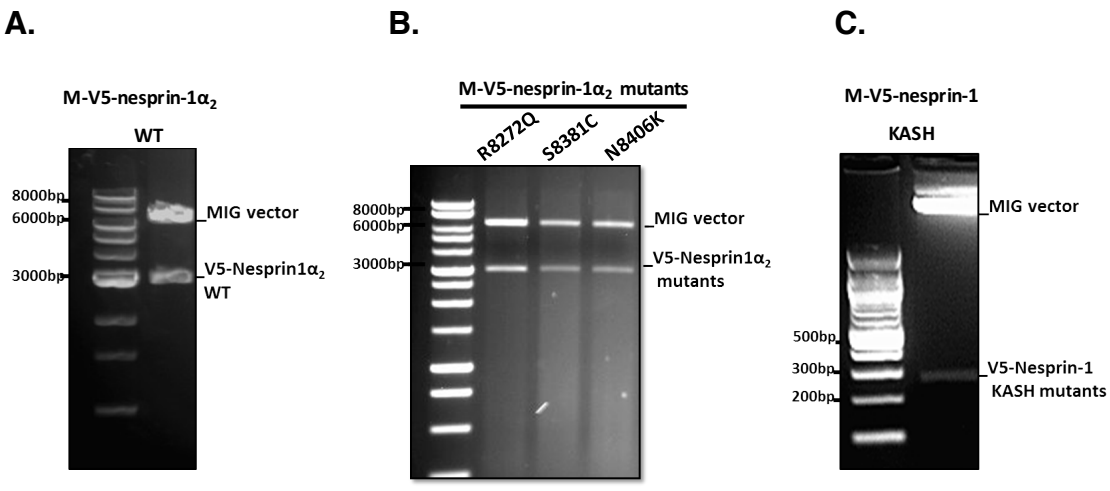


Figure 4.8 Generation of V5-tagged nesprin-1α$_2$ WT, mutants and KASH constructs using retroviral vectors

V5-tagged nesprin-1α$_2$ WT, mutants and KASH were extracted from the pGEM T-easy vectors, then ligated with retroviral MIG vector digested by NotI and EcoRI. The successful insertions and colonies were confirmed by the restriction enzyme digestions using NotI and EcoRI. MIG vector was shown on the gel with 6000bp size, while V5-nesprin-1α$_2$ and mutants were shown as the 3000bp and KASH was around 300bp. All the constructs were subjected to DNA sequencing for further confirmation.

4.2.3 Infection of C2C12 myoblasts with retroviral nesprin-1α_2 WT, mutants and KASH

The retroviral constructs of V5-nesprin-1α_2 WT, mutants and KASH, together with an ecotropic packaging plasmid (RV helper), were transiently co-transfected into HEK 293T cells to produce non-replicating retroviruses (RVs), and the supernatants were collected 48, 60 and 72 hours after infecting the C2C12 myoblasts [237]. The infected cells were purified by Fluorescence-Activated Cell Sorting (FACS) machine. The uninfected cells served as a negative control, and the cells infected with MIG only (GFP only) served as the selective marker. As the infection efficiency could be various among different cells, we chose the highest fluorescence intensity range from the MIG only populations as the threshold to select the cells infected with nesprin-1 RVs. The RVs transduction efficiency was as high as 90%, but only the cells expressed similar intensity of GFP were selected and used in subsequent muscle cell differentiation experiments (Figure 4.9).

IF showed V5-tagged WT nesprin-1α_2, three mutants (R8272Q, S8381C, N8406K) and KASH1 were present at the NE of the infected myoblasts. GFP localised throughout the whole cell, and served as a reporter for retroviral infection (Figure 4.10).

4.2.4 Nesprin-1 mutants led to defects in myotube formation

Efficient differentiation of C2C12 cells transduced with GFP alone (MIG only) or nesprin-1α_2 WT was observed, with many multinucleated myotubes formed within 6 days. However, more single myoblasts and fewer myotubes were observed in the cells transduced with either nesprin-1α mutants or KASH1 (Figure 4.11).

The fusion index that represent the percentage of nuclei incorporated into MHC positive multinucleated cells vs. the total number of nuclei, was used to quantify myotube fusion. In cells overexpressing nesprin-1α_2 WT or MIG only, the fusion index was similar at around 50%. However, a significant reduction of fusion index was observed in cells transduced with the mutants, in particular, R8272Q and N8406K, as well as KASH1 when compared to WT and MIG only (Figure 4.12A). Further analysis

to assess the size of myofibers by dividing the MHC positive populations into 4 groups (1-5 nuclei, 6-10 nuclei, 11-15 nuclei and >15 nuclei) was performed[263].

Small sized myotubes (1-5 nuclei/each myotube) were increased in all mutants and KASH1, accompanied with a reduction of larger size myotubes (6-10 nuclei/each myotube) compared to WT (Figure 4.12B). These findings revealed that myotubes expressing nesprin-1 mutants had a reduced capacity to form myotubes, the majority of which were a small size and contained fewer nuclei compared to the WT.

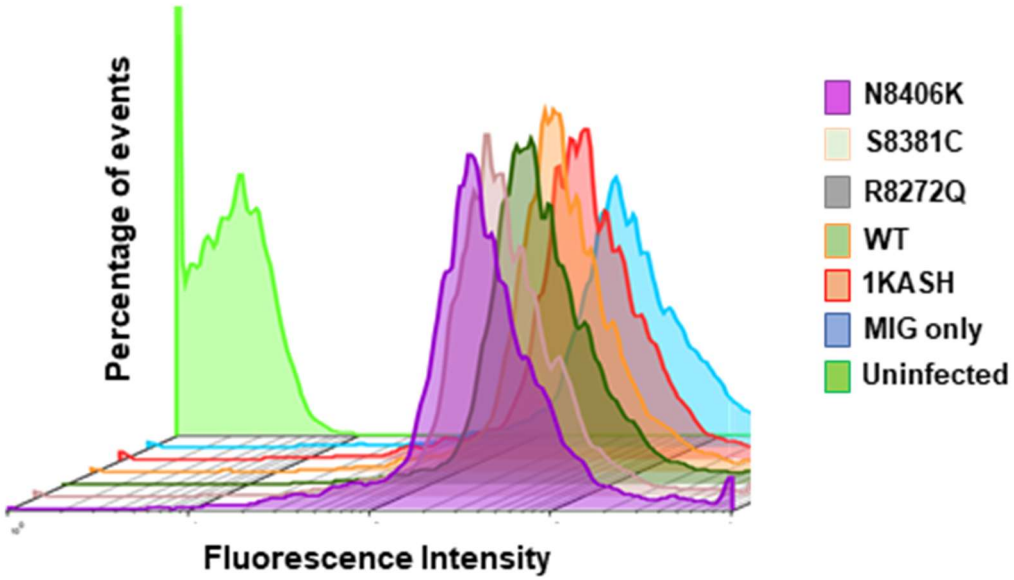


Figure 4.9 C2C12 myoblasts were highly infected with retroviral nesprin-1α_2 WT, mutants and KASH1

C2C12 myoblasts were infected with retroviral nesprin-1α_2 WT/mutants/DN KASH1 respectively. Fluorescence-Activated Cell Sorting (FACS) was performed to purify the infected GFP positive populations and these were used in subsequent muscle cell differentiation experiments.

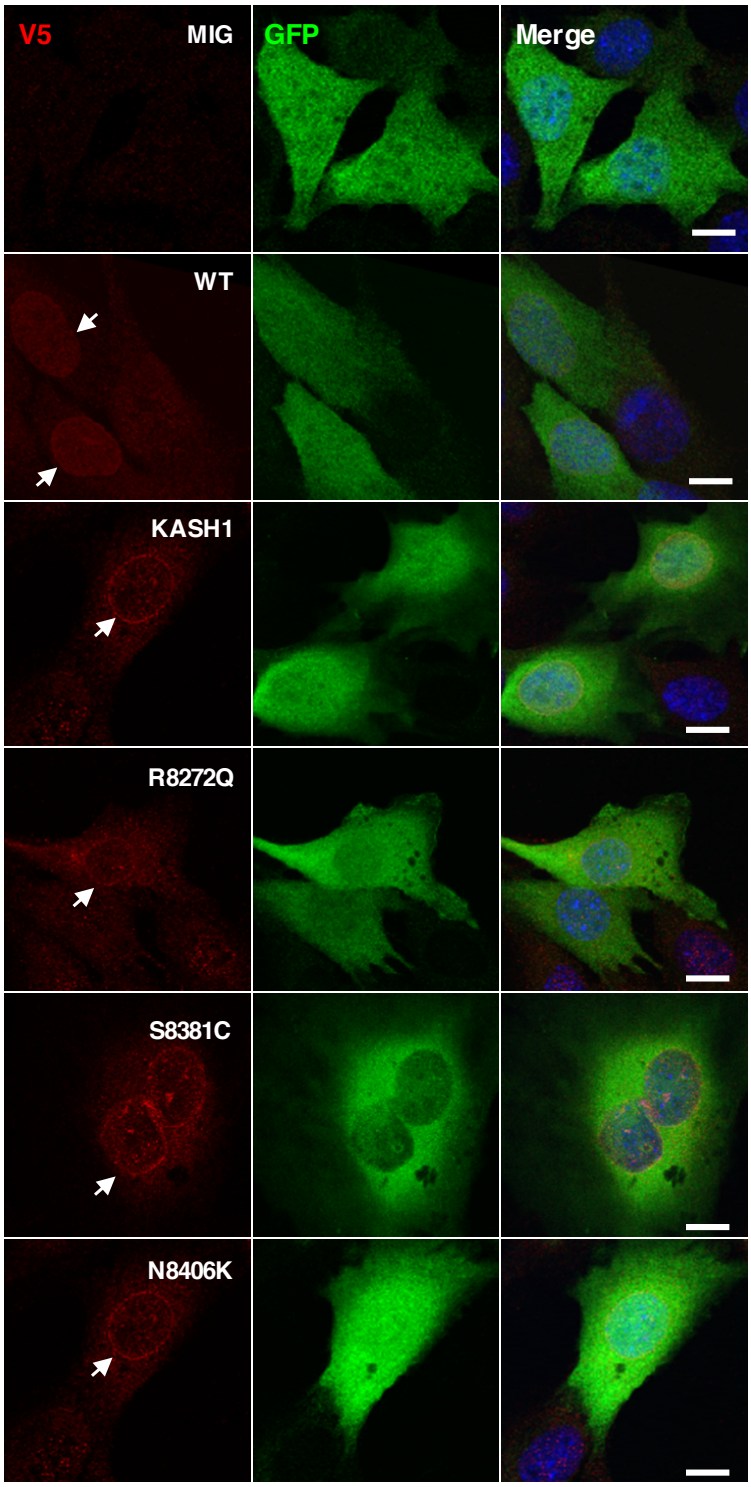


Figure 4.10 Exogenous nesprin-1 WT/mutants/KASH1 localised at the NE in C2C12 myoblasts.

IF showed that exogenously expressed V5-tagged WT-1α_2, mutants and DN KASH1 were localised at the NE. V5 staining (red) indicated the localisation of nesprin-1α_2 WT, mutants (R8272Q, S8381C, N8406K), as well as KASH1. GFP (green) was expressed as a reporter for retroviral infection. Scale bar=25μm.

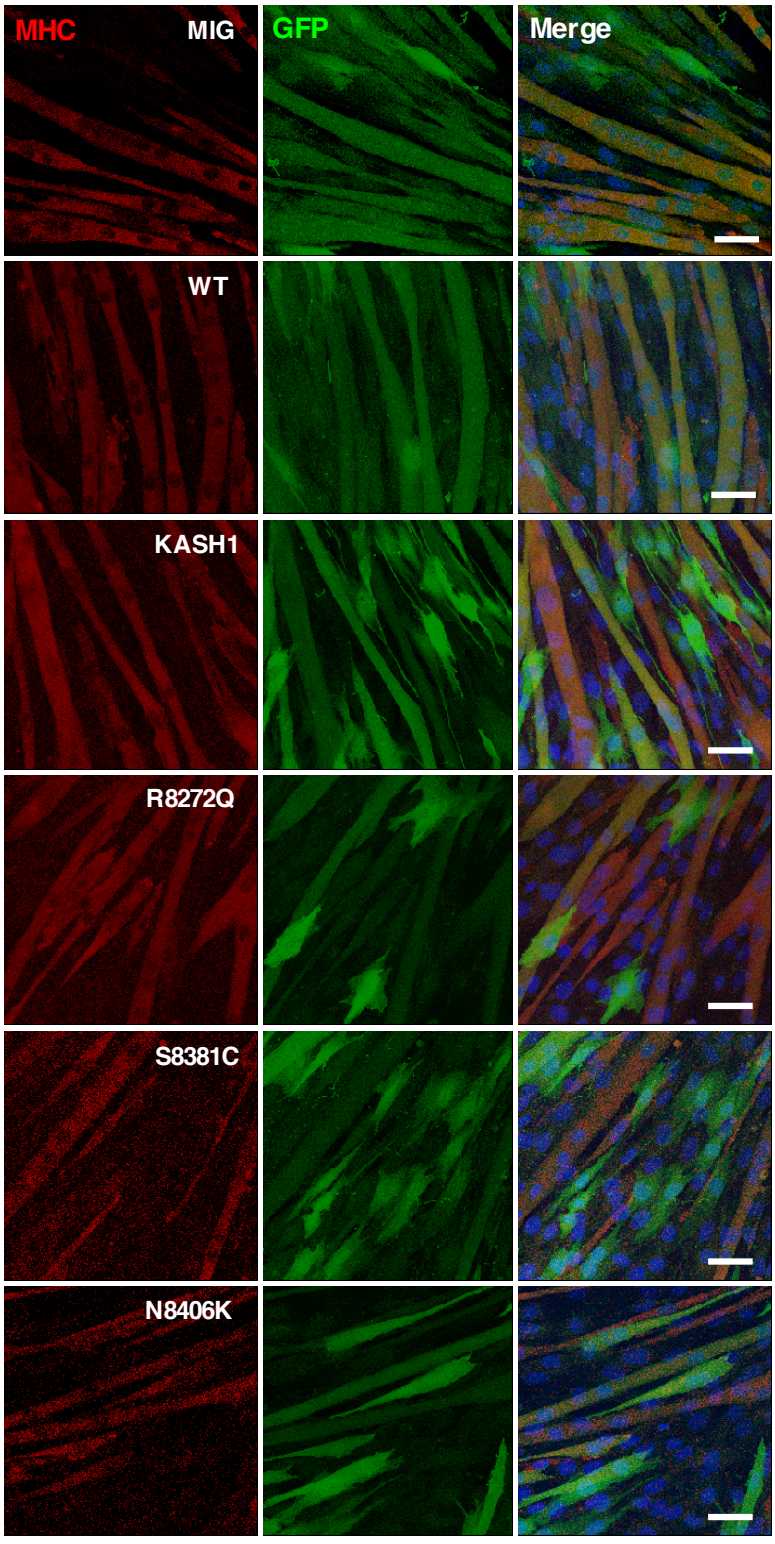
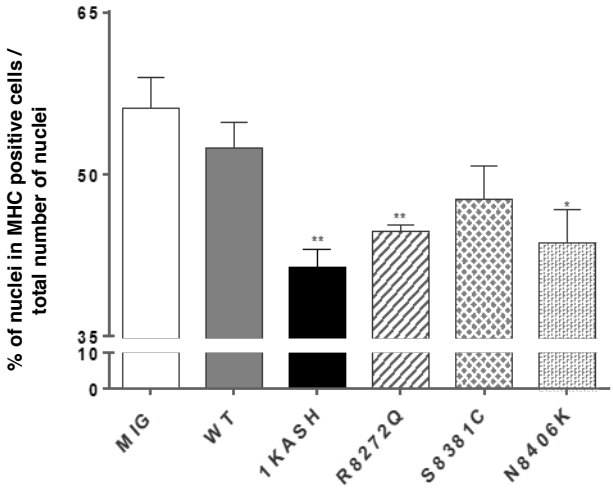


Figure 4.11 Nesprin-1 mutants led to fewer myotube formation

Upon differentiation, fewer multinucleated myotubes (red) were observed in the cells infected with three mutants and DN KASH1 compared with the C2C12 cells infected with GFP alone (MIG only) or nesprin-1α_2 WT. GFP (green) was expressed as a reporter for retroviral infection. Scale bar=50μm.

A.



B.

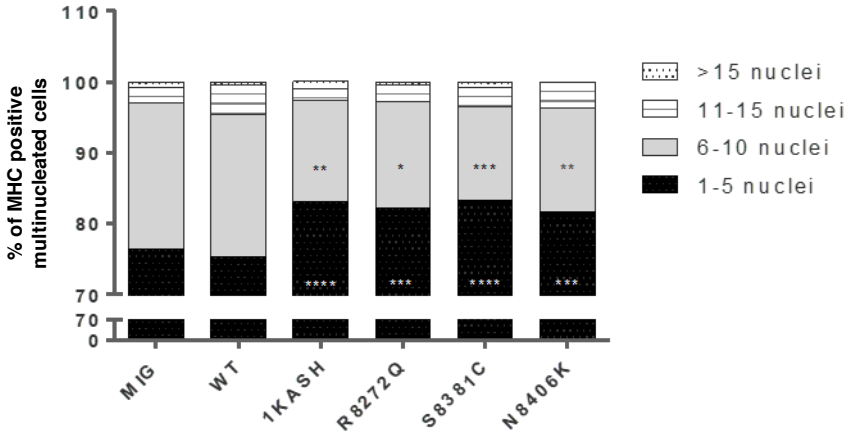


Figure 4.12 Nesprin-1 mutants caused defects in myoblast differentiation

The fusion index was reduced in cells infected with the mutant R8272Q and DN KASH1 compared with $1\alpha_2$ WT (A), more than 600 nuclei for each clone were counted under microscopy (63x objective) at day 6, three independent experiments were performed for each clone. Further analysis of the MHC positive multinucleated populations revealed that myotubes expressing nesprin-1 mutants contained more population of myotubes with fewer nuclei compared to the controls (B). Three independent experiments were performed shown as mean±SEM, *P<0.05 using Student's t-tests or two-way ANOVA analysis.

4.2.5 Nesprin-1 mutants led to dysregulation of MRFs

Cell lysates were extracted every two days the during differentiation process for analysis of protein and RNA levels of MRFs. The levels of myogenin and MHC were dramatically reduced in cells transduced with the three mutants, particularly R8272Q and KASH1 when compared with nesprin-1α_2 WT at day 2 and 6 respectively (Figure 4.13A-C). qPCR also demonstrated that MyoD was significantly reduced in cells transduced with KASH1 at Day 2 (Figure 4.13A). It is noteworthy that RNA expression levels of myogenin and MHC and protein level of MHC was elevated in the WT compared with MIG, indicating nesprin-1α_2 WT promoted myoblast differentiation during the process of myotube formation, whereas the mutants reduced these effects.

4.2.6 Nesprin-1α WT interacted with KLC-1/2 and nesprin-1 mutants disrupted this binding

Recent data showed that nesprin-2 interacts with KLC-1/2 via a conserved "LEWD" motif at the C-terminus of nesprin-2 [114]. This motif is also present in nesprin-1 (Figure 4.1) [22, 23, 114], suggesting nesprin-1 may also bind to KLC-1/2 and be involved in connecting the nucleus to the microtubule network and therefore plays a role in myonuclear positioning.

Previous data has shown small nesprin isoforms including nesprin-1α, localise at the INM to bind with lamin A/C and emerin at the NE [35, 61]. However, there was no direct evidence showing if small nesprin-1 isoforms, particularly nesprin-1α_2 localise only at the INM or at both INM and ONM. C2C12 cells expressing the V5-tagged nesprin-1α_2 WT were permeabilized with either digitonin (only breaking down the ONM) or NP-40 (breaking down both INM and ONM).

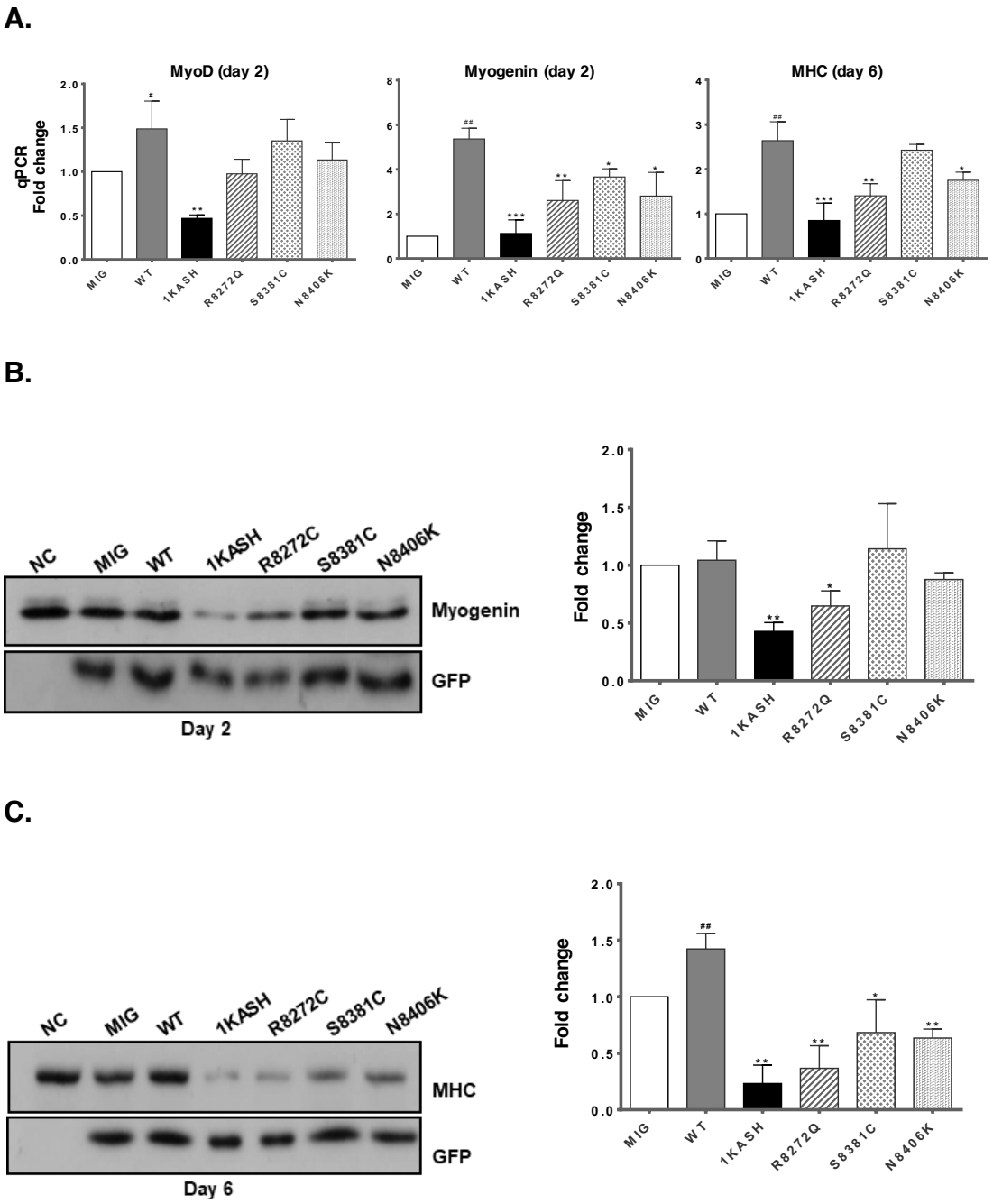


Figure 4.13 Nesprin-1 mutants caused dysregulation of MRFs during differentiation.

qPCR and WB showed that nesprin-1 mutant R8272Q and dominant negative-KASH1 caused significant reduction of myogenin (A, B) and MHC (A, C) levels at DM day 2 and day 6 respectively, qPCR also showed that dominant negative KASH1 caused significant reduction of MyoD (A) levels at DM day 2. All were normalised to GFP, three independent experiments were performed shown as mean±SEM. *P<0.05:compared with WT; #P<0.05: compared with MIG, using Student's t-tests.

Upon digitonin treatment, IFs showed nesprin-1α_2 can be detected at the NE, whereas INM protein SUN2 was unable to be detected (Figure 4.14A). When permeabilized with NP40, both nesprin-1α_2 and SUN2 could be detected at the NE (Figure 4.14B), suggesting nesprin-1α_2 localises at the ONM in addition to its previously identified INM localisation.

Then, we tested the binding of nesprin-1α_2 and KLC-1/2 *in vitro*. GFP-1α_2 WT or nesprin-1α_2 LEAA (mutated WD/AA within the LEWD motif, generated by our collaborator Dr. Sue Shackleton's lab in University of Leicester) were co-expressed with Flag-tagged KLC-2 WT (a dominant light chain isoform in muscle) or the KLC-2 N287L mutant, previously shown to disrupt nesprin-2/KLC binding [114] in U2OS cells. IP and WB showed that nesprin-1α_2 could efficiently bind to KLC-2, and this binding was disrupted by either nesprin-1 LEAA (mutated WD/AA within the LEWD motif) or the KLC-2 N287L mutant [114] (Figure 4.15). We then tested the nesprin-1 mutants using this system and found that the R8272Q mutant which contains the closest mutation to the binding motif, had significantly reduced binding to KLC-2 compared with nesprin-1α_2 WT, while the S8381C mutant appeared to enhance KLC-2 binding (Figure 4.15).

4.2.7 Nesprin-1 mutants affected the binding between nesprin-1 and KLC in both myoblasts and myotubes

Next, I tested whether these mutants affected nesprin-1/KLC-1/2 binding during muscle cell differentiation. Firstly, WB showed that, similar to nesprin-1α, the endogenous expression level of KLC-1/2 increased during myoblast differentiation (Figure 4.16). In C2C12 myoblasts, GST pull-down assays further confirmed that nesprin-1α_2 WT efficiently binds to KLC-1/2, and this binding was disrupted by the mutated LEWD motif-LEAA. In addition, the R8272Q mutant had significantly reduced binding to KLC-1/2 compared with WT in C2C12 cells, while the S8381C showed increased binding with KLC-1/2 (Figure 4.17A). This reduced interaction was especially evident in myotubes where expression of both nesprin-1 and KLC-1/2 was highest (Figure 4.17B). This part of the data was consistent with IP results and showed the interaction between nesprin-1α_2 WT and KLC-1/2 existed in both myoblasts and myotubes, whereas this binding was perturbed by the three novel nesprin-1α_2 mutants especially R8272Q during the dynamic myogenesis.

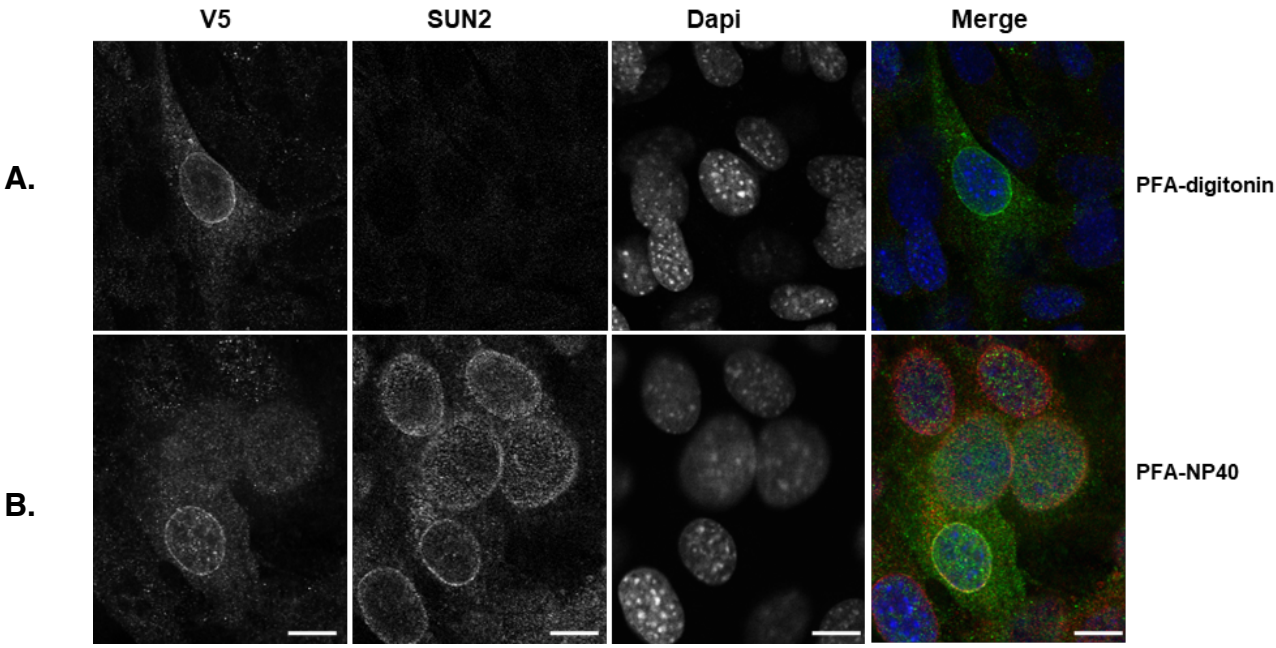


Figure 4.14 Nesprin-1α$_2$ localised at the ONM

IF staining showed that V5-nesprin-1α$_2$ was present at the ONM (A: digitonin treatment, only breaking down the ONM; B: NP-40 treatment, breaking down both INM and ONM). SUN2, the INM protein, indicated if the INM was broken down by either digitonin or NP-40 treatment. Scale bar=12.5µm.

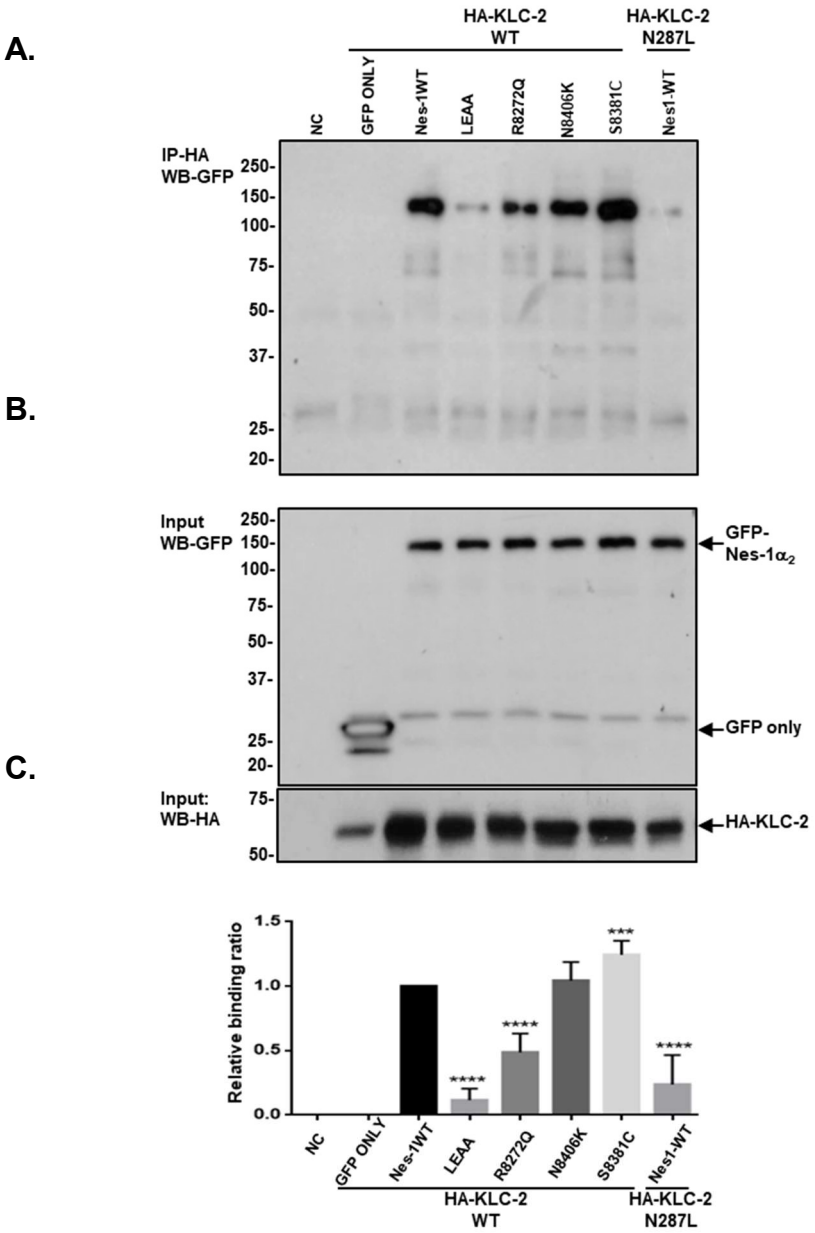
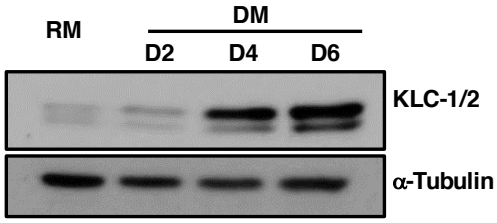


Figure 4.15 Nesprin-1α WT interacted with KLC-1/2 and nesprin-1 mutants disrupted this binding

Overexpression and IP showed the binding between nesprin-1 WT/mutants and KLC WT/mutants in U2OS cells. HA-KLC2-N287L co-expressed with GFP-nesprin-1α_2 WT and HA-KLC2 WT co-expressed with GFP-nesprin-1α_2 LEAA (mutated WD/AA within the LEWD motif) served as positive controls. GFP empty vector with HA-KLC-2 WT was a negative control. IP showed that nesprin-1α_2 could efficiently bind to KLC-2, and this binding was disrupted by either nesprin-1α_2 LEAA or the KLC-2 N287L mutant. The R8272Q mutant showed significantly reduced binding with KLC-2, while the S8381C mutant appeared to enhance KLC-2 binding (A, C). Three independent experiments were performed shown as mean±SEM, *P<0.05 using Student's t-tests.

A.



B.

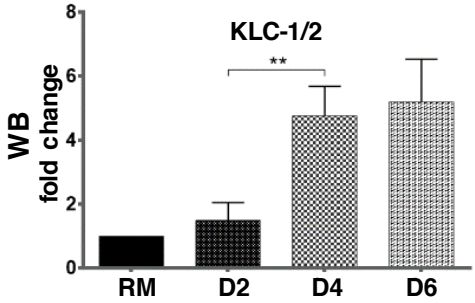


Figure 4.16 Endogenous KLC-1/2 increased during differentiation process

WB showed endogenous expression levels of KLC-1/2 increased during myotube formation, similar to the changes of endogenous nesprin-1α. Three independent experiments were performed shown as mean±SEM, *P<0.05 using Student's t-tests.

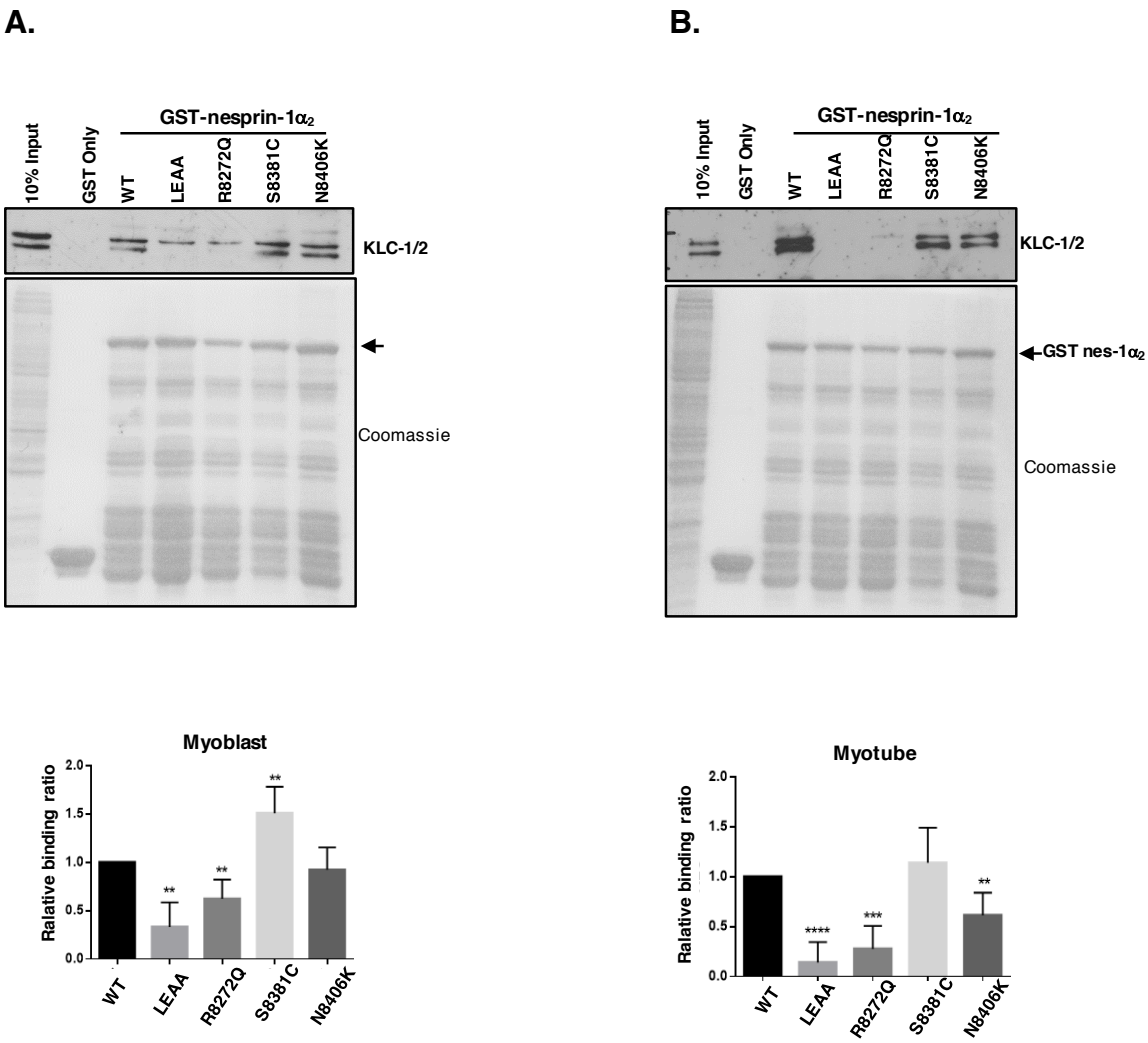


Figure 4.17 Defects in nesprin-1 and KLC-1/2 interaction

GST pull-down showed the binding between nesprin-1 and KLC-1/2 using either GST-WT or mutant nesprin-1 beads in myoblasts (A) and myotubes (B) respectively. The binding for each mutant was quantified by densitometry, and expressed as a ratio of the value obtained for WT protein. Three independent experiments were performed shown as mean±SEM, *P<0.05 using Student's t-tests. (The majority part of this experiment was done by Victoria Koullourou, King's College London.)

4.2.8 Depletion of KLC-1/2 affected myoblast differentiation

The KLC-1/2 was predominately localised at the NE, but was also present in the cytoplasm in myotubes formed with uninfected C2C12 or cells infected with the nesprin-1α_2 WT (Figure 4.18). However, KLC-1/2 staining was reduced at the NE in myotubes infected with DN KASH1, indicating the mis-localised endogenous nesprin-1 may lead to defects in recruiting KLC to the NE during the differentiation (Figure 4.18).

To further investigate the functional roles of nesprin-1α_2 and KLC-1/2, we tested whether depletion of KLC-1/2 using multiple siRNA oligos would affect fusion of myoblasts and differentiation in a similar manner to that observed in the cells infected by the R8272Q mutant. Three different oligos (named as A, B and C) were used to individually target different regions of mouse KLC-1 and KLC-2 genes thus excluding off-target effects (Figure 4.19). siRNA oligos KLC-1A and KLC-2A were used in the first group (group 1), KLC-1B&C and KLC-2B&C were combined and used in the second group (group 2). WB showed the expression levels of both KLC-1 and -2 were reduced in myoblasts upon the KLC-1/2 depletion using oligos group 1 and 2 respectively (Figure 4.20A & 4.20C). The KLC-1/2 siRNA also worked efficiently in the myotubes (Figure 4.20B & 4.20D). IF further confirmed a reduced KLC-1/2 staining at NE in myotubes (Figure 4.21B), and a weaker cytoplasmic staining in both myoblasts and myotubes (Figure 4.21A & 4.21B). However, the localisation of endogenous nesprin-1 still remained at the NE, irrespective of KLC-1/2 depletion (Figure 4.22). Moreover, MHC levels and the fusion index were significantly reduced in myotubes upon KLC-2 knockdown (Figure 4.23A-B & 4.24A-B). Further analysis of MHC positive multinucleated cells (myotubes) revealed that KLC-2 depletion resulted in significantly fewer nuclei per myotube (majority myotubes with 1-5 nuclei, and fewer myotubes containing more than 6 nuclei) (Figure 4.23C, 4.24C & 4.25), indicating a defect in myoblast fusion. In contrast, KLC-1 depletion led to significantly more clustered nuclei per myotube (reduced number of myotube with 1-5 nuclei, increased number of myotube with 6-10, 11-15 and >15 nuclei) (Figure 4.23C, 4.24C & 4.25).

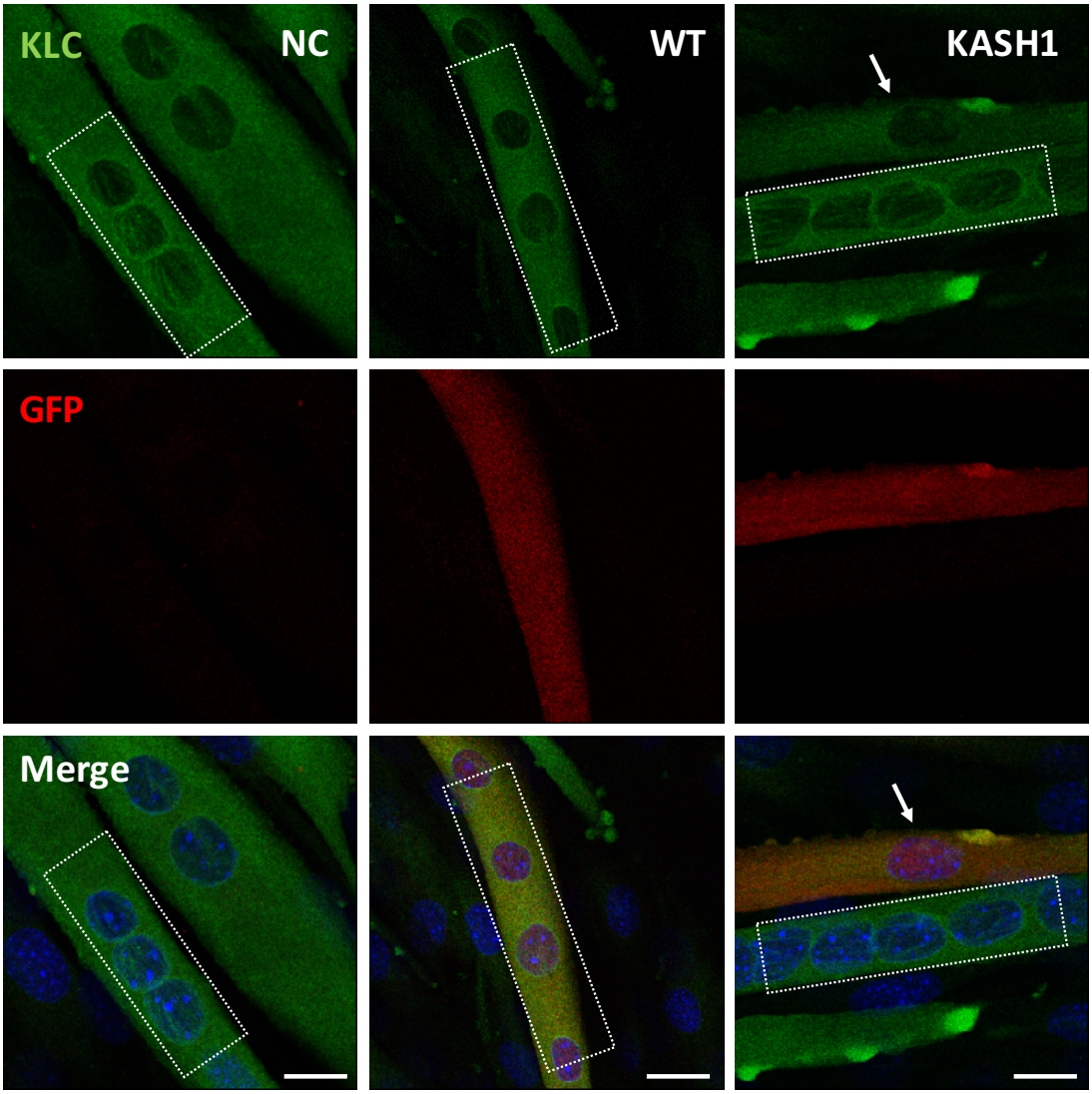


Figure 4.18 Overexpression of DN KASH1 mis-localised KLC-1/2 from the NE

C2C12 myoblasts infected with retroviral V5 tagged nesprin-1α_2 WT and DN KASH1 respectively and induced to differentiate. In myotubes formed with uninfected myoblasts (negative control) or exogenous nesprin-1α_2 WT, the KLC-1/2 was concentrated at the NE and cytoplasm (dotted rectangle), while in the cells infected with DN KASH1, the staining of KLC-1/2 (arrow) was reduced at the NE. Notably, GFP was stained with anti-rabbit Alexa Fluor 546 dye and shown in red. Scale bar=25µm.

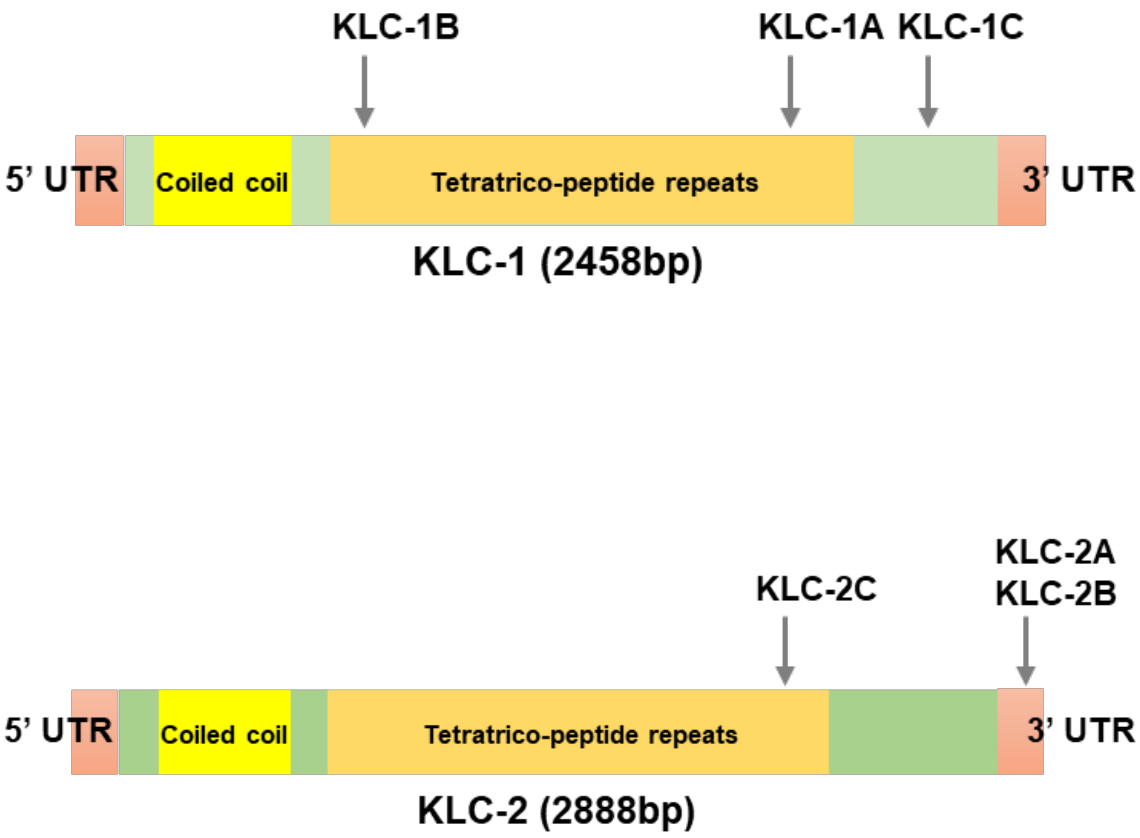


Figure 4.19 The localisation of siRNA oligos targeted to different regions of KLC-1/2 genes

KLC-1 and -2 genes are homologous, and consist of a coiled-coil region (interacting with kinesin heavy chain) and tetratrico-peptide repeats (mediating protein-protein interaction), with divergent C-terminus. Three different siRNA oligos (named as A, B and C) were used to individually target different regions of mouse KLC-1 and KLC-2 genes. The targeted regions are labelled on the schematic. (Gene bank accession number for mouse KLC-1 and KLC-2 are NM_001025361 and BC014845 respectively)

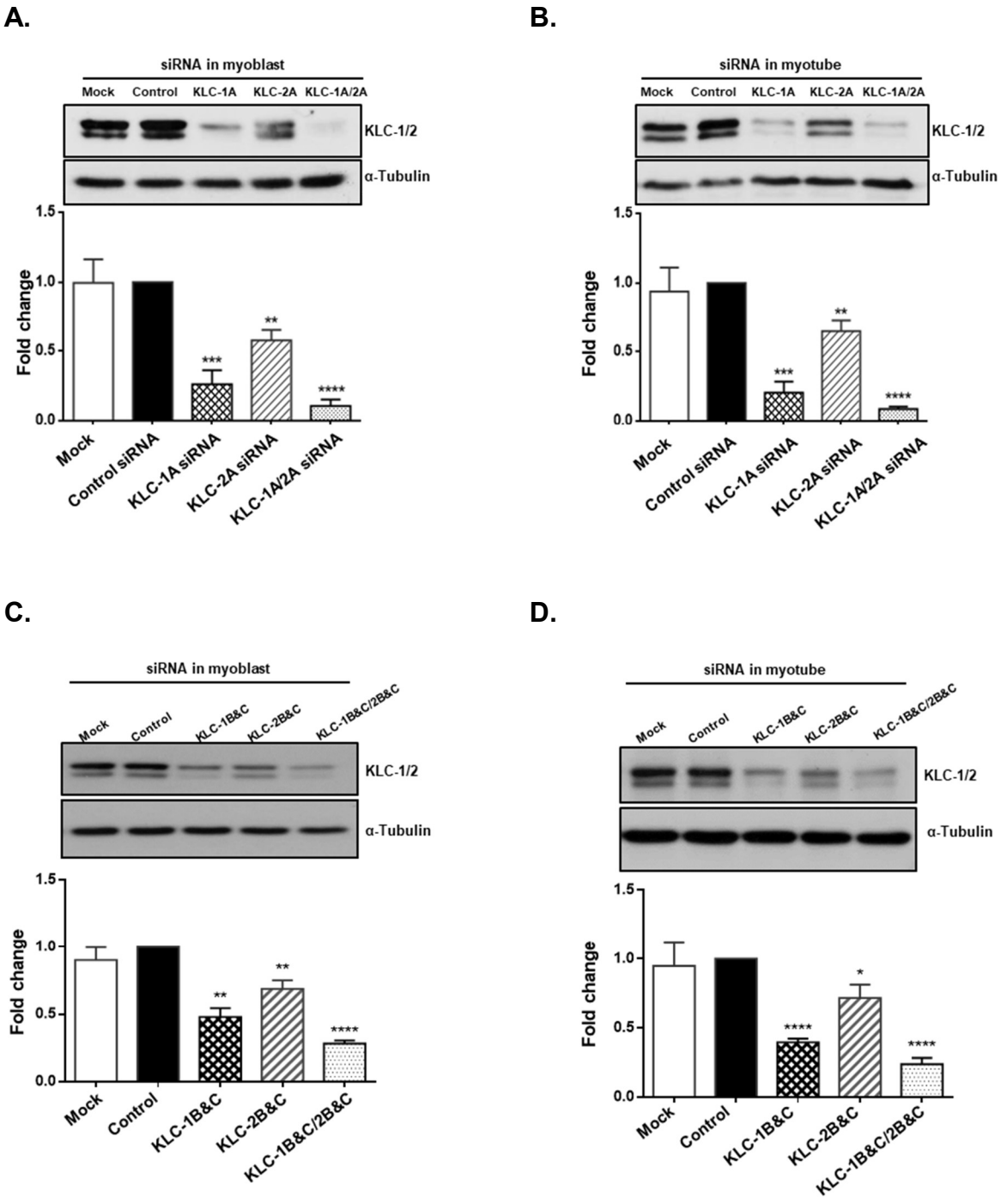


Figure 4.20 WB showed KLC-1/2 was knocked down in myoblasts and myotubes by using multiple siRNA oligos

Multi-oligos were used to knock down the KLC-1/2. A, B was using the single oligo that targeted to KLC-1/2; C, D were using anther double oligos that targeted to KLC-1/2. WB showed the expression levels of both KLC-1 and -2 were reduced in myoblasts (A, C) and myotubes (B, D) upon KLC-1/2 depletion using different siRNA oligos. Three independent experiments were performed shown as mean±SEM, *P<0.05 using Student's t-tests.

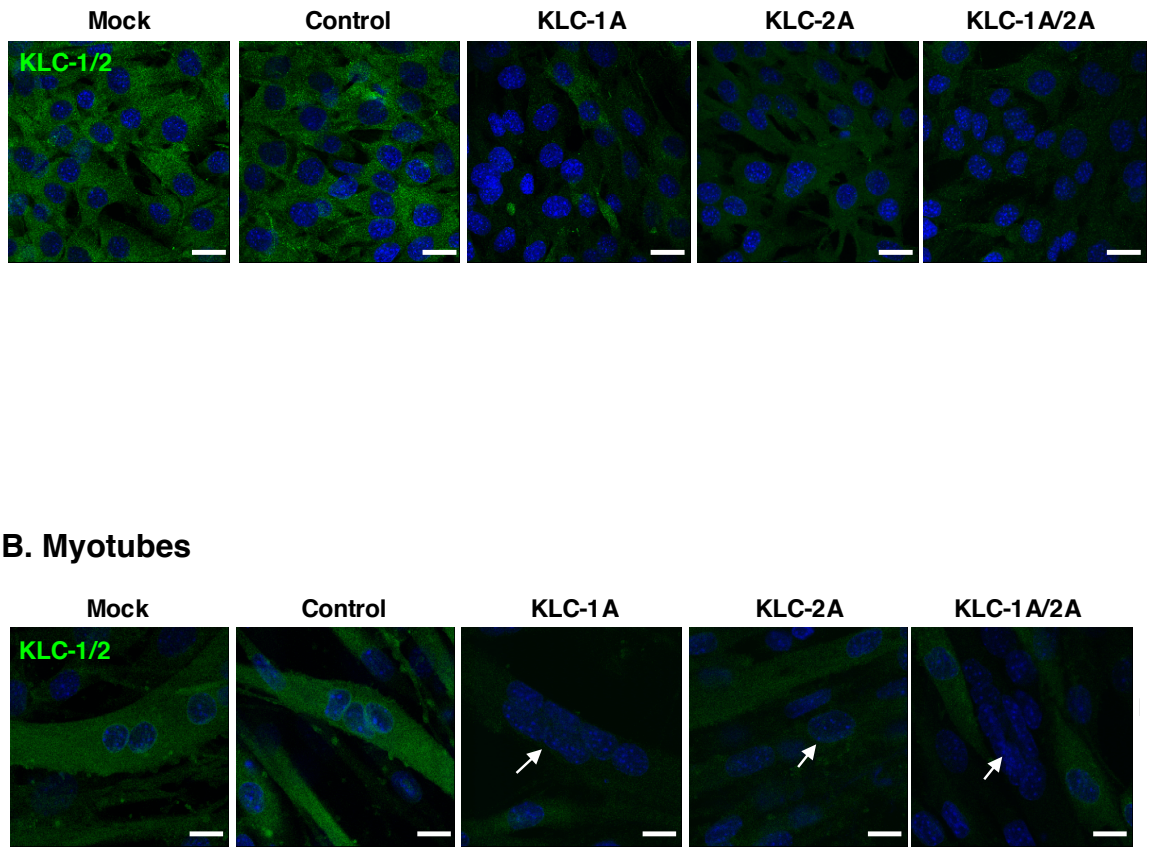


Figure 4.21 IF showed KLC-1/2 was knocked down in myoblasts and myotubes by using siRNA oligos

IF showed KLC-1/2 staining at the NE (arrowed) was reduced in myotubes upon KLC-1/2 siRNA knock down (B), the cytoplasmic staining of KLC-1/2 was reduced in both myoblasts and myotubes (A, B). A: Scale bar=25μm, B: Scale bar=12.5μm.

Myoblasts

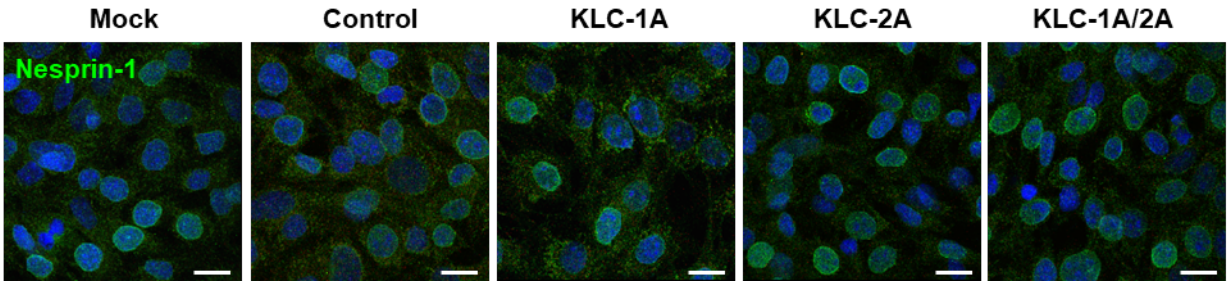


Figure 4.22 Endogenous nesprin-1α remained at the NE upon KLC-1/2 knockdown in myoblasts

IF showed endogenous nesprin-1α staining remained at the NE upon KLC-1/2 siRNA knocking down. Scale bar=25μm.

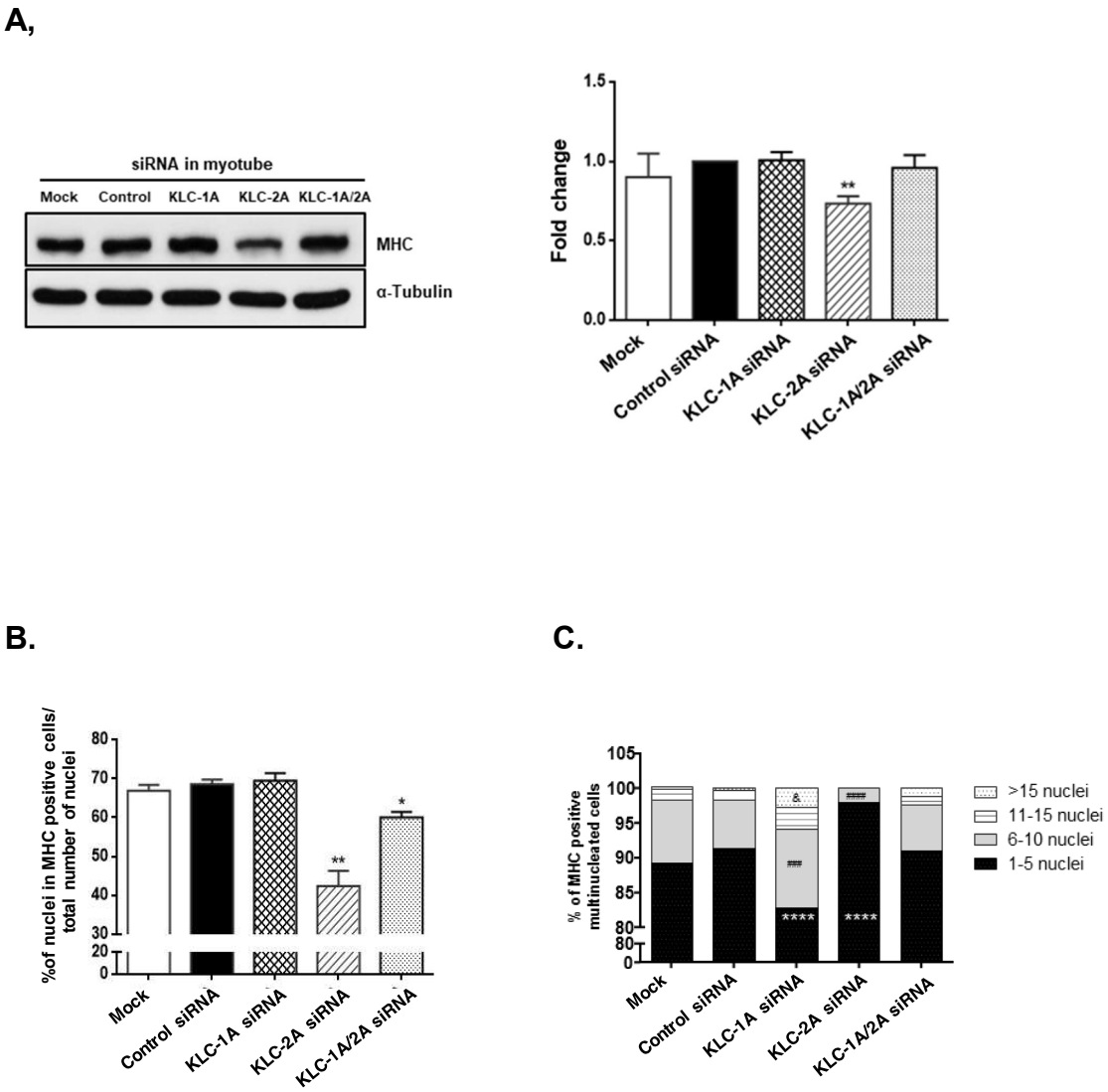


Figure 4.23 Knockdown of KLC-1/2 caused defects in myoblast fusion and differentiation (I)

The expression level of MHC (A) and the fusion index (B) were significantly reduced in myotubes especially upon KLC-2 depletion (using KLC-2A oligo). More than 800 nuclei for each clone were counted by microscopy (63x objective) at day 6, three independent experiments were performed for each clone. Further analysis of MHC positive multinucleated cells revealed that KLC-2 depletion resulted in fewer nuclei per myotube. In contrast, KLC-1 depletion (using KLC-1A oligo) led to significantly more clustered nuclei per myotube when compared with controls (C). Three independent experiments were performed shown as mean±SEM or mean, *P<0.05 using Student's t-tests or two-way ANOVA analysis.

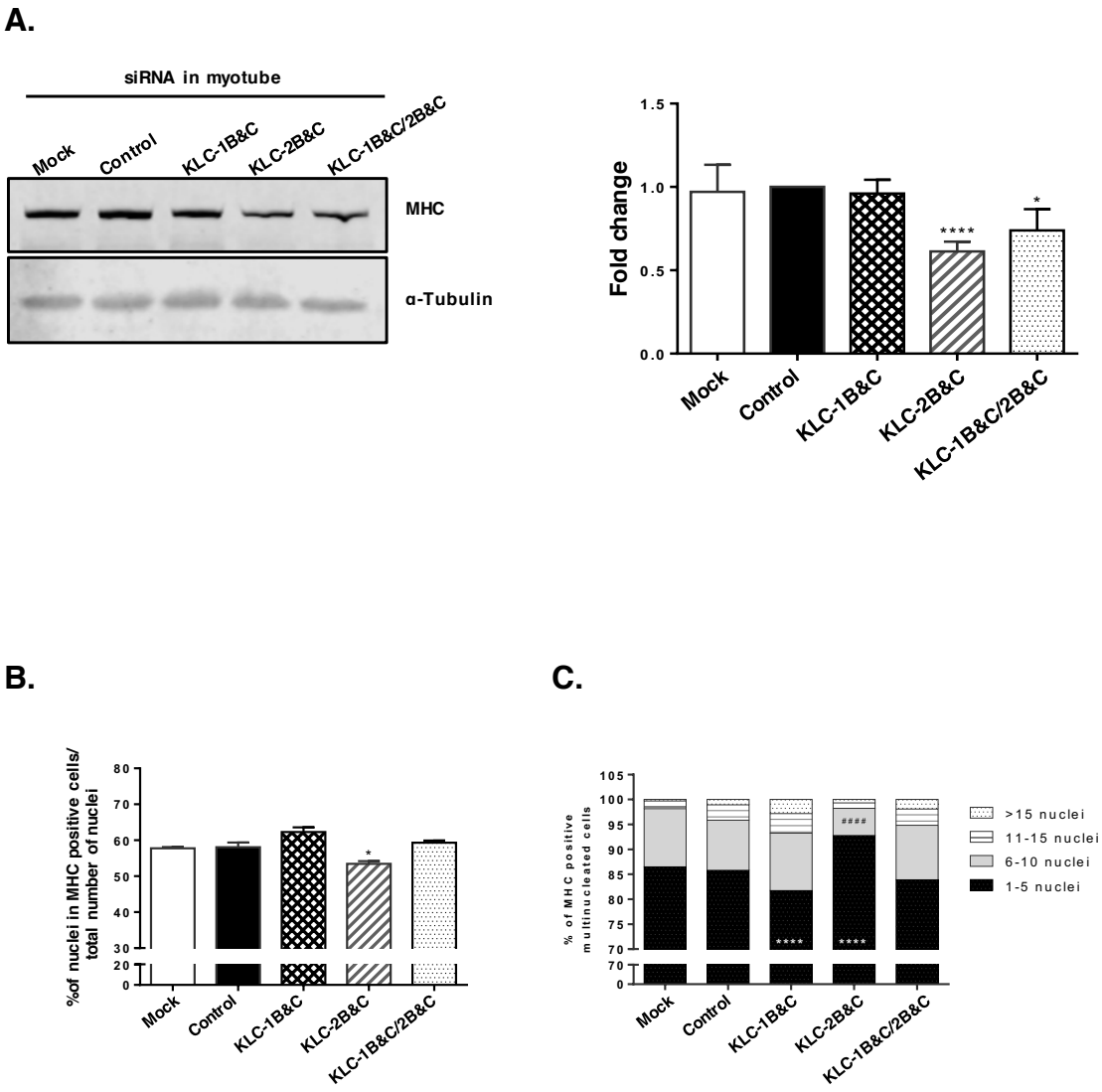


Figure 4.24 Knockdown of KLC-1/2 caused defects in myoblast fusion and differentiation (II)

The expression level of MHC (A) and the fusion index (B) were significantly reduced in myotubes especially upon KLC-2 depletion (using KLC-2B&C oligos). More than 800 nuclei for each clone were counted under microscopy (63x objective). Further analysis of MHC positive multinucleated cells revealed that KLC-2 depletion resulted in fewer nuclei per myotube (C). Three independent experiments were performed shown as mean±SEM or mean, *P<0.05 using Student's t-tests or two-way ANOVA analysis.

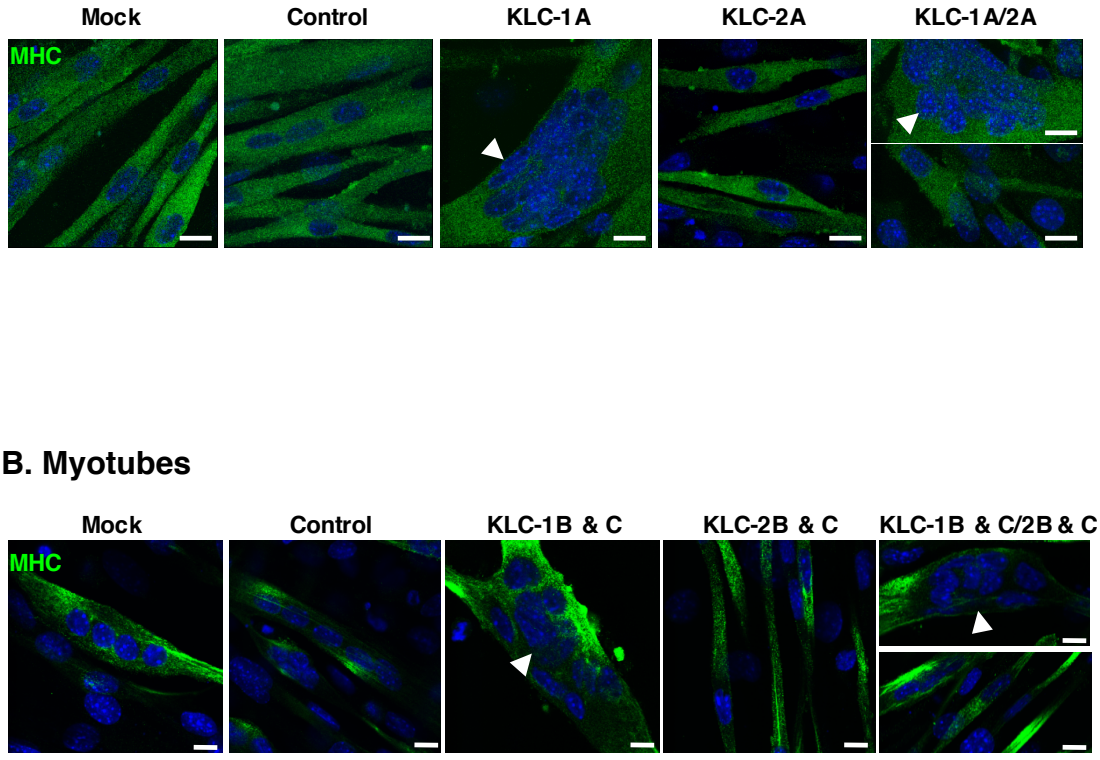


Figure 4.25 IF showed knockdown of KLC-1/2 caused defects in myoblast fusion and differentiation

IF showed the nuclei aggregation and clustering (arrow-headed) were observed upon KLC-1 and -1/2 knockdown via using different KLC-1/2 siRNA oligos. The smaller size of myotubes (with fewer nuclei in each myotube) were observed upon KLC-2 and KLC-1/2 knockdown via using different KLC-1/2 siRNA oligos. Scale bar=12.5μm.

4.2.9 Generation of flag-tagged nesprin-1α_2 WT and mutant constructs for investigating the roles of nesprin-1 in cardiac cell function in zebrafish embryos

We have shown that nesprin-1 mutants affected muscle cell differentiation *in vitro*. To investigate whether the nesprin mutants affected cardiac structure or function *in vivo*, we set out to generate a zebrafish model by expressing nesprin-1α_2 WT and mutants (R8272Q, S8381C and N8406K) in zebrafish embryos. The constructs were generated following the similar strategy as retroviral constructs described in 4.2.2. First, flag-tagged nesprin-1α_2 WT was amplified from the previously generated 'GFP-nesprin-1α_2 WT', by using flag tagged forward primer containing NotI site from the 5' end of nesprin-1α_2 of and a reverse primer targeted to the 3' end of nesprin-1α_2. Following the strategy, the amplified PCR product was inserted into the pGEM T-easy vector. Mutants R8272Q, S8381C and N8406K were generated by the site directed mutagenesis using the 'flag-nesprin-1α_2 WT' as a template. Lastly, flag-tagged nesprin-1α_2 WT, mutants (R8272Q, S8381C and N8406K) in T-easy vectors were extracted from the agarose gel after the NotI and EcoRI digestion and ligated with mammalian vector pcDNA3.1(-) (Figure 4.26A). The sequence of nesprin-1α_2 WT and mutants were verified using two methods: the first was that restriction enzyme digestion using NotI and EcoRI. pcDNA3.1(-) vector was shown on the gel with 5600bp size, while flag-nesprin-1α_2 and mutants were shown with the 3000bp (Figure 4.26B). Then all the constructs were subjected to DNA sequencing for further confirmation.

A.

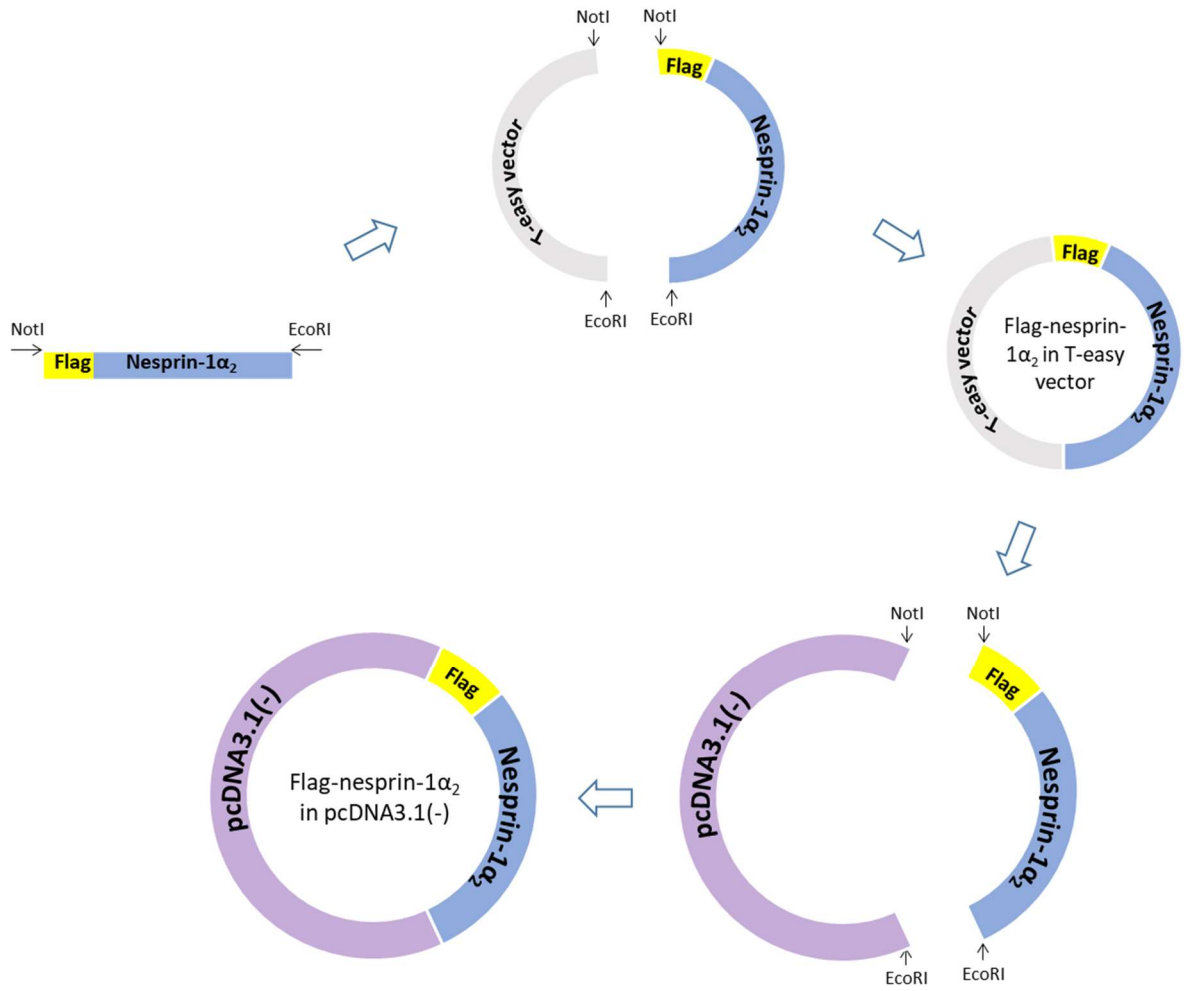


Figure 4.26 Generation of flag-tagged nesprin-1α$_2$ WT and mutants constructs using pcDNA3.1(-) vectors

(A) Flag-tagged nesprin-1α$_2$ WT was amplified from the previously generated 'GFP-nesprin-1α$_2$ WT' construct, then inserted into pGEM T-easy vectors. Mutants were generated by site directed mutagenesis using the flag-nesprin-1α$_2$ WT as a template. The Flag-nesprin-1α$_2$ WT/mutants were digested and extracted from the T-easy vectors by restriction enzyme digestion (NotI, EcoRI and XmnI), then ligated with mammalian pcDNA3.1(-) vectors.

B.

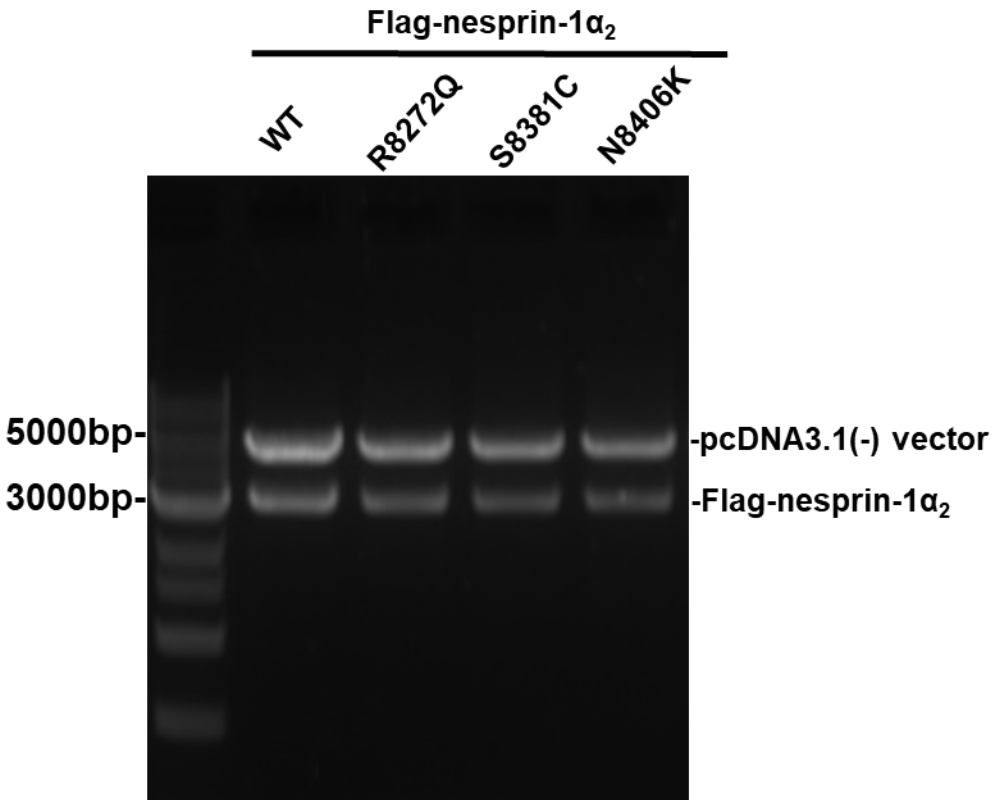


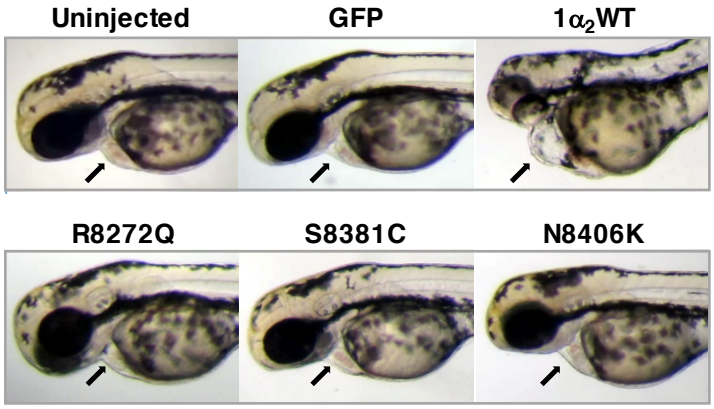
Figure 4.26 Generation of flag-tagged nesprin-1α$_2$ WT and mutants constructs using pcDNA3.1(-) vectors

(B) The sequences of nesprin-1α$_2$ WT and mutants were verified by the restriction enzyme digestion using NotI and EcoRI. pcDNA3.1(-) vector was shown on the gel with 5600bp size, while flag-nesprin-1α$_2$ and mutants were shown around 3000bp (B). All the constructs were subjected to DNA sequencing for further confirmation.

4.2.10 Human nesprin-1α_2 WT causes heart developmental and conduction defects in zebrafish embryos while mutants induce a less severe heart phenotype

Plasmid DNAs of human nesprin-1α_2 WT and mutants (R8272Q, S8381C and N8406K) were transcribed into capped mRNAs, then injected in zebrafish embryos at the one-cell stage. At 48 hours post-fertilization (hpf), zebrafish embryos expressing human nesprin-1α_2 WT showed heart defects including dilated atrial chambers with reduced heart rate (Figure 4.27). Furthermore, whole-mount *in situ* hybridization (WISH) demonstrated that the expression of myosin light chain polypeptide 7 (MYL7), the ortholog of the human regulatory myosin light chain (RLC) gene [267, 268], was reduced in 30% of the embryos expressing human nesprin-1α_2 WT. The MLY7 staining also highlighted the dilated atrial chambers and heart developmental defects such as abnormal looping (Figure 4.28A-B & 4.29A-B). In contrast, expression of the human nesprin-1α_2 mutants induced some heart developmental defects, such as abnormal heart looping and malpositioning of heart chambers (Figure 4.29A & 4.29B), but without heart enlargement or heart rate defects. There was also evidence of abnormal anterior-posterior axis development in all the embryos, when compared with uninjected and GFP expressed embryos (Figure 4.29C & 4.29D). Taken together this zebrafish larvae data suggests that overexpression of human nesprin-1α_2 WT leads to cardiac developmental defects while nesprin-1α_2 mutants induced a less severe heart phenotype.

A.



B.

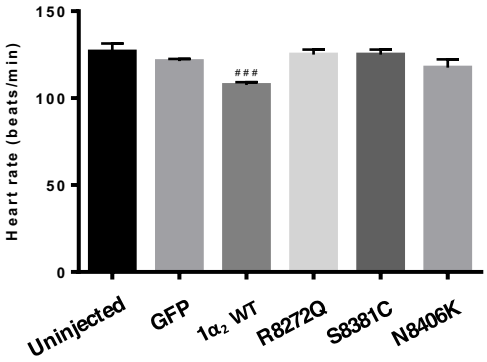
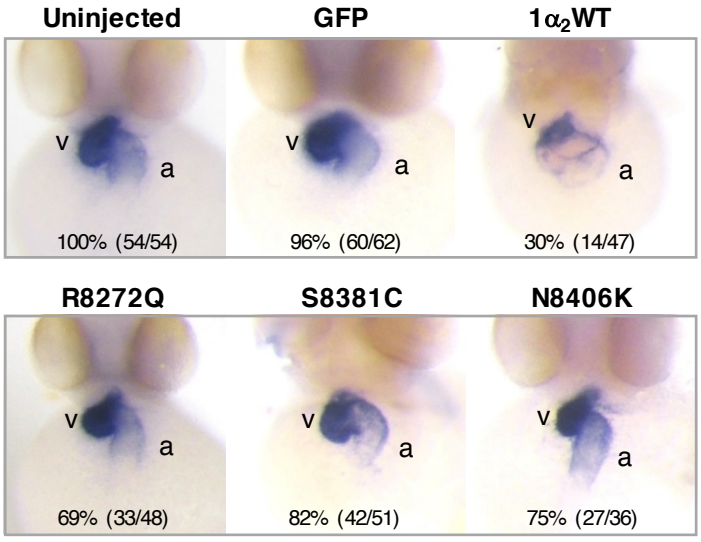


Figure 4.27 Human nesprin-1α$_2$ WT induced dilated atrial chamber and reduced heart rate

Lateral views of zebrafish live embryos at 48 hpf. The pericardium (A, arrowed) and heart rate were shown for each corresponding mRNA injected (B), zebrafish embryos with nesprin-1α$_2$ WT mRNA showed slow heart rate and dilated atrial chambers. About 4-7 embryos for each injection were measured. Means and SEM were obtained from three independent experiments for each treatment. #P<0.05 using Student's t-tests. (This experiment was done by our collaborators in Sichuan University, China.)

A.



B.

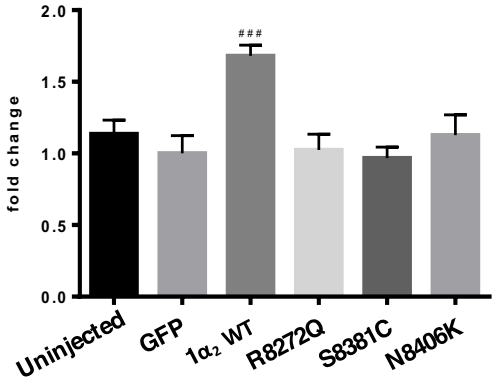


Figure 4.28 Expression of MYL7 indicated the dilated heart in zebrafish overexpressing human nesprin-1α$_2$ WT

Whole-mount *in situ* hybridization (WISH) monitored the expression of cardiac fetal gene MYL7 at 48 hpf (A), the numbers (left in brackets) indicated the percentage of embryos displaying the phenotype represented in the picture shown, the numbers (right in brackets) was the total numbers counted of observed embryos. The relative atrium area of embryos for the corresponding mRNA injection was measured and calculated by the area of MYL7 expression using ImageJ (B), which was normalised to the atrium area of the embryos injected with GFP mRNA. Embryos were in ventral views with the anterior at the top. About 4-7 embryos for each injection were measured. Mean±SEM were obtained from three independent experiments for each treatment. #P<0.05 using Student's t-tests. a: atrium, v: ventricle. (This experiment was done by our collaborators in Sichuan University, China.)

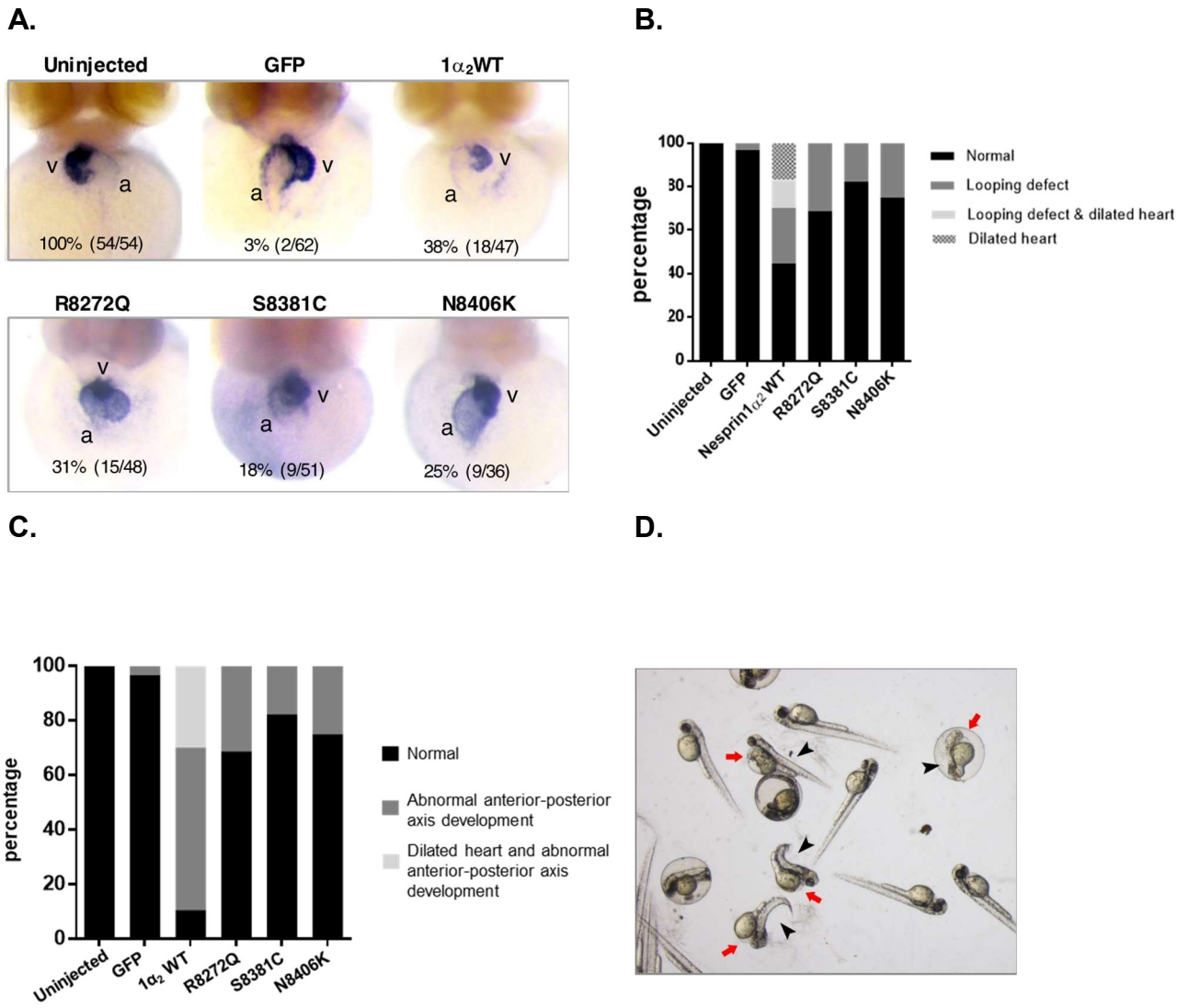


Figure 4.29 Human nesprin-1α$_2$ WT induced heart development defects while mutants induced a less severe heart phenotype in zebrafish embryos

WISH monitored the expression of MYL7 gene at 48 hpf (A), the numbers (left in brackets) indicated the percentage of embryos displaying the phenotype represented in the picture shown, the numbers (right in brackets) were the total numbers counted of observed embryos. Human nesprin-1α$_2$ WT caused a dilated heart phenotype (B-D), and both WT and mutants caused defects in heart looping when compared with uninjected shown (A, B) and abnormal anterior-posterior axis development (C, D) in the injected embryos when compared with uninjected and GFP expressing embryos. Approximately 36 to 62 embryos for each injection were counted; the representative picture (D) showed abnormal anterior-posterior axis development (black arrowhead) and dilated heart (red arrow) for the affected embryos. (This experiment was done by our collaborator from Sichuan University, China.)

4.3 Discussion

In this chapter of thesis, we infected C2C12 myoblasts with retroviral V5-tagged nesprin-1α_2 WT and mutants to investigate their effects on myogenesis *in vitro*. The C2C12 overexpressed nesprin-1 mutants or DN KASH1 showed significantly reduced fusion index, with increased population of multinucleated myotubes with fewer nuclei and dysregulated MRFs. Those changes suggested the nesprin-1α_2 mutants resulted in a compromised differentiation of these cells. Interestingly, we showed for the first time the interaction between nesprin-1α_2 and microtubule motor proteins KLC-1/2 and found the mutant nesprins affected their binding.

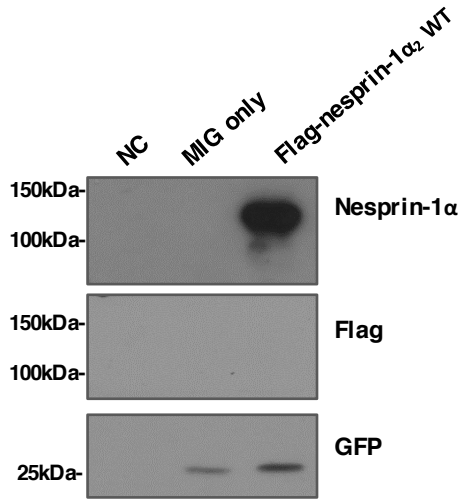
Depletion of KLC-1/2 exhibited the similar differentiation defects which caused by nesrin-1 mutants. *In vivo*, human nesprin-1α_2 WT causes heart developmental and conduction defects in zebrafish embryos while mutants induce a less severe heart phenotype due to disrupted LINC complex. These data further strengthened that an intact NE-LINC complex is critical for nuclear distribution, muscle cell differentiation and heart development.

4.3.1 Generation of retroviral nesprin-1 WT and mutant constructs

To investigate the effects of nesprin-1 mutants in a C2C12 differentiation model *in vitro*, retroviral constructs were generated. The initial aim was to generate flag-tagged nesprin-1α_2 WT and mutant versions of nesprin-1 retroviral constructs. Following the strategy described in 4.2.2, we successfully generated these constructs. Then the expression levels of nesprin-1α_2 and mutants were checked via transfecting the plasmids in C2C12 cells. Unfortunately, WB showed the exogenous flag-nesprin could not be detected by the flag antibody while it could be detected by anti-nesprin-1α antibody (Figure 4.30A). After optimisation of the experimental conditions, we still could not resolve this issue. Thus, the flag-tag was replaced by V5-tag, and the exogenous protein level was successfully detected by both anti-V5 and anti-nesprin-1α antibodies (Figure 4.30B).

Another challenge for retroviral experiments was how to choose the proper internal control to analyse data. The V5-tag was the best candidate as it was fused to the nesprin-1α, which would directly indicate how much proteins was overexpressed

A.



B.

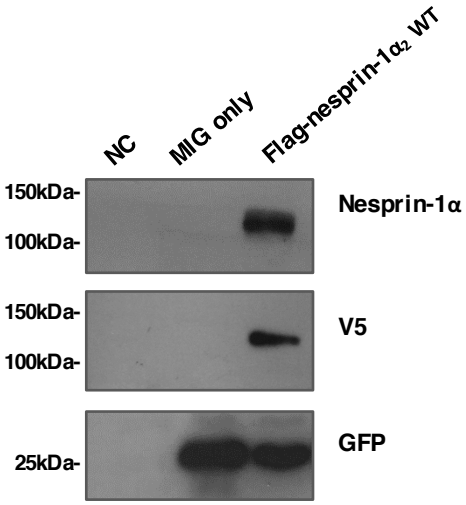


Figure 4.30 Overexpression of flag/V5-tagged nesprin-1α$_2$ in C2C12 cells

The exogenous flag tagged nesprin-1α could be detected via anti-nesprin-1 antibody, but not the anti-flag antibody in C2C12 cells transfected with flag-tagged nesprin-1α$_2$ WT and MIG only (A). While the exogenous V5 tagged nesprin-1α could be detected via both anti-nesprn-1 and V5 antibodies in the cells transfected with V5-tagged nesprin-1α$_2$ WT and MIG only (B). Untreated cells served as a negative control (NC); GFP served as the markers for transfected cells.

after RVs infection. However, V5-KASH was only 10kDa and too small to be detected by immunoblotting; additionally, V5 was not present in the MIG-only vector. GFP was the other candidate as it was expressed under the same promotor with V5 fused nesprin-1α, but independently. GFP was contained in all the constructs as well as MIG only, and could easily be detected by WB. qPCR showed a very positive correlation of the expression levels (CT value) between GFP and V5-nesprin-1α_2 (Figure 4.31). Therefore, GFP was chosen as the standard to measure the expression level of exogenous nesprin-1 for further experiments.

4.3.2 Nesprin-1 mutations caused dysregulation of MTFs in myoblast differentiation

Nesprin-1α_2 is highly expressed in both skeletal and cardiac muscles as previously shown [1, 37, 38]. Although there were no obvious muscle phenotypes recorded in these DCM patients harbouring these mutations, it is plausible that in the patients presenting with the *SYNE-1* mutations, the skeletal muscle dysfunction was too subtle or underestimated at clinical examination. Alternatively, in addition to these *SYNE-1* mutations, another cardiac disease gene is potentially mutated thus enhancing the phenotype. Therefore, due to restricted accessibility to patient samples, we focused on investigating if these three novel mutants cause muscle dysfunctions by using the C2C12 mouse myoblast differentiation model.

Myogenesis involves a series of sequential steps. Myoblasts originating from the mesoderm are converted to skeletal muscle lineage myoblasts after MyoD expression, enter the cell cycle and proliferate, then withdraw from the cell cycle and initiate differentiation with expression of MTFs such as myogenin. Next cell fusion occurs to form multinucleated myotubes and expression of the muscle specific protein MHC [259-262]. Increasing evidence indicates that multiple cell signalling pathways play critical roles in myoblast fusion, including those involved in cytoskeleton organisation, cell adhesion and migration [262] as well as extracellular signalling molecules and components of extracellular matrix [259, 269]. Recent literature shows that LINC complex components, including nesprins and SUN1/2, mechanically couple the nucleus to the extracellular matrix and play an important role in differentiating muscle. In addition, these proteins have been implicated in regulating chromatin structure and gene expression. For example, C2C12 cells expressing a *LMNA* R453W mutant have

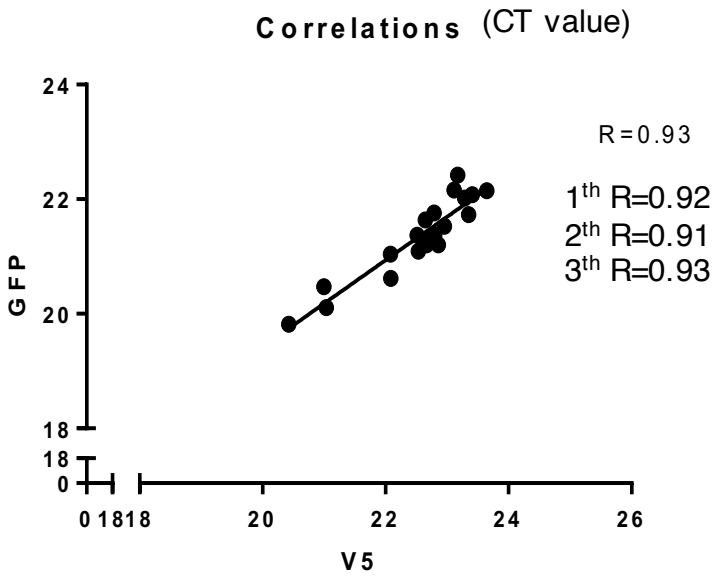


Figure 4.31 Expression level of V5-tagged nesprin-1α$_2$ and GFP was positively correlated

C2C12 myoblasts were infected with retroviral nesprin-1α$_2$ WT/mutants respectively. qPCR showed a positive correlation of the expression levels (CT value) between GFP and V5-nesprin-1α$_2$.

reduced capacity to differentiate, yet retain an unaltered morphology [263, 264], suggesting that subtle abnormal changes in lamina structure or composition may impair the anchoring of chromatin to the NE, affecting gene activities and regulation which are indispensable for muscle differentiation, thus perturbing myogenesis.

Using retroviral transduction in mouse C2C12 myoblasts in the current study, our data showed myoblasts expressing mutant nesprin-1α_2 R8272Q or dominant negative-KASH1 had a significantly lower capacity to differentiate, and form multinucleated cells than those expressing 1α_2 WT, although exogenously expressed 1α_2 WT and mutants were observed to be properly localised at the NE. Importantly, the inhibition of multi-nucleation by dominant negative-KASH1 and 1α_2 mutants, especially R8272Q, is potentially linked to the inhibition of myogenin and MHC expression in transduced C2C12 cells. Our data also showed that nesprin-1α_2 was expressed in the initial stage crucial for converting C2C12 myoblasts into myotubes, and promoted myoblast differentiation during the process of myotube formation, whereas the mutants reduced or abolished the effects, suggesting that expression of nesprin-1α_2 mutants does not alter the proliferation of myoblasts, but rather impairs their capacity to express muscle-specific genes (myogenin and MHC). This results in an inability to fuse, especially observed in the R8272Q mutant, which also explains why nesprin-1 mutants affect the expression levels of myogenin more severely than MyoD, because MyoD is already expressed prior to initiation of differentiation at a stage when the expression level of nesprin-1 is still low. Therefore, we propose the following mechanisms whereby nesprin mutants may affect muscle differentiation: regulation of myogenin and expression of MHC are influenced by the LINC complex; nesprin mutants may fail to build a functional scaffold and/or to maintain chromatin compartmentalisation with lamin A/C, leading to an alteration in the amount of heterochromatin formed and/or its localisation. Potentially this causes defects in initiation of the terminal differentiation process resulting in decreased or delayed expression of myogenin and MHC, thus causing a delayed differentiation. This effect may be similar to that observed in C2C12 cells expressing an *LMNA* R453W mutant [263, 264] that showed a reduced capacity to differentiate. However, further experimentation on how nesprin-1 mutants affect regulation of MTFs is required to elucidate the precise function of nesprin in muscle cell differentiation.

4.3.3 Nesprin-1 mutations disrupted nesprin-1/KLC interaction and myoblast fusion

Proper nuclear positioning and movement is critical in muscle cell differentiation and development. In the nucleus, changes in gene activity that occur during terminal cell differentiation correlate with gene migration and relocation [270, 271]. Nuclear movement and positioning are driven by cytoskeletal networks of microtubules, actin and/or IFs and involve a connection between the cytoskeleton and the NE, mediated by the LINC complex [181, 191]. KO mouse studies have shown that nesprin-1 and SUN1/SUN2 play critical roles in anchoring nuclei in skeletal muscle [81, 135, 138]. Similarly, mutations identified in SUN1 and SUN2 genes associated with EDMD like phenotypes cause defective nuclear positioning when expressed in mouse fibroblasts [87]. The microtubule-based kinesin motor, kinesin-1, consisting of two KHCs and two KLCs, is localised at the NE. Binding of the dominant light chain isoform in muscle, KLC-2 [272], to nesprin-2 has been shown to be responsible for nuclear rotations and movement along microtubules [114]. There is evidence that nuclear position can influence gene expression. For example, nuclei at the neuromuscular junction (NMJ) have a unique transcriptional profile relative to the non-synaptic nuclei [271]. Nesprin-1 (*SYNE-1*) levels are much higher in synaptic nuclei than extrasynaptic nuclei, and also higher in myotubes than myoblasts in culture and central nuclei during regeneration [13, 38]. In addition, maintaining proper nuclear positioning is thought to ensure sufficient transcriptional capacity and minimise transport distances between the nuclei and the cytoplasm in highly organised long muscle cells [181, 273]. Our data confirmed that nesprin-1 binds to KLC-1/2, and nesprin-1 mutants, particularly R8272Q, disrupted this interaction. Overexpression of the DN KASH1 protein prevented recruitment of the kinesin to the NE in myotubes which were consistent with the findings in the nesprin-1α_2 KO mouse model [124]. Furthermore, depletion of KLC-1 resulted in nuclear clustering, whereas depletion of KLC-2, a dominant muscle isoform, caused a reduction of MHC levels and the fusion index in myotubes that was consistent with those observed in the R8272Q mutant. This disruption of nesprin-1/KLC interaction in C2C12 myoblasts may result in defects in nuclear movement along microtubules, leading to abnormal nuclear positioning. Further investigations

are required to elucidate the precise roles of nesprin-1 and KLC-1 and -2 in myonuclear positioning in muscle cell differentiation.

4.3.4 Expression of nesprin-1α$_2$ mutants induced less severe heart defects during zebrafish heart development compared to 1α$_2$ WT

To investigate whether the nesprin mutants affect cardiac structure or function *in vivo*, we generated a zebrafish model by expressing human nesprin-1α$_2$ WT and mutants (R8272Q, S8381C and N8406K) in zebrafish embryos via injection of the corresponding human *SYNE-1*α$_2$ (nesprin-1α$_2$) mRNAs. The nesprin-1α$_2$ in zebrafish is 50% homologous to human nesprin-1α$_2$ (protein sequence was from [22] and compared with BLAST sequence analysis tool). Our data showed that human nesprin-1α$_2$ WT causes heart developmental and conduction defects in zebrafish embryos, and all three 1α$_2$ mutants caused less severe heart developmental defects. Although these results are unexpected, there are some potential explanations. The literature shows that myoblasts originating from the mesoderm are converted to skeletal muscle lineage myoblasts after MyoD expression, enter the cell cycle and proliferate, then withdraw from the cell cycle and initiate differentiation with expression of MTFs such as myogenin [259-262]. So far, there is no direct evidence showing the expression profile of nesprin-1 and -2 during the embryos development either in murine or human species. However, there is evidence that the expression of nesprin-1α$_2$ is relatively low in human myoblasts, while massively upregulated in human myotubes [37]. Analysis of expression profile of nesprins during human muscle development revealed an increase in nesprin-1 giant during early myogenesis *in vitro* [38]. Our data also showed there is very limited amount of nesprin-1α$_2$ expression in the initial stage of muscle cell differentiation. Therefore, it is plausible to suggest there is no nesprin-1α$_2$ expression in the zebrafish egg given there is no muscle cell differentiation at this stage. Forced expression of human nesprin-1α$_2$ mRNA in the injected zebrafish larvae at the one-cell stage when there was no expression of endogenous nesprin-1α$_2$ led to ectopic expression of nesprin-1α$_2$, potentially causing differentiation defects in heart development. All three nesprin-1α$_2$ mutants showed much less dilated heart phenotype compared to nesprin-1α$_2$ WT, suggesting that the altered binding interactions of these

mutants with binding partners caused less severe disruption to heart development, consistent with the *in vitro* binding data in Chapter 3.

4.3.5 Summary

In this chapter, we focused on the roles of nesprin-1 in myogenesis and heart development, and identified:

I) *In vitro*:

1. Nesprin-1α_2 mutants delayed myoblast fusion and dysregulated MRFs, resulting in myogenesis defects in C2C12 differentiation models;
2. Nesprin-1α_2 interacted with microtubule motor proteins KLC-1/2 and regulated nuclear migration and positioning during muscle cell differentiation, while the mutants caused defects in myogenesis via perturbing their interaction;

II) *In vivo*:

Expression of nesprin-1α_2 mutants induced less severe heart defects during zebrafish heart development compared to 1α_2 WT. This indicated the current zebrafish model is not an ideal *in vivo* model as forced expression of nesprin-1α_2 caused ectopic expression of nesprin-1 before expression of the endogenous isoform. Future studies utilising the zebrafish model with either cardiac (tissue specific) [274] / heat shock protein (timing dependent) promotors [275] or CRISPR/Cas9-mediated knock-in [276] is required to physiologically expressed nesprin-1 and characterised the impact of nesprin-1 mutants during zebrafish heart development.

The literature and the data I have presented showed the NE-LINC complex disruption caused by nesprin mutants is the key step that leads to muscular dystrophy. Therefore, I am going to target the NE and multiple nesprin KASH containing isoforms, and generate cardiac specific nesprin-2 KASH transgenic mice and further characterise the roles of nesprin in heart in Chapter 5.

Chapter 5: Generation and characterisation of cardiac specific nesprin-2 KASH transgenic mice

5.1 Introduction

In Chapters 3 and 4, the data I have shown suggest that nesprin-1 plays multi-functional roles at the NE. These nesprin-1 mutants and DN KASH1 compromised the NE-LINC complex, leading to defects in NE organisation and myogenesis, and reinforcing the importance of an intact NE-LINC complex in linking the nucleus to the cytoskeleton and maintaining normal physiology and homeostasis. However, the roles of nesprins-1/-2 in heart have not been properly investigated *in vivo*, and there are a number of issues that still need to be resolved, in particular the lack of specific mouse models.

Existing nesprin-1 and/or -2 mouse models provide valuable information regarding nesprin functions in maintaining nuclear morphology and regulating nuclear migration and positioning [4, 83, 85, 123, 124, 135-138, 221, 273]. However, two of the existing nesprin-1 KO mice exhibited cardiac phenotypes, but the origin of the phenotype may not even be directly due to nesprin-1 depletion. In one model, an aberrant 61 amino acid substitution of the KASH domain was generated upon global ablation of nesprin-1 KASH [4, 221]. In the other, cardiac specific nesprin-1 depletion was performed in addition to nesprin-2 global KO model [85]. It is plausible the cardiac defects observed in these two mouse models resulted from the aberrant 61 amino acid substitution of KASH in the first mouse model and partly due to the global effect of nesprin-2 KO in the second model [4, 85, 221]. Of note, most of the mouse models do not recapitulate the human disease, as these models require homozygous expression of the mutant alleles to show the disease phenotype. These strategies ignore the potential role of the presence of the WT allele in disease pathogenesis as most of human diseases, especially EDMD and DCM, are autosomal dominant [3, 4, 122].

To further investigate the roles of nesprin-1/-2 via NE-LINC complex disruption in regulating pathogenesis in hearts, I aimed to target the NE and multiple nesprin KASH containing isoforms using a DN-KASH strategy, by taking advantage of the existing KASH2 Tg mouse strain [238, 239] and MLC2V Cre mice [277] to establish

a novel cardiac specific nesprin KASH2 Tg (csKASH-Tg) mouse line. In the csKASH-Tg mice, the multiple nesprin KASH containing isoforms were dislodged from the NE by overexpressing KASH2 and generating the specific NE-LINC complex disruption model in the cardiomyocytes (CMs) (Figure 5.1).

The Tg KASH mouse strain (CAG-LacZ-V5/EGFP-KASH2) was generated by our collaborator Dr. Didier Hodzic in Washington University [238, 239]. This mouse harbours a genetic construct consisting of an open reading frame (ORF) encoding mouse nesprin-2 KASH domain fused to EGFP (EGFP-KASH2), cloned downstream of a Lox-flanked ORF encoding β-galactosidase fused to a V5 epitope (LacZ-V5) with a flanked STOP codon at the end [238] (Figure 5.2A). This model has been successfully used to investigate the functions of nesprin in cerebellum and retina development, and exhibits efficient KASH2 overexpression, mis-localisation of the endogenous nesprin to the endoplasmic reticulum (ER) and NE-LINC complex disruption in a tissue specific manner [238, 239] (Figure 5.1).

Myosin light chain 2 ventricular (MLC2V) Cre mice were originally generated by Prof. Ju Chen in San Diego University [277]. These mice carry the Cre-recombinase gene under control of endogenous MLC2V. MLC2V encoded by *MYL2* gene, as a ventricular-restricted marker, presents as early as E8.75 during mammalian cardiogenesis [278], and is involved in maintaining cardiac contractility and ventricular chamber morphogenesis [279, 280]. The MLC2V Cre mice have been widely used for generating cardiac specific mouse models for over 20 years (Figure 5.2B).

In this chapter, I aimed to:

1. Generate a cardiac specific NE-LINC complex disruption mouse model by overexpressing the DN KASH2 under the cardiac specific promotor MLC2V;
2. Characterise the phenotypes of this csKASH-Tg mouse model at the basal line;
3. Further characterise the heart phenotypes of the csKASH-Tg mice after subjected to pathological hemodynamic stress.

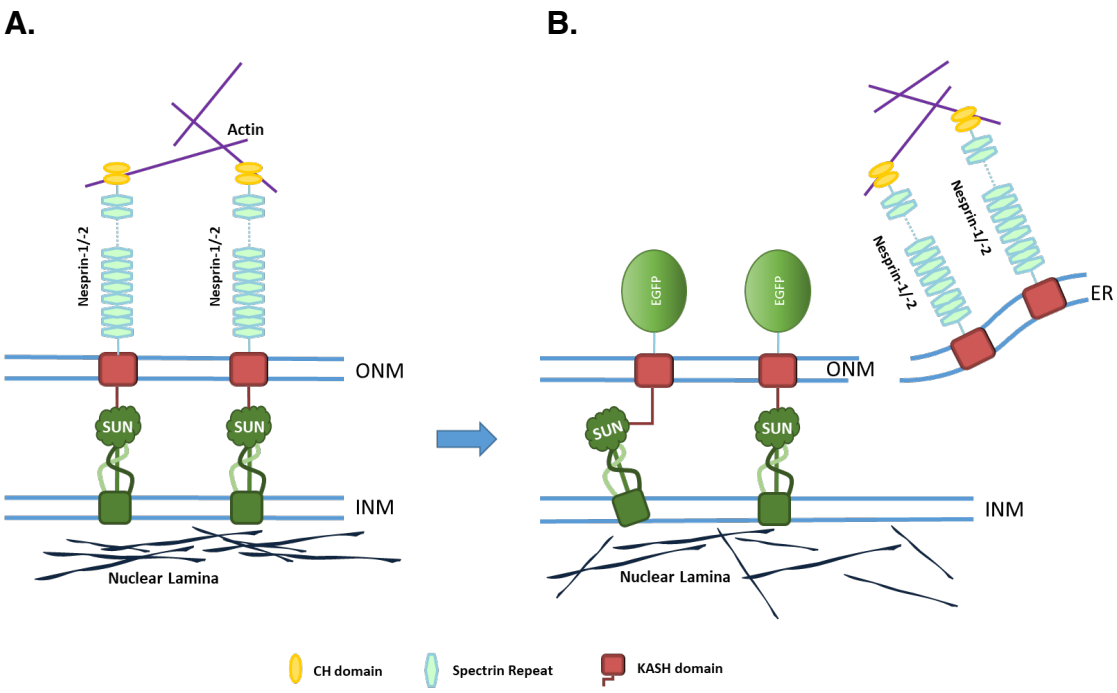


Figure 5.1 Overexpression of EGFP-KASH2 result in NE-LINC complex disruption

SUN domain containing proteins interact with KASH domain containing proteins to form the 'hub' of LINC complex, linking the nucleus to the cytoskeleton(A). Overexpression of EGFP-KASH2 displaces endogenous nesprin-1 and -2 from the NE to the endoplasmic reticulum (ER), in a dominant negative fashion, thus uncoupling the nucleoskeleton from the surrounding actin cytoskeleton (B).

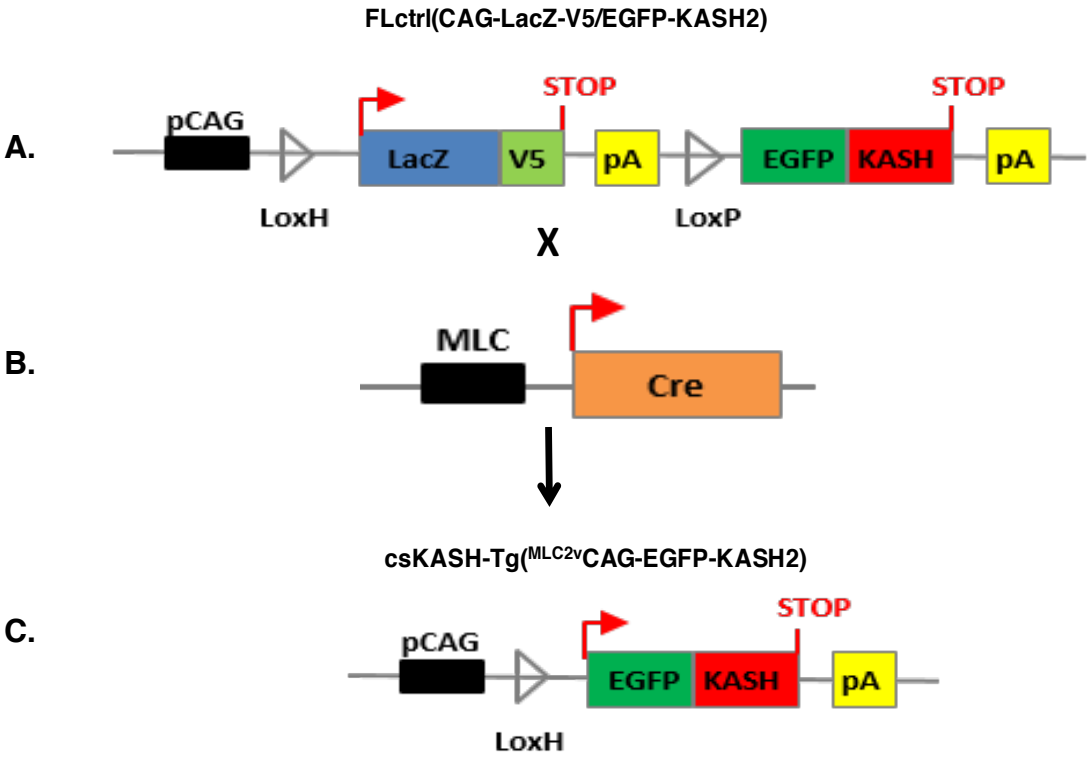


Figure 5.2 Breeding strategy of cardiac specific KASH2 Tg mice

Breeding of Tg KASH (CAG-LacZ/EGFP-KASH2) with Tg (MLC2V Cre) mice produced Tg (^{MLC2V}CreCAG-EGFP-KASH2) offspring in which Cre recombinase was expressed specifically in cardiomyocytes, allowing expression of GFP-KASH2 in heart tissue under a MLC2V promotor.

5.2 Results

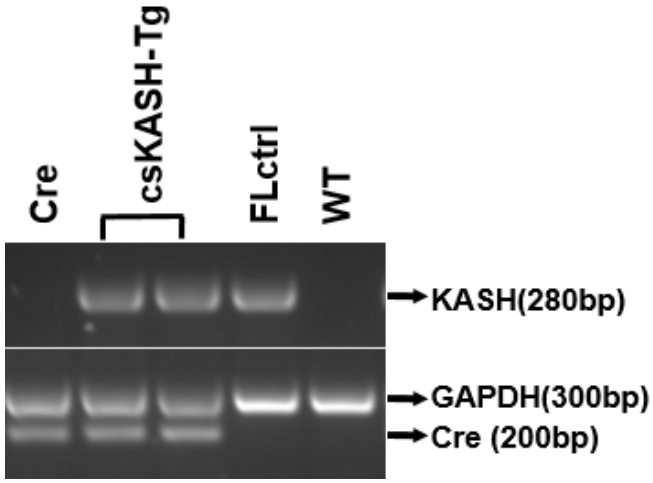
5.2.1 Establishment of a novel cardiac specific KASH2 Tg mouse model

By breeding MLC2V Cre mice with Tg KASH mice, Cre-recombinase mediated somatic excision of the LacZ/V5 ORF and STOP codon, allowed activation of transcription of EGFP-KASH2 specifically in CMs under the MLC2V promotor (Figure 5.2).

All mice used in this study are of C57/BL6 strain. Offspring were genotyped after birth using primers designed to identify the 'GFP-KASH2' and 'MLC2V Cre' simultaneously. The control group was Tg KASH2 mice that were referred to as floxed control (FLctrl). Mice with both EGFP-KASH2 and Cre expression were named as cardiac specific Tg KASH2 (csKASH-Tg). MLC2V Cre only mice were referred as Cre. Mice containing neither the GFP-KASH2 nor Cre were named as WT (Figure 5.3A). Genotypic analysis of total 193 pups showed that the expression of the GFP-KASH2 gene did not affect Mendelian birth ratios (Figure 5.3B).

WB showed EGFP-KASH2 was specifically expressed in csKASH-Tg heart when compared with the FLctrl heart (Figure 5.4A). qPCR further showed the expression level of exogenous KASH2 in csKASH-Tg was 12-fold high when compared with FLctrl, which only had endogenous KASH2 expression (Figure 5.4B). There was no expression of GFP-KASH2 in other tissues including skeletal muscle, lung, aorta, liver and kidney in both csKASH-Tg and FLctrl (Figure 5.4A). IF showed the subcellular localisation of GFP-KASH2 only present at the NE of CMs in csKASH-Tg mice compared with FLctrl mice (Figure 5.4C). There was no staining of GFP-KASH2 in other organs including skeletal muscle, lung, aorta, liver and kidney in both csKASH-Tg and FLctrl groups (Figure 5.4C). These data validated the success of overexpression of GFP-KASH2 in heart.

A.



B.

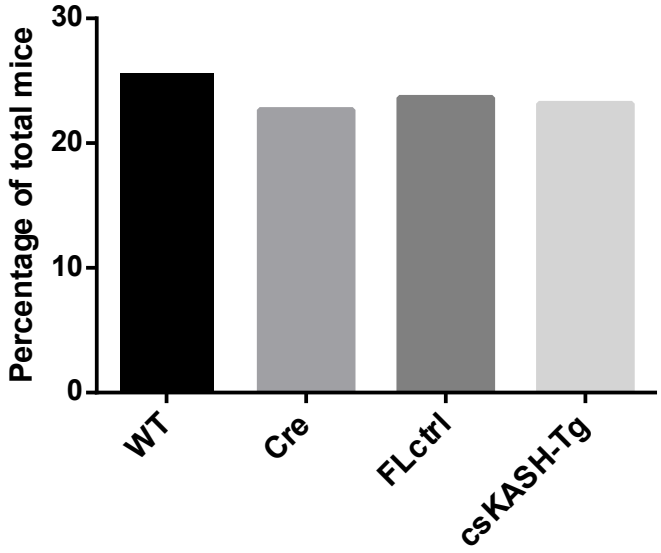
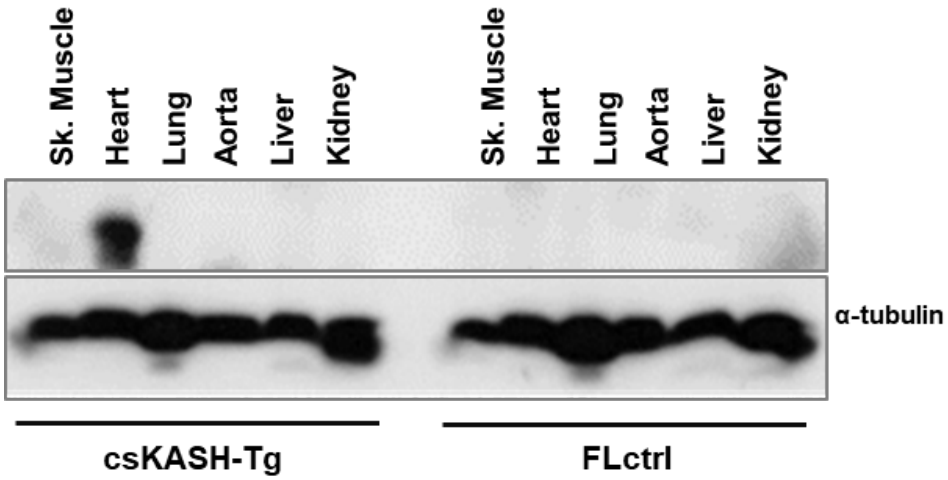


Figure 5.3 Transgenic mice were born at the expected Mendelian ratios

PCR genotyping of DNA extracted from the ear biopsy was performed with primers targeted to the 'GFP-KASH2' (~280bp) or 'Cre' (~200bp) sequence. GAPDH (~300bp) served as an internal control. The 'GFP-KASH2' only mice were referred to as floxed control (FLctrl). Mice with both 'EGFP-KASH2' and 'Cre' expression were named as cardiac specific Tg KASH2 (csKASH-Tg). Cre mice were the MLC2V Cre only. WT mice were the original C57/BL6 strain mice neither containing the GFP-KASH2 nor Cre. (B) Genotype ratios were present as a percentage of the total number of mice, which were born at the expected Mendelian pattern of 1:1:1:1. n=193 (WT=52; Cre=46; FLctrl=48; csKASH-Tg=47).

A.



B.

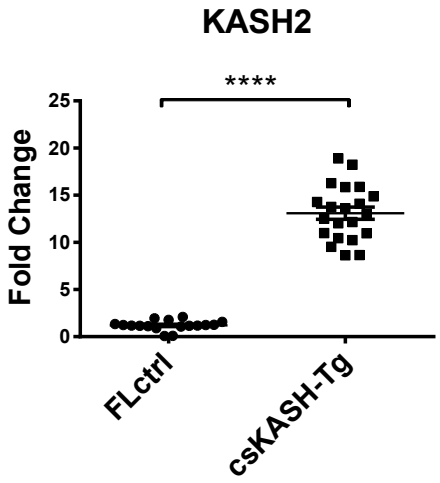


Figure 5.4 GFP-KASH was cardiac specifically expressed

(A) Using an antibody targeted to GFP protein, WB showed GFP-KASH2 was specifically expressed in csKASH-Tg heart compared with FLctrl. There was no expression of GFP-KASH in other tissues including skeletal muscle, lung, aorta, liver and kidney in both csKASH-Tg and FLctrl mice. (B) qPCR showed the expression level of exogenous KASH2 in csKASH-Tg was 12-fold high when compared with FLctrl, which only had endogenous KASH2 expression. FLctrl n=17; csKASH-Tg n=21 Data was analysed by Student's t-tests, shown as mean±SEM. *P<0.05.

C.

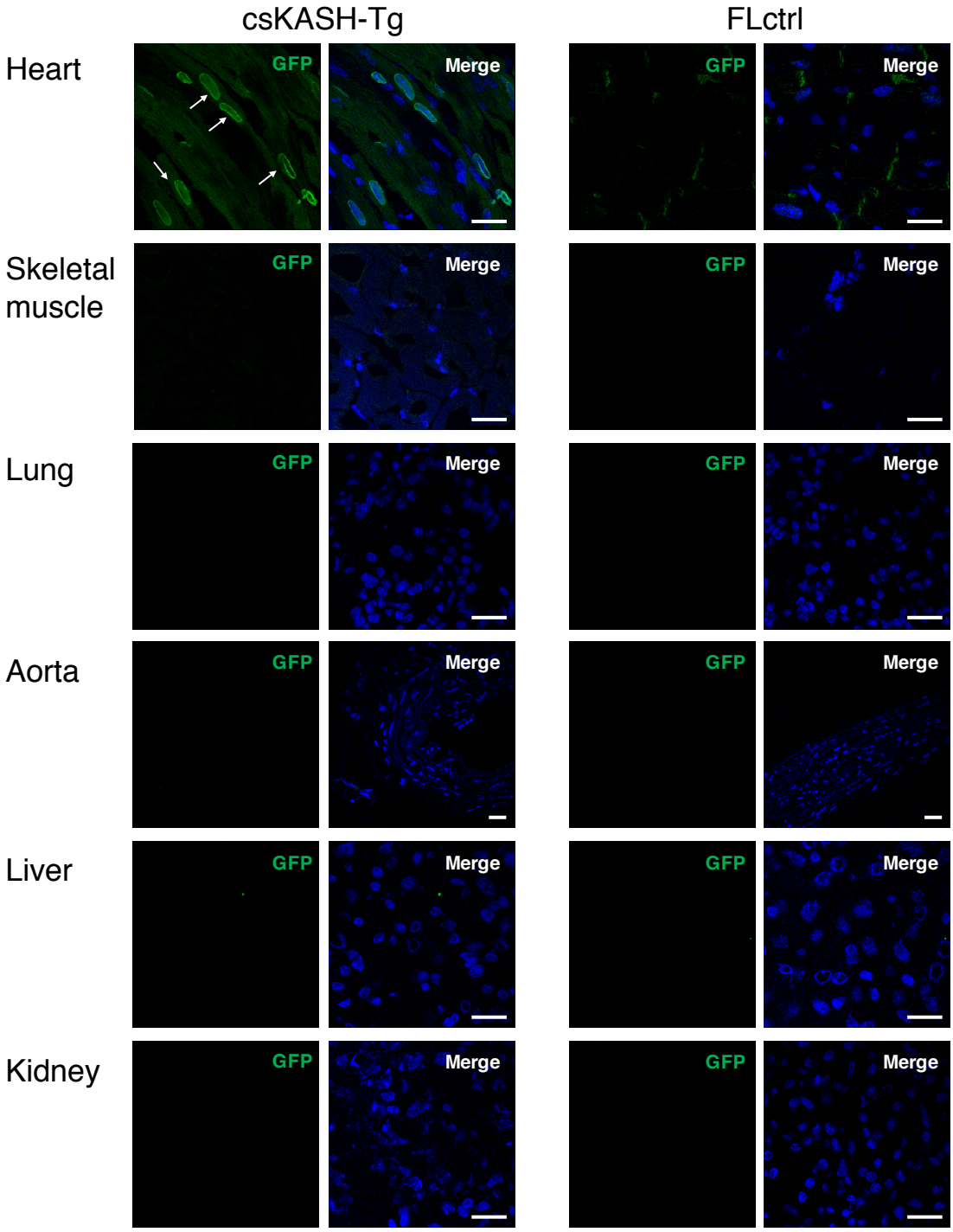


Figure 5.4 GFP-KASH was cardiac specifically expressed

(C) IF showed GFP-KASH2 wasmainly present at the NE of cardiomyocytes in csKASH-Tg mice compared with FLctrl mice. There was no observed GFP-KASH staining at the NE in other tissues including skeletal muscle, lung, aorta, liver and kidney in both csKASH-Tg and FLctrl groups. Scale bar=25μm.

5.2.2 Characterisation of cardiac specific KASH2 Tg mouse model at basal line

5.2.2.1 Cardiac specific KASH2 Tg mice developed normally up to one year

csKASH-Tg offspring developed normally up to 1 year after birth (Figure 5.5A). There was no observed gender difference and all mice survived during the first year of observation. Male pups were used for this study. There was no difference in body weight (BW), heart weight (HW), tibia length (TL) (Figure 5.5B), as well as the ratios of HW/BW and HW/TL (Figure 5.5C) between csKASH-Tg and FLctrl groups when observed at week 52.

5.2.2.2 Echocardiography showed the cardiac hypertrophic response was induced in csKASH-Tg mice

To evaluate cardiac structure and functions, non-invasive transthoracic echocardiography was performed on the csKASH-Tg and FLctrl mice at week 15, week 30 and week 52 respectively (Figure 5.6A). There was no difference in heart rate between the csKASH-Tg and FLctrl mice during echocardiographic assessment (Figure 5.6B)

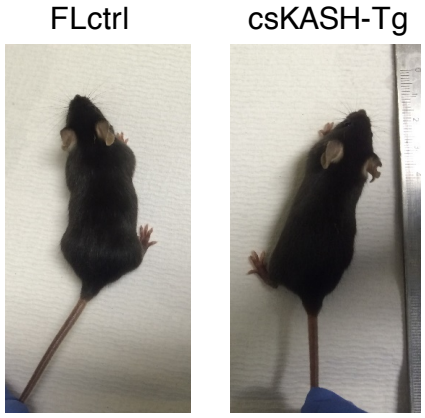
However, the cardiac structure showed significant changes at week 52. Firstly, structural parameters were analysed by comparing csKASH-Tg with FLctrl groups. In csKASH-Tg: echocardiography showed thickness of left ventricle (LV) wall including LV posterior wall during diastole and systole (LVPWd and LVPWs), was significantly increased (Figure 5.6C & 5.7A). The interventricular septum (IVS) showed a trend of mild increase, but no statistical significance (Figure 5.7B). The LV internal diameter at the end of diastole and systole (LVIDd and LVIDs) was significantly decreased (Figure 5.7C), and both LV end-systolic (ESV) and -diastolic volume (EDV) were reduced (Figure 5.7D). There was a reduction of stroke volume (SV) (SV=EDV-ESV) (the volume of blood pumped from the LV per beat) in csKASH-Tg compared with FLctrl (Figure 5.7E).

Following this, the functional parameters were then analysed. Heart function was evaluated by measuring ejection fraction (EF=SV/EDV) or fractional shortening

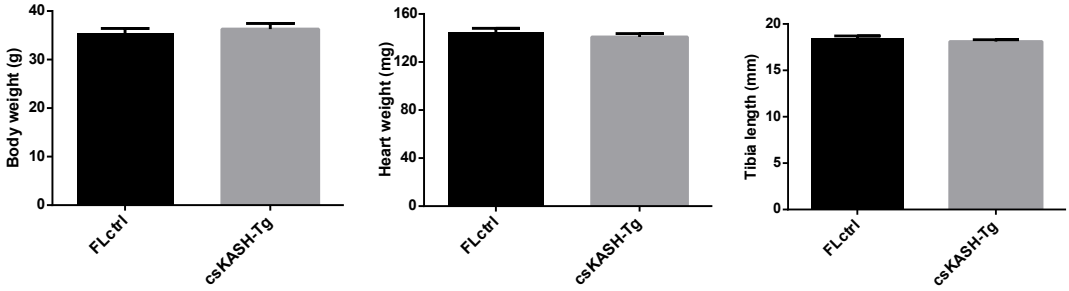
(FS=(LVIDd-LVIDs)/LVIDd), which are the important index of heart systolic function [240]. Echocardiography showed there was no difference in either EF or FS between csKASH-Tg and FLctrl mice (Figure 5.7F).

In summary (Table 5.1), the echocardiographic data indicated a hypertrophic response was induced by accumulation of DN-KASH in csKASH-Tg mouse hearts.

A.



B.



C.

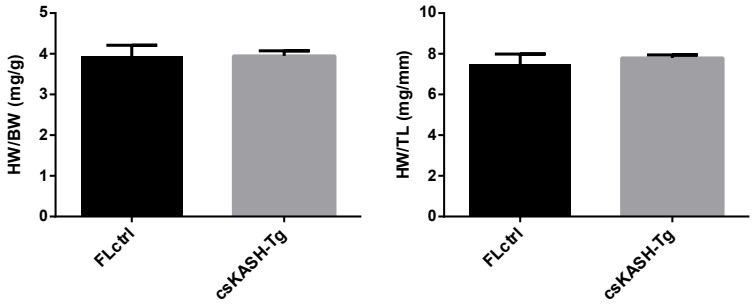
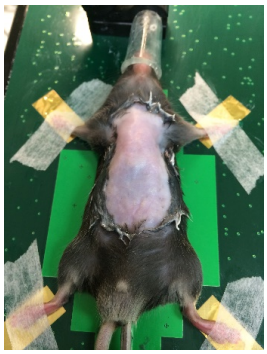


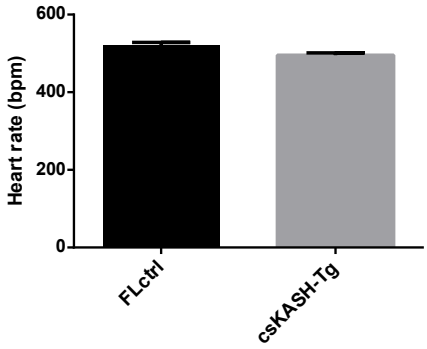
Figure 5.5 csKASH-Tg mice developed normally up to 1 year

csKASH-Tg offspring developed normally up to 1 year after birth. There were no observed gender difference and all mice survived during the first year of observation (A). Male pups were used for this study. There was no difference in body weight (BW), heart weight (HW), tibia length (TL) (B), as well as the ratios of HW/BW and HW/TL (C) between csKASH-Tg and FLctrl groups when observed at week 52. FLctrl n=11; csKASH-Tg n=15. Data was analysed using Student's t-tests, shown as mean±SEM.

A.



B.



C.

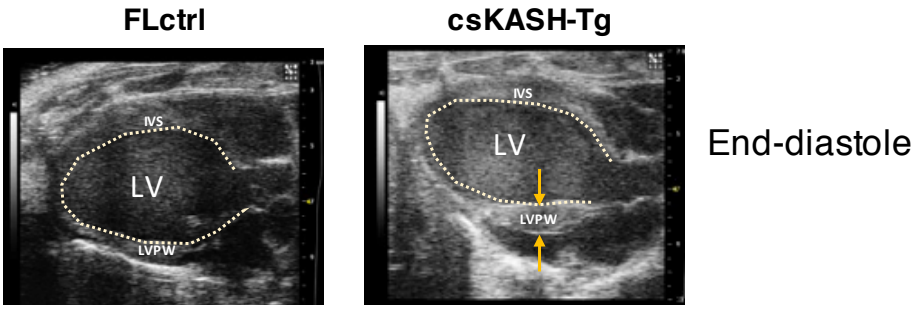


Figure 5.6 Echocardiography showed an increased LV wall thickness in csKASH-Tg mice

Cardiac structure and function were measured by echocardiography when mice were under anaesthesia (A). There was no difference in heart rate between the csKASH-Tg and FLctrl mice during echocardiographic assessment (B). LV parasternal long axis showed an increased LV wall thickness, especially the left ventricular posterior wall (LVPW) (yellow arrow) at the end-diastole in csKASH-Tg compared with FLctrl (C). FLctrl n=11; csKASH-Tg n=15. Data was analysed by Student's t-tests, shown as mean±SEM.

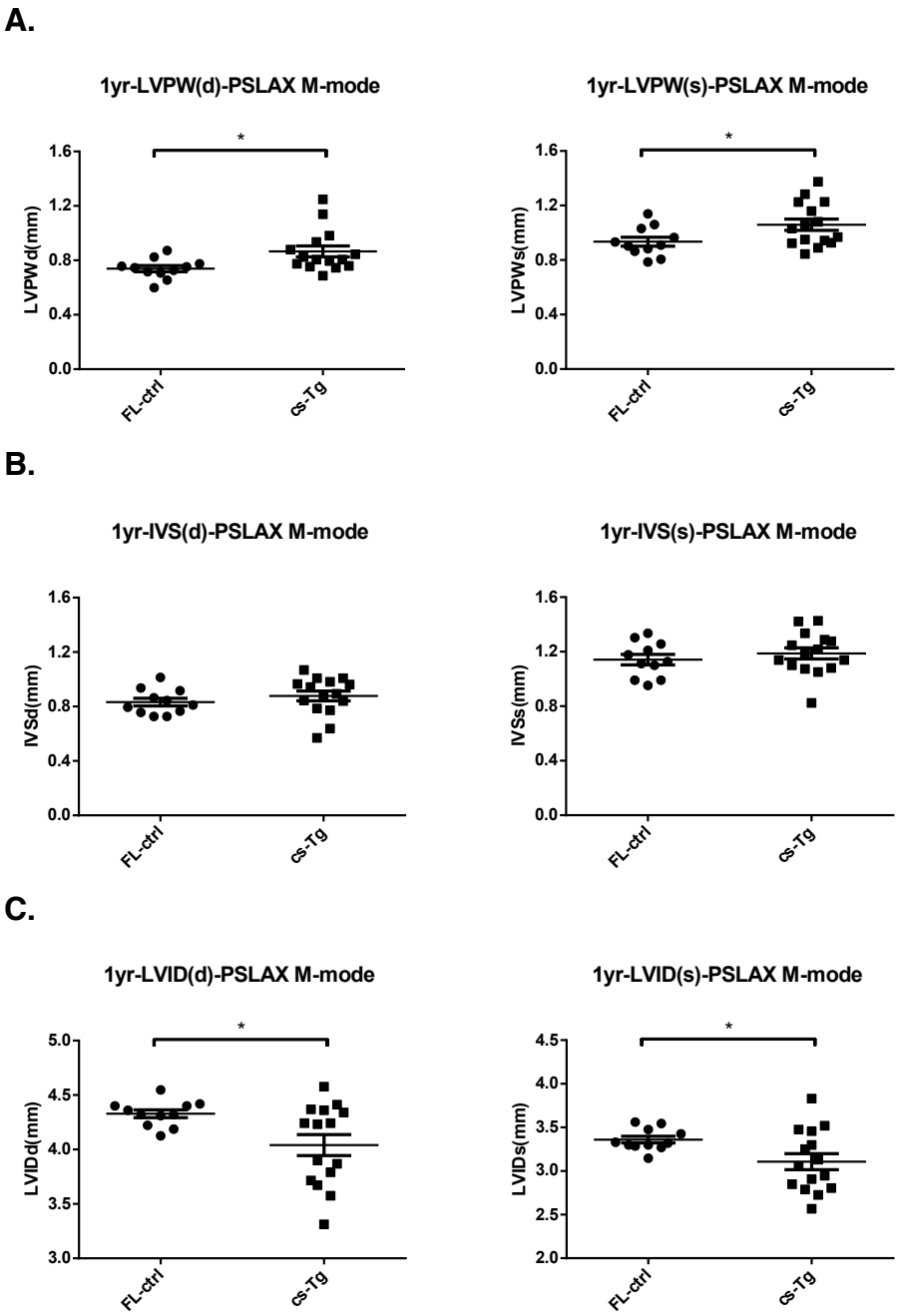
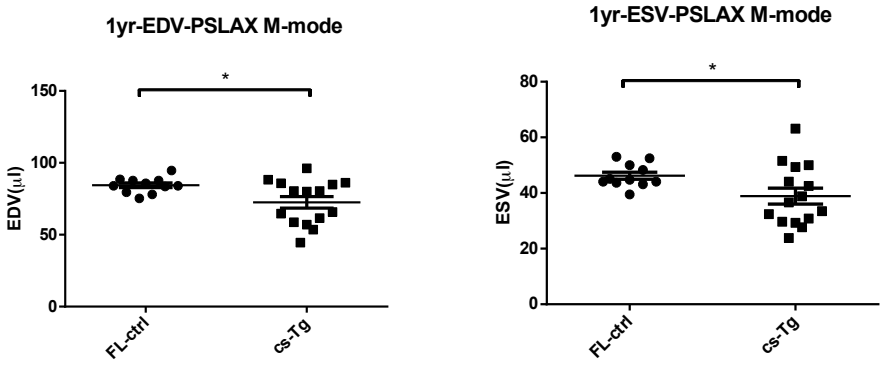


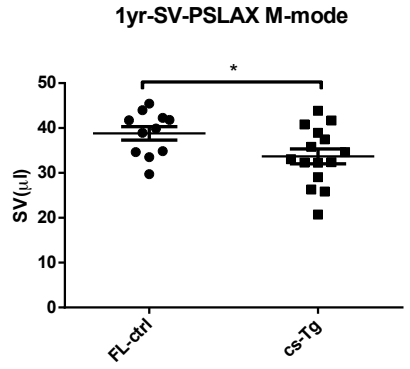
Figure 5.7 Echocardiography showed the cardiac hypertrophic response was induced in csKASH-Tg mice

Echocardiography were analysed by comparing csKASH-Tg with FLctrl groups. In csKASH-Tg mice, there was a significant increased thickness of the left ventricular posterior wall during diastole and systole (A: LVPWd and LVPWs); a trend of increased interventricular septum (IVS) (B); decreased left ventricular internal diameter at the end of diastole and systole (LVIDd and LVIDs) (C).

D.



E.



F.

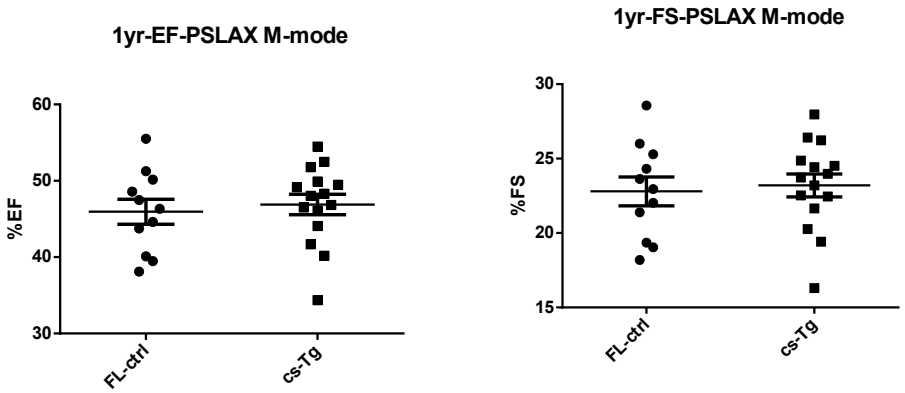


Figure 5.7 Echocardiography showed the cardiac hypertrophic response was induced in csKASH-Tg mice

There was a reduced left ventricular end-systolic (ESV) and -diastolic volume (EDV) (D) as well as stroke volume (SV) (E). There was no difference in either ejection fraction (EF) or fractional shortening (FS) between csKASH-Tg and FLctrl mice (F). FLctrl n=11; csKASH-Tg n=15. Data was analysed by Student's t-tests, shown as mean±SEM. *P<0.05.

Table 5.1 Echocardiographic analysis showed a cardiac hypertrophic response was induced in csKASH-Tg mice at 52 weeks

	Parameter	**Units**	**FLctrl**	**csKASH-Tg**	**P value**	**Significant**
	Heart rate	bpm	521.6±6.9	503.9±5.4	0.0544	ns
LV wall	LVPWd	mm	0.74±0.02	0.87±0.04	0.0196	*
	LVPWs	mm	0.93±0.03	1.06±0.04	0.0358	*
	IVSd	mm	0.83±0.02	0.88±0.03	0.3645	ns
	IVSs	mm	1.14±0.04	1.19±0.04	0.4370	ns
LV internal diameter	LVIDd	mm	4.33±0.04	4.04±0.10	0.0214	*
	LVIDs	mm	3.36±0.04	3.11±0.09	0.0345	*
LV volume	EDV	μl	84.48±1.64	72.58±3.97	0.0221	*
	ESV	μl	46.22±1.27	38.90±2.84	0.0476	*
	SV	μl	38.80±1.49	33.68±1.66	0.0372	*
Heart function	EF	%	45.95±1.63	46.89±1.34	0.6571	ns
	FS	%	22.80±0.97	23.20±0.77	0.7451	ns
ns: not significant; * P<0.05						

5.2.2.3 Histological examination showed thicker LV wall and fibrosis in csKASH-Tg mouse hearts

To evaluate the morphological feature of hearts in csKASH-Tg mice, Haematoxylin and Eosin (H&E) staining was performed on frozen heart sections (long axis). Analysing the four heart chambers under the light microscopy with low power, there was an increased thickness of LV wall in csKASH-Tg mice compared with FLctrl mice at 1-year time point (Figure 5.8).

To investigate if there was any interstitial collagen deposition in csKASH-Tg mouse hearts, Masson's trichrome staining was performed on the frozen heart sections (short axis). There was some fibrosis staining present in csKASH Tg mouse hearts at 1 year old, but no fibrosis was detected in FLctrl mouse hearts (Figure 5.9).

5.2.2.4 Size of cardiomyocytes was increased in csKASH-Tg mice

To determine if there were differences in cardiomyocyte size caused by DN KASH2 expression, wheat germ agglutinin (WGA) staining was performed to stain the cell membranes on frozen heart sections (short axis) [281, 282]. Quantitation indicated there was a significant increased CM size in csKASH-Tg mice compared with FLctrl at 1-year-old (Figure 5.10).

5.2.2.5 Cardiomyocyte nuclear morphology was changed in csKASH-Tg hearts

To investigate if there were any changes of cardiomyocyte nuclear morphology in csKASH-Tg mice, nuclei were stained with DAPI and overexpressed GFP-KASH2 in CMs was detected by GFP staining. IF showed the exogenous GFP-KASH2 was only localised at the NE in the CMs in csKASH-Tg mice when compared with FLctrl mice (Figure 5.11A). The GFP-KASH2 positive CMs in csKASH-Tg exhibited an elongated nuclear shape compared with CMs in FLctrl mice (Figure 5.11A). Computational morphometric analyses showed dramatically increased nuclear length (long axis), perimeter and area in csKASH-Tg CMs when compared with the FLctrl mice (Figure 5.11B), however, no observed change of nuclear width (short axis). These

changes indicated there was enlarged nuclear size and altered nuclear morphology in CMs in csKASH-Tg mice.

5.2.2.6 Hypertrophic and fibrotic genes were expressed in csKASH-Tg mouse hearts

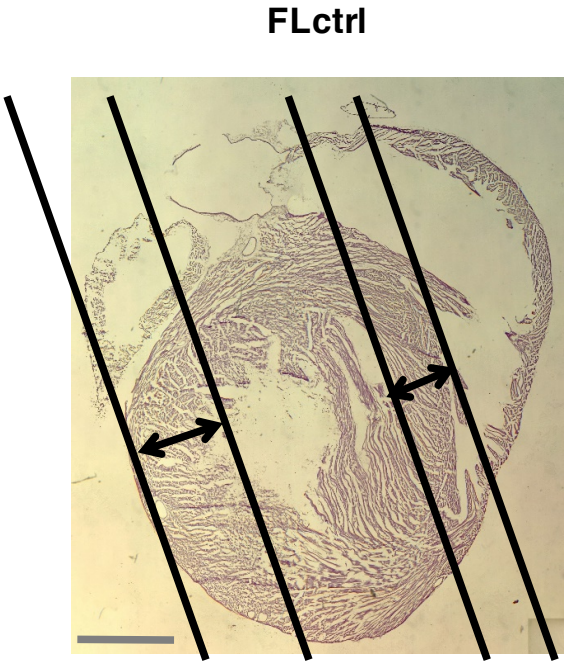
At the molecular level, the hypertrophic response or development of heart failure (HF) can be evaluated via reliable markers such as αMHC, βMHC, atrial natriuretic peptide (ANP) and brain natriuretic peptide (BNP) [283-286]. Gene expression of these fetal genes in our mouse model was analysed: βMHC, a marker for the major thick filaments in ventricles [284] was significantly increased in csKASH-Tg mice compared with FLctrl (Figure 5.12A). ANP, a hypertrophic marker [287], was 3-fold higher than FLctrl (Figure 5.12B). The fibrosis markers, pro-fibrotic genes procollagen1α1 and procollagen3α1 [288, 289] both showed an upregulation in csKASH-Tg mice compared with FLctrl (Figure 5.12C). There was no significant changes of other fetal genes including αMHC (the major isoforms expressed predominantly in cardiac atria [283]) and BNP (heart failure marker [286]) (Figure 5.12A & 5.12B). Those data further implied the LV was under the hypertrophic response, with modulation of expression of cardiac fetal genes and fibrotic genes.

5.2.2.7 Endogenous NE-LINC components were mis-localised from NE in csKASH-Tg mice

Our data in Chapter 3 and previous literatures suggest that nesprin mutants and DN KASH lead to mis-localisation of endogenous nesprin from the NE and also affect the localisation of its binding partners such as lamin A/C, emerin and SUN at the NE [3, 35, 178]. Therefore, the localisation of endogenous nesprin and its binding partners at the NE were further examined in the CMs of csKASH-Tg mice.

IF showed GFP-KASH2 accumulated at the NE of csKASH-Tg CMs, however, the staining of endogenous nesprin-1α was reduced at the NE in these CMs when compared with FLctrl mice (Figure 5.13A). IF also showed the mis-localisation of endogenous lamin A/C and emerin in the CMs upon overexpression of DN KASH2 (Figure 5.13B & 5.13C), suggesting NE-LINC complex was disrupted in csKASH-Tg mouse hearts.

A.



B.

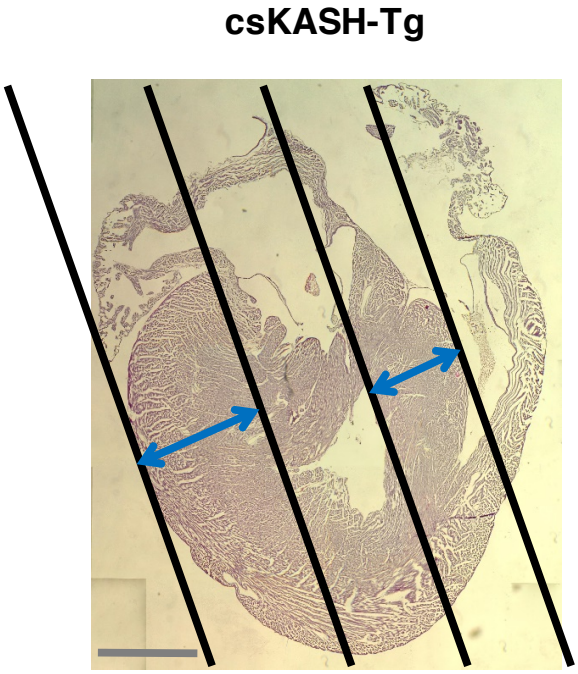


Figure 5.8 HE staining showed an increased LV wall thickness in csKASH-Tg mouse hearts

Haematoxylin and Eosin (H&E) staining was performed on frozen heart sections (long axis) to evaluate the morphological feature of hearts. The LV wall was thicker in csKASH-Tg (B, blue double-headed arrow) compared with FLctrl mice (A, black double-headed arrow) at 1 year time point. n=3/each group, Scale bar=2mm.

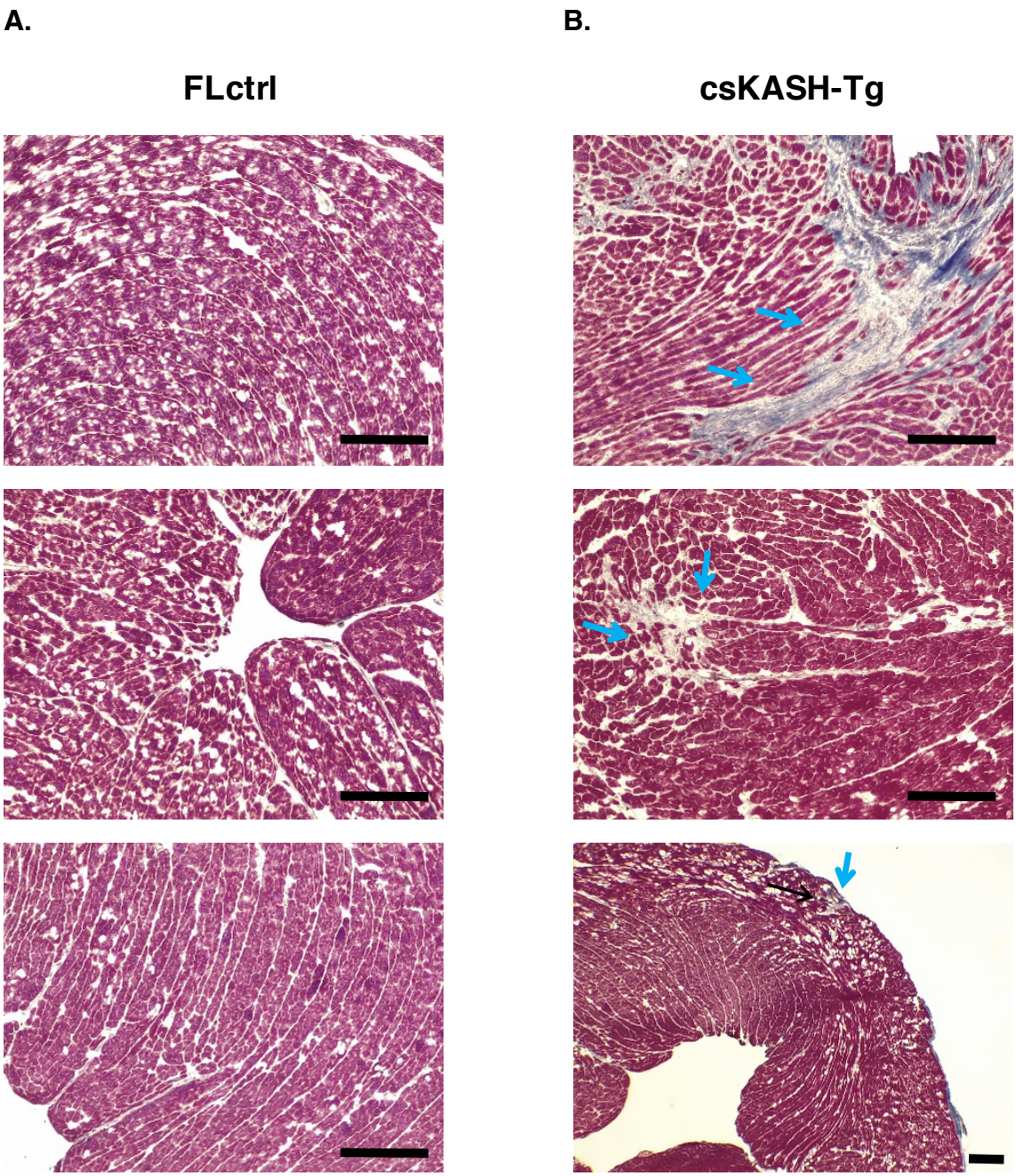
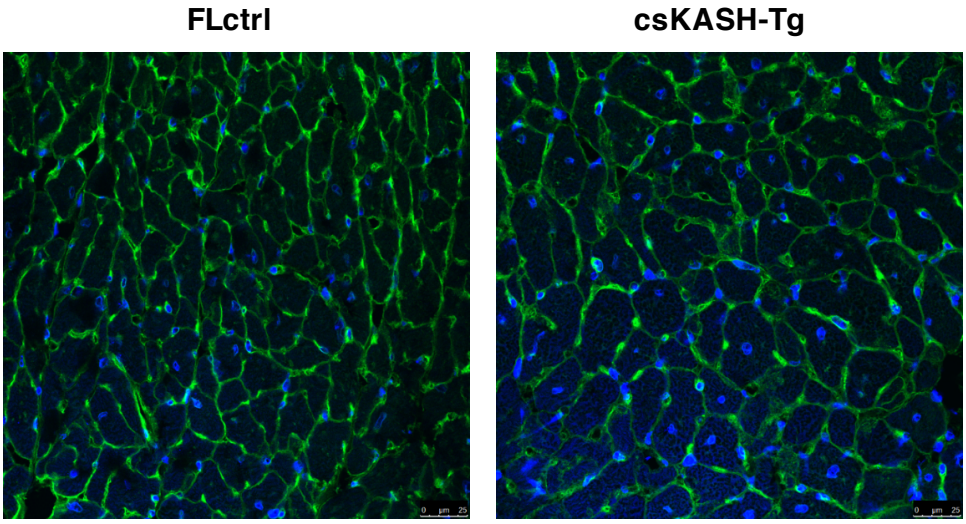


Figure 5.9 Myocardial fibrosis was observed in csKASH-Tg mice

Masson's trichrome was performed on frozen heart sections (short axis). There was some fibrosis staining present in csKASH Tg mouse hearts (B, blue arrow) at 1 year old, but no fibrosis was detected in FLctrl mouse hearts (A). Scale bar=20μm.

A.



B.

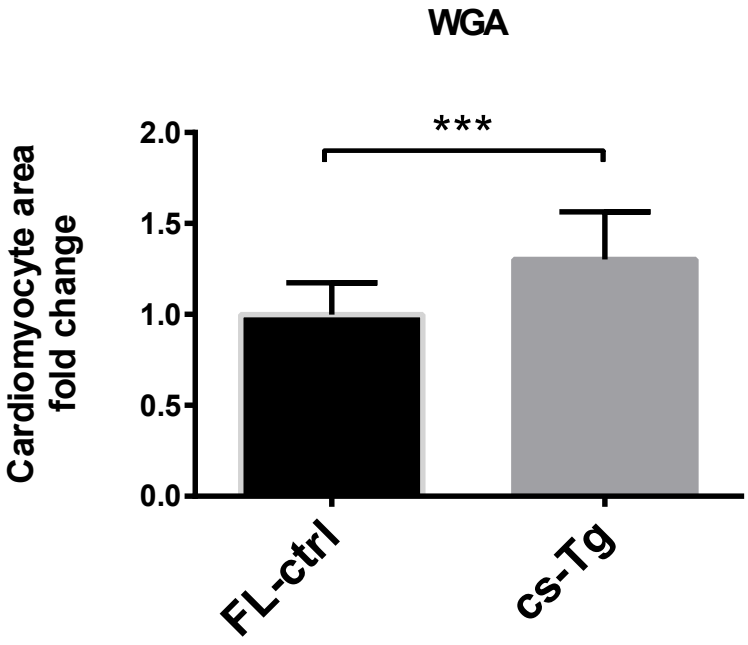


Figure 5.10 Size of cardiomyocytes was increased in csKASH-Tg mice

The sarcolemma of CMs from the heart cross section was labelled by the wheat germ agglutinin (WGA) staining (green staining) in both FLctrl and csKASH-Tg mice at 1 year old (A). Quantitation indicated there was a significant increased CM size in csKASH-Tg mice compared with FLctrl at 1-year-old (B). n=10 individual hearts/group; around 250 CMs/heart were quantified. Data was analysed by performed Student's t-tests, shown as mean±SEM. *P<0.05, Scale bar=50μm.

A.

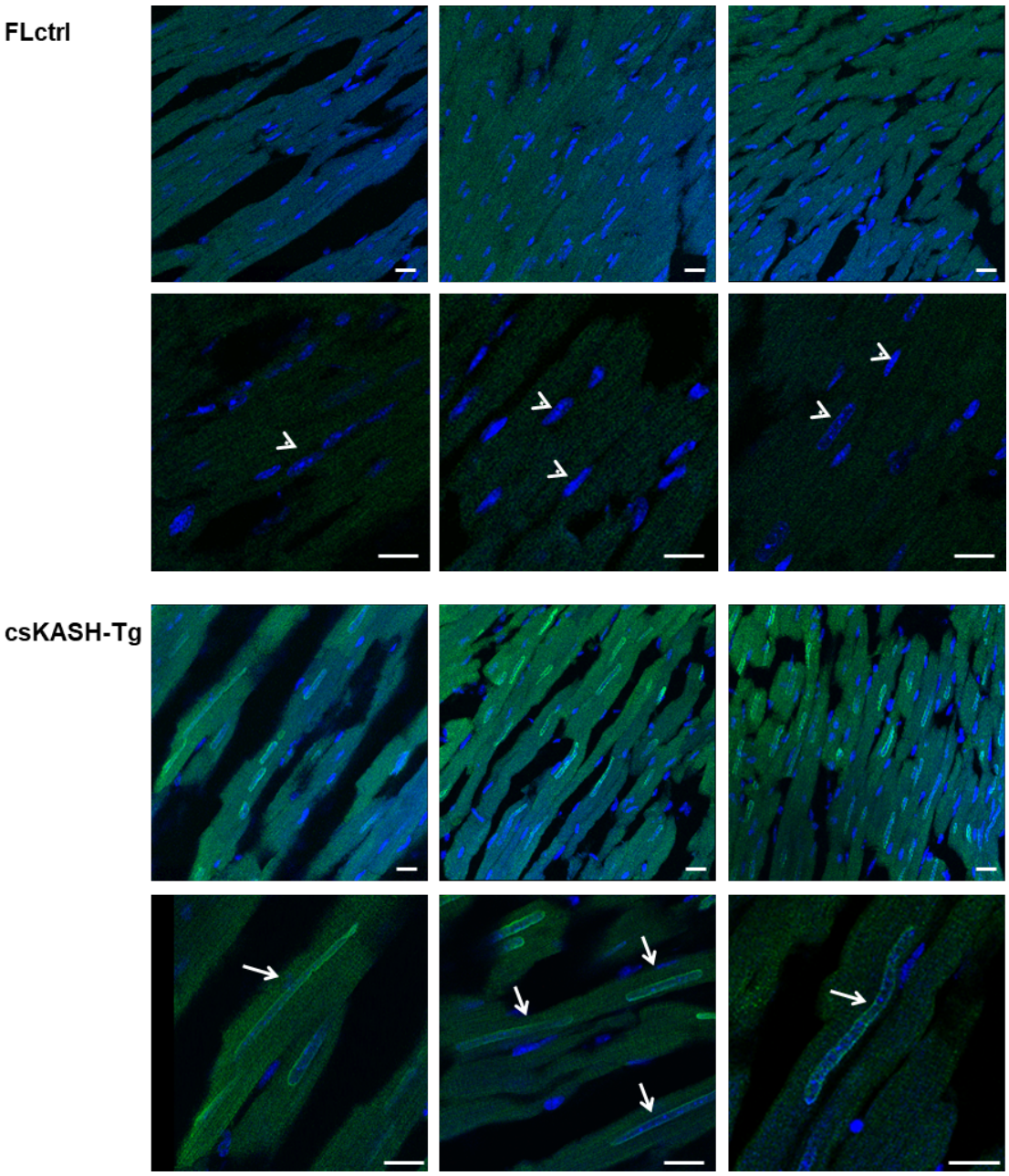


Figure 5.11 Cardiomyocyte nuclear morphology was altered in csKASH-Tg mice

(A) Representative of the cardiomyocyte nuclei in both FLctrl and csKASH-Tg at 1 year old (Blue was DAPI staining, Green was the GFP-KASH2 stained by GFP antibody). The exogenous GFP-KASH2 was only present at the NE in the CMs in csKASH-Tg heart compared with FLctrl. The GFP-KASH positive nuclei (A, bottom two panels) exhibited an elongated nuclear shape compared with CMs in FLctrl (A, top two panels. Scale bar=20μm.

B.

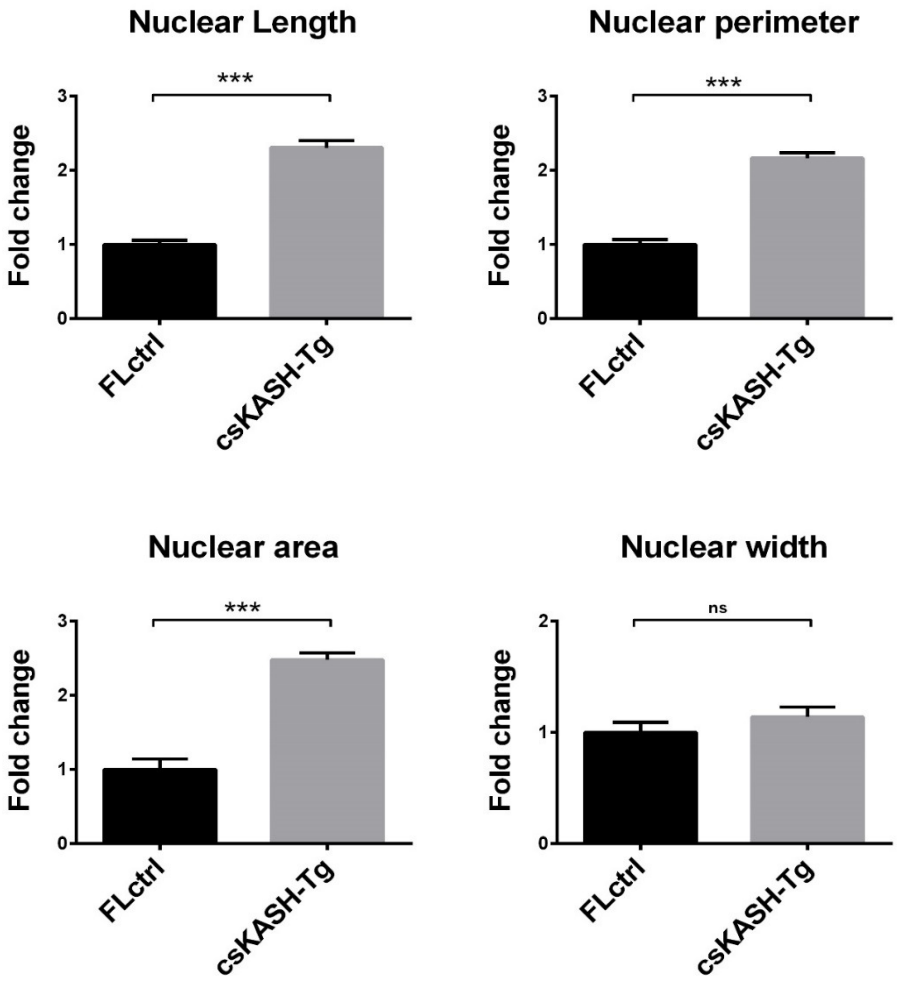


Figure 5.11 Cardiomyocyte nuclear morphology was altered in csKASH-Tg mice

(B) Nuclear morphology parameters further revealed the irregular shape of nuclei in csKASH-Tg mouse hearts including increased nuclear length (long axis), perimeter/area compared with the FLctrl, however, no observed change of nuclear width (short axis). n=3 hearts/each group, 100 nuclei/heart were counted. Data was analysed by Student's t-tests, shown as mean±SEM. *P<0.05.

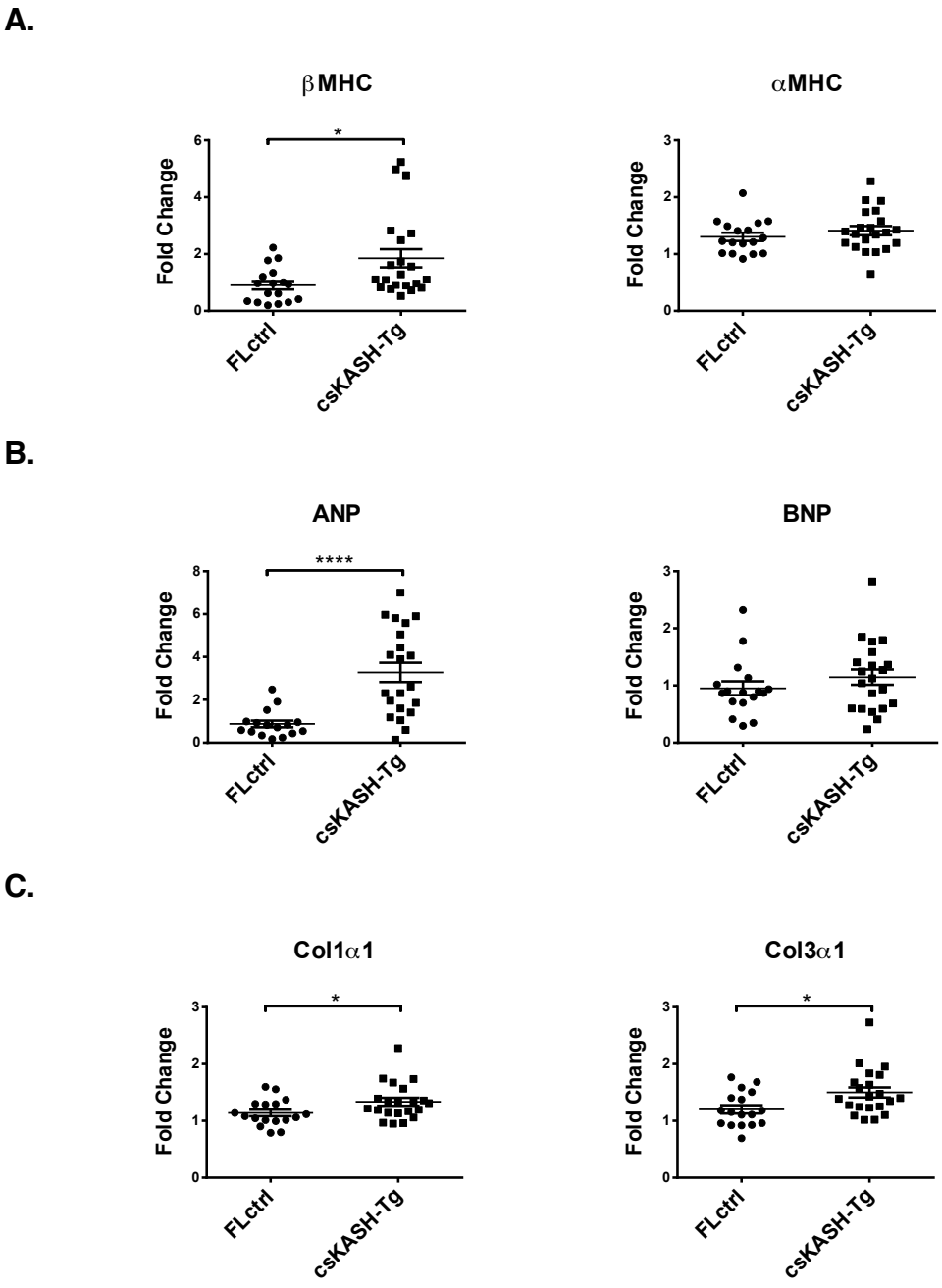


Figure 5.12 Hypertrophic and fibrotic genes were expressed in csKASH-Tg mouse hearts

Evaluating the expression of fetal genes in csKASH-Tg and FLctrl hearts at 1-year time point. Fetal genes βMHC (A) and ANP (B), as well as fibrotic genes procollagen1α1 and 3α1 (C) were upregulated in csKASH-Tg compared with FLctrl. There were no significant changes of other fetal genes including αMHC and BNP in csKASH-Tg compared with FLctrl (A, B). FLctrl n=17; csKASH-Tg n=21. Data was analysed by Student's t-tests, shown as mean±SEM. *P<0.05.

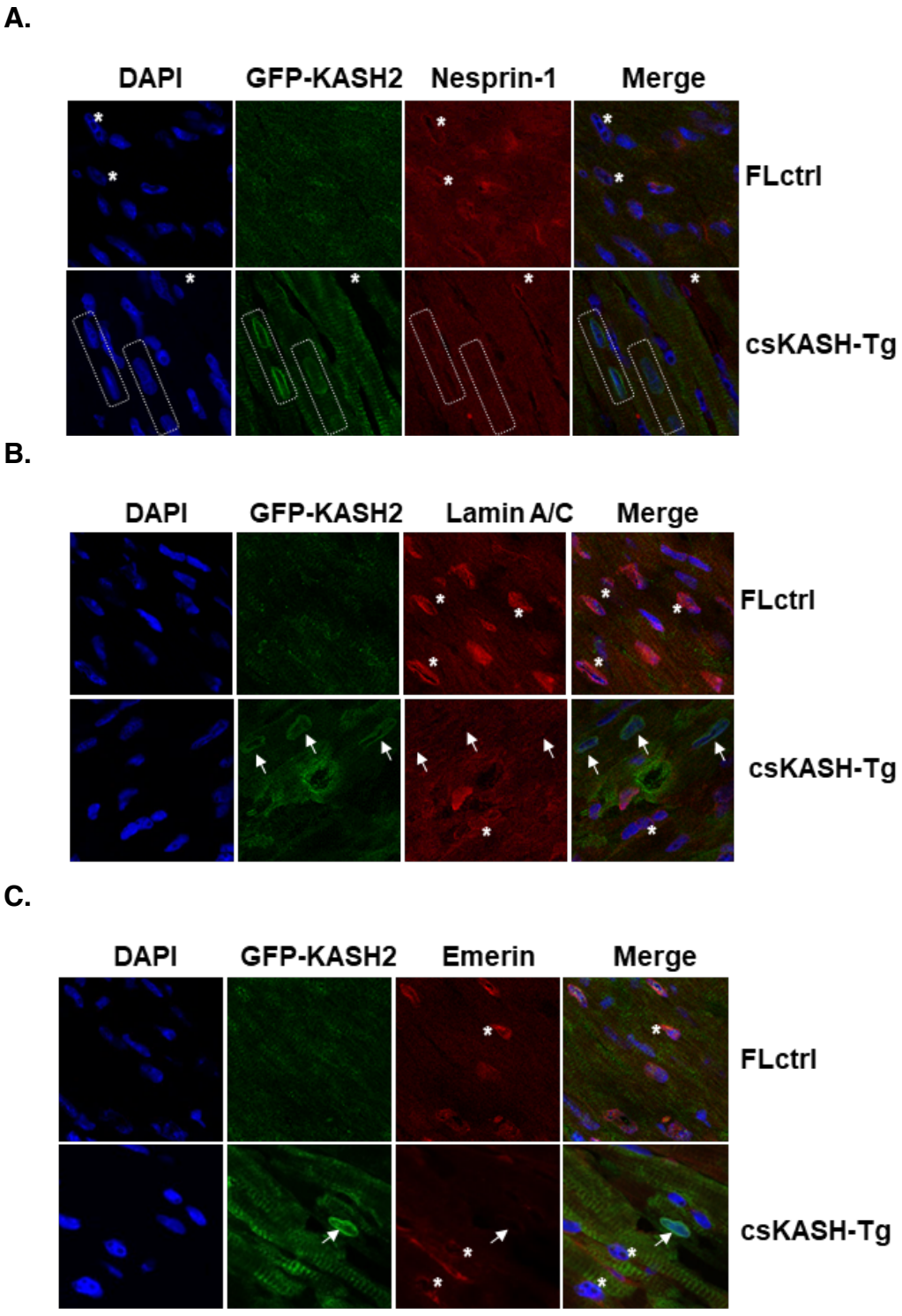


Figure 5.13 Endogenous NE-LINC complex components were mis-localised from NE in csKASH-Tg mice

IF showed mis-localisation of endogenous nesprin-1α (A, dashed boxes), lamin A/C and emerin (B & C, arrow) while GFP-KASH2 accumulated at the NE of CMs in csKASH-Tg mice when compared with FLctrl. * indicates the representative cells without GFP-KASH expression. Scale bar=20μm.

5.2.2.8 Subtle changes of expression levels of NE-LINC complex components in csKASH-Tg mice

To investigate if overexpression of DN KASH2 cause defects in expression levels of various nesprin-1/-2 isoforms and NE-LINC complex components, qPCR and WB were performed. qPCR showed there was no difference of expression of nesprin endogenous isoforms containing nesprin-2 CH domain or nesprin-1 KASH domain between csKASH-Tg and FLctrl groups (Figure 5.14A). The expression level of SUN1 was increased in csKASH-Tg compared with FLctrl (Figure 5.14B). Other NE-LINC complex components such as lamin A/C, emerin, SUN2 and nesprin-1α were unchanged at both RNA and protein levels in csKASH-Tg compared with FLctrl (Figure 5.14 B & 5.15).

Taken together, the data at the basal line showed: overexpression of DN-KASH in CMs of csKASH-Tg mice disrupted the NE-LINC complex, induced a hypertrophic response with activated fetal gene expression.

5.2.3 Characterisation of cardiac specific KASH2 Tg mouse model under pressure overload

5.2.3.1 The csKASH-Tg mice was subjected to pressure overload

To further validate any increased susceptibility to mechanical stress resulted from disrupted NE-LINC complex in CMs and its accompanied cardiac structure and function changes, transverse aortic constriction (TAC) were performed on both FLctrl and csKASH-Tg mice.

11-week old, male mice around 25g were subjected to severe pressure overload surgery in collaboration with Prof. Ajay Shah's lab (King's College London). Echocardiographic images were collected for all the mice before and after surgery. The bound descending aorta showed restricted forward flow and 4-fold increase in flow velocity (Figure 5.16). The hemodynamic changes resulted in overloaded pressure for the LV. The heart function was assessed 2 weeks post-operation prior to harvesting due to the severe TAC procedure which accelerated the LV remodelling and heart failure process [241]. All the mice were divided into four groups including FLctrl Sham (n=5), FLctrl TAC (n=4), csKASH-Tg Sham (n=1) and csKASH-Tg TAC

(n=3). As the mouse experiments were performed in the last year of my research, we were not able to acquire enough mice for the csKASH-Tg Sham group due to limited time. Therefore, we only compared the FLctrl Sham vs. FLctrl TAC and FLctrl TAC vs csKASH-Tg TAC in further experiments.

5.2.3.2 LV hypertrophy was induced by pressure overload in both FLctrl and csKASH-Tg

The body weight (BW) was measured before and after surgery and there was no difference among each group (Figure 5.17A). The ratio of HW/BW and HW/TL were used to assess the changes in heart mass. Both HW/BW and HW/TL were significantly increased in FLctrl TAC group compared with FLctrl Sham, suggesting that LV hypertrophy was induced by acute pressure overload in two weeks (Figure 5.17B). In the csKASH-Tg and FLctrl TAC groups, there was an increased trend in csKASH-Tg compared with FLctrl, indicating the csKASH-Tg TAC may have a more severe LV hypertrophic response than FLctrl TAC (Figure 5.17B).

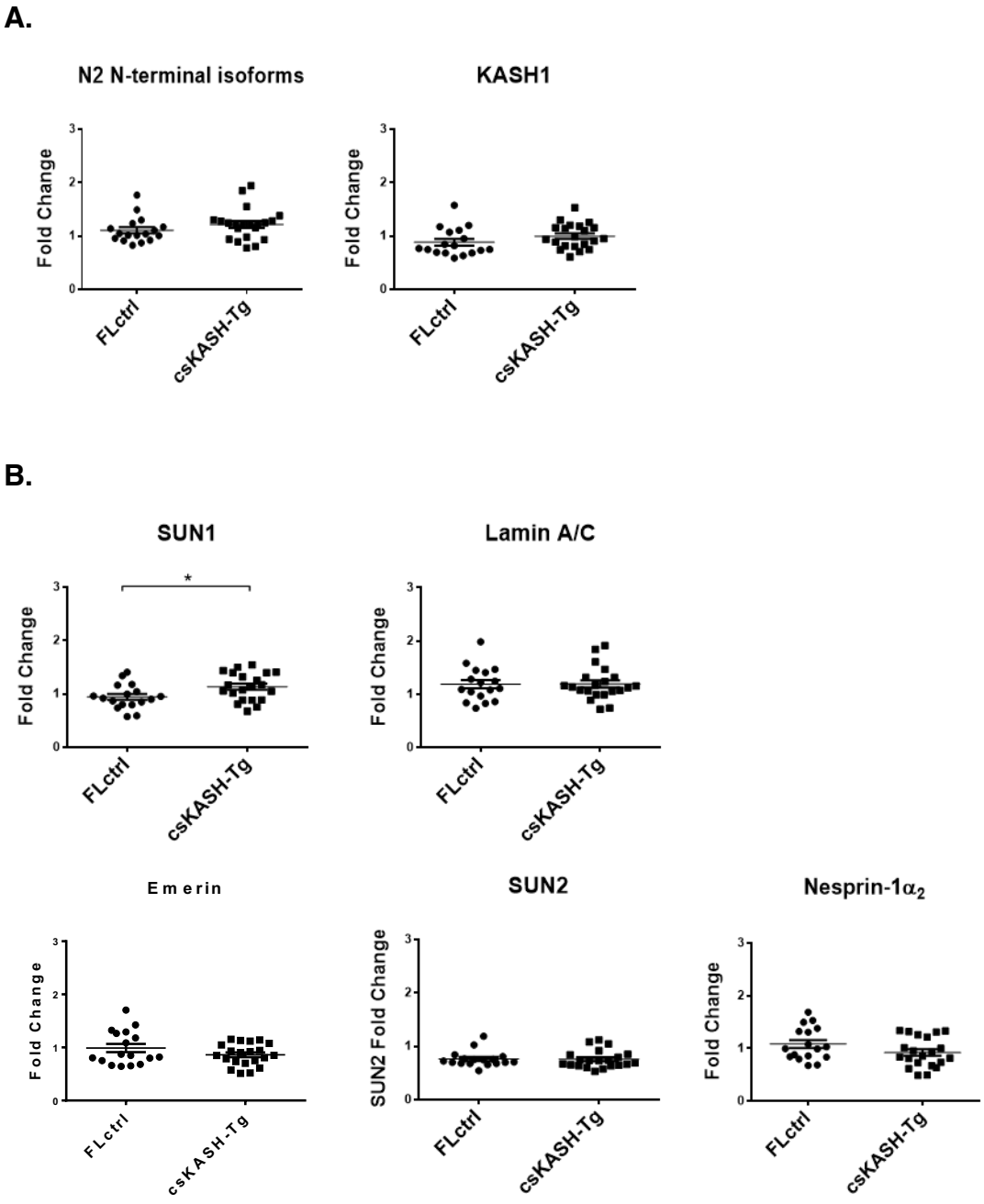


Figure 5.14 qPCR showed SUN1 was increased in csKASH-Tg mice

The RNA levels of NE-LINC complex components were examined from both FLctrl and csKASH-Tg hearts at 1 year old. There was no difference of expression of nesprin isoforms containing nesprin-2 CH domain or nesprin-1 KASH domain between csKASH-Tg and FLctrl groups (A). The expression level of SUN1 was increased and other NE-LINC complex proteins lamin A/C, emerin, SUN2 and nesprin-1α_2 were unchanged in csKASH-Tg compared with FLctrl (B). FLctrl n=17; csKASH-Tg n=21. Data was analysed by Student's t-tests, shown as mean±SEM. *P<0.05.

A.

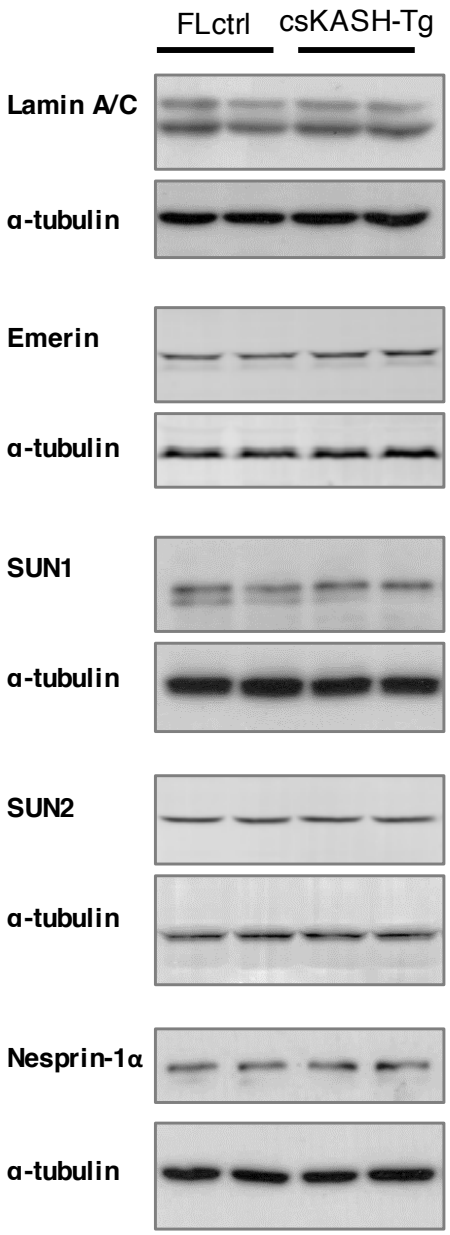


Figure 5.15 WB showed unchanged protein levels of NE-LINC complex components

(A) The protein levels of NE-LINC complex components including lamin A/C, emerin, SUN1/2 and nesprin-1α were examined from both FLctrl and csKASH-Tg hearts at 1 year old.

B.

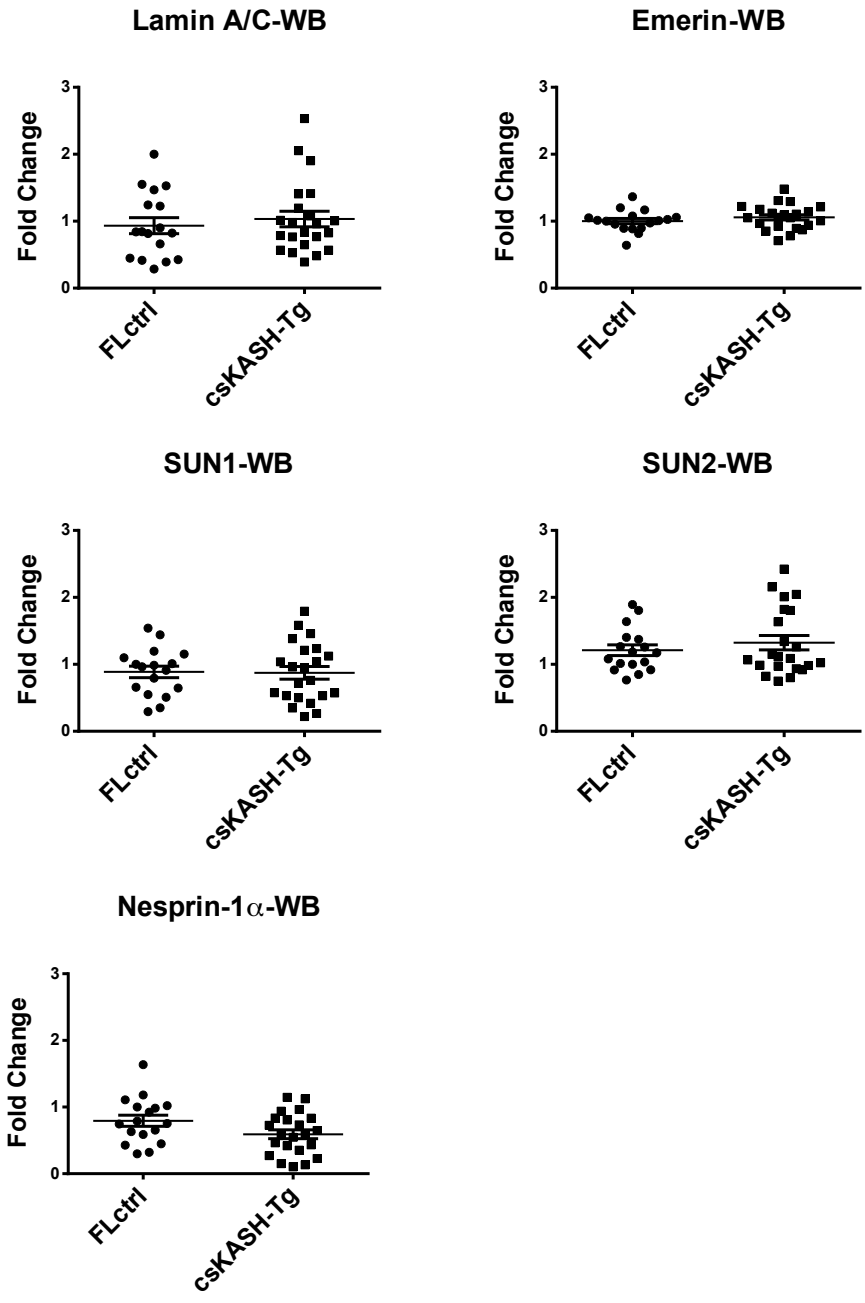
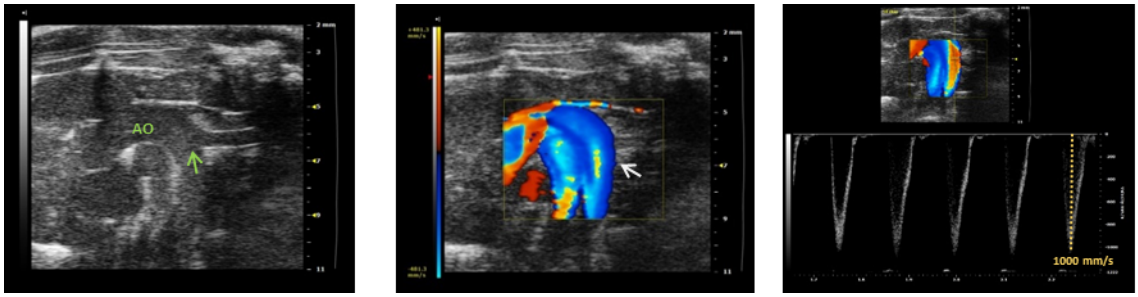


Figure 5.15 WB showed unchanged protein levels of NE-LINC complex components

(B) Statistical analysis showed there were no significant differences in protein levels of lamin A/C, emerin, SUN1, SUN2 and nesprin-1α between csKASH-Tg and FLctrl mice (B). FLctrl n=17; csKASH-Tg n=21. Data was analysed by Student's t-tests, shown as mean±SEM.

A. Before TAC



B. After TAC

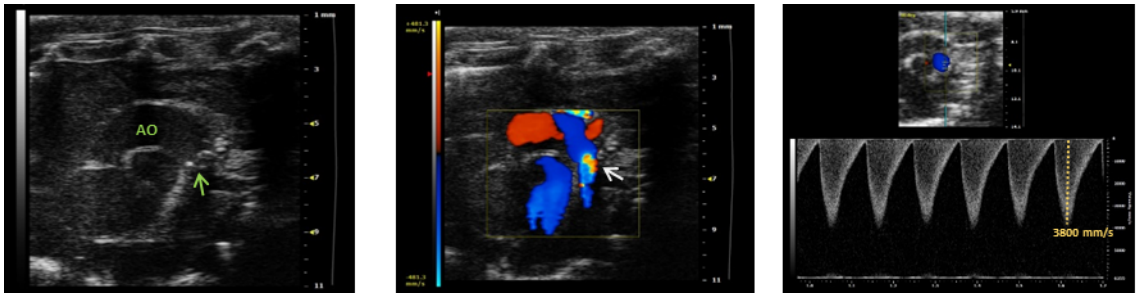
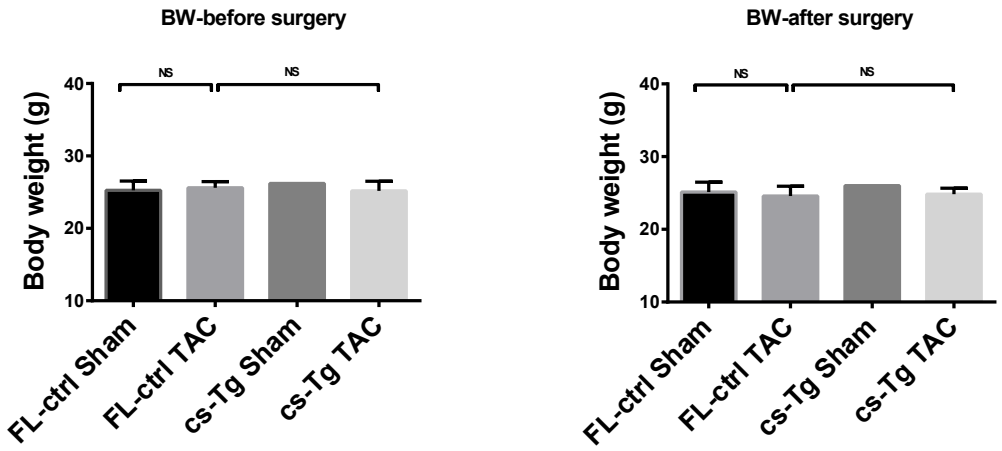


Figure 5.16 Echocardiographic images of the aorta in TAC mice

Aortic images were acquired before and after TAC surgery by echocardiography. Images of the aorta before TAC were shown in group A. B-mode of aorta arch was well shown (green arrow). The velocity of forward flow (white arrow) in the descending aorta was around 1000mm/s (yellow labelling). B group represented the aortic images two weeks post-operation. The descending aorta was bound (green arrow), with restricted forward flow (white arrow) and increased velocity to 3800mm/s (yellow labelling). AO: aorta.

A.



B.

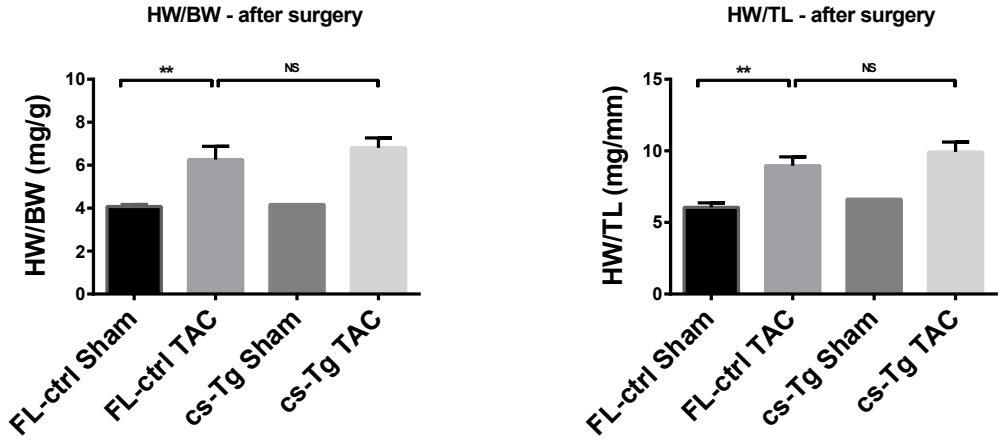


Figure 5.17 Heart mass was increased by pressure overload in both FLctrl and csKASH-Tg mice

The BW in csKASH-Tg and FLctrl groups were measured before and after surgery respectively. There was no significant difference among four groups (A). The ratios of HW/BW and HW/TL were significantly increased in FLctrl TAC compared with FLctrl Sham, however only showed an increased trend in csKASH-Tg TAC compared with FLctrl TAC (B). FLctrl Sham n=5, FLctrl TAC n=4, csKASH-Tg Sham n=1 and csKASH-Tg TAC n=3. Data was analysed by Student's t-tests, shown as mean±SEM. *P<0.05, BW-body weight, HW-heart weight; TL-tibia length.

5.2.3.3 Echocardiography showed severe defects in cardiac structure and function in csKASH-Tg TAC mice

Echocardiography monitored the changes of heart structure and functions in both csKASH-Tg and FLctrl groups before and after surgeries. Using 1D M-Mode, the flattened LV wall motion in FLctrl and csKASH-Tg after TAC indicated the reduced LV contraction and compromised systolic function when compared to the same group before surgery (Figure 5.18B & 5.18D). There was no observed difference of LV wall movement in csKASH-Tg Sham and FLctrl Sham before and after surgery (Figure 5.18A & 5.18C).

Then the echocardiographic data was analysed within the three groups (csKASH-Tg Sham was excluded due to the data collected from only 1 mouse): I) In the FLctrl Sham, there were no changes in heart structure and functions after Sham surgery compared with the same mice before surgery, excluding any changes caused by surgical intervention (Figure 5.19A-G). II) In the FLctrl TAC group, there were significant increases in LVPW (LVPWd, LVPWs) (Figure 5.19A), LV diameter and LV volume (LVIDs, ESV) (Figure 5.19C, 5.19D), as well as decreased EF (Figure 5.19G) in FLctrl mice after TAC compared with same mice before TAC. III) In the csKASH-Tg TAC group, these mice displayed similar changes to those observed in FLctrl TAC group before and after surgery (Figure 5.19A-G).

Next, echocardiographic data were further analysed between two groups after surgery (csKASH-Tg Sham was excluded due to the data collected from only 1 mouse): I) There was an enlarged LV volume (ESV) (Figure 5.19D) and reduced EF (Figure 5.19F & Figure 5.19G) in FLctrl TAC compared with FLctrl Sham. II) There was a trend towards thicker LV wall (Figure 5.19A & 5.19B), larger LV chamber diameter and volume (Figure 5.19C & 5.19D) and more reduced EF (Figure 5.19F & 5.19G) in csKASH-Tg TAC compared with FLctrl TAC.

Those changes suggested LV hypertrophy and heart failure were induced in FLctrl mice due to the acute pressure overload, and may potentially be exacerbated in the hearts with overexpression of DN KASH.

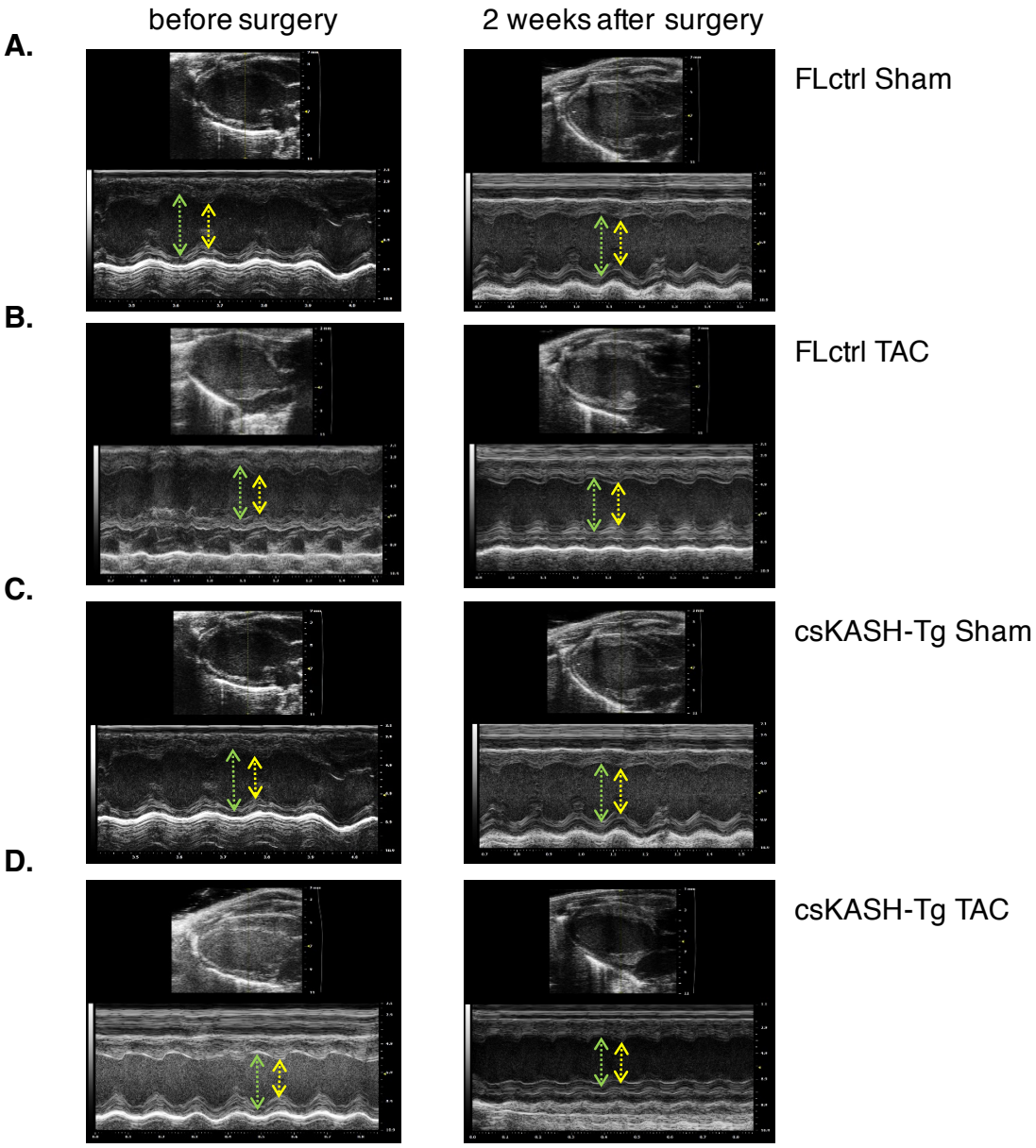
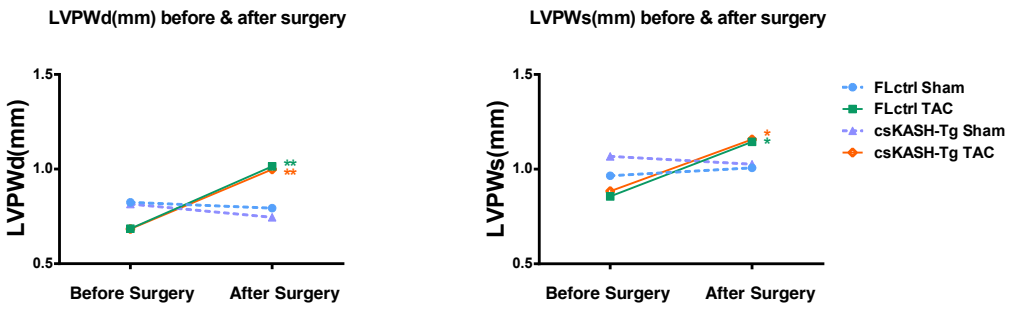


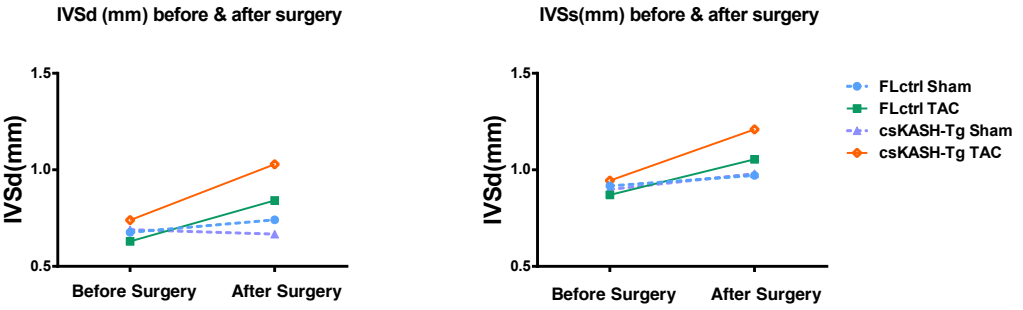
Figure 5.18 Echocardiography showed reduced heart contraction after TAC surgery

M-mode images were acquired by echocardiography before and after surgery to monitor the dynamic changes of heart structure and functions in each individual mouse (A-D). This 1-D view recorded the LV wall movement, which reflected the LV systolic function. Green double arrow line represented the LV internal diameter at the end of diastole, while the yellow double arrow line represented the LV internal diameter at the end of systole. The flattened LV wall motion in FLctrl and csKASH-Tg after TAC indicated the reduced LV contraction and compromised systolic function when compared to the same group before surgery (B, D). There was no observed difference of LV wall movement in csKASH-Tg Sham and FLctrl Sham before and after surgery respectively (A, C).

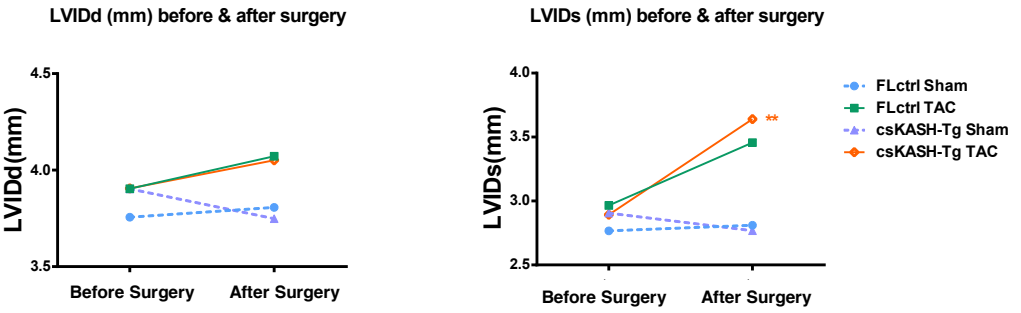
A.


LVPWd(mm) before & after surgery
LVPWd(mm)
1.5
1.0
0.5
Before Surgery
After Surgery
**
**
LVPWs(mm) before & after surgery
LVPWs(mm)
1.5
1.0
0.5
Before Surgery
After Surgery
*
*
FLctrl Sham
FLctrl TAC
csKASH-Tg Sham
csKASH-Tg TAC

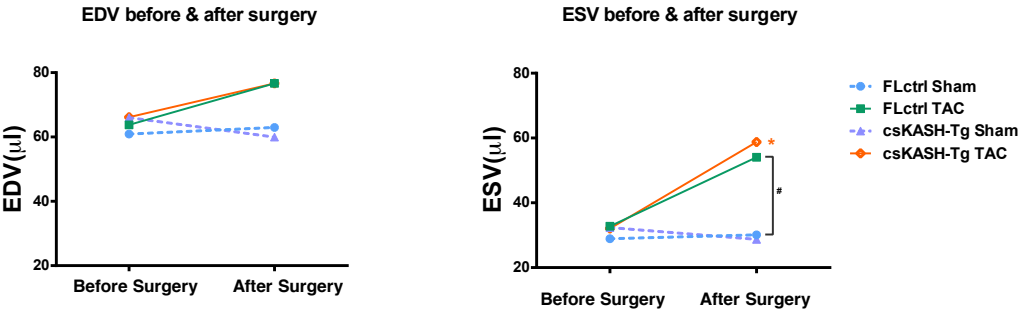
B.


IVSd (mm) before & after surgery
IVSd(mm)
1.5
1.0
0.5
Before Surgery
After Surgery
IVSs(mm) before & after surgery
IVSd(mm)
1.5
1.0
0.5
Before Surgery
After Surgery
FLctrl Sham
FLctrl TAC
csKASH-Tg Sham
csKASH-Tg TAC

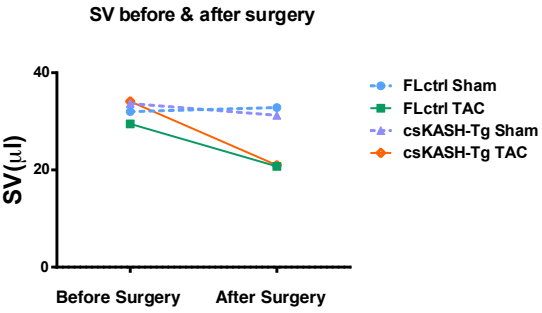
C.


LVIDd (mm) before & after surgery
LVIDd(mm)
4.5
4.0
3.5
Before Surgery
After Surgery
LVIDs (mm) before & after surgery
LVIDs(mm)
4.0
3.5
3.0
2.5
Before Surgery
After Surgery
**
FLctrl Sham
FLctrl TAC
csKASH-Tg Sham
csKASH-Tg TAC

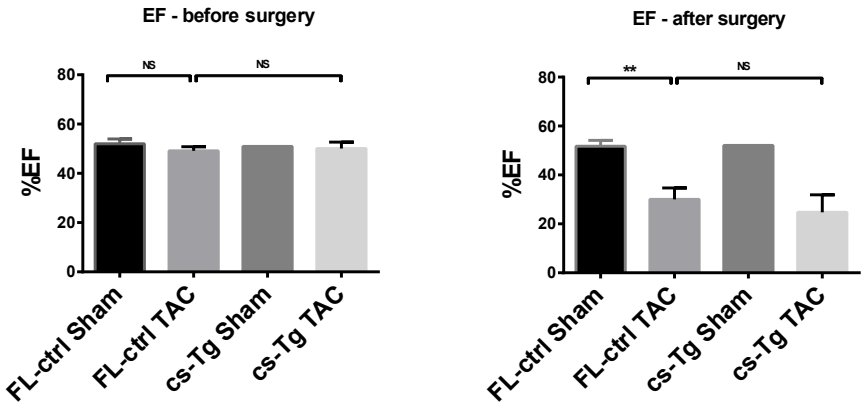
D.


EDV before & after surgery
EDV(μl)
80
60
40
20
Before Surgery
After Surgery
ESV before & after surgery
ESV(μl)
80
60
40
20
Before Surgery
After Surgery
*
#
FLctrl Sham
FLctrl TAC
csKASH-Tg Sham
csKASH-Tg TAC

E.


SV before & after surgery
SV(μl)
40
20
0
Before Surgery
After Surgery
FLctrl Sham
FLctrl TAC
csKASH-Tg Sham
csKASH-Tg TAC

F.



G.

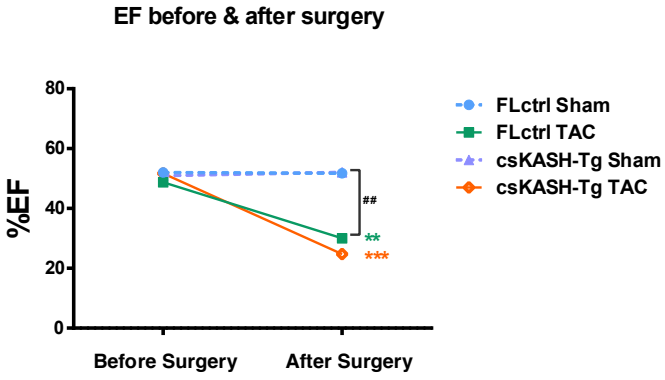


Figure 5.19 Echocardiography showed severe cardiac structural and functional changes in csKASH-Tg TAC mice

Echocardiography monitored the LV structural and functional parameters. Within each group I) FLctrl Sham: there was no changes in heart structure and functions after Sham surgery compared with the same mice before surgery (A-G). II) FLctrl TAC: there were significant increases in LVPW (LVPWd, LVPWs) (A), LV diameter and LV volume (LVIDs, ESV) (C & D), as well as decreased EF (G) in mice after TAC compared with same mice before TAC. III) csKASH-Tg TAC: these mice displayed similar changes to those observed in FLctrl TAC group before and after surgery (A-G).

Between two groups I) There was an enlarged LV volume (ESV) (D) and recued EF (F & G) in FLctrl TAC compared with FLctrl Sham. II) There was a trend towards thicker LV wall (A & B), larger LV chamber diameter and volume (C & D) and decreased EF (F & G) in csKASH-Tg TAC compared with FLctrl TAC.

FLctrl Sham n=5, FLctrl TAC n=4, csKASH-Tg Sham n=1 and csKASH-Tg TAC n=3. Data was analysed by Student's t-tests or Two-way ANOVA Turkey's test, shown as mean±SEM. *P<0.05 compared within the group; # P<0.05 compared between two groups.

5.2.3.4 Histological examination showed massive myocardial fibrosis in csKASH-Tg TAC mice

Myocardial fibrosis was assessed in Masson's trichrome stained LV sections (short axis) at 2 weeks after surgery. In the Sham group, there was no visible difference in the extents of fibrosis in both FLctrl and csKASH-Tg hearts (Figure 5.20A & 5.20C). However, there was massive fibrosis across the whole LV cross sections in the csKASH-Tg TAC mice (Figure 5.20D), when compared with FLctrl TAC mice that only showed limited area of fibrosis (Figure 5.20B).

5.2.3.5 Up-regulated expression of hypertrophic and fibrotic genes in csKASH-Tg TAC mouse hearts

The mRNA levels of fetal and fibrotic genes were evaluated by qPCR. In the FLctrl group: there were down-regulated βMHC and αMHC expression (Figure 5.21A), up-regulated ANP and BNP expression (Figure 5.21B), as well as increased expression of fibrotic genes Procol1α1 and Procol3α1 (Figure 5.21C) in the FLctrl TAC mice when compared with the FLctrl Sham.

Comparing the two TAC groups, the ANP, Procol1α1 and Procol3α1 in csKASH-Tg TAC group was significantly increased, with 3-fold higher in csKASH-Tg TAC hearts compared with FLctrl TAC (Figure 5.21B & 5.21C). There were no significant changes in other fetal genes including α/βMHC and BNP in csKASH-Tg TAC when compared with FLctrl TAC (Figure 5.21A & 5.21B).

These results were consistent with the echocardiographic and histological staining data, indicating overexpression of the DN KASH promoted pressure overload-induced LV dysfunction.

5.2.3.6 Disruption of NE-LINC complex was induced by pressure overload in csKASH-Tg mice

To investigate whether the expression levels of endogenous NE-LINC complex associated proteins were altered in csKASH-Tg TAC mice, WB and qPCR were used.

Nesprin-2 KASH domain containing isoforms were 7-fold high than endogenous KASH2 isoforms in FLctrl group due to overexpression of EGFP-KASH2 in the

csKASH-Tg mouse hearts. KASH2 isoform expression was not altered by the TAC procedure in both csKASH-Tg and FLctrl groups (Figure 5.22A). Other nesprin isoforms that contained nesprin-2 CH or nesprin-1 KASH domains were also unchanged in all groups before and after surgery (Figure 5.22A).

SUN2 was significantly down-regulated in the FLctrl TAC compared to the FLctrl Sham (Figure 5.22B). Moreover, lamin A/C showed an upregulated trend in FLctrl TAC when compared with FLctrl Sham, but significantly increased in the csKASH-Tg TAC compared with FLctrl TAC (Figure 5.22B). Other NE-LINC complex components including emerin, SUN1 and nessprin-1α were unchanged in FLctrl and csKASH-Tg before and after TAC (Figure 5.22B & 5.23). These results suggested that pressure overload alone was enough to alter the expression level of SUN2, whilst increased lamin A/C was induced by both overexpression of KASH and pressure overload.

5.2.3.7 Biomechanical response was altered in csKASH-Tg mice under the pressure overload

The cells response to mechanical strain can be measured by the expression of the mechanosensitive genes [211, 212]. Literatures showed attenuated mechanical induction of egr-1, iex-1, c-fos and c-jun under mechanical strain in MEFs derived from *LMNA* or *EMD* null mice, and the CMs derived from nesprin-1/-2 KO mice [85, 153, 213, 214], suggesting the critical role of the integral NE-LINC complex in mechanotransduction and gene regulation.

We examined the changes of mechanosensitive genes in the csKASH-Tg and FLctrl mice. In the FLctrl group, qPCR data showed significant upregulated egr-1 after TAC procedure compared with the Sham group (Figure 5.24). Next, two TAC groups were compared: egr-1 and c-myc were significantly elevated in csKASH-Tg TAC compared with FLctrl TAC (Figure 5.24). These data indicated that the mechanosensitive gene such as egr-1 responded to the abnormal hemodynamic changes, and could be exacerbated in the heart in conjunction with overexpression of KASH.

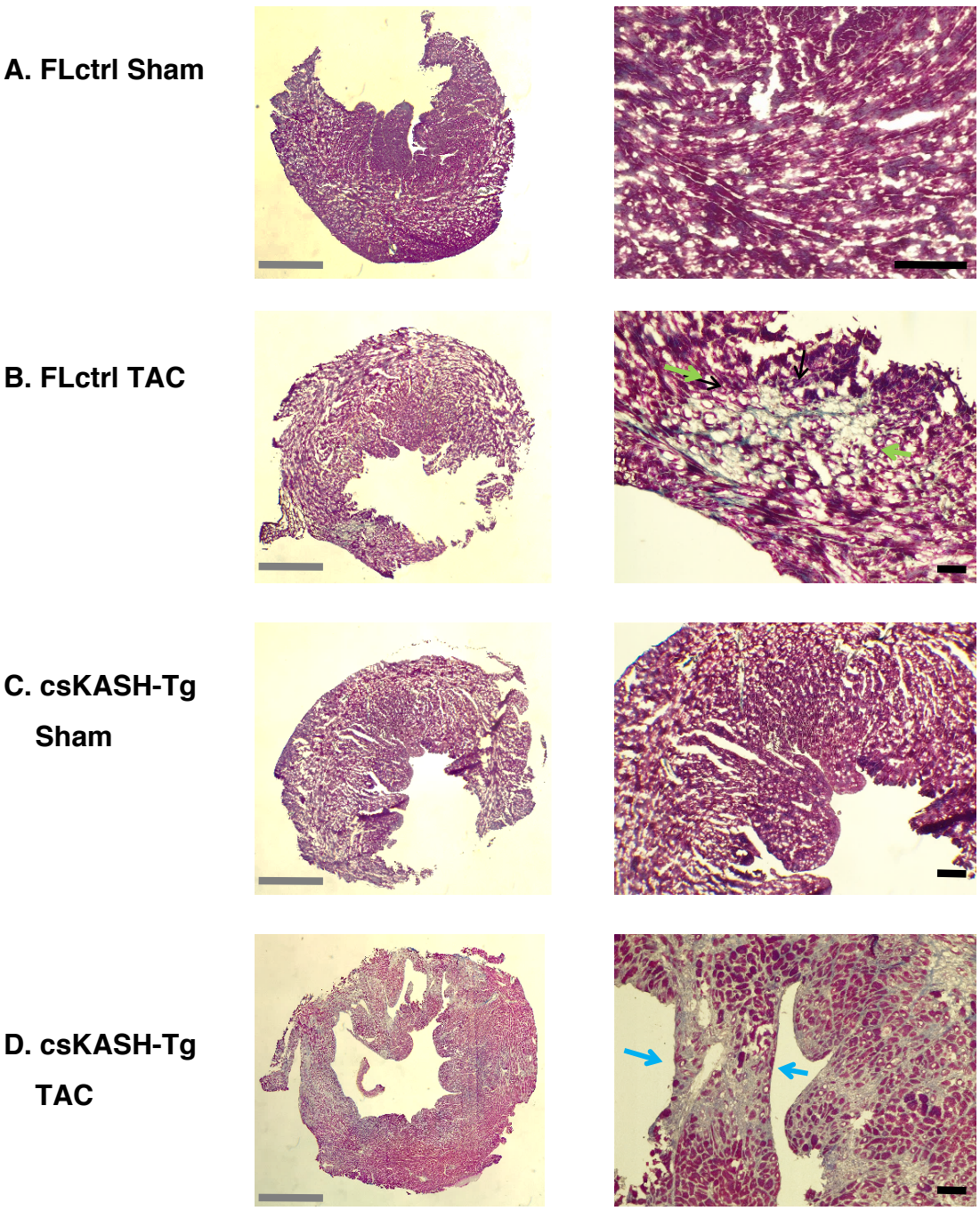


Figure 5.20 Massive myocardial fibrosis was present in csKASH-Tg TAC mice

Masson's trichrome were performed on the frozen heart sections (short axis). In the Sham group, there was no visible difference in the extents of fibrosis in both FLctrl and csKASH-Tg heart (A, C). In TAC group, there was massive fibrosis across the whole LV cross sections in the csKASH-Tg TAC mice (D, blue arrow), when compared with FLctrl TAC mice that only showed limited area of fibrosis (B, green arrow). Scale bar: 2mm (grey), 20μm (black).

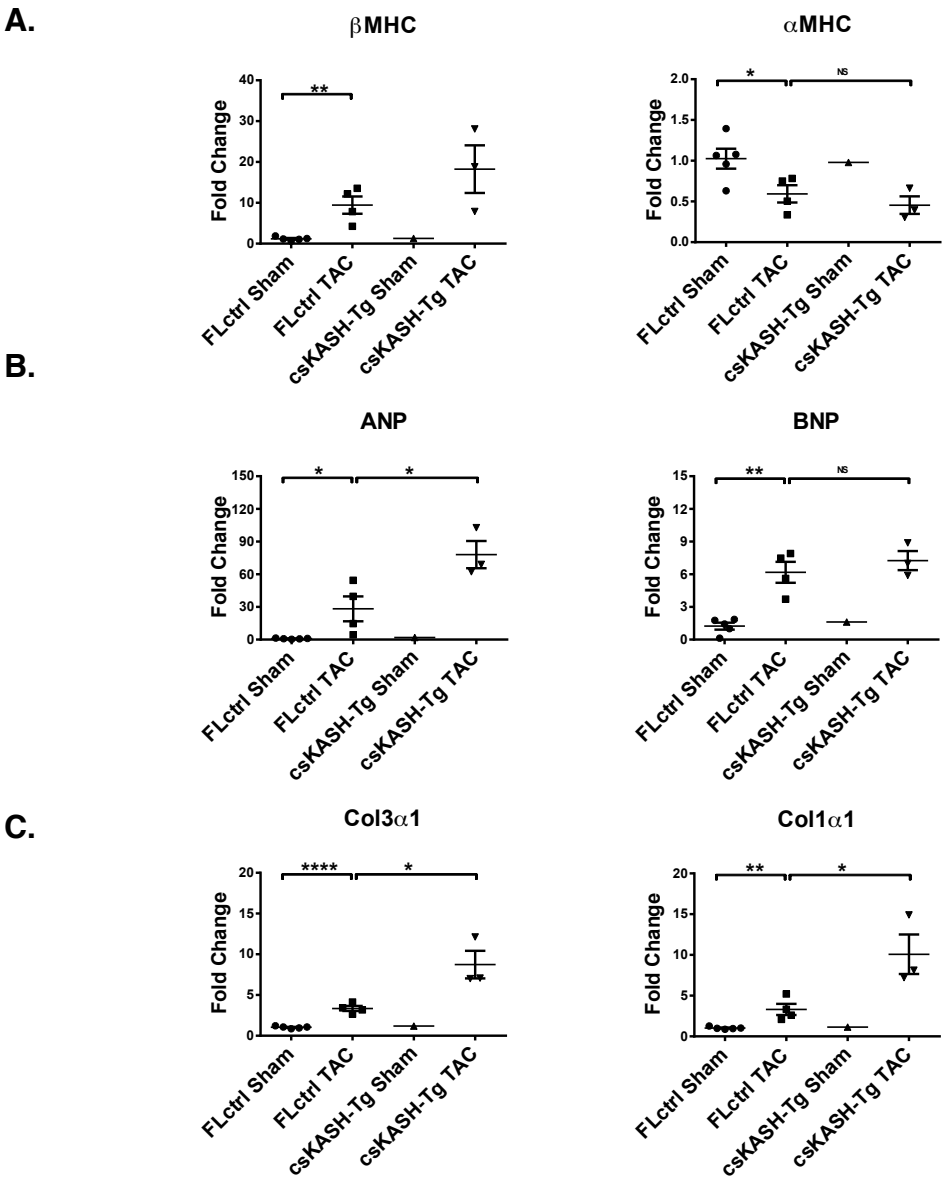


Figure 5.21 Upregulated expression of hypertrophic and fibrotic genes in csKASH-Tg TAC mouse hearts

qPCR analyses showed: in the FLctrl group, there were down-regulated βMHC and αMHC expression (A), up-regulated ANP and BNP expression (B), as well as increased expression of fibrotic genes Procol1α1 and Procol3α1 (C) in the FLctrl TAC mice when compared with the FLctrl Sham.

Comparing the two TAC groups, the ANP, Procol1α1 and Procol3α1 in csKASH-Tg TAC group was significantly increased in csKASH-Tg TAC hearts compared with FLctrl TAC (B, C). There were no significant changes in other fetal genes including α/βMHC and BNP in csKASH-Tg TAC when compared with FLctrl TAC (A, B). FLctrl Sham n=5, FLctrl TAC n=4, csKASH-Tg Sham n=1 and csKASH-Tg TAC n=3. Data was analysed by Student's t-tests, shown as mean±SEM; *P<0.05.

A.

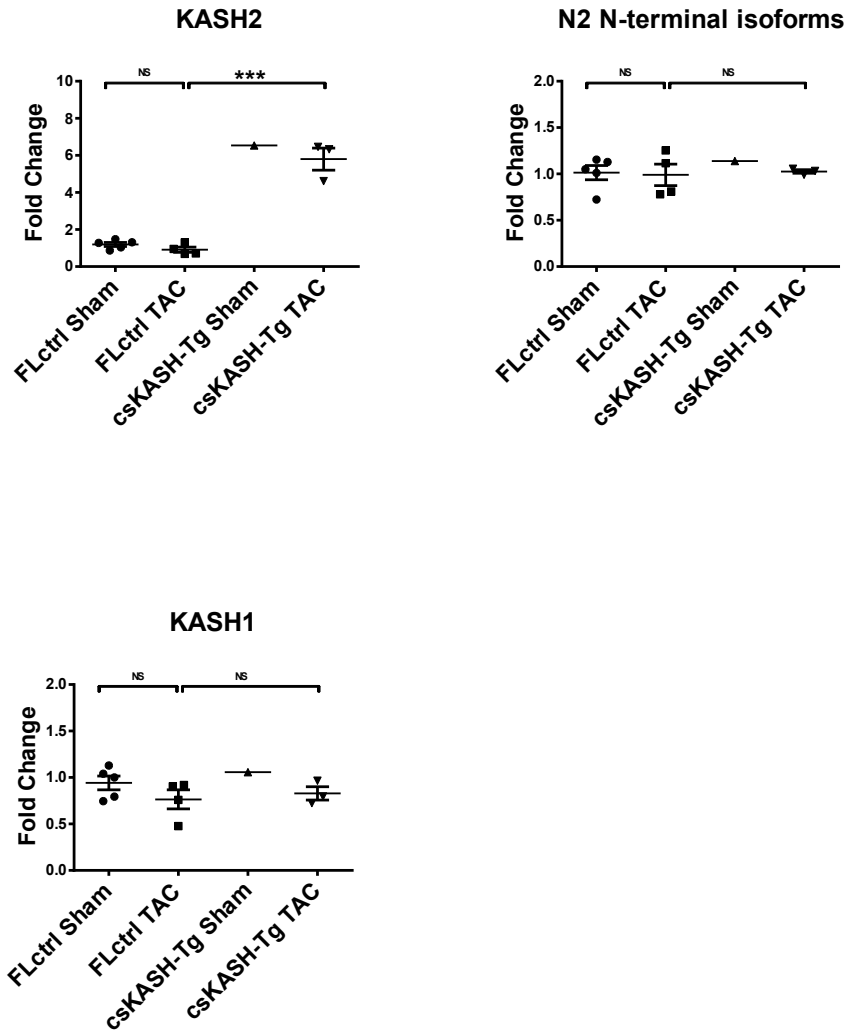


Figure 5.22 qPCR showed SUN2 was reduced in FLctrl TAC mice and lamin A/C was increased in csKASH-Tg TAC mice

(A) Changes in nesprin isoforms: nesprin-2 KASH domain containing isoforms were 7-fold high than endogenous KASH2 isoforms in FLctrl group due to overexpression of EGFP-KASH2 in the csKASH-Tg mouse hearts. KASH2 isoform expression was not altered by the TAC procedure in both csKASH-Tg and FLctrl groups. Other nesprin isoforms that contained nesprin-2 CH or nesprin-1 KASH domains were also unchanged in all groups.

B.

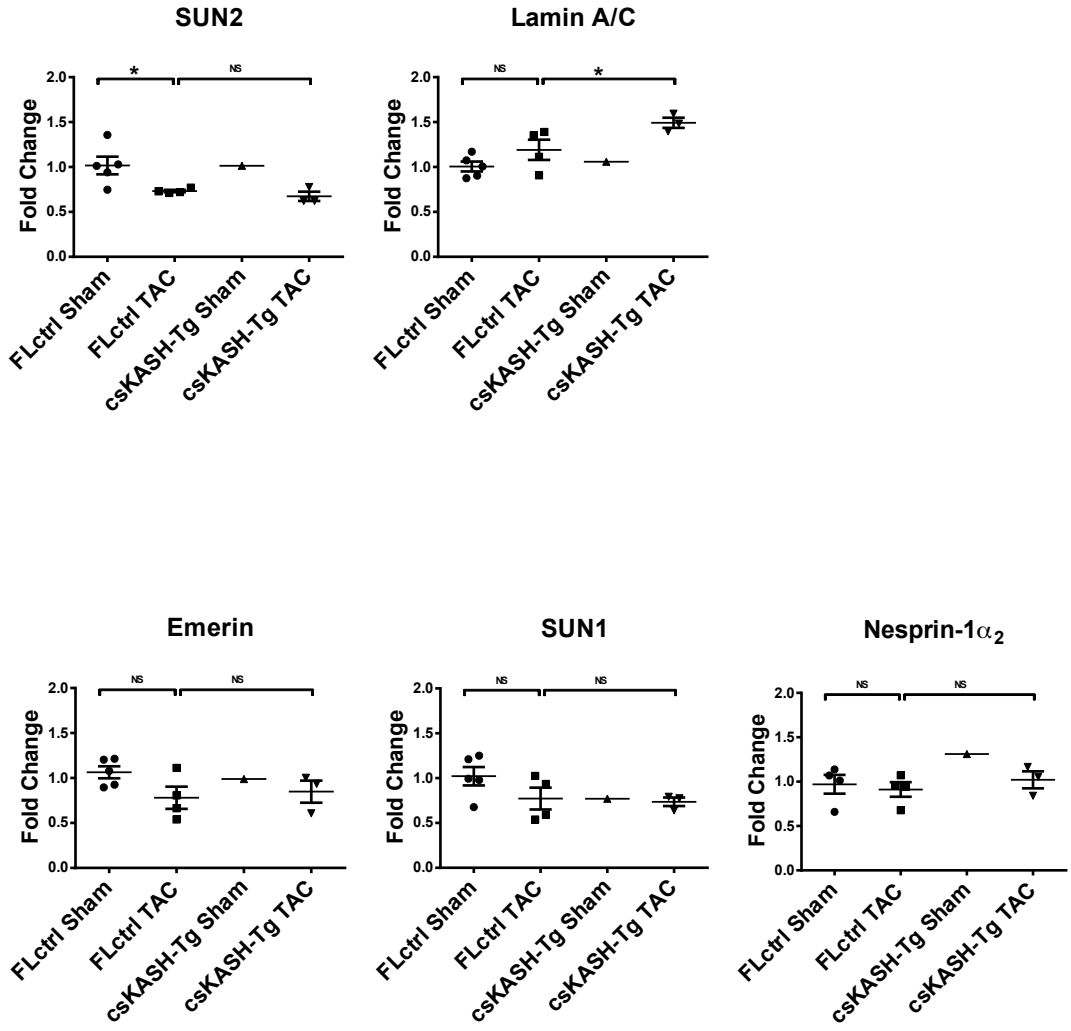


Figure 5.22 qPCR showed SUN2 was reduced in FLctrl TAC mice and lamin A/C was increased in csKASH-Tg TAC mice

(B) Changes in NE-LINC complex components: SUN2 was significantly down-regulated in the FLctrl TAC compared to the FLctrl Sham. Lamin A/C showed an upregulated trend in FLctrl TAC when compared with FLctrl Sham, but significantly increased in the csKASH-Tg TAC compared with FLctrl TAC. Other NE-LINC complex components including emerin, SUN1 and nesprin-1α_2 were not altered in all groups. FLctrl Sham n=5, FLctrl TAC n=4, csKASH-Tg Sham n=1 and csKASH-Tg TAC n=3. Data was analysed by Student's t-tests, shown as mean±SEM. *P<0.05.

A.

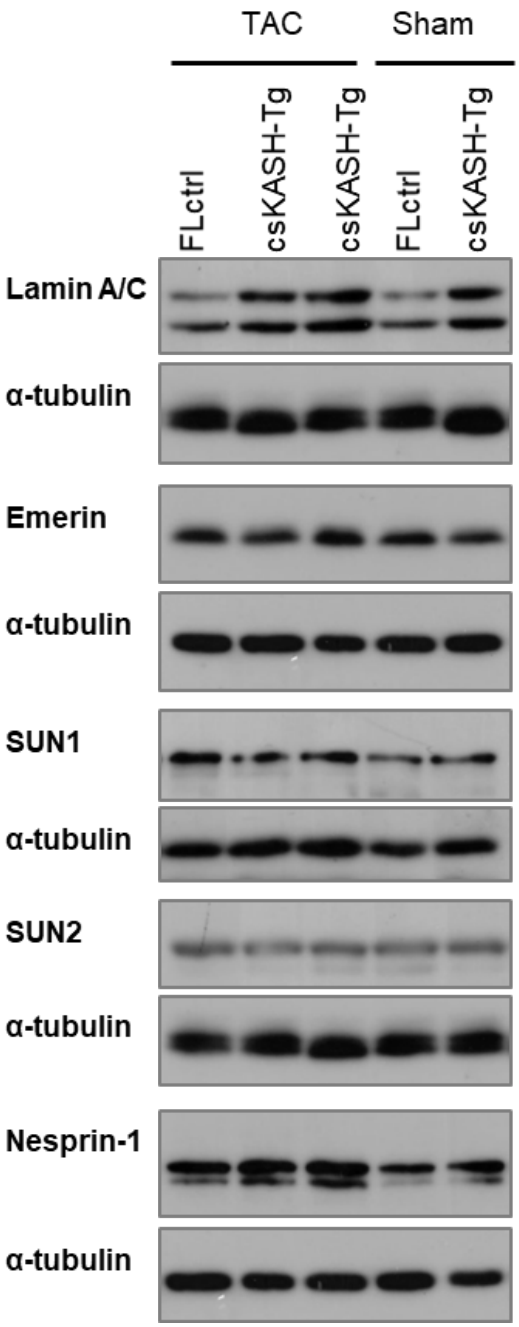


Figure 5.23 WB showed no significant changes of expression levels of NE-LINC complex components in csKASH-Tg after TAC

(A) Protein levels of NE-LINC complex components including lamin A/C, emerin, SUN1/2 and nesprin-1α were analysed by WB using the heart tissue derived from FLctrl and csKASH-Tg mice before and after surgery.

B.

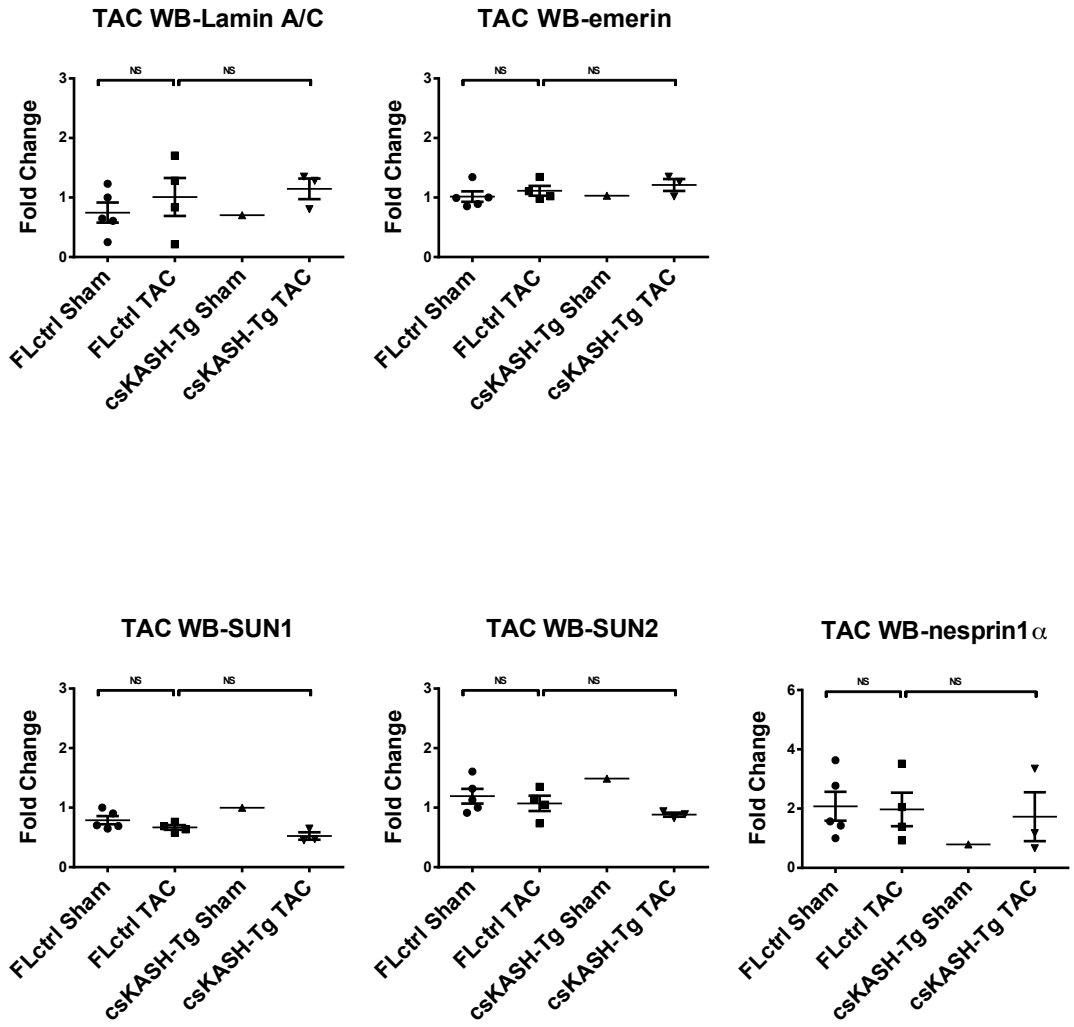


Figure 5.23 WB showed no significant changes of protein levels of NE-LINC complex components in csKASH-Tg after TAC

(B) Statistical analysis showed there were no significant differences in protein levels of lamin A/C, emerin, SUN1/2 and nesprin-1α in csKASH-Tg and FLctrl groups before and after surgery. FLctrl Sham n=5, FLctrl TAC n=4, csKASH-Tg Sham n=1 and csKASH-Tg TAC n=3. Data was analysed by Student's t-tests, shown as mean±SEM.

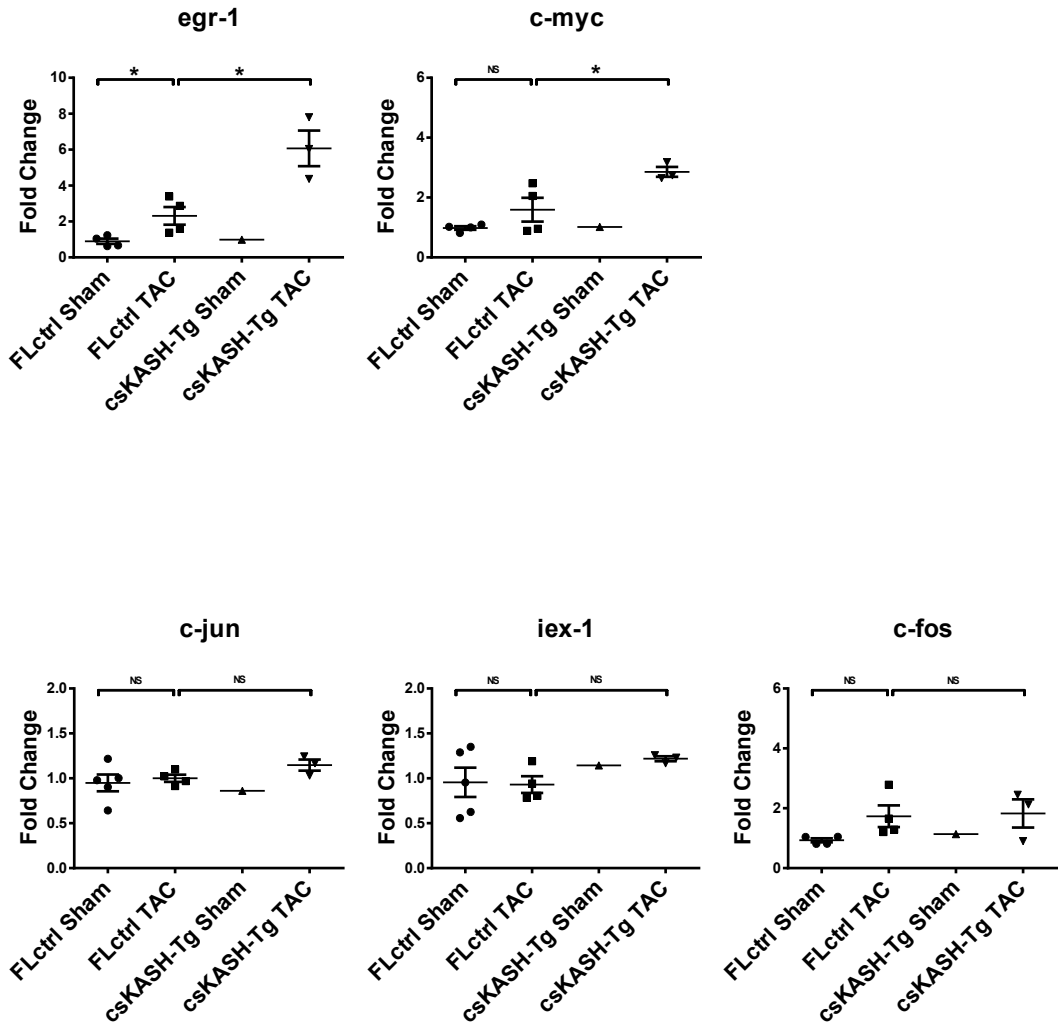


Figure 5.24 Mechanosensitive genes were altered in csKASH-Tg mice under the pressure overload

The changes of mechanosensitive genes in the csKASH-Tg and FLctrl mice before and after TAC were investigated. In the FLctrl group, qPCR data showed significant upregulated egr-1 after TAC procedure compared with the Sham group. Next, two TAC groups were compared. egr-1 and c-myc were significantly elevated in csKASH-Tg TAC compared with FLctrl TAC. Other mechanosensitive genes including c-jun, iex-1 and c-fos were unchanged in all groups. FLctrl Sham n=5, FLctrl TAC n=4, csKASH-Tg Sham n=1 and csKASH-Tg TAC n=3. Data was analysed by Student's t-tests, shown as mean±SEM. *P<0.05.

5.3 Discussion

In this chapter, we successfully generated a cardiac specific KASH2 overexpression mouse model which exhibited the NE-LINC complex disruption in CMs under the MLC2V promotor. The cardiac phenotype and cellular changes of csKASH-Tg mice are summarised in Table 5.2. At the basal line, csKASH-Tg mice developed normally up to 1 year, and showed a cardiac hypertrophy response with re-expression of fetal gene βMHC, ANP and fibrotic gene procollagen1α1/3α1 in the heart. The mis-localisation of lamin A/C, emerin and endogenous nesprin-1α, indicated a disrupted NE-LINC complex in csKASH-Tg mice, which also contributed to irregular nuclear morphology in CMs. Under pathological hemodynamic stress, the csKASH-Tg TAC mouse hearts showed more severe LV hypertrophic response and systolic dysfunction compared to the FLctrl, with increased expression of fetal gene ANP and fibrotic genes procollagen1α1/3α1 in hearts. The fibrotic heart in csKASH-Tg also showed abnormal expression of mechanosensitive genes egr-1 and c-myc, indicating that uncoupling of the NE-LINC complex impaired the transduction of mechanical stimuli into biochemical signals, exacerbated the pathological process in the heart.

Table 5.2 Characterisation of cardiac phenotype and cellular changes in csKASH-Tg mice

	csKASH-Tg	
	Basal line (compared with FLctrl)	**Under TAC (compared with FLctrl TAC)**
Echocardiography	Thicker LV wall, reduced LV chamber size, unchanged systolic function	Increased trends: thicker LV wall, enlarged LV chamber size, exacerbated systolic function
Histology	Thicker LV wall, minor fibrosis	Massive fibrosis
CMs	Enlarged CMs area, irregular nuclear morphology	-
Cardiac fetal genes and fibrotic genes	Increased βMHC, ANP and fibrotic genes procollagen1α1/3α1	Increased ANP and fibrotic genes procollagen1α1/3α1
NE-LINC complex	Expression level: increased SUN1 Localisation: mis-localised lamin A/C, emerin and nesprin-1α	Expression level: increased lamin A/C Localisation: -
Mechanosensitive genes	-	Upregulated egr-1 and c-myc
-: have not been investigated yet		

5.3.1 Rationale for generation of cardiac specific nesprin-2 KASH overexpression mice

Recent studies focused on the NE-LINC complex have shown this structure is not only the physical linker between nucleoskeleton and cytoskeleton, but also responsible for mechanical force transduction and gene regulation [2, 111, 112, 176, 178, 190]. The mutations identified in the genes encoding NE-LINC complex associated proteins nesprin, SUN, lamin A/C and emerin have all been found to associate with the muscle specific diseases DCM and EDMD [3, 4, 53, 86, 87, 145, 221]. Various animal models have been generated via different strategies to mimic the physiological and pathophysiological functions of the NE-LINC complex in muscle disease [223, 290]. In particular, the nesprins form the SUN-KASH interaction which is a fundamental part of the NE-LINC complex [111, 115]. To date, 13 nesprin murine models have been established and have highlighted the critical roles of nesprin-1 and -2 in nuclear positioning, mechanotransduction and cardiac or skeletal muscle functions [290]. Interestingly, two of these models have shown cardiac related phenotypes [4, 85, 221]. Based on the strategy utilised in those mouse models, nesprin-1 KASH domain or nesprin-2 were globally deleted from the double alleles [85, 221], which ignore the potential role of the presence of the WT allele in human disease.

In our mouse model, the nesprin-2 KASH domain specifically overexpressed in the hearts using a DN strategy and driven by the cardiac specific MLC2V promotor. The rationales behind using cardiac specific Tg strategy include: 1) Nesprin KASH is a well-documented experimental tool that leads to LINC complex disruption, as it is the key element in the interaction between nesprin-1/-2 and their NE-LINC complex partners [2]. Thus, disruption of the KASH and SUN interaction at NE-LINC complex will disrupt endogenous nesprin functions [238, 291], and provide a better model to examine the role of the LINC itself rather than individual proteins. 2) Both nesprin-1 and -2 share a high degree of homology and are highly conserved in this C-terminal region, especially the KASH domain. Overexpression the recombinant DN-KASH constructs of nesprins-1, -2 and -3 saturates endogenous nesprins from the NE to ER, leading to a significant loss of mechanical stiffness and myogenesis defects, similar to the effects caused by nesprin-1/-2 mutants as reported [112]. 3) The zebrafish embryo data in Chapter 4 showed the expression of nesprin-1α_2 WT had the biggest effect in

causing heart developmental and conduction defects while the mutations caused less severe phenotypes via compromised the binding with other NE-LINC complex components. The limitation of this *in vivo* zebrafish model was the forced expression of muscle specific isoform nesprin-1α_2 at the one egg stage earlier before myogenesis initiation, leading to an ectopic expression effect. In our KASH2 Tg mouse model, the expression of DN KASH was initialled from E8.75 under the MLC2V promoter in CMs [278]. At this time point, three cardiac regions can be distinguished by the bulging morphology: bulbus cordis (future right ventricle), primitive left ventricle, and common atrial chamber behind the primitive left ventricle [292, 293]. Therefore, the expression of DN-KASH in csKASH-Tg followed the physiological heart developmental time point *in vivo*.

5.3.2 Cardiac specific nesprin-2 KASH Tg mice induced a hypertrophic response especially under the mechanical stress

Under basal conditions, csKASH-Tg mice developed a cardiac hypertrophic response from 30 weeks up to 1 year. Echocardiography showed increased LV wall thickness with unchanged heart systolic function. In addition, the CMs size had increased significantly in the csKASH-Tg with deformation of nuclear morphology. The fetal genes βMHC and ANP were re-expressed, along with upregulated fibrotic gene procollagen1α1/3α1. Those findings indicated that there was a cardiac hypertrophic response due to the overexpression of DN KASH in hearts.

There is widespread agreement that the hypertrophic response is a transition phenotype to heart failure (HF). It initially compensates to the physiology or pathological changes, but this is then followed by progression of worsening of symptoms that lead to HF [294, 295]. LV hypertrophy is a complex phenotype that may be influenced by hemodynamic overload and non-hemodynamic variables such as ethnicity, gender, neurohumoral, environment etc. [295, 296]. The main factor hemodynamic changes can be either physiological (exercise) or pathological. In our studies, the mice were not subjected to exercise, and no hypertrophic symptom from the original founders (FLctrl) was reported [238, 239]. Therefore, physiology hemodynamic changes such as exercise capacity induced hypertrophic hearts in athletes can be excluded from the hypertrophy observed in the csKASH-Tg hearts

[297]. In addition, when the csKASH-Tg mouse hearts were subjected to pressure overload, the LV exhibited an enlarged internal diameter and volume at the end of diastole, with massive fibrosis and altered biomechanical gene expression profile compared with FLctrl TAC. The deteriorated cardiac response to the hemodynamic stress further confirmed that the pathological process induced by DN KASH would lead to a more fragile heart.

LV hypertrophy as the intermediate phenotype of heart failure, can lead to this final outcome with reduced EF (HFrEF) or preserved EF (HFpEF) [298]. The latter HF accounts for 50% HF, and is characterised with the prolonged isovolumic LV relaxation, slow LV filling and increased diastolic LV stiffness [299]. The subcellular changes of HFpEF include an increase in the size of CMs, alteration in the ECM with accumulation of fibrosis. In our csKASH-Tg mice, the increased LV wall, with maintained EF, enlarged CMs, increased accumulation of collagen in ECM and fibrosis, indicated the hypertrophic cardiomyopathy (HFpEF) was induced by overexpression of DN KASH2. In further studies, the assessment of myocardial strain (LV segment movement and deformation) and diastolic functions by echocardiography [300] will be needed for the diagnostic evaluation and linking the cellular changes with clinical symptoms to elucidate the pathogenesis of the cardiomyopathy evident in csKASH-Tg mice.

5.3.3 csKASH-Tg mice exhibited a late onset and mild cardiac phenotype

In this study, csKASH-Tg mice exhibited a deleterious cardiac phenotype with a late-onset manner. There are several potential explanations. Firstly, the well characterised *LMNA* mice which showed early onset DCM and HF were due to the homozygous KO or mutants (*H222P*, *N195K*) knock-in strategy [224, 250, 301]. However, the heterozygous *LMNA* KO mice showed a milder phenotype, with slightly decreased EF only at one-year-old [229]. The different severity of DCM can be influenced by whether there is a functional WT allele. In our Tg mouse model, the expression level of nesprin WT alleles were preserved. Secondly, nesprin-1 and -2 generate multiple isoforms can act in a compensatory role in cardiac tissue functions [34]. Studies indicated the heart phenotype would not have been induced when either *SYNE-1* or *SYNE-2* was knocked out, but required both to be absent [85, 135].

Interestingly, the DCM phenotype did not show in other nesprin KO mouse models that targeted on either nesprin-1 or -2 isoforms [124, 136-138], further strengthening the compensation hypothesis. Nesprin-2 isoforms have been shown to dynamically switch between the nucleus and cytoplasm in CMs under the hypertrophic stimuli *in vitro* or TAC procedure *in vivo* (Catherine Shanahan lab, unpublished data). Nesprin-1 showed these isoforms switch during the C2C12 differentiation (Catherine Shanahan lab, unpublished data). In csKASH-Tg mice, overexpression DN KASH2 would theoretically displace the endogenous nesprin-1 and -2 isoforms containing the KASH domain, but the efficiency also depended on the expressed amount/level of GFP-KASH2. Notably the multiple unidentified nesprin isoforms generated by alternative initiation and splicing may contribute to the compensation of NE-LINC complex disruption and result in the late onset and milder cardiac phenotype in csKASH-Tg mice.

5.3.4 NE-LINC complex was disrupted in csKASH-Tg mice

The overexpressed DN KASH was shown to mis-localise endogenous nesprin from the NE, and disrupt the NE-LINC complex [178, 238, 239]. The fold changes of exogenous GFP-KASH2 relative to endogenous KASH2 containing isoform was only quantified by qPCR instead of combination of WB. It was due to two reasons: i) there are no specific nesprin antibodies generated specifically against the region of KASH2 domain; ii) there are numerous nesprin-2 KASH containing isoforms which vary in size (nesprin-2 giant is around 800kDa whereas GFP-KASH2 is 31kDa). It is very challenging to detect all of them on one blotting and compare the intensity of multiple bands with GPF-KASH2. In our mouse model, the expression level of SUN1 was increased in csKASH-Tg compared with FLctrl in the basal line. The expression of SUN2 was upregulated under the TAC procedure in FLctrl TAC compared with FLctrl Sham, and lamin A/C was increased in conjunction with overexpressing KASH and pressure overload. Other NE-LINC complex components emerin and nesprin-1α were unchanged in csKASH-Tg and FLctrl before and after TAC. Those subtle changes in expression level of the NE-LINC complex components were consistent with other nesprin mouse models. In nesprin-1 KASH KO mice, lamin A/C level was unchanged in the heart [4]. Global nesprin-1 KO mice have only increased SUN1 in the heart lysate [135]. Even in the double *SYNE-1* and *SYNE-2* KO mice, both the protein and

RNA levels of those LINC complex components are more variable, but without statistical difference [85]. Combined with all the nesprin mouse models, it is reasonably to postulate that: loss of either nesprin-1 and/or -2 would not dramatically alter expression profiles of NE-LINC complex associated proteins; SUN1 may serve as the dominant SUN protein to form the SUN-KASH bridge in the heart; the minimal changes of expression levels of the NE-LINC complex components may be amplified by the pathological changes such as pressure overload and result in HF in csKASH-Tg mice.

In addition, with such minimal changes of the expression level, the localisation of those NE-LINC complex factors were surprisingly reduced at the NE in the csKASH-Tg heart. Overexpression of GFP-KASH2 reduced endogenous nesprin-1α, lamin A/C and emerin from the CMs, similar to the effect caused by nesprin-1 mutants from DCM patients in Chapter 3. In nesprin double KO mice, loss of both nesprin-1 and -2 have a significant impact on the localisation of both lamin A/C and emerin in the CMs [85]. Those findings indicated that dysfunction of nesprin have more impact on changing the localisation of associated proteins rather than altering their expression levels. In addition to the reduced bindings between nesprin and lamin A/C and SUN2 caused by nesprin-1α mutations in Chapter 3, it is plausible that the disrupted NE-LINC complex in CMs was induced by the mis-localisation of NE-LINC complex components and their perturbed bindings.

5.3.5 Functions of NE-LINC complex were perturbed in csKASH-Tg mice

The force transmission from the ECM to the nucleus is dependent on the intact NE-LINC complex [112, 176, 215]. Components of NE-LINC complex such as lamin A/C, emerin and nesprin-1/-2 have been shown to participate in mechanotransduction and regulate the mechanosensitive genes (egr-1, iex-1, c-fos, c-myc and c-jun) [85, 211, 213, 214]. MEFs derived from *LMNA* or *EMD* null mice had reduced expression of the mechanosensitive genes egr-1 and iex-1 [213, 214]. Isolated CMs lacking both nesprin-1 and -2 displayed attenuated biomechanical genes (egr-1, iex-1, c-fos, c-myc and c-jun) in response to stretching [85]. *In vivo* pressure overload models, egr-1 null mice had reduced LV hypertrophic response to the pressure overload [302], suggesting egr-1 was a crucial regulator in pathological cardiovascular processes. In addition,

heterozygous *LMNA* null mice exhibited attenuated hypertrophy with absent induction of egr-1 and iex-1 at 1-week post-surgery compared to the WT mice [229]. Thus, hyper-activation of mechanosensitive genes egr-1 and iex-1 might be positive correlated to the ventricular and CMs hypertrophy. In our csKASH-Tg mice, the LV remodelling was accelerated by pressure overload, and this was associated with an increased response of mechanosensitive genes egr-1 and c-myc, whereas other mechanosensitive genes iex-1, c-fos and c-myc were similar to the FLctrl TAC. These data further reinforce the hypothesis that the disrupted NE-LINC complex impairs mechanotransduction signalling and influences the eventual biochemical response. One explanation is that the nucleus as the mechanosensor is impaired and is made deficient by the disrupted NE-LINC complex. The changed nuclear morphology and stiffness increased the susceptibility of nuclei to the mechanical strain. Moreover, another intriguing explanation could be that the up-regulated lamin A/C in csKASH-Tg mice contributed to the dysregulation of mechanical sensitive genes. Lamin A/C has been shown to directly interact with another biomechanical gene c-fos at the NE to suppress Activating Protein 1 (AP-1). Meanwhile, c-fos in the nucleus can down-regulate egr-1 [303]. Increased lamin A/C with unchanged c-fos expression in our csKASH-Tg TAC mice may sequester more c-fos at the NE and result in fewer c-fos in the nuclear interior and cause increased gene expression of egr-1 in response to pressure overload.

Of note, all those mechanosensitive genes showed a rapid response to mechanical stretch. *In vitro*, these genes show induction response within 1-2 hours and go back to basal line within 2 days [211, 304]; while *in vivo*, the rapid response can be detected at 1 week and returns to normal at 3 weeks [229, 305]. Due to the different experimental conditions and the various severity of the pressure overload models, it is necessary to examine the dynamic changes of mechanosensitive genes in the csKASH-Tg mouse model and to choose the appropriate time point to investigate the impact of disrupted NE-LINC complex on transduction of mechanical stimuli into biochemical signals *in vivo*.

5.3.6 Summary

Taken together, the data from csKASH-Tg mice suggested that:

1. Overexpression of DN-KASH in CMs disrupted the NE-LINC complex and induced a hypertrophic response with activated fetal gene re-expression, which was likely a compensatory response at the early phase of developing DCM.
2. The disrupted NE-LINC complex in csKASH-Tg mice led to a more susceptible heart under the mechanical stress, resulting in a decline in cardiac cell functions and defects in force transmission and mechanotransduction. This was consistent with the late-onset of DCM in general, which again validated the model compared to other existing nesprin KO models.
3. In future work, we will focus on investigating the roles of nesprin-1/-2 and NE-LINC complex in nuclear migration, sarcomeric structure and functions in CMs using this csKASH-Tg mouse model.

Chapter 6: General discussion and future directions

6.1 Thesis summary

In this study, three novel rare variants (R8272Q, S8381C, and N8406K) in the C-terminus of the *SYNE-1* gene (nesprin-1) were identified in 7 DCM patients by mutation screening. These nesprin-1 mutants caused increased NE fragility and NE-LINC complex disruption, leading to defects in mechanotransduction and myogenesis *in vitro*, which was further investigated preliminarily in zebrafish embryos and a cardiac specific KASH2 Tg mouse model. These data suggest that nesprin-1 plays multi-functional roles at the NE. These nesprin-1 mutants and DN-KASH comprise NE-LINC complex, leading to defects in NE organisation, myogenesis, which may contribute to pathogenesis of DCM.

6.2 Discussion and future direction

6.2.1 Roles of nesprin-1/-2 in NE-LINC complex

The multi-isometric scaffolding proteins nesprin-1/-2 play multiple functions at the NE-LINC complex (Figure 6.1). In general, large nesprin-1/-2 isoforms localise at the ONM, forming the SUN-KASH trimetric interaction at the perinuclear space, and linking the nucleus to the cytoskeleton via their CH domains binding to F-actin [111, 183]. Meanwhile, small nesprin-1/-2 isoforms localise at the INM, interacting with NE proteins, emerin, SUN1/2 and the nuclear lamina to form the NE complex [35]. In addition, lamin A/C and emerin can directly bind with chromatin-associated proteins such as HP-1, BAF and H2A-H2B histone dimers, which is important for maintaining chromatin architecture, regulating cell signalling and gene expression during different cellular activities. This NE-LINC complex strengthen the connection from inside of the nucleus to the cytoskeleton and further to the ECM.

In Chapter 4, it was shown for the first time that small nesprin isoforms lacking CH domains such as nesprin-1α_2 also localise at the ONM. These isoforms interacted with microtubule motor proteins kinesin-1 to drive the nuclear distribution during

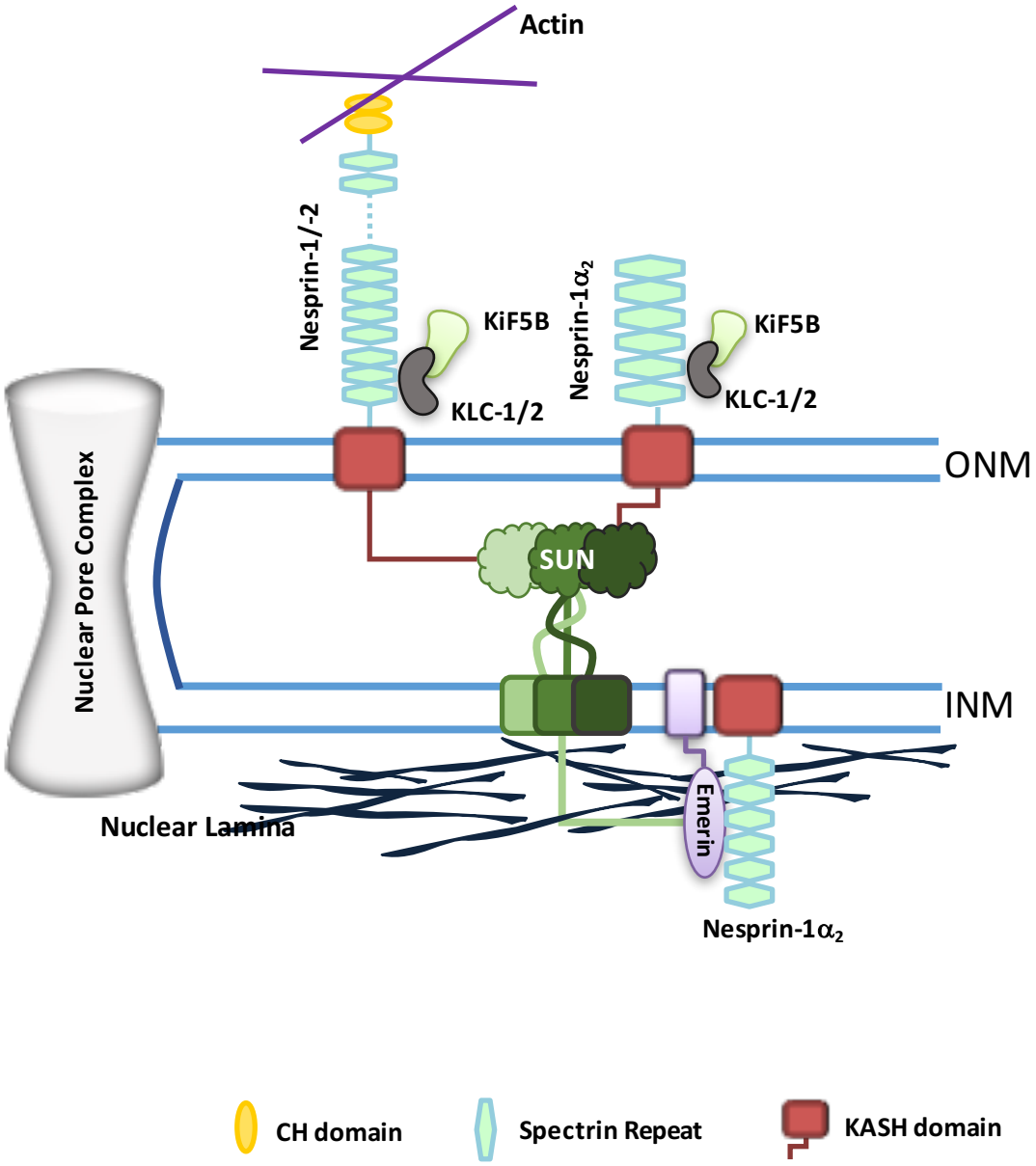


Figure 6.1 Working model for the roles of nesprin-1/-2

The schematic figure shows nesprin-1/-2 play multiple-functions at both INM and ONM. Large nesprin-1/-2 isoforms localise at the ONM, forming the SUN-KASH bridge at the perinuclear space, and linking the nucleus to the cytoskeleton via the CH domains binding to the F-actin. Small nesprin isoforms lacking the CH domains such as nesprin-1α_2 also localise at the ONM, forming the microtubule LINC via the interaction with microtubule motor proteins kinesin-1. Meanwhile, small nesprin-1/-2 isoforms in the INM can interact with NE proteins, emerin, SUN1/2 and nuclear lamina to form NE complex. The NE complex at INM and LINC complex at ONM together form the NE-LINC architecture strengthen the connection from inside of the nucleus to the cytoskeleton and build the cellular homeostasis.

muscle cell differentiation. Nesprin-1 mutations perturbed myoblast fusion and differentiation in a similar manner to the depletion of KLC-1/2. The expanding interactions of nesprins with cytoskeleton elements at both the ONM and INM facilitate scaffolding of the overall cellular structure and maintain cellular homeostasis.

6.2.2 Genotype and phenotype correlation of nesprin-1 mutations

Nesprins, especially nesprin-1, have been implicated in a wide range of diseases, including EDMD, DCM, AMC, CMD, ARCA1, ASD and bipolar disorder [3, 4, 122, 155-157, 159, 161, 166-168]. Summarisation of all mutations in the *SYNE-1* gene: the majority (around 85%) of known mutations associated with muscle disease such as EDMD and DCM are heterozygous missense mutations localised at the C-terminus of nesprin-1 giant, equivalent to muscle specific isoform nesprin-1α_2. Mutated nucleotides in this region can cause amino acid substitution and loss/gain of protein functions [306]. Mutated nesprin-1 may increase the instability of the NE-LINC complex scaffolding in muscle cells, leading to structural disruption. In contrast, mutations affecting CNS development are homozygous and scatter along the whole *SYNE-1* gene. The nonsense mutations cause amino acids substitution that introduce a stop codon [306]. This premature stop codon results in many truncated nesprin-1 variants lacking SRs and KASH domain or absence of nesprin-1 due to nonsense-mediated decay of mutant mRNA [162, 164]. The varied positions of mutations in the *SYNE* gene and their related diseases indicate: 1) The KASH domain and CH domain containing isoforms have tissue specific scaffolding functions in muscle and CNS respectively; 2) The mutations localised at the nesprin-1α_2 region resulting in the EDMD and DCM further highlight that muscle specific isoforms are indispensable for maintaining normal heart and skeletal muscle function.

In my studies, I utilised the novel nesprin-1 mutants identified in DCM patients and investigated their impacts on the NE-LINC complex *in vitro* and *in vivo* (zebrafish embryos development), and further characterised the effects of nesprin mutants in heart via generating the cardiac specific KASH2 Tg mouse model. The compromised functions of NE-LINC complex caused by nesprin-1/-2 mutants can be summarised into three major aspects: 1). Nesprin-1 mutations and DN KASH2 altered nuclear

morphology, mis-localised its binding partners lamin A/C and SUN2 from the NE, which have both been confirmed both *in vitro* and *in vivo*. Furthermore, the three novel nesprin-1 mutants perturbed interactions between nesprin-1 and NE-LINC complex associated proteins including lamin A/C and SUN2 at the INM, as well as the microtubule motor proteins KLC-1/2 at the ONM. These changes resulted in the disrupted NE-LINC complex, uncoupling the nucleoskeleton from the cytoskeleton (F-actin and microtubule), and compromised the functions of NE-LINC complex as a physical linker and force transmission propagator. 2) Nesprin-1 can recruit KCL-1/2 to the NE through a highly conserved 'LEWD' motif and drive nuclei distribution during myotube formation. The altered interaction between nesprin-1 and KLC-1/2 in myoblasts and myotubes affected microtubule mediated nuclear migration and positioning, leading to defects in myogenesis. 3) The disrupted NE-LINC complex and irregular nuclear morphology is likely to influence chromatin structural integrity. Mis-localised emerin and lamin A/C may also alter binding with chromatin-associated proteins such as HP-1 and BAF. Disruption of these interactions would affect cell signalling and gene regulation including : augmented cell signalling (hyperactivation of MAPK kinase induced by nesprin-1 mutants), dysregulated gene expression (perturbed myogenic regulatory factors by nesprin-1 mutants in muscle cell differentiation *in vitro* and upregulated cardiac fetal genes and fibrotic genes by overexpression of DN KASH2 in heart *in vivo*) and abnormal mechanotransduction (altered mechanosensitive genes in csKASH-Tg mice under pressure overload). The compromised NE-LINC complex functions shown in these three aspects (Figure 6.2) may reveal the shared common pathogenic mechanisms underlying muscle specific laminopathies.

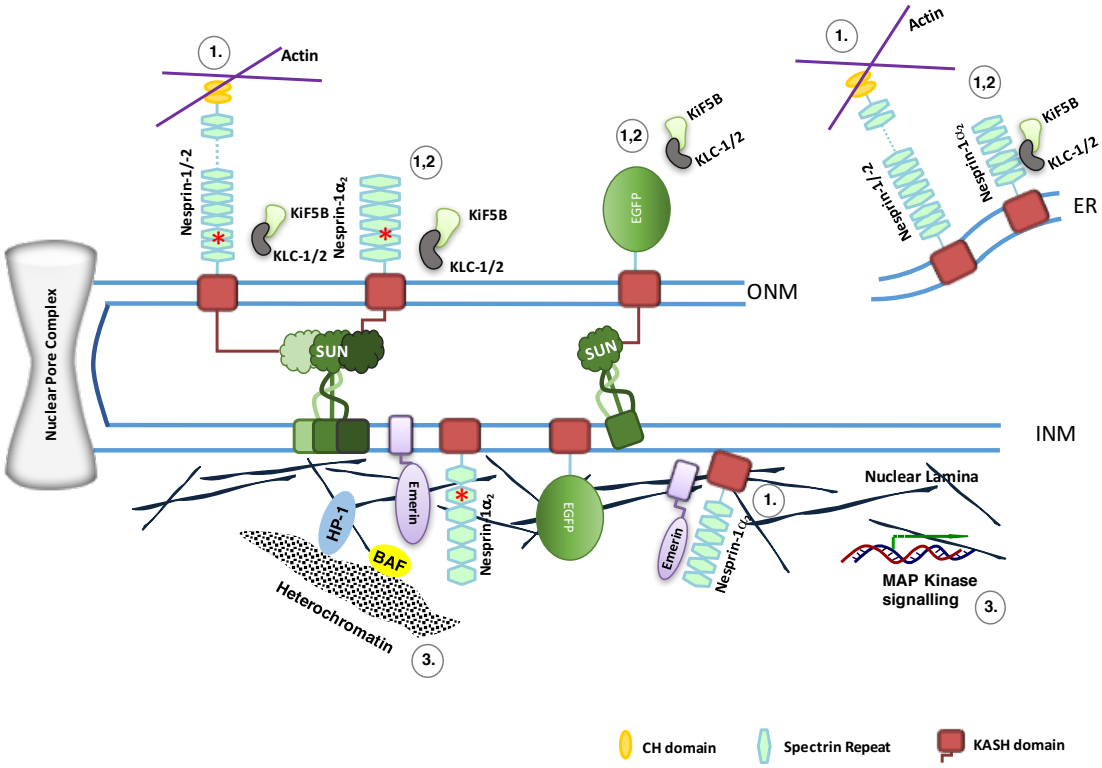


Figure 6.2 Working model for nesprin-1/-2 mutants

The schematic figure shows how nesprin-1/-2 mutants disrupt the NE-LINC complex, contributing the pathogenesis of muscle disease. * indicates where the nesprin-1 mutants are; GFP-KASH indicates the strategy of mouse model in Chapter 5; number 1-3 indicate the affected NE-LINC complex functions by nesprin-1 mutants or DN KASH2 (1. structural disruption; 2. defects in nuclear migration and positioning; 3. dysregulated cell signalling and gene expression.).

6.2.3 Further characterisation of csKASH-Tg mice

6.2.3.1 Investigating the roles of NE-LINC complex in nuclear positioning in CMs

NE-LINC complex plays a critical role in nuclear migration and positioning [69, 118, 180, 185, 191]. In EDMD patients carrying SUN mutations or C2C12 myoblasts overexpressing SUN mutants, gross defects in myonuclear arrangement were detected which was caused by impaired microtubule nucleation [87]. In Chapter 4, the three novel nesprin-1α_2 mutants perturbed the interaction with microtubule motor proteins and this resulted in defects of myonuclear fusion and positioning in C2C12 myoblasts. In contrast to skeletal muscle cells, it remains unknown if there is a nuclear migration defect in CMs in our csKASH-Tg mice. In murine animals, CMs stop proliferation and finish karyokinesis within several days after birth and then maintain a diploid nucleus for the rest of their lives [307, 308]. Studies show during this short period, centrosome integrity is disassembled and microtubule-organizing centre (MTOC) factors such as pericentrin and pericentriolar material 1 protein (PCM-1) are re-localised to the NE depending on the recruitment of microtubule motor proteins kinesin-1 and dynein/dynactin to achieve the post-mitotic state in CMs [309, 310]. PCM-1 [310] and pericentrin (personal communications with Dr. Sue Shackleton's lab, University of Leicester, unpublished data) have been shown to interact with nesprin-1α_2 at the ONM. In addition to that we have confirmed the interaction between nesprin-1α_2 and microtubule motor proteins kinesin-1 in Chapter 4. Therefore, it will be interesting to investigate if there is any defect in microtubule organisation and how they are related to nuclear positioning in CMs in our csKASH-Tg model, and explore the role of the NE-LINC complex in the post-mitotic state of mammalian cardiomyocytes.

6.2.3.2 Investigating the potential roles of nesprin-1 in nuclear Ca^{2+} transient in CMs

The cardiomyopathy related LV remodelling is a complex process involving cardiac myocyte growth and death, vascular rarefaction, fibrosis, inflammation, and electrophysiological remodelling [311, 312]. The hypertrophic response in csKASH-Tg at basal line and the more severe LV remodelling under pathological hemodynamic

stress is similar to the cardiomyopathy phenotypes developed in the late-onset DCM patients in our study.

Literatures showed intracellular Ca^{2+} plays central roles in physiology and pathology of CMs, such as excitation-contraction coupling and secondary messengers, and alteration of the nuclear Ca^{2+} transient is an early event in cardiac remodelling [313, 314]. Recent data showed the NE protein emerin plays a role in nuclear transient in CMs, as EDMD induced pluripotent stem (iPS) cell-derived cardiomyocytes carrying emerin mutations were shown to have increased half decay time of nuclear Ca^{2+} transient [247]. However, the underlying mechanism regarding how emerin mutants cause defects in nuclear Ca^{2+} transient is unknown. In addition, literature showed nesprin-1α could anchor muscle A-kinase anchoring protein (mAKAP) at the NE to control the Ca^{2+} release channel of the sarcoplasmic reticulum in CMs [258]. We propose nesprin and emerin regulate the intracellular Ca^{2+} transients through the NE-LINC complex. Therefore, the Ca^{2+} transients in CMs will be investigated using our csKASH-Tg mouse model. This may provide us with additional information for the roles of NE-LINC complex in CM dysfunction and could be used as potential therapeutic targets in DCM/EDMD and cardiac remodelling.

6.2.3.3 Gene expression profile analysis in hearts from csKASH-Tg mice

NE-LINC complex disruption has been shown to alter the levels and distribution of heterochromatin and thus may have an effect on the epigenetic status of myocyte nuclei, in turn altering the transcriptome of the cell in response to normal contractile activity or mechanical stress [315-317]. In the published LINC complex mouse models, genome-wide expression analysis has shown MAPK activation is significantly elevated in *LMNA*^{H222P} and *EMD* null mice [194, 195]. Using MAPK inhibitors prior to the onset of cardiomyopathy and muscular dystrophy can prevent the development of DCM and EDMD [207-209, 226, 227]. In this thesis, the augmentation of ERK activation was shown in HDFs carrying EDMD mutations and KASH1 KO mouse hearts, as well as C2C12 cells overexpressing nesprin-1α_2 mutations. Thus, it will be interesting to examine csKASH-Tg and FLctrl mice after TAC via Affymetrix microarray analysis, to explore the expression profiles of dysregulated genes and associated signalling pathways in additional to the well characterised MAPK pathway.

This additional information would provide novel cues for further mechanistic investigations of CM dysfunction and DCM.

6.3 Conclusions

In this thesis, I have characterised how nesprin-1/-2 mutants affect NE organisation, myogenesis and how this can contribute to DCM via the NE-LINC complex associated structural disruption and gene dysregulation. In future, improved knowledge of the diverse nesprin isoforms that exist, elucidation of the myriad of nesprin binding partners and their functions in NE-LINC complex in cardiomyocytes will help to uncover novel mechanisms whereby disruption of the NE-LINC complex contribute to development of cardiac cell dysfunction and pathogenesis of DCM, thus leading to potential therapeutic targets for DCM.

Bibliography

1. Zhang, Q., et al., *Nesprins: a novel family of spectrin-repeat-containing proteins that localize to the nuclear membrane in multiple tissues.* J Cell Sci, 2001. **114**(Pt 24): p. 4485-98.
2. Crisp, M., et al., *Coupling of the nucleus and cytoplasm: role of the LINC complex.* J Cell Biol, 2006. **172**(1): p. 41-53.
3. Zhang, Q., et al., *Nesprin-1 and -2 are involved in the pathogenesis of Emery Dreifuss muscular dystrophy and are critical for nuclear envelope integrity.* Hum Mol Genet, 2007. **16**(23): p. 2816-33.
4. Puckelwartz, M.J., et al., *Nesprin-1 mutations in human and murine cardiomyopathy.* J Mol Cell Cardiol, 2010. **48**(4): p. 600-8.
5. Fletcher, D.A. and R.D. Mullins, *Cell mechanics and the cytoskeleton.* Nature, 2010. **463**(7280): p. 485-92.
6. Djinovic-Carugo, K., et al., *The spectrin repeat: a structural platform for cytoskeletal protein assemblies.* FEBS Lett, 2002. **513**(1): p. 119-23.
7. Liem, R.K., *Cytoskeletal Integrators: The Spectrin Superfamily.* Cold Spring Harb Perspect Biol, 2016. **8**(10).
8. Nicolas, A., et al., *The spectrin family of proteins: a unique coiled-coil fold for various molecular surface properties.* J Struct Biol, 2014. **186**(3): p. 392-401.
9. Wilhelmsen, K., et al., *Nesprin-3, a novel outer nuclear membrane protein, associates with the cytoskeletal linker protein plectin.* J Cell Biol, 2005. **171**(5): p. 799-810.
10. Roux, K.J., et al., *Nesprin 4 is an outer nuclear membrane protein that can induce kinesin-mediated cell polarization.* Proc Natl Acad Sci U S A, 2009. **106**(7): p. 2194-9.
11. Behrens, T.W., et al., *Jaw1, A lymphoid-restricted membrane protein localized to the endoplasmic reticulum.* J Immunol, 1994. **153**(2): p. 682-90.
12. Morimoto, A., et al., *A conserved KASH domain protein associates with telomeres, SUN1, and dynactin during mammalian meiosis.* J Cell Biol, 2012. **198**(2): p. 165-72.
13. Apel, E.D., et al., *Syne-1, a dystrophin- and Klarsicht-related protein associated with synaptic nuclei at the neuromuscular junction.* J Biol Chem, 2000. **275**(41): p. 31986-95.
14. Mislow, J.M., et al., *Myne-1, a spectrin repeat transmembrane protein of the myocyte inner nuclear membrane, interacts with lamin A/C.* J Cell Sci, 2002. **115**(Pt 1): p. 61-70.
15. Shanahan, C.M., P.L. Weissberg, and J.C. Metcalfe, *Isolation of gene markers of differentiated and proliferating vascular smooth muscle cells.* Circ Res, 1993. **73**(1): p. 193-204.
16. Zhen, Y.Y., et al., *NUANCE, a giant protein connecting the nucleus and actin cytoskeleton.* J Cell Sci, 2002. **115**(Pt 15): p. 3207-22.

17. Behrens, T.W., et al., *Carboxyl-terminal targeting and novel post-translational processing of JAW1, a lymphoid protein of the endoplasmic reticulum.* J Biol Chem, 1996. **271**(38): p. 23528-34.

18. Lindeman, R.E. and F. Pelegri, *Localized products of futile cycle/lrmp promote centrosome-nucleus attachment in the zebrafish zygote.* Curr Biol, 2012. **22**(10): p. 843-51.

19. Shindo, Y., et al., *Lrmp/Jaw1 is expressed in sweet, bitter, and umami receptor-expressing cells.* Chem Senses, 2010. **35**(2): p. 171-7.

20. Horn, H.F., et al., *A mammalian KASH domain protein coupling meiotic chromosomes to the cytoskeleton.* J Cell Biol, 2013. **202**(7): p. 1023-39.

21. Rajgor, D. and C.M. Shanahan, *Nesprins: from the nuclear envelope and beyond.* Expert Rev Mol Med, 2013. **15**: p. e5.

22. Simpson, J.G. and R.G. Roberts, *Patterns of evolutionary conservation in the nesprin genes highlight probable functionally important protein domains and isoforms.* Biochem Soc Trans, 2008. **36**(Pt 6): p. 1359-67.

23. Zhong, Z., et al., *Stabilization of the spectrin-like domains of nesprin-1alpha by the evolutionarily conserved "adaptive" domain.* Cell Mol Bioeng, 2010. **3**(2): p. 139-150.

24. Mosley-Bishop, K.L., et al., *Molecular analysis of the klarsicht gene and its role in nuclear migration within differentiating cells of the Drosophila eye.* Curr Biol, 1999. **9**(21): p. 1211-20.

25. Zhang, Q., et al., *The nesprins are giant actin-binding proteins, orthologous to Drosophila melanogaster muscle protein MSP-300.* Genomics, 2002. **80**(5): p. 473-81.

26. Schneider, M., A.A. Noegel, and I. Karakesisoglou, *KASH-domain proteins and the cytoskeletal landscapes of the nuclear envelope.* Biochem Soc Trans, 2008. **36**(Pt 6): p. 1368-72.

27. Kim, D.I., K.C. Birendra, and K.J. Roux, *Making the LINC: SUN and KASH protein interactions.* Biol Chem, 2015. **396**(4): p. 295-310.

28. Grum, V.L., et al., *Structures of two repeats of spectrin suggest models of flexibility.* Cell, 1999. **98**(4): p. 523-35.

29. Autore, F., et al., *Large-scale modelling of the divergent spectrin repeats in nesprins: giant modular proteins.* PLoS One, 2013. **8**(5): p. e63633.

30. Castresana, J. and M. Saraste, *Does Vav bind to F-actin through a CH domain?* FEBS Lett, 1995. **374**(2): p. 149-51.

31. Broderick, M.J. and S.J. Winder, *Towards a complete atomic structure of spectrin family proteins.* J Struct Biol, 2002. **137**(1-2): p. 184-93.

32. Winder, S.J., et al., *Utrophin actin binding domain: analysis of actin binding and cellular targeting.* J Cell Sci, 1995. **108 (Pt 1)**: p. 63-71.

33. Djinovic Carugo, K., S. Banuelos, and M. Saraste, *Crystal structure of a calponin homology domain.* Nat Struct Biol, 1997. **4**(3): p. 175-9.

34. Rajgor, D., et al., *Multiple novel nesprin-1 and nesprin-2 variants act as versatile tissue-specific intracellular scaffolds.* PLoS One, 2012. **7**(7): p. e40098.

35. Zhang, Q., et al., *Nesprin-2 is a multi-isomeric protein that binds lamin and emerin at the nuclear envelope and forms a subcellular network in skeletal muscle.* J Cell Sci, 2005. **118**(Pt 4): p. 673-87.

36. Duong, N.T., et al., *Nesprins: tissue-specific expression of epsilon and other short isoforms.* PLoS One, 2014. **9**(4): p. e94380.

37. Holt, I., et al., *Specific localization of nesprin-1-alpha2, the short isoform of nesprin-1 with a KASH domain, in developing, fetal and regenerating muscle, using a new monoclonal antibody.* BMC Cell Biol, 2016. **17**(1): p. 26.

38. Randles, K.N., et al., *Nesprins, but not sun proteins, switch isoforms at the nuclear envelope during muscle development.* Dev Dyn, 2010. **239**(3): p. 998-1009.

39. Dawe, H.R., et al., *Nesprin-2 interacts with meckelin and mediates ciliogenesis via remodelling of the actin cytoskeleton.* J Cell Sci, 2009. **122**(Pt 15): p. 2716-26.

40. Kobayashi, Y., et al., *Identification and characterization of GSRP-56, a novel Golgi-localized spectrin repeat-containing protein.* Exp Cell Res, 2006. **312**(16): p. 3152-64.

41. Rajgor, D., et al., *Mammalian microtubule P-body dynamics are mediated by nesprin-1.* J Cell Biol, 2014. **205**(4): p. 457-75.

42. Warren, D.T., et al., *Novel nuclear nesprin-2 variants tether active extracellular signal-regulated MAPK1 and MAPK2 at promyelocytic leukemia protein nuclear bodies and act to regulate smooth muscle cell proliferation.* J Biol Chem, 2010. **285**(2): p. 1311-20.

43. Lamond, A.I. and W.C. Earnshaw, *Structure and function in the nucleus.* Science, 1998. **280**(5363): p. 547-53.

44. Watson, M.L., *The nuclear envelope; its structure and relation to cytoplasmic membranes.* J Biophys Biochem Cytol, 1955. **1**(3): p. 257-70.

45. Cain, N.E. and D.A. Starr, *SUN proteins and nuclear envelope spacing.* Nucleus, 2015. **6**(1): p. 2-7.

46. Ma, J. and W. Yang, *Three-dimensional distribution of transient interactions in the nuclear pore complex obtained from single-molecule snapshots.* Proc Natl Acad Sci U S A, 2010. **107**(16): p. 7305-10.

47. Gerace, L. and B. Burke, *Functional organization of the nuclear envelope.* Annu Rev Cell Biol, 1988. **4**: p. 335-74.

48. Dreger, M., et al., *Nuclear envelope proteomics: novel integral membrane proteins of the inner nuclear membrane.* Proc Natl Acad Sci U S A, 2001. **98**(21): p. 11943-8.

49. Schirmer, E.C., et al., *Nuclear membrane proteins with potential disease links found by subtractive proteomics.* Science, 2003. **301**(5638): p. 1380-2.

50. Schirmer, E.C. and L. Gerace, *The nuclear membrane proteome: extending the envelope.* Trends Biochem Sci, 2005. **30**(10): p. 551-8.

51. Koch, A.J. and J.M. Holaska, *Emerin in health and disease.* Semin Cell Dev Biol, 2014. **29**: p. 95-106.

52. Bione, S., et al., *Identification of a novel X-linked gene responsible for Emery-Dreifuss muscular dystrophy.* Nat Genet, 1994. **8**(4): p. 323-7.

53. Manilal, S., et al., *The Emery-Dreifuss muscular dystrophy protein, emerin, is a nuclear membrane protein.* Hum Mol Genet, 1996. **5**(6): p. 801-8.

54. Wagner, N. and G. Krohne, *LEM-Domain proteins: new insights into lamin-interacting proteins.* Int Rev Cytol, 2007. **261**: p. 1-46.

55. Ostlund, C., et al., *Intracellular trafficking of emerin, the Emery-Dreifuss muscular dystrophy protein.* J Cell Sci, 1999. **112 (Pt 11)**: p. 1709-19.

56. Tsuchiya, Y., et al., *Distinct regions specify the nuclear membrane targeting of emerin, the responsible protein for Emery-Dreifuss muscular dystrophy.* Eur J Biochem, 1999. **259**(3): p. 859-65.

57. Ostlund, C., et al., *Dependence of diffusional mobility of integral inner nuclear membrane proteins on A-type lamins.* Biochemistry, 2006. **45**(5): p. 1374-82.

58. Nagano, A., et al., *Emerin deficiency at the nuclear membrane in patients with Emery-Dreifuss muscular dystrophy.* Nat Genet, 1996. **12**(3): p. 254-9.

59. Cartegni, L., et al., *Heart-specific localization of emerin: new insights into Emery-Dreifuss muscular dystrophy.* Hum Mol Genet, 1997. **6**(13): p. 2257-64.

60. Holaska, J.M., *Emerin and the nuclear lamina in muscle and cardiac disease.* Circ Res, 2008. **103**(1): p. 16-23.

61. Mislow, J.M., et al., *Nesprin-1alpha self-associates and binds directly to emerin and lamin A in vitro.* FEBS Lett, 2002. **525**(1-3): p. 135-40.

62. Holaska, J.M., K.L. Wilson, and M. Mansharamani, *The nuclear envelope, lamins and nuclear assembly.* Curr Opin Cell Biol, 2002. **14**(3): p. 357-64.

63. Haque, F., et al., *Mammalian SUN protein interaction networks at the inner nuclear membrane and their role in laminopathy disease processes.* J Biol Chem, 2010. **285**(5): p. 3487-98.

64. Margalit, A., et al., *Barrier-to-autointegration factor--a BAFfling little protein.* Trends Cell Biol, 2007. **17**(4): p. 202-8.

65. Berk, J.M., K.E. Tifft, and K.L. Wilson, *The nuclear envelope LEM-domain protein emerin.* Nucleus, 2013. **4**(4): p. 298-314.

66. Wheeler, M.A., et al., *Distinct functional domains in nesprin-1alpha and nesprin-2beta bind directly to emerin and both interactions are disrupted in X-linked Emery-Dreifuss muscular dystrophy.* Exp Cell Res, 2007. **313**(13): p. 2845-57.

67. Burke, B. and C.L. Stewart, *Life at the edge: the nuclear envelope and human disease.* Nat Rev Mol Cell Biol, 2002. **3**(8): p. 575-85.

68. Hagan, I. and M. Yanagida, *The product of the spindle formation gene sad1+ associates with the fission yeast spindle pole body and is essential for viability.* J Cell Biol, 1995. **129**(4): p. 1033-47.

69. Malone, C.J., et al., *UNC-84 localizes to the nuclear envelope and is required for nuclear migration and anchoring during C. elegans development.* Development, 1999. **126**(14): p. 3171-81.

70. Jaspersen, S.L., et al., *The Sad1-UNC-84 homology domain in Mps3 interacts with Mps2 to connect the spindle pole body with the nuclear envelope.* J Cell Biol, 2006. **174**(5): p. 665-75.

71. Graumann, K., J. Runions, and D.E. Evans, *Characterization of SUN-domain proteins at the higher plant nuclear envelope.* Plant J, 2010. **61**(1): p. 134-44.

72. Gob, E., et al., *Mammalian sperm head formation involves different polarization of two novel LINC complexes.* PLoS One, 2010. **5**(8): p. e12072.

73. Shao, X., et al., *Spag4, a novel sperm protein, binds outer dense-fiber protein Odf1 and localizes to microtubules of manchette and axoneme.* Dev Biol, 1999. **211**(1): p. 109-23.

74. Calvi, A., et al., *SUN4 is essential for nuclear remodeling during mammalian spermiogenesis.* Dev Biol, 2015. **407**(2): p. 321-30.

75. Jiang, X.Z., et al., *SPAG4L, a novel nuclear envelope protein involved in the meiotic stage of spermatogenesis.* DNA Cell Biol, 2011. **30**(11): p. 875-82.

76. Hodzic, D.M., et al., *Sun2 is a novel mammalian inner nuclear membrane protein.* J Biol Chem, 2004. **279**(24): p. 25805-12.

77. Haque, F., et al., *SUN1 interacts with nuclear lamin A and cytoplasmic nesprins to provide a physical connection between the nuclear lamina and the cytoskeleton.* Mol Cell Biol, 2006. **26**(10): p. 3738-51.

78. Zhou, Z., et al., *Structure of Sad1-UNC84 homology (SUN) domain defines features of molecular bridge in nuclear envelope.* J Biol Chem, 2012. **287**(8): p. 5317-26.

79. Gob, E., et al., *Expression of individual mammalian Sun1 isoforms depends on the cell type.* Commun Integr Biol, 2011. **4**(4): p. 440-2.

80. Liu, Q., et al., *Functional association of Sun1 with nuclear pore complexes.* J Cell Biol, 2007. **178**(5): p. 785-98.

81. Lei, K., et al., *SUN1 and SUN2 play critical but partially redundant roles in anchoring nuclei in skeletal muscle cells in mice.* Proc Natl Acad Sci U S A, 2009. **106**(25): p. 10207-12.

82. Horn, H.F., et al., *The LINC complex is essential for hearing.* J Clin Invest, 2013. **123**(2): p. 740-50.

83. Yu, J., et al., *KASH protein Syne-2/Nesprin-2 and SUN proteins SUN1/2 mediate nuclear migration during mammalian retinal development.* Hum Mol Genet, 2011. **20**(6): p. 1061-73.

84. Ding, X., et al., *SUN1 is required for telomere attachment to nuclear envelope and gametogenesis in mice.* Dev Cell, 2007. **12**(6): p. 863-72.

85. Banerjee, I., et al., *Targeted ablation of nesprin 1 and nesprin 2 from murine myocardium results in cardiomyopathy, altered nuclear morphology and inhibition of the biomechanical gene response.* PLoS Genet, 2014. **10**(2): p. e1004114.

86. Li, P., et al., *Contribution of SUN1 mutations to the pathomechanism in muscular dystrophies.* Hum Mutat, 2014. **35**(4): p. 452-61.

87. Meinke, P., et al., *Muscular dystrophy-associated SUN1 and SUN2 variants disrupt nuclear-cytoskeletal connections and myonuclear organization.* PLoS Genet, 2014. **10**(9): p. e1004605.

88. Turgay, Y., et al., *The molecular architecture of lamins in somatic cells.* Nature, 2017. **543**(7644): p. 261-264.

89. Lin, F. and H.J. Worman, *Structural organization of the human gene encoding nuclear lamin A and nuclear lamin C.* J Biol Chem, 1993. **268**(22): p. 16321-6.

90. Davidson, P.M. and J. Lammerding, *Broken nuclei--lamins, nuclear mechanics, and disease.* Trends Cell Biol, 2014. **24**(4): p. 247-56.

91. Machiels, B.M., et al., *An alternative splicing product of the lamin A/C gene lacks exon 10.* J Biol Chem, 1996. **271**(16): p. 9249-53.

92. Alsheimer, M., et al., *Meiotic lamin C2: the unique amino-terminal hexapeptide GNAEGR is essential for nuclear envelope association.* Proc Natl Acad Sci U S A, 2000. **97**(24): p. 13120-5.

93. Constantinescu, D., et al., *Lamin A/C expression is a marker of mouse and human embryonic stem cell differentiation.* Stem Cells, 2006. **24**(1): p. 177-85.

94. Stick, R., *The gene structure of B-type nuclear lamins of Xenopus laevis: implications for the evolution of the vertebrate lamin family.* Chromosome Res, 1994. **2**(5): p. 376-82.

95. Stewart, C. and B. Burke, *Teratocarcinoma stem cells and early mouse embryos contain only a single major lamin polypeptide closely resembling lamin B.* Cell, 1987. **51**(3): p. 383-92.

96. Rober, R.A., K. Weber, and M. Osborn, *Differential timing of nuclear lamin A/C expression in the various organs of the mouse embryo and the young animal: a developmental study.* Development, 1989. **105**(2): p. 365-78.

97. Nigg, E.A., G.T. Kitten, and K. Vorburger, *Targeting lamin proteins to the nuclear envelope: the role of CaaX box modifications.* Biochem Soc Trans, 1992. **20**(2): p. 500-4.

98. Young, S.G., L.G. Fong, and S. Michaelis, *Prelamin A, Zmpste24, misshapen cell nuclei, and progeria--new evidence suggesting that protein farnesylation could be important for disease pathogenesis.* J Lipid Res, 2005. **46**(12): p. 2531-58.

99. Davies, B.S., et al., *The posttranslational processing of prelamin A and disease.* Annu Rev Genomics Hum Genet, 2009. **10**: p. 153-74.

100. Swift, J., et al., *Nuclear lamin-A scales with tissue stiffness and enhances matrix-directed differentiation.* Science, 2013. **341**(6149): p. 1240104.

101. Kubben, N., J.W. Voncken, and T. Misteli, *Mapping of protein- and chromatin-interactions at the nuclear lamina.* Nucleus, 2010. **1**(6): p. 460-71.

102. Simon, D.N. and K.L. Wilson, *Partners and post-translational modifications of nuclear lamins.* Chromosoma, 2013. **122**(1-2): p. 13-31.

103. Ye, Q. and H.J. Worman, *Interaction between an integral protein of the nuclear envelope inner membrane and human chromodomain proteins homologous to Drosophila HP1.* J Biol Chem, 1996. **271**(25): p. 14653-6.

104. Goldberg, M., et al., *The tail domain of lamin Dm0 binds histones H2A and H2B.* Proc Natl Acad Sci U S A, 1999. **96**(6): p. 2852-7.

105. Lee, K.K., et al., *Distinct functional domains in emerin bind lamin A and DNA-bridging protein BAF.* J Cell Sci, 2001. **114**(Pt 24): p. 4567-73.

106. Sakaki, M., et al., *Interaction between emerin and nuclear lamins.* J Biochem, 2001. **129**(2): p. 321-7.

107. Dechat, T., et al., *Lamina-associated polypeptide 2alpha binds intranuclear A-type lamins.* J Cell Sci, 2000. **113 Pt 19**: p. 3473-84.

108. Dorner, D., et al., *Lamina-associated polypeptide 2alpha regulates cell cycle progression and differentiation via the retinoblastoma-E2F pathway.* J Cell Biol, 2006. **173**(1): p. 83-93.

109. Gonzalez, J.M., et al., *Fast regulation of AP-1 activity through interaction of lamin A/C, ERK1/2, and c-Fos at the nuclear envelope.* J Cell Biol, 2008. **183**(4): p. 653-66.

110. Lloyd, D.J., R.C. Trembath, and S. Shackleton, *A novel interaction between lamin A and SREBP1: implications for partial lipodystrophy and other laminopathies.* Hum Mol Genet, 2002. **11**(7): p. 769-77.

111. Razafsky, D. and D. Hodzic, *Bringing KASH under the SUN: the many faces of nucleo-cytoskeletal connections.* J Cell Biol, 2009. **186**(4): p. 461-72.

112. Lombardi, M.L., et al., *The interaction between nesprins and sun proteins at the nuclear envelope is critical for force transmission between the nucleus and cytoskeleton.* J Biol Chem, 2011. **286**(30): p. 26743-53.

113. Simon, D.N. and K.L. Wilson, *The nucleoskeleton as a genome-associated dynamic 'network of networks'.* Nat Rev Mol Cell Biol, 2011. **12**(11): p. 695-708.

114. Wilson, M.H. and E.L. Holzbaur, *Nesprins anchor kinesin-1 motors to the nucleus to drive nuclear distribution in muscle cells.* Development, 2015. **142**(1): p. 218-28.

115. Sosa, B.A., et al., *LINC complexes form by binding of three KASH peptides to domain interfaces of trimeric SUN proteins.* Cell, 2012. **149**(5): p. 1035-47.

116. Sosa, B.A., U. Kutay, and T.U. Schwartz, *Structural insights into LINC complexes.* Curr Opin Struct Biol, 2013. **23**(2): p. 285-91.

117. Wang, N., J.D. Tytell, and D.E. Ingber, *Mechanotransduction at a distance: mechanically coupling the extracellular matrix with the nucleus.* Nat Rev Mol Cell Biol, 2009. **10**(1): p. 75-82.

118. Luxton, G.W., et al., *TAN lines: a novel nuclear envelope structure involved in nuclear positioning.* Nucleus, 2011. **2**(3): p. 173-81.

119. Folker, E.S., et al., *Lamin A variants that cause striated muscle disease are defective in anchoring transmembrane actin-associated nuclear lines for nuclear movement.* Proc Natl Acad Sci U S A, 2011. **108**(1): p. 131-6.

120. Khatau, S.B., et al., *A perinuclear actin cap regulates nuclear shape.* Proc Natl Acad Sci U S A, 2009. **106**(45): p. 19017-22.

121. Lu, W., et al., *Nesprin interchain associations control nuclear size.* Cell Mol Life Sci, 2012. **69**(20): p. 3493-509.

122. Zhou, C., et al., *Novel nesprin-1 mutations associated with dilated cardiomyopathy cause nuclear envelope disruption and defects in myogenesis.* Hum Mol Genet, 2017. **26**(12): p. 2258-2276.

123. Zhang, X., et al., *SUN1/2 and Syne/Nesprin-1/2 complexes connect centrosome to the nucleus during neurogenesis and neuronal migration in mice.* Neuron, 2009. **64**(2): p. 173-87.

124. Stroud, M.J., et al., *Nesprin 1alpha2 is essential for mouse postnatal viability and nuclear positioning in skeletal muscle.* J Cell Biol, 2017. **216**(7): p. 1915-1924.

125. Morgan, J.T., et al., *Nesprin-3 regulates endothelial cell morphology, perinuclear cytoskeletal architecture, and flow-induced polarization.* Mol Biol Cell, 2011. **22**(22): p. 4324-34.

126. Ketema, M. and A. Sonnenberg, *Nesprin-3: a versatile connector between the nucleus and the cytoskeleton.* Biochem Soc Trans, 2011. **39**(6): p. 1719-24.

127. Stewart, C.L. and B. Burke, *The missing LINC: a mammalian KASH-domain protein coupling meiotic chromosomes to the cytoskeleton.* Nucleus, 2014. **5**(1): p. 3-10.

128. Lee, C.Y., et al., *Mechanism and regulation of rapid telomere prophase movements in mouse meiotic chromosomes.* Cell Rep, 2015. **11**(4): p. 551-63.

129. Borradori, L. and A. Sonnenberg, *Structure and function of hemidesmosomes: more than simple adhesion complexes.* J Invest Dermatol, 1999. **112**(4): p. 411-8.

130. Koster, J., L. Borradori, and A. Sonnenberg, *Hemidesmosomes: molecular organization and their importance for cell adhesion and disease.* Handb Exp Pharmacol, 2004(165): p. 243-80.

131. Ketema, M., et al., *Requirements for the localization of nesprin-3 at the nuclear envelope and its interaction with plectin.* J Cell Sci, 2007. **120**(Pt 19): p. 3384-94.

132. Postel, R., et al., *Nesprin-3 augments peripheral nuclear localization of intermediate filaments in zebrafish.* J Cell Sci, 2011. **124**(Pt 5): p. 755-64.

133. Ketema, M., et al., *Nesprin-3 connects plectin and vimentin to the nuclear envelope of Sertoli cells but is not required for Sertoli cell function in spermatogenesis.* Mol Biol Cell, 2013. **24**(15): p. 2454-66.

134. Rodriguez, O.C., et al., *Conserved microtubule-actin interactions in cell movement and morphogenesis.* Nat Cell Biol, 2003. **5**(7): p. 599-609.

135. Zhang, J., et al., *Nesprin 1 is critical for nuclear positioning and anchorage.* Hum Mol Genet, 2010. **19**(2): p. 329-41.

136. Luke, Y., et al., *Nesprin-2 Giant (NUANCE) maintains nuclear envelope architecture and composition in skin.* J Cell Sci, 2008. **121**(11): p. 1887-98.

137. Grady, R.M., et al., *Syne proteins anchor muscle nuclei at the neuromuscular junction.* Proc Natl Acad Sci U S A, 2005. **102**(12): p. 4359-64.

138. Zhang, X., et al., *Syne-1 and Syne-2 play crucial roles in myonuclear anchorage and motor neuron innervation.* Development, 2007. **134**(5): p. 901-8.

139. Fan, J. and K.A. Beck, *A role for the spectrin superfamily member Syne-1 and kinesin II in cytokinesis.* J Cell Sci, 2004. **117**(Pt 4): p. 619-29.

140. Worman, H.J., et al., *Laminopathies and the long strange trip from basic cell biology to therapy.* J Clin Invest, 2009. **119**(7): p. 1825-36.

141. Towbin, J.A. and N.E. Bowles, *The failing heart.* Nature, 2002. **415**(6868): p. 227-33.

142. Hershberger, R.E., D.J. Hedges, and A. Morales, *Dilated cardiomyopathy: the complexity of a diverse genetic architecture.* Nat Rev Cardiol, 2013. **10**(9): p. 531-47.

143. Weintraub, R.G., C. Semsarian, and P. Macdonald, *Dilated cardiomyopathy.* Lancet, 2017. **390**(10092): p. 400-414.

144. Emery, A.E. and F.E. Dreifuss, *Unusual type of benign x-linked muscular dystrophy.* J Neurol Neurosurg Psychiatry, 1966. **29**(4): p. 338-42.

145. Bonne, G., et al., *Mutations in the gene encoding lamin A/C cause autosomal dominant Emery-Dreifuss muscular dystrophy.* Nat Genet, 1999. **21**(3): p. 285-8.

146. Capell, B.C. and F.S. Collins, *Human laminopathies: nuclei gone genetically awry.* Nat Rev Genet, 2006. **7**(12): p. 940-52.

147. Helbling-Leclerc, A., G. Bonne, and K. Schwartz, *Emery-Dreifuss muscular dystrophy.* Eur J Hum Genet, 2002. **10**(3): p. 157-61.

148. Vytopil, M., et al., *Mutation analysis of the lamin A/C gene (LMNA) among patients with different cardiomuscular phenotypes.* J Med Genet, 2003. **40**(12): p. e132.

149. Bonne, G., et al., *108th ENMC International Workshop, 3rd Workshop of the MYO-CLUSTER project: EUROMEN, 7th International Emery-Dreifuss Muscular Dystrophy (EDMD) Workshop, 13-15 September 2002, Naarden, The Netherlands.* Neuromuscul Disord, 2003. **13**(6): p. 508-15.

150. Gotzmann, J. and R.P. Foisner, *Lamins and Emerin in muscular dystrophy: the nuclear envelope connection*, in *Madame Curie Bioscience Database [Internet]*. 2013, Landes Bioscience; 2000-2013.

151. Chen, Z., et al., *A novel SYNE1 gene mutation in a Chinese family of Emery-Dreifuss muscular dystrophy-like.* BMC Med Genet, 2017. **18**(1): p. 63.

152. Fanin, M., et al., *Dominant muscular dystrophy with a novel SYNE1 gene mutation.* Muscle Nerve, 2015. **51**(1): p. 145-7.

153. Sullivan, T., et al., *Loss of A-type lamin expression compromises nuclear envelope integrity leading to muscular dystrophy.* J Cell Biol, 1999. **147**(5): p. 913-20.

154. Taranum, S., et al., *LINC complex alterations in DMD and EDMD/CMT fibroblasts.* Eur J Cell Biol, 2012. **91**(8): p. 614-28.

155. Voit, T., et al., *C.O.4 Congenital muscular dystrophy with adducted thumbs, mental retardation, cerebellar hypoplasia and cataracts is caused by mutation of Enaptin (Nesprin-1): The third nuclear envelopathy with muscular dystrophy.* Neuromuscular Disorders. **17**(9): p. 833-834.

156. Attali, R., et al., *Mutation of SYNE-1, encoding an essential component of the nuclear lamina, is responsible for autosomal recessive arthrogryposis.* Hum Mol Genet, 2009. **18**(18): p. 3462-9.

157. Baumann, M., et al., *Homozygous SYNE1 mutation causes congenital onset of muscular weakness with distal arthrogryposis: a genotype-phenotype correlation.* Eur J Hum Genet, 2017. **25**(2): p. 262-266.

158. Gao, F., et al., *[Effect of nesprin-1 in the differentiation of mouse embryonic stem cells into cardiomyocytes].* Sichuan Da Xue Xue Bao Yi Xue Ban, 2012. **43**(2): p. 161-5.

159. Gros-Louis, F., et al., *Mutations in SYNE1 lead to a newly discovered form of autosomal recessive cerebellar ataxia.* Nat Genet, 2007. **39**(1): p. 80-5.

160. Noreau, A., et al., *SYNE1 mutations in autosomal recessive cerebellar ataxia.* JAMA Neurol, 2013. **70**(10): p. 1296-31.

161. Izumi, Y., et al., *Cerebellar ataxia with SYNE1 mutation accompanying motor neuron disease.* Neurology, 2013. **80**(6): p. 600-1.

162. Synofzik, M., et al., *SYNE1 ataxia is a common recessive ataxia with major non-cerebellar features: a large multi-centre study.* Brain, 2016. **139**(Pt 5): p. 1378-93.

163. Fogel, B.L. and S. Perlman, *Clinical features and molecular genetics of autosomal recessive cerebellar ataxias.* Lancet Neurol, 2007. **6**(3): p. 245-57.

164. Brogna, S. and J. Wen, *Nonsense-mediated mRNA decay (NMD) mechanisms.* Nat Struct Mol Biol, 2009. **16**(2): p. 107-13.

165. Razafsky, D. and D. Hodzic, *A variant of Nesprin1 giant devoid of KASH domain underlies the molecular etiology of autosomal recessive cerebellar ataxia type I.* Neurobiol Dis, 2015. **78**: p. 57-67.

166. O'Roak, B.J., et al., *Exome sequencing in sporadic autism spectrum disorders identifies severe de novo mutations.* Nat Genet, 2011. **43**(6): p. 585-9.

167. Yu, T.W., et al., *Using whole-exome sequencing to identify inherited causes of autism.* Neuron, 2013. **77**(2): p. 259-73.

168. Green, E.K., et al., *Association at SYNE1 in both bipolar disorder and recurrent major depression.* Mol Psychiatry, 2013. **18**(5): p. 614-7.

169. Akinrinade, O., et al., *Genetics and genotype-phenotype correlations in Finnish patients with dilated cardiomyopathy.* Eur Heart J, 2015. **36**(34): p. 2327-37.

170. Laquerriere, A., et al., *Mutations in CNTNAP1 and ADCY6 are responsible for severe arthrogryposis multiplex congenita with axoglial defects.* Hum Mol Genet, 2014. **23**(9): p. 2279-89.

171. Edens, L.J., et al., *Nuclear size regulation: from single cells to development and disease.* Trends Cell Biol, 2013. **23**(4): p. 151-9.

172. Webster, M., K.L. Witkin, and O. Cohen-Fix, *Sizing up the nucleus: nuclear shape, size and nuclear-envelope assembly.* J Cell Sci, 2009. **122**(Pt 10): p. 1477-86.

173. Jevtic, P., et al., *Sizing and shaping the nucleus: mechanisms and significance.* Curr Opin Cell Biol, 2014. **28**: p. 16-27.

174. Chancellor, T.J., et al., *Actomyosin tension exerted on the nucleus through nesprin-1 connections influences endothelial cell adhesion, migration, and cyclic strain-induced reorientation.* Biophys J, 2010. **99**(1): p. 115-23.

175. Mazumder, A. and G.V. Shivashankar, *Emergence of a prestressed eukaryotic nucleus during cellular differentiation and development.* J R Soc Interface, 2010. **7 Suppl 3**: p. S321-30.

176. Lombardi, M.L. and J. Lammerding, *Keeping the LINC: the importance of nucleocytoskeletal coupling in intracellular force transmission and cellular function.* Biochem Soc Trans, 2011. **39**(6): p. 1729-34.

177. Maniotis, A.J., C.S. Chen, and D.E. Ingber, *Demonstration of mechanical connections between integrins, cytoskeletal filaments, and nucleoplasm that stabilize nuclear structure.* Proc Natl Acad Sci U S A, 1997. **94**(3): p. 849-54.

178. Stewart-Hutchinson, P.J., et al., *Structural requirements for the assembly of LINC complexes and their function in cellular mechanical stiffness.* Exp Cell Res, 2008. **314**(8): p. 1892-905.

179. Anno, T., N. Sakamoto, and M. Sato, *Role of nesprin-1 in nuclear deformation in endothelial cells under static and uniaxial stretching conditions.* Biochem Biophys Res Commun, 2012. **424**(1): p. 94-9.

180. Dupin, I. and S. Etienne-Manneville, *Nuclear positioning: mechanisms and functions.* Int J Biochem Cell Biol, 2011. **43**(12): p. 1698-707.

181. Gundersen, G.G. and H.J. Worman, *Nuclear positioning.* Cell, 2013. **152**(6): p. 1376-89.

182. Starr, D.A. and M. Han, *Role of ANC-1 in tethering nuclei to the actin cytoskeleton.* Science, 2002. **298**(5592): p. 406-9.

183. Starr, D.A. and H.N. Fridolfsson, *Interactions between nuclei and the cytoskeleton are mediated by SUN-KASH nuclear-envelope bridges.* Annu Rev Cell Dev Biol, 2010. **26**: p. 421-44.

184. Hedgecock, E.M. and J.N. Thomson, *A gene required for nuclear and mitochondrial attachment in the nematode Caenorhabditis elegans.* Cell, 1982. **30**(1): p. 321-30.

185. Meyerzon, M., et al., *UNC-83 is a nuclear-specific cargo adaptor for kinesin-1-mediated nuclear migration.* Development, 2009. **136**(16): p. 2725-33.

186. Fridolfsson, H.N. and D.A. Starr, *Kinesin-1 and dynein at the nuclear envelope mediate the bidirectional migrations of nuclei.* J Cell Biol, 2010. **191**(1): p. 115-28.

187. Schneider, M., et al., *Molecular mechanisms of centrosome and cytoskeleton anchorage at the nuclear envelope.* Cell Mol Life Sci, 2011. **68**(9): p. 1593-610.

188. Wilson, M.H. and E.L. Holzbaur, *Opposing microtubule motors drive robust nuclear dynamics in developing muscle cells.* J Cell Sci, 2012. **125**(Pt 17): p. 4158-69.

189. Maninova, M., M.P. Iwanicki, and T. Vomastek, *Emerging role for nuclear rotation and orientation in cell migration.* Cell Adh Migr, 2014. **8**(1): p. 42-8.

190. Brosig, M., et al., *Interfering with the connection between the nucleus and the cytoskeleton affects nuclear rotation, mechanotransduction and myogenesis.* Int J Biochem Cell Biol, 2010. **42**(10): p. 1717-28.

191. Chang, W., et al., *Linker of nucleoskeleton and cytoskeleton (LINC) complex-mediated actin-dependent nuclear positioning orients centrosomes in migrating myoblasts.* Nucleus, 2015. **6**(1): p. 77-88.

192. Gomes, E.R., S. Jani, and G.G. Gundersen, *Nuclear movement regulated by Cdc42, MRCK, myosin, and actin flow establishes MTOC polarization in migrating cells.* Cell, 2005. **121**(3): p. 451-63.

193. Dupin, I., E. Camand, and S. Etienne-Manneville, *Classical cadherins control nucleus and centrosome position and cell polarity.* J Cell Biol, 2009. **185**(5): p. 779-86.

194. Muchir, A., et al., *Activation of MAPK pathways links LMNA mutations to cardiomyopathy in Emery-Dreifuss muscular dystrophy.* J Clin Invest, 2007. **117**(5): p. 1282-93.

195. Muchir, A., et al., *Activation of MAPK in hearts of EMD null mice: similarities between mouse models of X-linked and autosomal dominant Emery Dreifuss muscular dystrophy.* Hum Mol Genet, 2007. **16**(15): p. 1884-95.

196. Markiewicz, E., et al., *The inner nuclear membrane protein emerin regulates beta-catenin activity by restricting its accumulation in the nucleus.* EMBO J, 2006. **25**(14): p. 3275-85.

197. Van Berlo, J.H., et al., *A-type lamins are essential for TGF-beta1 induced PP2A to dephosphorylate transcription factors.* Hum Mol Genet, 2005. **14**(19): p. 2839-49.

198. Cohen, T.V., O. Kosti, and C.L. Stewart, *The nuclear envelope protein MAN1 regulates TGFbeta signaling and vasculogenesis in the embryonic yolk sac.* Development, 2007. **134**(7): p. 1385-95.

199. Scaffidi, P. and T. Misteli, *Lamin A-dependent misregulation of adult stem cells associated with accelerated ageing.* Nat Cell Biol, 2008. **10**(4): p. 452-9.

200. Pearson, G., et al., *Mitogen-activated protein (MAP) kinase pathways: regulation and physiological functions.* Endocr Rev, 2001. **22**(2): p. 153-83.

201. Kim, E.K. and E.J. Choi, *Pathological roles of MAPK signaling pathways in human diseases.* Biochim Biophys Acta, 2010. **1802**(4): p. 396-405.

202. Mebratu, Y. and Y. Tesfaigzi, *How ERK1/2 activation controls cell proliferation and cell death: Is subcellular localization the answer?* Cell Cycle, 2009. **8**(8): p. 1168-75.

203. Petrich, B.G., et al., *c-Jun N-terminal kinase activation mediates downregulation of connexin43 in cardiomyocytes.* Circ Res, 2002. **91**(7): p. 640-7.

204. Gillespie-Brown, J., et al., *The mitogen-activated protein kinase kinase MEK1 stimulates a pattern of gene expression typical of the hypertrophic phenotype in rat ventricular cardiomyocytes.* J Biol Chem, 1995. **270**(47): p. 28092-6.

205. Thorburn, J., et al., *Inhibition of a signaling pathway in cardiac muscle cells by active mitogen-activated protein kinase kinase.* Mol Biol Cell, 1995. **6**(11): p. 1479-90.

206. Emerson, L.J., et al., *Defects in cell spreading and ERK1/2 activation in fibroblasts with lamin A/C mutations.* Biochim Biophys Acta, 2009. **1792**(8): p. 810-21.

207. Muchir, A., et al., *Inhibition of extracellular signal-regulated kinase signaling to prevent cardiomyopathy caused by mutation in the gene encoding A-type lamins.* Hum Mol Genet, 2009. **18**(2): p. 241-7.

208. Muchir, A., et al., *Inhibition of extracellular signal-regulated kinase 1/2 signaling has beneficial effects on skeletal muscle in a mouse model of Emery-Dreifuss muscular dystrophy caused by lamin A/C gene mutation.* Skelet Muscle, 2013. **3**(1): p. 17.

209. Wu, W., et al., *Mitogen-activated protein kinase inhibitors improve heart function and prevent fibrosis in cardiomyopathy caused by mutation in lamin A/C gene.* Circulation, 2011. **123**(1): p. 53-61.

210. Warren, D.T., et al., *Nesprin-2-dependent ERK1/2 compartmentalisation regulates the DNA damage response in vascular smooth muscle cell ageing.* Cell Death Differ, 2015. **22**(9): p. 1540-50.

211. De Keulenaer, G.W., et al., *Identification of IEX-1 as a biomechanically controlled nuclear factor-kappaB target gene that inhibits cardiomyocyte hypertrophy.* Circ Res, 2002. **90**(6): p. 690-6.

212. Granet, C., et al., *MAPK and SRC-kinases control EGR-1 and NF-kappa B inductions by changes in mechanical environment in osteoblasts.* Biochem Biophys Res Commun, 2001. **284**(3): p. 622-31.

213. Lammerding, J., et al., *Abnormal nuclear shape and impaired mechanotransduction in emerin-deficient cells.* J Cell Biol, 2005. **170**(5): p. 781-91.

214. Lammerding, J., et al., *Lamin A/C deficiency causes defective nuclear mechanics and mechanotransduction.* J Clin Invest, 2004. **113**(3): p. 370-8.

215. Guilluy, C., et al., *Isolated nuclei adapt to force and reveal a mechanotransduction pathway in the nucleus.* Nat Cell Biol, 2014. **16**(4): p. 376-81.

216. Booth-Gauthier, E.A., et al., *Hutchinson-Gilford progeria syndrome alters nuclear shape and reduces cell motility in three dimensional model substrates.* Integr Biol (Camb), 2013. **5**(3): p. 569-77.

217. Schwartz, C., et al., *Lamins and nesprin-1 mediate inside-out mechanical coupling in muscle cell precursors through FHOD1.* Sci Rep, 2017. **7**(1): p. 1253.

218. Piccolo, S., S. Dupont, and M. Cordenonsi, *The biology of YAP/TAZ: hippo signaling and beyond.* Physiol Rev, 2014. **94**(4): p. 1287-312.

219. Connelly, J.T., et al., *Actin and serum response factor transduce physical cues from the microenvironment to regulate epidermal stem cell fate decisions.* Nat Cell Biol, 2010. **12**(7): p. 711-8.

220. Ho, C.Y., et al., *Lamin A/C and emerin regulate MKL1-SRF activity by modulating actin dynamics.* Nature, 2013. **497**(7450): p. 507-11.

221. Puckelwartz, M.J., et al., *Disruption of nesprin-1 produces an Emery Dreifuss muscular dystrophy-like phenotype in mice.* Hum Mol Genet, 2009. **18**(4): p. 607-20.

222. Johnson, J.E., B.J. Wold, and S.D. Hauschka, *Muscle creatine kinase sequence elements regulating skeletal and cardiac muscle expression in transgenic mice.* Mol Cell Biol, 1989. **9**(8): p. 3393-9.

223. Zhang, H., J.E. Kieckhaefer, and K. Cao, *Mouse models of laminopathies.* Aging Cell, 2013. **12**(1): p. 2-10.

224. Arimura, T., et al., *Mouse model carrying H222P-Lmna mutation develops muscular dystrophy and dilated cardiomyopathy similar to human striated muscle laminopathies.* Hum Mol Genet, 2005. **14**(1): p. 155-69.

225. Mounkes, L.C., et al., *Expression of an LMNA-N195K variant of A-type lamins results in cardiac conduction defects and death in mice.* Hum Mol Genet, 2005. **14**(15): p. 2167-80.

226. Wu, W., et al., *Pharmacological inhibition of c-Jun N-terminal kinase signaling prevents cardiomyopathy caused by mutation in LMNA gene.* Biochim Biophys Acta, 2010. **1802**(7-8): p. 632-8.

227. Muchir, A., et al., *Treatment with selumetinib preserves cardiac function and improves survival in cardiomyopathy caused by mutation in the lamin A/C gene.* Cardiovasc Res, 2012. **93**(2): p. 311-9.

228. Muchir, A., et al., *Mitogen-activated protein kinase kinase 1/2 inhibition and angiotensin II converting inhibition in mice with cardiomyopathy caused by lamin A/C gene mutation.* Biochem Biophys Res Commun, 2014. **452**(4): p. 958-61.

229. Cupesi, M., et al., *Attenuated hypertrophic response to pressure overload in a lamin A/C haploinsufficiency mouse.* J Mol Cell Cardiol, 2010. **48**(6): p. 1290-7.

230. Stroud, M.J., et al., *Linker of nucleoskeleton and cytoskeleton complex proteins in cardiac structure, function, and disease.* Circ Res, 2014. **114**(3): p. 538-48.

231. Al-Tubuly, A.A., *SDS-PAGE and Western Blotting.* Methods Mol Med, 2000. **40**: p. 391-405.

232. Cobb, A.M., et al., *Prelamin A impairs 53BP1 nuclear entry by mislocalizing NUP153 and disrupting the Ran gradient.* Aging Cell, 2016.

233. Heid, C.A., et al., *Real time quantitative PCR.* Genome Res, 1996. **6**(10): p. 986-94.

234. Deepak, S., et al., *Real-Time PCR: Revolutionizing Detection and Expression Analysis of Genes.* Curr Genomics, 2007. **8**(4): p. 234-51.

235. Garibyan, L. and N. Avashia, *Polymerase chain reaction.* J Invest Dermatol, 2013. **133**(3): p. e6.

236. Liu, H. and J.H. Naismith, *An efficient one-step site-directed deletion, insertion, single and multiple-site plasmid mutagenesis protocol.* BMC Biotechnol, 2008. **8**: p. 91.

237. Scharner, J., et al., *Novel LMNA mutations in patients with Emery-Dreifuss muscular dystrophy and functional characterization of four LMNA mutations.* Hum Mutat, 2011. **32**(2): p. 152-67.

238. Razafsky, D. and D. Hodzic, *Temporal and tissue-specific disruption of LINC complexes in vivo.* Genesis, 2014. **52**(4): p. 359-65.

239. Razafsky, D., C. Potter, and D. Hodzic, *Validation of a Mouse Model to Disrupt LINC Complexes in a Cell-specific Manner.* J Vis Exp, 2015(106): p. e53318.

240. Gao, S., et al., *Echocardiography in Mice.* Curr Protoc Mouse Biol, 2011. **1**: p. 71-83.

241. deAlmeida, A.C., R.J. van Oort, and X.H. Wehrens, *Transverse aortic constriction in mice.* J Vis Exp, 2010(38).

242. Westerfield, M., *The Zebrafish Book. A Guide for The Laboratory Use of Zebrafish (Danio rerio)*. Vol. 385. 2000.

243. Kimmel, C.B., et al., *Stages of embryonic development of the zebrafish.* Dev Dyn, 1995. **203**(3): p. 253-310.

244. Thisse, C. and B. Thisse, *High-resolution in situ hybridization to whole-mount zebrafish embryos.* Nat Protoc, 2008. **3**(1): p. 59-69.

245. Sun, H., et al., *Zili inhibits transforming growth factor-beta signaling by interacting with Smad4.* J Biol Chem, 2010. **285**(6): p. 4243-50.

246. Reichart, B., et al., *Expression and localization of nuclear proteins in autosomal-dominant Emery-Dreifuss muscular dystrophy with LMNA R377H mutation.* BMC Cell Biol, 2004. **5**: p. 12.

247. Shimojima, M., et al., *Emerin plays a crucial role in nuclear invagination and in the nuclear calcium transient.* Sci Rep, 2017. **7**: p. 44312.

248. Biro, J.C., *Amino acid size, charge, hydropathy indices and matrices for protein structure analysis.* Theor Biol Med Model, 2006. **3**: p. 15.

249. Schreiber, K.H. and B.K. Kennedy, *When lamins go bad: nuclear structure and disease.* Cell, 2013. **152**(6): p. 1365-75.

250. Nikolova, V., et al., *Defects in nuclear structure and function promote dilated cardiomyopathy in lamin A/C-deficient mice.* J Clin Invest, 2004. **113**(3): p. 357-69.

251. Nikolova-Krstevski, V., et al., *Nesprin-1 and actin contribute to nuclear and cytoskeletal defects in lamin A/C-deficient cardiomyopathy.* J Mol Cell Cardiol, 2011. **50**(3): p. 479-86.

252. Muchir, A., et al., *Nuclear envelope alterations in fibroblasts from LGMD1B patients carrying nonsense Y259X heterozygous or homozygous mutation in lamin A/C gene.* Exp Cell Res, 2003. **291**(2): p. 352-62.

253. Libotte, T., et al., *Lamin A/C-dependent localization of Nesprin-2, a giant scaffolder at the nuclear envelope.* Mol Biol Cell, 2005. **16**(7): p. 3411-24.

254. Al-Saaidi, R. and P. Bross, *Do lamin A and lamin C have unique roles?* Chromosoma, 2015. **124**(1): p. 1-12.

255. Muchir, A., W. Wu, and H.J. Worman, *Reduced expression of A-type lamins and emerin activates extracellular signal-regulated kinase in cultured cells.* Biochim Biophys Acta, 2009. **1792**(1): p. 75-81.

256. Rodriguez, J., et al., *ERK1/2 MAP kinases promote cell cycle entry by rapid, kinase-independent disruption of retinoblastoma-lamin A complexes.* J Cell Biol, 2010. **191**(5): p. 967-79.

257. Velours, G., et al., *Dual cell wall/mitochondria localization of the 'SUN' family proteins.* FEMS Microbiol Lett, 2002. **207**(2): p. 165-72.

258. Pare, G.C., et al., *Nesprin-1alpha contributes to the targeting of mAKAP to the cardiac myocyte nuclear envelope.* Exp Cell Res, 2005. **303**(2): p. 388-99.

259. Yun, K. and B. Wold, *Skeletal muscle determination and differentiation: story of a core regulatory network and its context.* Curr Opin Cell Biol, 1996. **8**(6): p. 877-89.

260. Charge, S.B. and M.A. Rudnicki, *Cellular and molecular regulation of muscle regeneration.* Physiol Rev, 2004. **84**(1): p. 209-38.

261. Berkes, C.A. and S.J. Tapscott, *MyoD and the transcriptional control of myogenesis.* Semin Cell Dev Biol, 2005. **16**(4-5): p. 585-95.

262. Hindi, S.M., M.M. Tajrishi, and A. Kumar, *Signaling mechanisms in mammalian myoblast fusion.* Sci Signal, 2013. **6**(272): p. re2.

263. Favreau, C., et al., *Expression of a mutant lamin A that causes Emery-Dreifuss muscular dystrophy inhibits in vitro differentiation of C2C12 myoblasts.* Mol Cell Biol, 2004. **24**(4): p. 1481-92.

264. Hakelien, A.M., et al., *Expression of the myodystrophic R453W mutation of lamin A in C2C12 myoblasts causes promoter-specific and global epigenetic defects.* Exp Cell Res, 2008. **314**(8): p. 1869-80.

265. Folker, E.S. and M.K. Baylies, *Nuclear positioning in muscle development and disease.* Front Physiol, 2013. **4**: p. 363.

266. Burattini, S., et al., *C2C12 murine myoblasts as a model of skeletal muscle development: morpho-functional characterization.* Eur J Histochem, 2004. **48**(3): p. 223-33.

267. Chen, Z., et al., *Depletion of zebrafish essential and regulatory myosin light chains reduces cardiac function through distinct mechanisms.* Cardiovasc Res, 2008. **79**(1): p. 97-108.

268. Hwang, P.M. and B.D. Sykes, *Targeting the sarcomere to correct muscle function.* Nat Rev Drug Discov, 2015. **14**(5): p. 313-28.

269. Krauss, R.S., et al., *Close encounters: regulation of vertebrate skeletal myogenesis by cell-cell contact.* J Cell Sci, 2005. **118**(Pt 11): p. 2355-62.

270. Kosak, S.T., et al., *Subnuclear compartmentalization of immunoglobulin loci during lymphocyte development.* Science, 2002. **296**(5565): p. 158-62.

271. Jevsek, M. and S.J. Burden, *Microarray screen for synaptic genes in the neuromuscular junction.* J Mol Neurosci, 2006. **30**(1-2): p. 29-30.

272. Rahman, A., D.S. Friedman, and L.S. Goldstein, *Two kinesin light chain genes in mice. Identification and characterization of the encoded proteins.* J Biol Chem, 1998. **273**(25): p. 15395-403.

273. Bruusgaard, J.C., et al., *Number and spatial distribution of nuclei in the muscle fibres of normal mice studied in vivo.* J Physiol, 2003. **551**(Pt 2): p. 467-78.

274. Huang, C.J., et al., *Germ-line transmission of a myocardium-specific GFP transgene reveals critical regulatory elements in the cardiac myosin light chain 2 promoter of zebrafish.* Dev Dyn, 2003. **228**(1): p. 30-40.

275. Shoji, W. and M. Sato-Maeda, *Application of heat shock promoter in transgenic zebrafish.* Dev Growth Differ, 2008. **50**(6): p. 401-6.

276. Hwang, W.Y., et al., *Efficient genome editing in zebrafish using a CRISPR-Cas system.* Nat Biotechnol, 2013. **31**(3): p. 227-9.

277. Chen, J., S.W. Kubalak, and K.R. Chien, *Ventricular muscle-restricted targeting of the RXRalpha gene reveals a non-cell-autonomous requirement in cardiac chamber morphogenesis.* Development, 1998. **125**(10): p. 1943-9.

278. O'Brien, T.X., K.J. Lee, and K.R. Chien, *Positional specification of ventricular myosin light chain 2 expression in the primitive murine heart tube.* Proc Natl Acad Sci U S A, 1993. **90**(11): p. 5157-61.

279. Chen, J., et al., *Selective requirement of myosin light chain 2v in embryonic heart function.* J Biol Chem, 1998. **273**(2): p. 1252-6.

280. Sheikh, F., R.C. Lyon, and J. Chen, *Functions of myosin light chain-2 (MYL2) in cardiac muscle and disease.* Gene, 2015. **569**(1): p. 14-20.

281. Kostrominova, T.Y., *Application of WGA lectin staining for visualization of the connective tissue in skeletal muscle, bone, and ligament/tendon studies.* Microsc Res Tech, 2011. **74**(1): p. 18-22.

282. Coelho-Filho, O.R., et al., *Quantification of cardiomyocyte hypertrophy by cardiac magnetic resonance: implications for early cardiac remodeling.* Circulation, 2013. **128**(11): p. 1225-33.

283. Reiser, P.J., et al., *Human cardiac myosin heavy chain isoforms in fetal and failing adult atria and ventricles.* Am J Physiol Heart Circ Physiol, 2001. **280**(4): p. H1814-20.

284. Krenz, M. and J. Robbins, *Impact of beta-myosin heavy chain expression on cardiac function during stress.* J Am Coll Cardiol, 2004. **44**(12): p. 2390-7.

285. Pandya, K., H.S. Kim, and O. Smithies, *Fibrosis, not cell size, delineates beta-myosin heavy chain reexpression during cardiac hypertrophy and normal aging in vivo.* Proc Natl Acad Sci U S A, 2006. **103**(45): p. 16864-9.

286. Sergeeva, I.A. and V.M. Christoffels, *Regulation of expression of atrial and brain natriuretic peptide, biomarkers for heart development and disease.* Biochim Biophys Acta, 2013. **1832**(12): p. 2403-13.

287. Federico, C., *Natriuretic Peptide system and cardiovascular disease.* Heart Views, 2010. **11**(1): p. 10-5.

288. Chapman, D., K.T. Weber, and M. Eghbali, *Regulation of fibrillar collagen types I and III and basement membrane type IV collagen gene expression in pressure overloaded rat myocardium.* Circ Res, 1990. **67**(4): p. 787-94.

289. Fan, D., et al., *Cardiac fibroblasts, fibrosis and extracellular matrix remodeling in heart disease.* Fibrogenesis Tissue Repair, 2012. **5**(1): p. 15.

290. Stewart, C.L., *Mouse models of the nuclear envelopathies and related diseases. Preface.* Curr Top Dev Biol, 2014. **109**: p. xi-xiii.

291. Zwerger, M., et al., *Myopathic lamin mutations impair nuclear stability in cells and tissue and disrupt nucleo-cytoskeletal coupling.* Hum Mol Genet, 2013. **22**(12): p. 2335-49.

292. Savolainen, S.M., J.F. Foley, and S.A. Elmore, *Histology atlas of the developing mouse heart with emphasis on E11.5 to E18.5.* Toxicol Pathol, 2009. **37**(4): p. 395-414.

293. de Boer, B.A., et al., *Growth of the developing mouse heart: an interactive qualitative and quantitative 3D atlas.* Dev Biol, 2012. **368**(2): p. 203-13.

294. Levy, D., et al., *Prognostic implications of echocardiographically determined left ventricular mass in the Framingham Heart Study.* N Engl J Med, 1990. **322**(22): p. 1561-6.

295. Drazner, M.H., *The progression of hypertensive heart disease.* Circulation, 2011. **123**(3): p. 327-34.

296. Kannel, W.B., *Left ventricular hypertrophy as a risk factor: the Framingham experience.* J Hypertens Suppl, 1991. **9**(2): p. S3-8; discussion S8-9.

297. Rawlins, J., A. Bhan, and S. Sharma, *Left ventricular hypertrophy in athletes.* Eur J Echocardiogr, 2009. **10**(3): p. 350-6.

298. Abebe, T.B., et al., *Patients with HFpEF and HFrEF have different clinical characteristics but similar prognosis: a retrospective cohort study.* BMC Cardiovasc Disord, 2016. **16**(1): p. 232.

299. Borlaug, B.A. and M.M. Redfield, *Diastolic and systolic heart failure are distinct phenotypes within the heart failure spectrum.* Circulation, 2011. **123**(18): p. 2006-13; discussion 2014.

300. Dandel, M., et al., *Strain and strain rate imaging by echocardiography - basic concepts and clinical applicability.* Curr Cardiol Rev, 2009. **5**(2): p. 133-48.

301. Fatkin, D., et al., *Missense mutations in the rod domain of the lamin A/C gene as causes of dilated cardiomyopathy and conduction-system disease.* N Engl J Med, 1999. **341**(23): p. 1715-24.

302. Khachigian, L.M., *Early growth response-1 in cardiovascular pathobiology.* Circ Res, 2006. **98**(2): p. 186-91.

303. Gius, D., et al., *Transcriptional activation and repression by Fos are independent functions: the C terminus represses immediate-early gene expression via CArG elements.* Mol Cell Biol, 1990. **10**(8): p. 4243-55.

304. Pollack, P.S., *Proto-oncogenes and the cardiovascular system.* Chest, 1995. **107**(3): p. 826-35.

305. Zhao, M., et al., *Microarray analysis of gene expression after transverse aortic constriction in mice.* Physiol Genomics, 2004. **19**(1): p. 93-105.

306. Lodish, H., *Molecular Cell Biology*. 2008: W. H. Freeman.

307. Malliaras, K. and J. Terrovitis, *Cardiomyocyte proliferation vs progenitor cells in myocardial regeneration: The debate continues.* Glob Cardiol Sci Pract, 2013. **2013**(3): p. 303-15.

308. Laflamme, M.A. and C.E. Murry, *Heart regeneration.* Nature, 2011. **473**(7347): p. 326-35.

309. Zebrowski, D.C., et al., *Developmental alterations in centrosome integrity contribute to the post-mitotic state of mammalian cardiomyocytes.* Elife, 2015. **4**.

310. Espigat-Georger, A., et al., *Nuclear alignment in myotubes requires centrosome proteins recruited by nesprin-1.* J Cell Sci, 2016. **129**(22): p. 4227-4237.

311. Burchfield, J.S., M. Xie, and J.A. Hill, *Pathological ventricular remodeling: mechanisms: part 1 of 2.* Circulation, 2013. **128**(4): p. 388-400.

312. Konstam, M.A., et al., *Left ventricular remodeling in heart failure: current concepts in clinical significance and assessment.* JACC Cardiovasc Imaging, 2011. **4**(1): p. 98-108.

313. Luo, M. and M.E. Anderson, *Mechanisms of altered Ca(2)(+) handling in heart failure.* Circ Res, 2013. **113**(6): p. 690-708.

314. Gorski, P.A., D.K. Ceholski, and R.J. Hajjar, *Altered myocardial calcium cycling and energetics in heart failure--a rational approach for disease treatment.* Cell Metab, 2015. **21**(2): p. 183-94.

315. Cremer, T. and C. Cremer, *Chromosome territories, nuclear architecture and gene regulation in mammalian cells.* Nat Rev Genet, 2001. **2**(4): p. 292-301.

316. Fraser, P. and W. Bickmore, *Nuclear organization of the genome and the potential for gene regulation.* Nature, 2007. **447**(7143): p. 413-7.

317. Bank, E.M. and Y. Gruenbaum, *The nuclear lamina and heterochromatin: a complex relationship.* Biochem Soc Trans, 2011. **39**(6): p. 1705-9.

Appendix

Appendix I. Clinical features of research subjects

	DCM patients (n=218)	**Healthy controls (n=210)**	**p-value**
Gender, % male	67.0 (158/218)	51.0 (117/210)	0.0007
Age at diagnosis/inclusion, year	48.3±15.2	49.2±9.2	0.4565
LVEDD, mm/m^2	66.3 ±9.1	45.1 ± 5.9	<0.0001
LVEF, %	33.2 ±13.3	59.3 ± 8.9	<0.0001

Clinical features refer to the time of presentation. LVEDD, left ventricular end diastolic diameter;
LVEF, left ventricular ejection fraction.

Appendix II. Rare (<1%) nesprin-1 variants identified in DCM patients

Exon	DNA variation	Amino acid exchange	Allele frequency in patients (%, n=436 alleles)	Allele frequency in a reference population (%, n=420 alleles)
136	c. 25417 G>A	**p. R8272Q**	0.46	0
139	c. 25743 A>T	**p. S8381C**	0.46	0
139	c. 25820 C>A	**p. N8406K**	0.69	0
133	c. 24299+12 G>A	intron	0.69	0
135	c.24308+3 A>G	intron	0.46	0
136	c.25463 C>T	p.H8287H	0.92	0
139	c.25730 G>C	p.L8376L	0.69	0
139	c.25748 C>T	p.S8382S	0.46	0

GenBank reference sequence: nesprin-1 giant (*SYNE-1*): AF495910.1; $1\alpha_2$: AY184203.1. Nucleotide and amino acid numbers are based on nesprin-1 giant. n, number of alleles analysed.

Appendix III: Clinical description of the patients harbouring the mutations identified in this study

Patient No.1 was a male carrying the R8272Q mutation. He had no family history of cardiovascular diseases and suffered shortness of breath after exertion since his forties. He was diagnosed with DCM and started receiving drug therapy including diuretics and digoxin since the age of 59. His symptom exaggerated at the age of 68, echocardiography showed the LV diameter was 90mm with very thin interventricular septum (IVS) and left ventricular posterior wall (LVPW). LVEF was 26%. N-terminal pro-B-type Natriuretic Peptide (pro-BNP) was 2912pg/ml, significantly greater than normal reference value (0-227pg/ml). ICD was subsequently implanted. The patient died of progressive left-sided heart failure one year later.

Patient No.2 was a male carrying the R8272Q mutation. He has no family history of cardiovascular diseases. He suffered shortness of breath after exertion since the age of 52, one year later he was diagnosed with DCM. Echocardiography showed the LV diameter was 72mm, LVEF was 37%.

Patient No.3 was a male carrying the S8381C mutation. He has no family history of cardiovascular diseases. He suffered shortness of breath after exertion at the age of 56, the LV diameter was 56 and LVEF was 34%. ECG showed sinus rhythm, the pro-BNP level was 1847pg/ml, greater than the normal reference value. He was treated with beta-blocker, diuretics and digoxin and then free of symptom. At the age of 62, echocardiography showed the LVEF was 24%. ECG showed atrial fibrillation (AF), pro-BNP increased to 4140pg/ml.

Patient No. 4 was a male carrying the N8406K mutation. He has no family history of cardiovascular diseases. His first symptom was repeated palpitation. At the age of 67, he began to feel fatigue after exertion. Ambulatory electrocardiogram revealed ventricular tachycardia. Echocardiography showed his LV diameter was 67mm and LVEF was 42%. He refused ICD implantation and thus was treated with beta-blocker and amiodarone.

Patient No. 5 was a male carrying the N8406K mutation. He has no family history of cardiovascular disease. He suffered shortness of breath after exertion at the age of 68, ECG showed AF. He was treated with beta-blocker, diuretics and digoxin. He died of cardiac arrest at the age of 68. The diagnosis of DCM was further confirmed by autopsy.

No clinical data was available for patient No. 6 (S8381C) and No.7 (N8406K).

Appendix IV: List of methods and results contributed by collaborators

Collaborator	Contributed Area	Methods/Results
Sichuan University	Nesprin-1/2 mutation screening in DCM patients	Result 3.1.1: Identification of three novel nesprin-1 mutants in DCM patients. Appendix I: Clinical features of research subjects; II: Rare (<1%) nesprin-1 variants identified in DCM patients; III: Clinical description of the patients harbouring the mutations identified in this study.
Sichuan University	The impact of nesprin-1α_2 WT and mutants during Zebrafish embryonic development	Method 2.6.8: Zebrafish. Result 4.2.10 Human nesprin-1α_2 WT causes heart developmental and conduction defects in zebrafish embryos while mutants induce a less severe heart phenotype.

Appendix V: Novel nesprin-1 mutations associated with dilated cardiomyopathy cause nuclear envelope disruption and defects in myogenesis

Human Molecular Genetics, 2017, Vol. 26, No. 12 2258–2276

doi: 10.1093/hmg/ddx116
Advance Access Publication Date: 7 April 2017
Original Article

ORIGINAL ARTICLE

Novel nesprin-1 mutations associated with dilated cardiomyopathy cause nuclear envelope disruption and defects in myogenesis

Can Zhou[1,2,†], Chen Li[1,2,†], Bin Zhou[3,4], Huaqin Sun[4,5], Victoria Koullourou[1,6], Ian Holt[7], Megan J. Puckelwartz[8], Derek T. Warren[1], Robert Hayward[1], Ziyuan Lin[4,5], Lin Zhang[3,4], Glenn E. Morris[7], Elizabeth M. McNally[8], Sue Shackleton[6], Li Rao[2], Catherine M. Shanahan[1,‡] and Qiuping Zhang[1,*,‡]

[1]King's College London British Heart Foundation Centre of Research Excellence, Cardiovascular Division, London SE5 9NU, UK, [2]Department of Cardiology, West China Hospital of Sichuan University, Chengdu 610041, China, [3]Laboratory of Molecular Translational Medicine, [4]Key Laboratory of Obstetric & Gynecologic and Pediatric Diseases and Birth Defects of Ministry of Education, [5]SCU-CUHK Joint Laboratory for Reproductive Medicine, West China Second University Hospital, Sichuan University, Chengdu, 610041, China, [6]Department of Molecular and Cell Biology, University of Leicester, Leicester LE1 9HN, UK, [7]Wolfson Centre for Inherited Neuromuscular Disease, RJAH Orthopaedic Hospital, Oswestry SY10 7AG, UK and Institute for Science and Technology in Medicine, Keele University, ST5 5BG, UK and [8]Center for Genetic Medicine, Northwestern University Feinberg School of Medicine, Chicago, IL 60611, USA

*To whom correspondence should be addressed at: King's College London, Cardiovascular Division, James Black Centre, 125 Coldharbour Lane, London SE5 9NU, UK. Tel: +44 20 78485222; Fax: +44 20 78485193; Email: qp.zhang@kcl.ac.uk

Abstract

Nesprins-1 and -2 are highly expressed in skeletal and cardiac muscle and together with SUN (Sad1p/UNC84)-domain containing proteins and lamin A/C form the LInker of Nucleoskeleton-and-Cytoskeleton (LINC) bridging complex at the nuclear envelope (NE). Mutations in nesprin-1/2 have previously been found in patients with autosomal dominant Emery–Dreifuss muscular dystrophy (EDMD) as well as dilated cardiomyopathy (DCM). In this study, three novel rare variants (R8272Q, S8381C and N8406K) in the C-terminus of the *SYNE1* gene (nesprin-1) were identified in seven DCM patients by mutation screening. Expression of these mutants caused nuclear morphology defects and reduced lamin A/C and SUN2 staining at the NE. GST pull-down indicated that nesprin-1/lamin/SUN interactions were disrupted. Nesprin-1 mutations were also associated with augmented activation of the ERK pathway *in vitro* and in hearts *in vivo*. During C2C12 muscle cell differentiation, nesprin-1 levels are increased concomitantly with kinesin light chain (KLC-1/2) and immunoprecipitation and GST pull-down showed that these proteins interacted via a recently identified LEWD domain in the C-terminus of nesprin-1. Expression of nesprin-1 mutants in C2C12 cells caused defects in myoblast differentiation and fusion associated with dysregulation of

[†]Authors contributed equally to this work.
[‡]Joint senior authors.

Received: February 10, 2017. **Revised:** March 22, 2017. **Accepted:** March 22, 2017

© The Author 2017. Published by Oxford University Press.
This is an Open Access article distributed under the terms of the Creative Commons Attribution License (http://creativecommons.org/licenses/by/4.0/), which permits unrestricted reuse, distribution, and reproduction in any medium, provided the original work is properly cited.

Downloaded from https://academic.oup.com/hmg/article-abstract/26/12/2258/3111721
by King's College London user
on 07 December 2017

myogenic transcription factors and disruption of the nesprin-1 and KLC-1/2 interaction at the outer nuclear membrane. Expression of nesprin-1α_2 WT and mutants in zebrafish embryos caused heart developmental defects that varied in severity. These findings support a role for nesprin-1 in myogenesis and muscle disease, and uncover a novel mechanism whereby disruption of the LINC complex may contribute to the pathogenesis of DCM.

Introduction

Dilated cardiomyopathy (DCM) is characterised by dilatation and impaired contraction of the left ventricle or both ventricles, and is an important cause of heart failure and sudden cardiac death, particularly in the young. The genetic causes of DCM are extremely complicated and over 50 genes have been implicated, many of them encoding components of the cytoskeleton and nuclear envelope (NE) (1,2).

Mutations in the *LMNA* gene, encoding the nuclear intermediate filament proteins lamin A/C, account for 6% of familial DCM patients in addition to causing a wide spectrum of diseases, named laminopathies. The laminopathies include Emery-Dreifuss muscular dystrophy (EDMD), which manifests with skeletal muscle wasting, heart conduction defects (CD) and DCM (3,4). Mutations in the *EMD* gene, encoding the inner nuclear membrane (INM) protein emerin, a binding partner of lamin A/C, also cause EDMD with CD (5). How mutations in both emerin and lamin A/C, which are ubiquitously expressed proteins, can lead to muscle-specific diseases has been a subject of debate for some time. However, evidence has shown that lamin A/C and emerin are both associated with the LInker of Nucleoskeleton and Cytoskeleton (LINC) bridge complex, which links the nucleus to the actin cytoskeleton. The major components of the LINC complex are: nesprins-1 and -2 (NE-spectrin repeat proteins) and SUN (Sad1p/UNC84)-domain containing proteins (SUN1/2) (6–8). Nesprin-1 and -2 can bind actin via a paired N-terminal Calponin Homology (CH) actin binding domains and the nuclear membrane via a C-terminal Klarsicht/ANC-1/Syne Homology (KASH) domain (9,10). The KASH domain also binds to SUN1/2 which span the INM and bind to lamin A/C directly via their N-terminal nucleoplasmic domain, thus providing a physical connection between the nucleus and the cytoskeleton (6,11,12). Mutations in nesprin-1 and -2 have been implicated in EDMD 4 (AD-EDMD 4, OMIM 612998) and 5 (AD-EDMD5, OMIM 612999), and SUN1 and SUN2 have also been implicated in EDMD (13–16). Thus, it has been suggested that disruption of the LINC complex by *LMNA* and *EMD* mutations, as well as *SYNE* (nesprin) and *SUN* mutations, may trigger effects on either chromatin structure causing deregulation of gene expression, or disruption of structural organisation of the cell, which is particularly important in muscle as it is subject to mechanical strain.

Another mechanism that may explain tissue specific disease is muscle-specific expression of LINC complex components. Alternative transcription and splicing of *SYNE1* and *SYNE2*, the genes encoding nesprin-1 and -2, generate multiple isoforms that vary greatly in size (17). The largest giant nesprin-1 and -2 isoforms localise at the outer nuclear membrane (ONM) and connect the nucleus to the actin cytoskeleton. However, smaller nesprin-1 and -2 isoforms, with a truncated N-terminus but sharing spectrin repeats (SRs) in common with the C-terminal regions of the giant proteins, also localise at the INM where they bind to emerin, lamin A/C and SUN1/2, forming a complex at the INM (18). These smaller isoforms, in particular, nesprin-1α_2 and -2α_1, are highly and specifically expressed in cardiac and skeletal muscle (7,19). Thus, mutations in *SYNE1/2* that disrupt these specific nesprin-1 and -2 isoforms, or mutations in other components of the LINC complex that disrupt their binding with nesprin-1 and -2, are likely to play a key role in muscle-specific laminopathies.

In support of this notion, mutations in the C-terminal regions of the nesprin-1 (*SYNE1*) and -2 (*SYNE2*) genes have been identified in patients with muscle specific disorders. This is in contrast to mutations located towards the N-terminus, which are associated with ataxia (13,14,20). For example, several missense mutations in the C-terminus were identified in several small family pedigrees, as well as in sporadic EDMD patients with DCM (13). Studies in fibroblasts from these patients showed abnormal localisation and binding of the LINC complex proteins lamin, emerin and SUN2, as well as nuclear morphology defects and loss of NE integrity. A missense mutation in the same C-terminal region of the *SYNE1* gene was identified in a DCM patient, which resulted in increased expression of nesprin-1 and lamin A/C, also indicating a perturbation of the LINC complex (14). Furthermore, nesprin-1 KASH domain knockout (KO) mice developed an EDMD-like phenotype and DCM (21), displaying muscle degeneration with elongated nuclei and reduced heterochromatin. Ablation of the C-terminal regions of both nesprin-1 and -2 in cardiomyocytes resulted in early onset cardiomyopathy (22). These mutant cardiomyocytes exhibited altered nuclear positioning, shape, and chromatin positioning, leading to impairment of gene expression in response to biomechanical stimuli due to loss of either nesprin -1 or -2 or both (22). Finally, in studies *in vitro*, overexpressing dominant-negative versions of nesprin KASH or SUN proteins in mouse C2C12 myoblasts perturbed the mechanical control of cell differentiation (23). In these studies, nuclear displacement and defects in nuclear rotation were also noted, implicating the LINC complex in myonuclear positioning.

Indeed, recent data have shown that the C-terminal region of nesprin mediates myonuclear positioning by attaching the microtubule (MT) network to the NE during embryonic muscle development and cell migration (24). These interactions occur via the MT motor proteins, dynein and kinesin, the latter being a heterotetramer of two kinesin heavy chain (KHC) subunits - Kif5A, Kif5B, or Kif5C- and two kinesin light chain (KLC)-1/2 subunits. Nesprin-2 was shown to interact with KLC-1/2 at the ONM via a newly identified four-residue tryptophan-acidic (W-acidic) 'LEWD' binding motif within an adaptive domain (AD) at its C-terminus, which is present in all muscle-specific isoforms (25–27). Disruption of the LINC complex with a dominant-negative nesprin-2 KASH impaired kinesin-1 association with the NE and induced nuclear aggregation in myotubes (24). As both nesprin-1 and -2 are highly conserved in this C-terminal region, it is likely that nesprin-1 may also mediate the nesprin/KLC interaction via the 'LEWD' binding motif but so far this has not been tested.

In this study, we screened the *SYNE1* and *SYNE2* genes in 218 DCM patients. We identified three novel nesprin-1 variants (R8272Q, S8381C, and N8406K) in seven patients and investigated their roles in NE organisation and myogenesis.

Downloaded from https://academic.oup.com/hmg/article-abstract/26/12/2258/3111721
by King's College London user
on 07 December 2017

Results

Identification of three novel nesprin-1 mutants in DCM patients

Mutation screening of both the *SYNE1* and *SYNE2* genes was performed in 218 sporadic cases of DCM and 210 ethnically matched controls (Supplementary Material, Table S1). 23 exons for nesprin-1 corresponding to nesprin-1α_1 and 1α_2 and 16 exons for nesprin-2 corresponding to isoforms nesprin-2α, 2β and 2ε were screened. This screening strategy was based on high and specific expression of these isoforms in cardiac and skeletal muscle as well as mapping of the lamin A/C, emerin, SUN and KLC binding sites to domains within these isoforms (19,28–30).

Twelve single nucleotide polymorphisms (SNPs)/variants in *SYNE1* were identified, which included intronic sequence variations ($n = 2$), synonymous ($n = 5$) and non-synonymous, amino acid exchanges ($n = 5$). Eight of the variants were not present in 420 control alleles of an ethnically matched reference population (Supplementary Material, Table S2). No nesprin-2 SNPs/variants were identified in the region screened. Interestingly, three of the identified nesprin-1 mutations were unique DNA variants, which resulted in R8272Q, S8381C, N8406K amino acid exchanges in the C-terminus of the nesprin-1 giant as well as within the muscle specific isoform nesprin-1α_2, and identified in seven unrelated DCM patients (Fig. 1A, Supplementary Material). The amino acids changed by these missense mutations were in regions that were evolutionarily well conserved and within the mapped emerin and lamin A/C binding domains (25) and also the proposed KLC-1/2 binding domain in nesprin-1 (24,27) (Fig. 1B). The rarity of these variants and their conservation and positioning suggest they may be causative for DCM in the patients examined. ExAC database search revealed that population frequencies for the R8272Q allele were 0.0002145 (26/121204). Further *in silico* functional analyses showed that all three variants are predicted to cause significant functional impairment for nesprin-1 (Polyphen-2: possibly damaging, SIFT: damaging and Mutation Taster: disease causing). Therefore, all three rare variants were included in further cell biological investigations.

Over-expression of nesprin-1 mutants disrupted nuclear morphology and reduced lamin A/C and SUN2 staining at the NE

We generated GFP-tagged wild-type (WT) and mutant R8272Q, S8381C, N8406K constructs in the context of the muscle specific isoform nesprin-1α_2 (Fig. 2A). When transfected into human osteosarcoma (U2OS) cells, abnormalities of nuclear morphology, measured by nuclei circularity, were induced by constructs harbouring the three novel nesprin-1 mutants when compared with WT (Fig. 2B and E). Immunofluorescence (IF) staining showed exogenous expression of the mutants, especially S8381C, caused weaker staining of lamin A/C at the NE (Fig. 2C and E and Supplementary Material, Fig. S1A), while all three mutants caused weaker staining of SUN2 at the NE, when compared with WT nesprin-1α_2 (Fig. 2D and E and Supplementary Material, Fig. S1B). In addition, emerin was mislocalised by both the WT and mutants when compared with GFP alone (Fig. 2E). When the same constructs were transfected into neonatal rat cardiomyocytes (NRCs), IF staining showed that both lamin A/C and SUN2 staining was weaker at the NE with all three mutants compared with WT nesprin-1α_2 (Fig. 2F and G and Supplementary Material, Fig S1C and D), indicating nesprin-1 mutants differentially affect the localisation of NE binding partners.

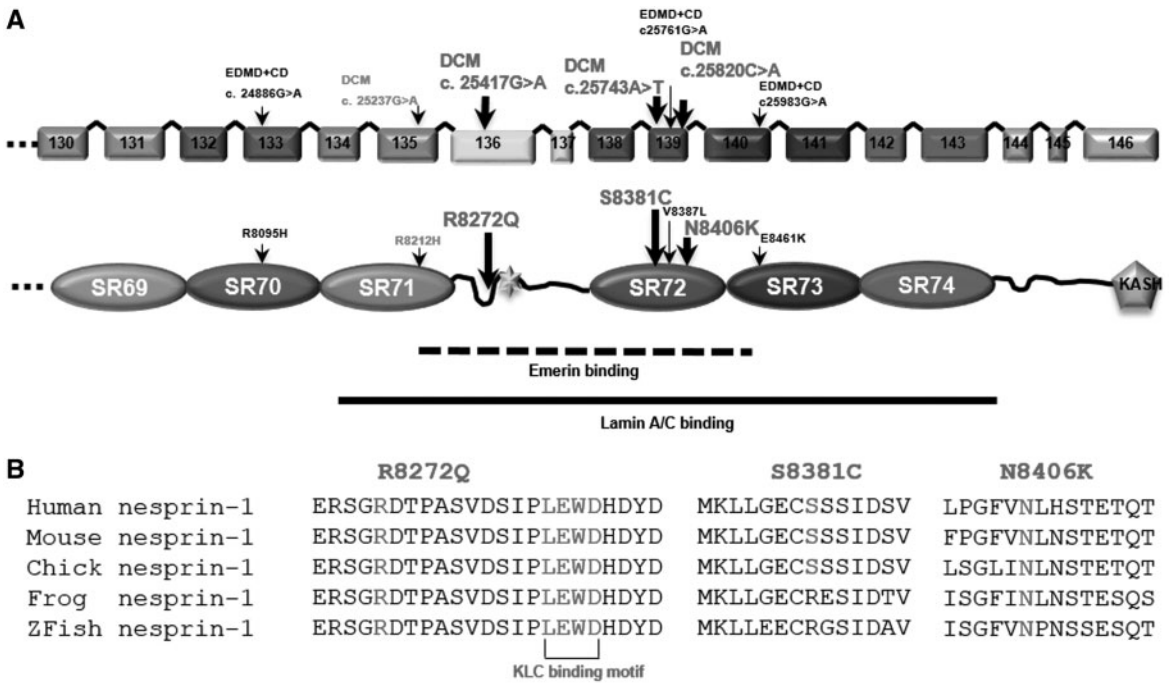


Figure 1. Identification of nesprin-1 variants in DCM patients. Mutation screening in *SYNE1* and 2 genes was performed in 218 DCM patients and 210 healthy controls, and identified seven patients harbouring three novel nesprin-1 mutations (R8272Q, S8381C, N8406K, shown in bold) in the C-terminus of nesprin-1 giant (**A**), equivalent to nesprin-1α, within an evolutionally conserved region containing the lamin and emerin binding domains (**A**, **B**). Previously identified nesprin-1 mutants in DCM (R8212H) and EDMD-CD patients (R8095H, V8387L and E8461K) were also shown (13,14). The KLC binding motif (LEWD) is shown in (B) (24,27).

Downloaded from https://academic.oup.com/hmg/article-abstract/26/12/2258/3111721
by King's College London user
on 07 December 2017

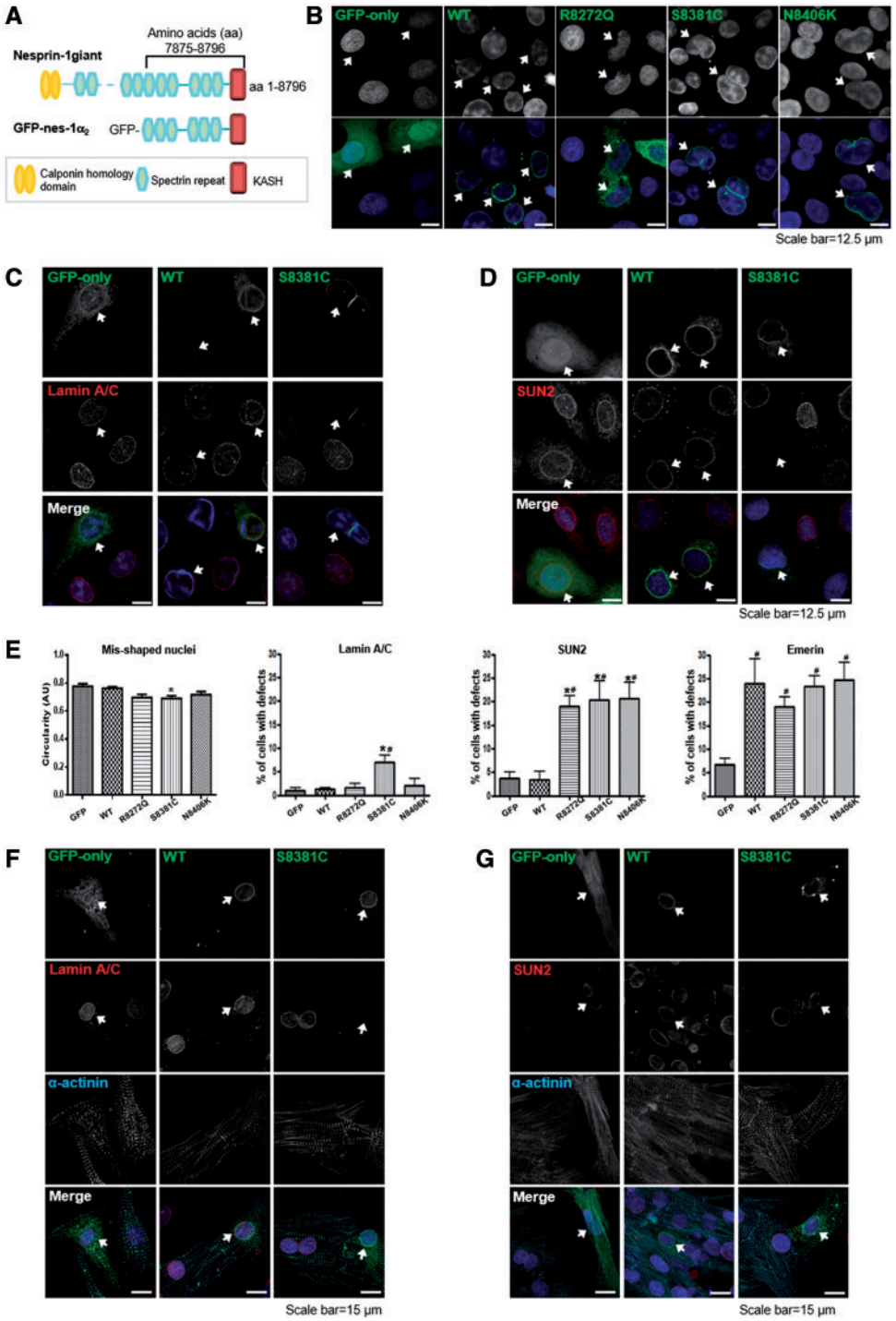


Figure 2. Overexpression of nesprin-1 mutants caused abnormal nuclear morphology and reduced NE staining of lamin A/C and SUN2. GFP-tagged nesprin-1α_2 WT and mutants are shown schematically (**A**). The full length of this isoform is 977 amino acids, equivalent to amino acids 7875–8796 in nesprin-1 Giant. U2OS cells were transfected with either GFP-nesprin-1α_2 WT or mutants. IF staining showed overexpression of mutants, especially S8381C, led to abnormalities in nuclear morphology (**B**), reduced lamin A/C and SUN2 staining at the NE (**C**, **D**, arrowed). The mis-shapen nuclei were measured by circularity, and mislocalisation of lamin A/C, SUN2 and emerin in the transfected cells was quantified by comparing the NE staining in non-transfected cells on the same slide. Graphical representation of the frequency of misshaped nuclei and defects in lamin A/C, SUN2, and emerin at the NE caused by all three mutants (**E**). At least 100 transfected nuclei were counted in more than three individual experiments and the results are presented as mean ± SEM and also analysed by Student's *t*-tests and one-way ANOVA. (*$P < 0.05$ compared with WT; #: $P < 0.05$ compared with GFP only). In addition, IF showed both lamin A/C and SUN2 staining at the NE was reduced in the transfected NRCs using GFP-tagged nesprin1α_2 mutant S8381C compared with GFP-tagged WT nesprin-1α_2 (**F**, **G**, arrowed).

Downloaded from https://academic.oup.com/hmg/article-abstract/26/12/2258/3111721
by King's College London user
on 07 December 2017

Nesprin-1 mutants disrupt the interactions between nesprin-1, lamin A/C and SUN2 within the NE complex

To investigate whether the mutants affected the binding between nesprin-1 and its NE binding partners, GST-tagged WT and mutant nesprin-1α_2 constructs lacking the KASH domain (equivalent to nesprin-1 giant amino acids 7875–8662) were generated (Fig. 3A left panel). Protein lysates from un-transfected U2OS cells and transfected cells with Myc-SUN2 (full length) were subjected to GST pull-down using either WT or mutant GST-nesprin-1α_2. All three mutants had significantly reduced binding to lamin A/C and SUN2, but not emerin (Fig. 3A right panel, and B) when compared with WT nesprin-1α_2. A reverse GST pull-down was also performed. Protein lysates from U2OS cells transfected with either GFP-nesprin-1α_2 WT or each of three mutants were subjected to pull-down using either GST-lamin A (amino acids 356–665, containing nesprin-1/2 binding domain) or GST-emerin (amino acids 1–176, lacking the TM domain). The results confirmed all three mutants had significantly reduced binding to lamin A (Fig. 3C), but not

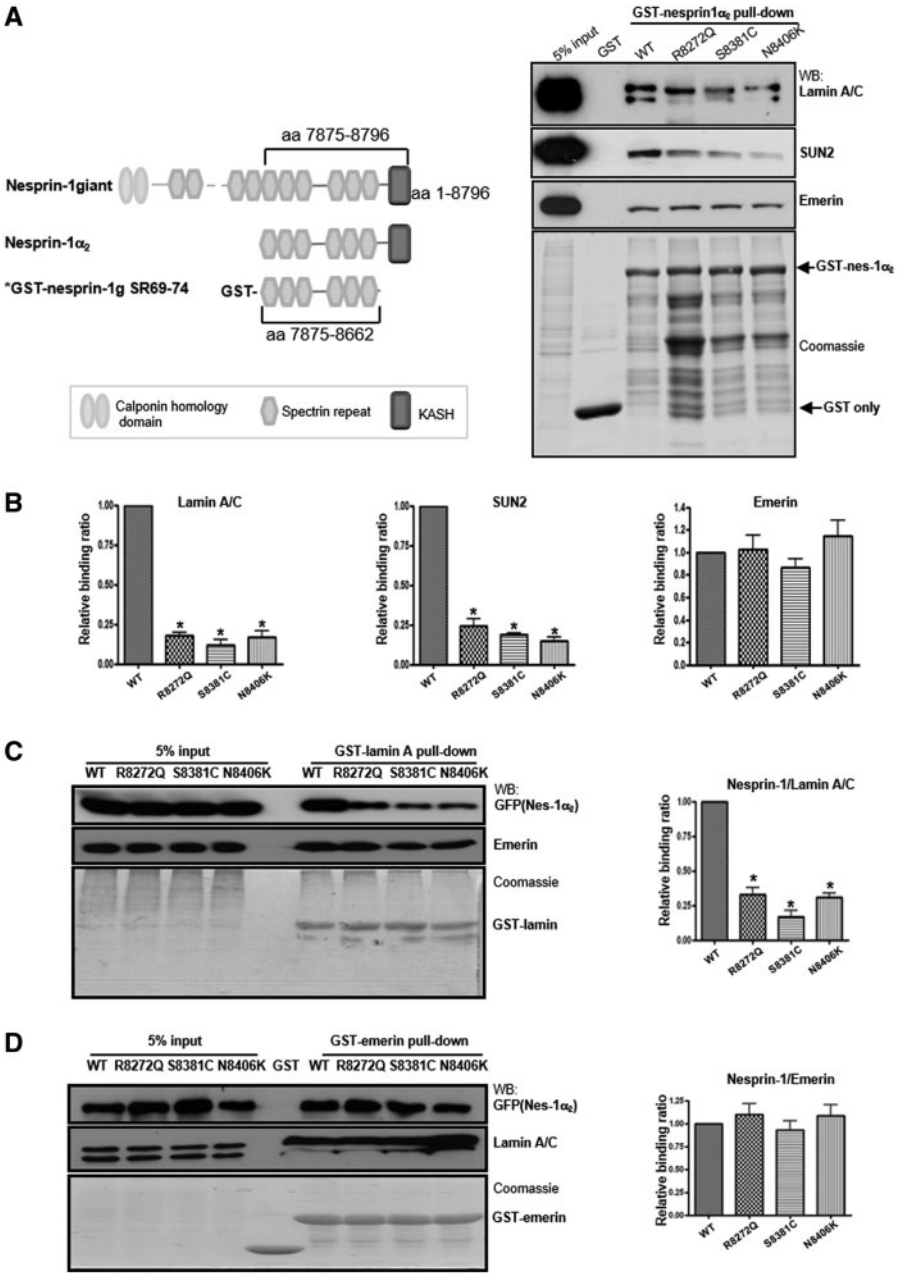


Figure 3. Nesprin-1 mutants affect the interaction between nesprin-1α_2 and lamin A/C or SUN2. GST-tagged WT nesprin-1α_2 SR1-6 (equivalent to nesprin-1 giant SR 69–74) and mutants are generated and shown schematically (3A left panel, labelled with *), which constructs consisted of 837 amino acids, lacking KASH domain, equivalent to amino acids 7875–8662 of nespin-1 giant. GST pull-down using either GST-WT or mutant nesprin-1 beads showed all three mutants affected binding between nesprin-1 and lamin A/C or SUN2, but not emerin (**A**, **B**), which was confirmed by reverse GST pull down by transfecting either GFP-nesprin-1α_2WT or each mutant and using either GST-lamin A (amino acids 356–665) (**C**) or GST-emerin (amino acids 1–176) beads (**D**). The binding for each mutant was quantified by densitometry with respect to the input material and expressed as a ratio of the value obtained for WT protein. Three independent experiments were performed shown as mean ± SEM, *$P < 0.05$ using one-way ANOVA analysis. Coomassie blue staining gel also showed equal amount of GST-nesprin 1α_2, lamin or emerin beads used.

Downloaded from https://academic.oup.com/hmg/article-abstract/26/12/2258/3111721
by King's College London user
on 07 December 2017

emerin (Fig. 3D). Taken together, these data indicated that these nesprin-1 mutations in the $1\alpha_2$ region cause disruption of the lamin A/C, SUN2 and nesprin-1 complex at the INM.

Nesprin-1 mutants augment activation of extracellular signal-regulated kinase (ERK) pathway

Previous studies have shown that cells harbouring lamin and emerin mutations have altered activation of ERK1/2 (31,32). To investigate whether nesprin-1 defects lead to aberrant ERK1/2 activation, protein lysates from human dermal fibroblasts (HDFs) derived from EDMD and DCM patients carrying either nesprin-1, lamin A/C or emerin mutations (13), and heart tissue from WT and nesprin-1 KASH KO mice with EDMD-like phenotype and DCM (21) were examined. Western blot (WB) showed significant up-regulation of ERK1/2 activity in patient fibroblasts (Fig. 4A) and nesprin-1 KASH KO mouse hearts (Fig. 4B). To determine whether the novel nesprin-1 mutants could also induce activation of ERK1/2 signalling, GFP-nesprin-$1\alpha_2$ WT and mutants, as well as a dominant-negative nesprin-1 KASH (1KASH), which has previously been shown to displace endogenous nesprin-1 and cause NE defects (6,33), were transiently transfected into C2C12 and H9C2 myoblasts. Immunoblotting with antibodies against phosphorylated ERK1/2 (pERK) and total ERK1/2 (tERK) as well as phosphorylated ELK1 (pELK1), a downstream target of ERK1/2, demonstrated that overexpression of the GFP tagged-nesprin-1 mutants and 1KASH increased the amount of pERK1/2 and pELK1 compared with GFP alone or WT nesprin-$1\alpha_2$, in both C2C12 cells (Fig. 4C) and H9C2 cells (Supplementary Material, Fig. S2).

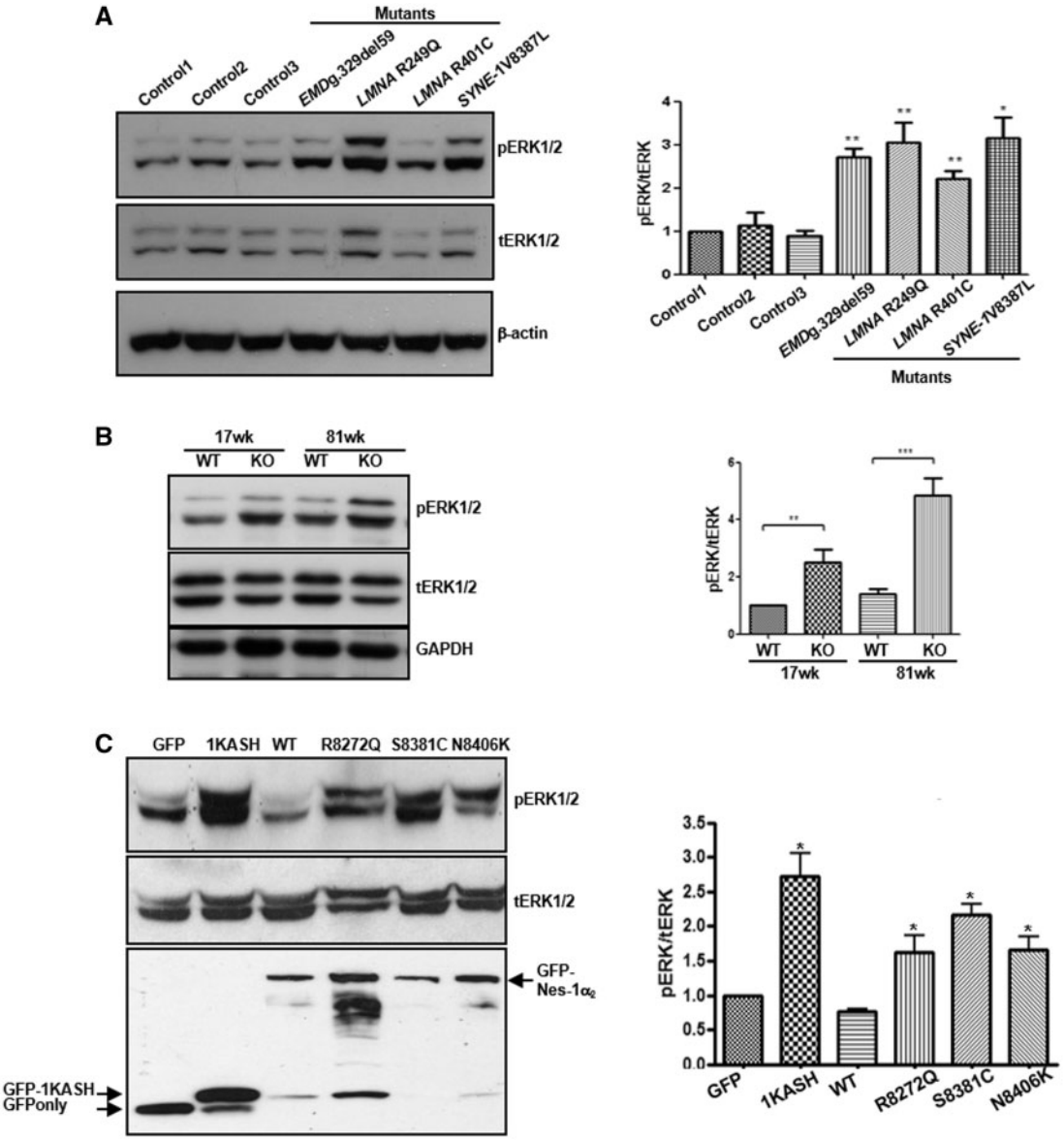


Figure 4. Nesprin-1 mutants cause aberrant activation of MAPKs. WB showed that aberrant activation of pERK was observed in human dermal fibroblasts from EDMD-DCM patients carrying nesprin-1 mutation (V8387L), lamin A/C (R249Q and R401C) and emerin (g.329del59) mutations (**A**), as well as nesprin-1 KASH KO mice heart collected at 17 and 81 weeks, respectively (**B**). WB also showed overexpression of all three nesprin-1 mutants and dominant negative-1KASH led to augmented pERK activity compared with WT nesprin-1 and GFP alone (**C**). GFP empty vector was used for negative control and a dominant negative-1KASH construct as a positive control. Three independent experiments were performed shown as mean ± SEM, $^*P < 0.05$ using one-way ANOVA analysis.

Downloaded from https://academic.oup.com/hmg/article-abstract/26/12/2258/3111721
by King's College London user
on 07 December 2017

Nesprin-1 mutants lead to dysregulation of myogenic transcription factors

To further investigate if these three novel mutants cause muscle cell dysfunction, we next used the C2C12 mouse myoblast differentiation model. Previous studies showed that mutations in *LMNA* and overexpression of 1KASH or SUN proteins in C2C12 cells disrupt myoblast differentiation (23,34,35). Myogenesis is driven by myogenic transcription factors (MTFs) such as MyoD and myogenin (36,37). To determine the expression levels of endogenous nesprin-1α, MyoD and myogenin as well as the skeletal muscle specific protein myosin heavy chain (MHC) during the differentiation process, protein lysates were collected at days 0, 2, 4 and 6 following induction (serum withdrawal). WB and/or qPCR showed that endogenous expression levels of nesprin-1α (including both $1\alpha_1$ and $1\alpha_2$), MyoD, myogenin and MHC were increased along with myotube formation (Fig. 5A–C, Supplementary Material, Fig. S3). Nesprin-1α levels peaked at day 6, whereas MyoD and myogenin levels peaked at day 2. MHC was detected from day 2 and increased until day 6. Therefore, day 2 for MyoD and myogenin, and day 6 for MHC were chosen as the optimised investigation time points for early and late differentiation in further experiments.

To investigate whether the novel nesprin-1 mutants could disrupt muscle cell differentiation, we used retroviral transduction to generate C2C12 cells stably expressing V5-tagged nesprin-$1\alpha_2$ WT and mutant constructs as well as dominant negative-1KASH, which were cloned into a MIG (IRES-GFP) retroviral vector. GFP protein was expressed independently as a reporter for retroviral infection. Fluorescence-activated cell sorting (FACS) was performed to purify the infected GFP positive populations and these were used in subsequent muscle cell differentiation experiments (Supplementary Material, Fig. S4A, B). IF staining showed that exogenously expressed V5-tagged WT nesprin-$1\alpha_2$, mutants and 1KASH were observed at the NE in myoblasts (Fig. 6A, Supplementary Material, Fig. S5A). Efficient differentiation of C2C12 cells transduced with eGFP alone (MIG only) or nesprin-$1\alpha_2$ WT was observed, with many multinucleated myotubes formed within 5–6 days. However, fewer myotubes were formed in the cells transduced with either nesprin-1α mutants or 1KASH (Fig. 6B, Supplementary Material, Fig. S5B). Quantification of the fusion index i.e. the percentage of nuclei incorporated into MHC positive multinucleated cells vs. the total number of nuclei, showed a significant reduction in cells transduced with the mutants, in particular, R8272Q and N8406K as well as 1KASH when compared to WT (Fig. 6C). Further analysis of the MHC positive populations revealed that myotubes expressing nesprin-1 mutants contained fewer nuclei compared to the controls (Fig. 6D), indicating a defect in myoblast fusion. Both qPCR and WB showed that the levels of myogenin and MHC were dramatically reduced in cells transduced with the mutants, particularly R8272Q and 1KASH when compared with nesprin-$1\alpha_2$ WT at day 2 and 6 respectively (Fig. 6E–G). qPCR also demonstrated that MyoD was significantly reduced in the cells transduced with 1KASH at Day 2 (Fig. 6E).

Nesprin-1 mutants cause disruption of nesprin-1 and KLC interaction

Recent data showed that nesprin-2 interacts with KLC-1/2 via a conserved 'LEWD' motif at the C-terminus of nesprin-2 (27). This motif is also present in nesprin-1 (Fig. 1B) (25–27), suggesting nesprin-1 may also bind to KLC-1/2 and be involved in connecting the nucleus to the microtubule network and therefore play a role in myonuclear positioning. By treatment of C2C12

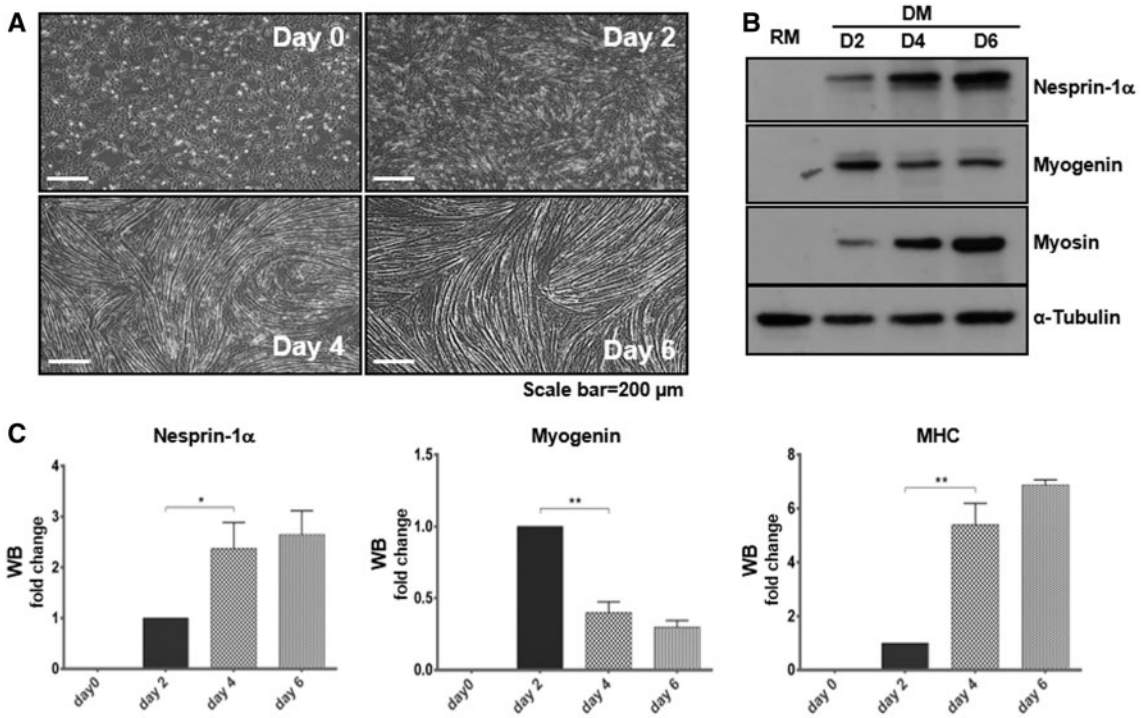


Figure 5. Expression level of nesprin-1α increase during C2C12 myoblast differentiation. C2C12 myoblasts in regular medium (RM) were stimulated with a low serum differentiation medium (DM), leading to myotube formation during the process (**A**). WB showed endogenous expression levels of nesprin-1, myogenin and myosin/MHC increased during myotube formation (**B**, **C**). Nesprin-1α protein levels (detected by MANNES1E) were highest at day 6, whereas myogenin was highest at day 2, and MHC was detected from day 2 and increased until day 6.

Downloaded from https://academic.oup.com/hmg/article-abstract/26/12/2258/3111721
by King's College London user
on 07 December 2017

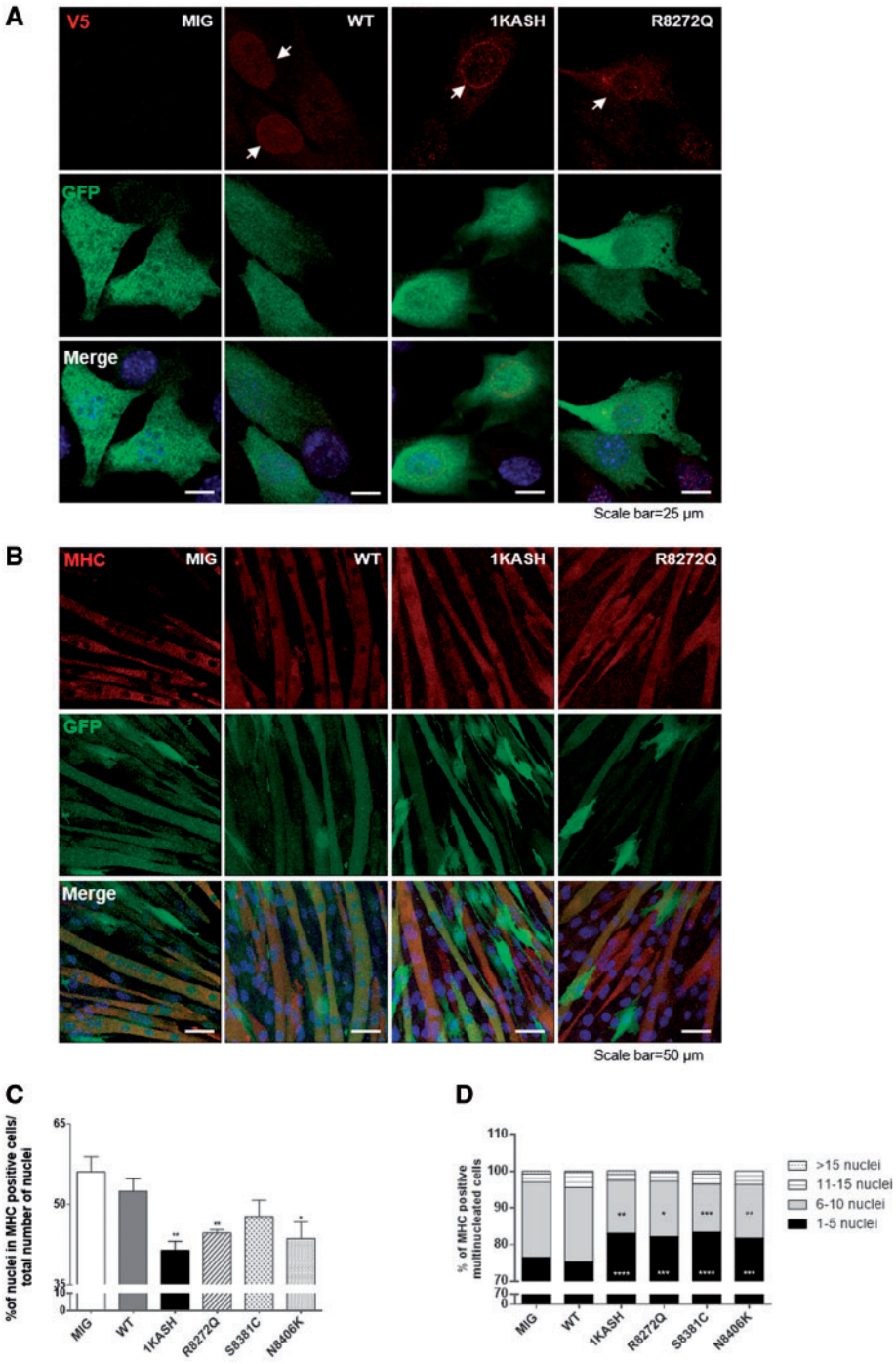


Figure 6. Nesprin-1 mutants cause defects in myoblast differentiation. IF showed that exogenously expressed V5-tagged WT-1α_2 or mutants and dominant genative-1KASH were localized at the NE. GFP was expressed as a reporter for retroviral infection (**A**). Upon differentiation, fewer multinucleated myotubes were observed in cells transduced with mutant R8272Q and dominant negative-1KASH compared with C2C12 cells transduced with eGFP alone (MIG only) or nesprin-1α_2 WT (**B**). The fusion index was reduced in cells transduced with the mutant R8272Q and dominant negative-1KASH compared with 1α_2 WT (**C**), more than 600 nuclei for each clone were counted by microscopy (63× objective) at day 6, three independent experiments were performed for each clone. Further analysis of the MHC positive multinucleated populations revealed that myotubes expressing nesprin-1 mutants contained fewer nuclei compared to the controls (**D**). qPCR and WB showed that nesprin-1 mutant R8272Q and dominant negative-1KASH caused significant reduction of myogenin (**E, F**) and MHC (E, G) levels at DM day 2 and day 6 respectively, qPCR also showed that dominant negative-1KASH caused significant reduction of MyoD (E) levels at DM day 2. All were normalized to GFP, three independent experiments were performed shown as mean ± SEM, *$P < 0.05$ using Student's *t*-tests or two-way ANOVA analysis.

cells expressing the plasmid containing V5-tagged nesprin-1α_2 WT with digitonin or NP-40, we showed that nesprin-1α_2 was also localised at the ONM in addition to its previously identified INM localisation where it co-localises and binds to lamin A/C (Supplementary Material, Fig. S6). Therefore, we set out to investigate whether nesprin-1 could also bind to KLC-1/2. GFP-1α_2 WT or nesprin-1α_2-LEAA (mutated WD/AA within the LEWD motif) were co-expressed with Flag-tagged KLC-2 WT

Downloaded from https://academic.oup.com/hmg/article-abstract/26/12/2258/3111721
by King's College London user
on 07 December 2017

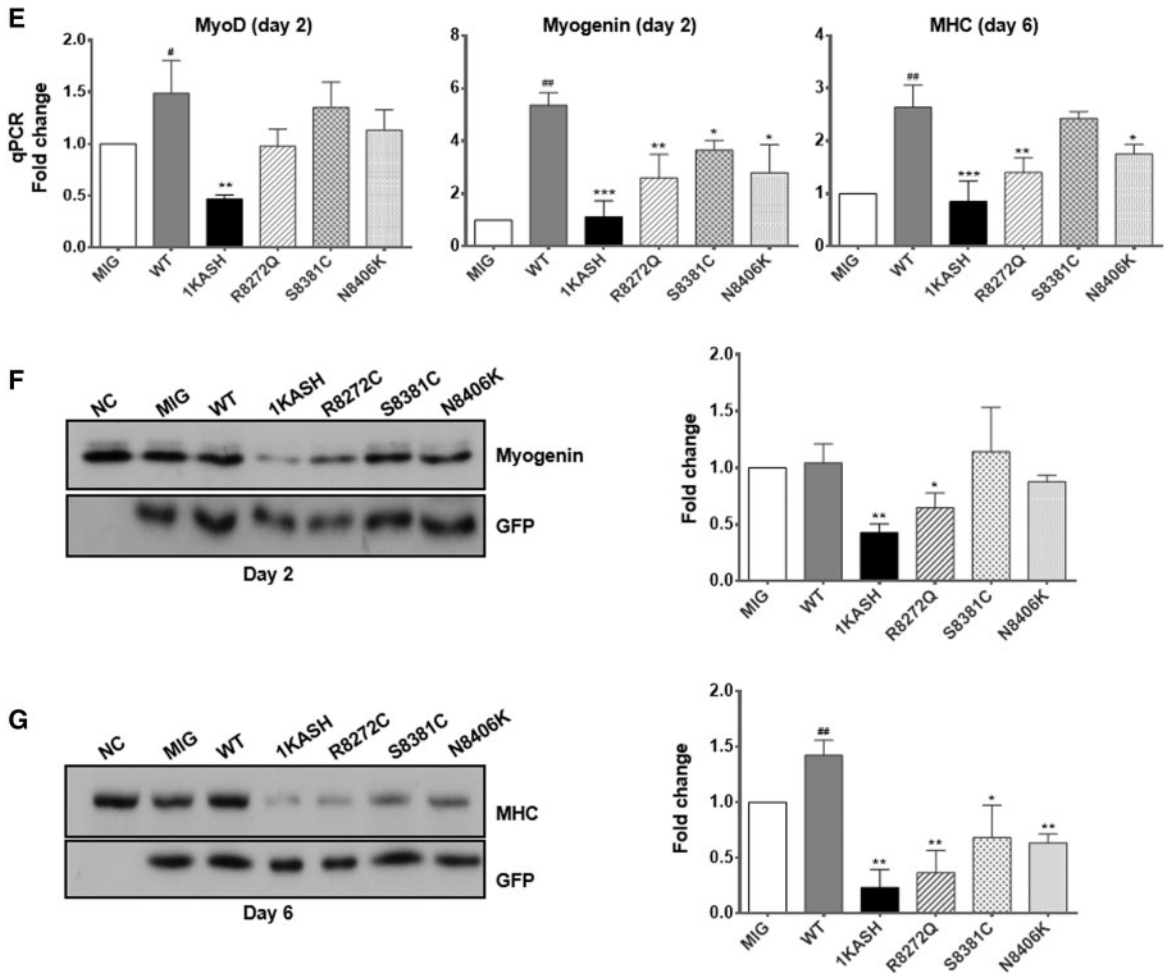


Figure 6. Continued.

(a dominant light chain isoform in muscle) or the KLC-2 N287L mutant, previously shown to disrupt nesprin-2/KLC binding (27) in U2OS cells. Immunoprecipitation (IP) and WB showed that nesprin-1α_2 could efficiently bind to KLC-2, and this binding was disrupted by either mutation (LEAA) in the conserved nesprin-1 LEWD motif or the KLC-2 N287L mutant (27) (Fig. 7A). We then tested the nesprin-1 mutants using this system and found that the R8272Q mutant had significantly reduced binding to KLC-2 compared with nesprin-1α_2 WT, while the S8381C mutant appeared to enhance KLC-2 binding (Fig. 7A).

Next we tested whether these mutants affect nesprin-1/KLC-1/2 binding during muscle cell differentiation. Firstly, WB showed that, similar to nesprin-1α, the endogenous expression level of KLC-1/2 increased during myoblast differentiation (Figs. 5B and 7B). Using GST-nesprin-1α_2 WT (lacking KASH domain), nesprin-1α_2-LEAA and the three mutants, pull-down further confirmed that nesprin-1α_2 efficiently binds to KLC-1/2, and this binding was disrupted by the mutated LEWD motif-LEAA. In addition, the R8272Q mutant had significantly reduced binding to KLC-1/2 compared with WT in C2C12 cells. This reduced interaction was especially evident in myotubes where expression of these two proteins is highest (Fig. 7C and D). Finally, we tested whether depletion of KLC-1/2 using multiple siRNA oligos would affect fusion of myoblasts and differentiation in a similar manner to that observed in the R8272Q mutant. WB showed the expression levels of both KLC-1 and -2 were reduced in both myoblasts and myotubes after KLC-1/2 depletion (Fig. 8A and B, Supplementary Material, Fig. S7C and D), and IF also showed a reduced KLC-1/2 staining at the NE, however, nesprin-1 remained at the NE (Supplementary Material, Fig. S7A). Moreover, MHC levels and the fusion index were significantly reduced in myotubes upon KLC-2 knockdown (Fig. 8C and D, Supplementary Material, Fig. S7E and F). Further analysis of MHC positive multinucleated cells (myotubes) revealed that KLC-2 depletion resulted in fewer nuclei per myotube (Fig. 8E, Supplementary Material, Fig. S7G), indicating a defect in myoblast fusion. In contrast, KLC-1 depletion led to significantly more clustered nuclei per myotube when compared with controls (Fig. 8E, Supplementary Material, Fig. S7B), indicating a defect in nuclear positioning in addition to myoblast fusion.

Human nesprin-1α_2 WT causes heart developmental and conduction defects in zebrafish embryos while mutants induce a less severe heart phenotype

To investigate whether the nesprin mutants affect cardiac structure or function *in vivo*, we generated a zebrafish model by expressing nesprin-1α_2 WT and mutants (R8272Q, S8381C and N8406K) in zebrafish embryos via injection of the corresponding human *SYNE1*α_2 (nesprin-1α_2) mRNAs at the one-cell stage. At 48 h post-fertilization (hpf), zebrafish embryos expressing

Downloaded from https://academic.oup.com/hmg/article-abstract/26/12/2258/3111721
by King's College London user
on 07 December 2017

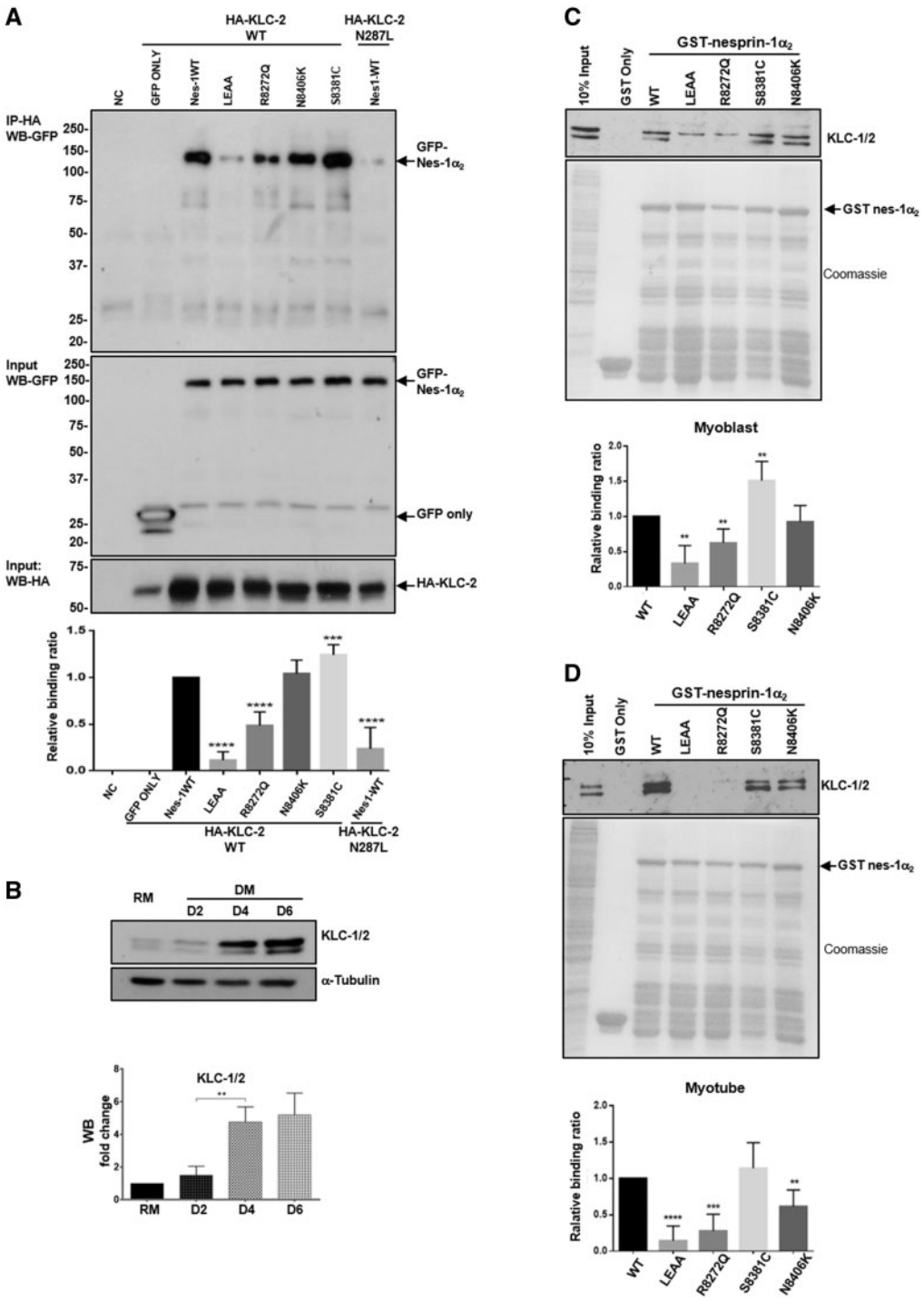


Figure 7. Defects in nesprin-1 and KLC-1/2 interaction. Overexpression and IP showed the binding between nesprin-1WT/mutants and KLC WT/mutants in U2OS cells, HA-KLC2-N287L was co-expressed with GFP-nesprin-1α_2 WT as a positive control, GFP empty vector with HA-KLC-2 WT as a negative control (**A**). WB showed endogenous expression levels of KLC-1/2 increased during myotube formation (**B**). GST pull-down showed the binding between nesprin-1 and KLC-1/2 using either GST-WT or mutant nesprin-1 beads in myoblasts (C) and myotubes (**D**), respectively. The binding for each mutant was quantified by densitometry and expressed as a ratio of the value obtained for WT protein. Three independent experiments were performed shown as mean ± SEM, $^*P < 0.05$ using Student's *t*-tests.

human nesprin-1α_2 WT showed heart defects including dilated atrial chambers with reduced heart rate (Fig. 9A and B, Supplementary Material, video). There was also evidence of abnormal anterior-posterior axis development and curved tails (Supplementary Material, video). Furthermore, whole-mount *in situ* hybridization (WISH) demonstrated that the expression of myosin light chain polypeptide 7 (*myl7*), the ortholog of the human regulatory myosin light chain (RLC) gene (38,39), was reduced in 30% of the embryos expressing human nesprin-1α_2 WT. The expression pattern of this gene also highlighted the dilated atrial chambers and heart developmental defects such as abnormal looping (Fig. 9C and D; Supplementary Material,

Downloaded from https://academic.oup.com/hmg/article-abstract/26/12/2258/3111721
by King's College London user
on 07 December 2017

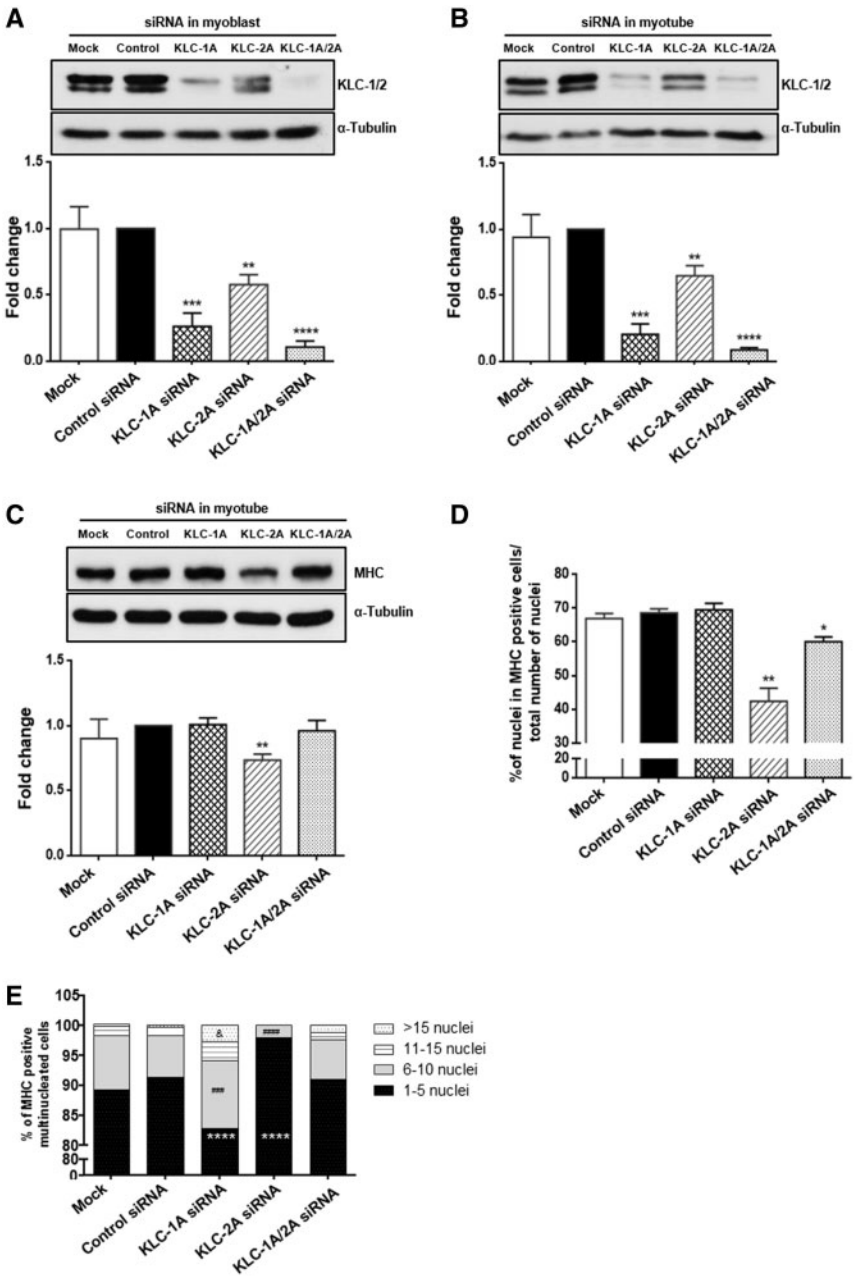


Figure 8. siRNA knockdown of KLC-1/2 cause defects in myoblast fusion and differentiation. WB showed the expression levels of both KLC-1 and -2 were reduced in myoblasts (**A**) and myotubes (**B**) upon KLC-1/2 depletion. The expression level of MHC (**C**) and the fusion index (**D**) were significantly reduced in myotubes especially upon KLC-2 depletion (using KLC-2A oligo), more than 800 nuclei for each clone were counted by microscopy (63× objective) at day 6, three independent experiments were performed for each clone. Further analysis of MHC positive multinucleated cells revealed that KLC-2 depletion resulted in fewer nuclei per myotube. In contrast, KLC-1 depletion (using KLC-1A oligo) led to significantly more clustered nuclei per myotube when compared with controls (**E**). Means and SEM were obtained from three independent experiments for each clone. *$P < 0.05$ using Student's *t*-tests or two-way ANOVA analysis.

Fig. S8A and B). In contrast, expression of the human nesprin-1α_2 mutants induced some heart developmental defects, such as abnormal heart looping and malpositioning of heart chambers (Supplementary Material, Fig. S8A and B), but without heart enlargement or heart rate defects. There was also evidence of abnormal anterior-posterior axis development in all the embryos, when compared with uninjected and GFP expressed embryos (Supplementary Material, Fig. S8C and D). Taken together these zebrafish larvae data suggests that overexpression of human nesprin-1α_2 WT leads to cardiac developmental defects while nesprin-1α_2 mutants induced a less severe heart phenotype.

Discussion

Mutations in lamin A/C and emerin, which form a complex at the INM, can cause EDMD with conduction system defects, as well as DCM. Similarly, missense mutations in the C-terminal region of the nesprin-1 (*SYNE1*) and -2 (*SYNE2*) genes and *SUN1/2* genes were identified in EDMD-DCM patients, leading to

Downloaded from https://academic.oup.com/hmg/article-abstract/26/12/2258/3111721
by King's College London user
on 07 December 2017

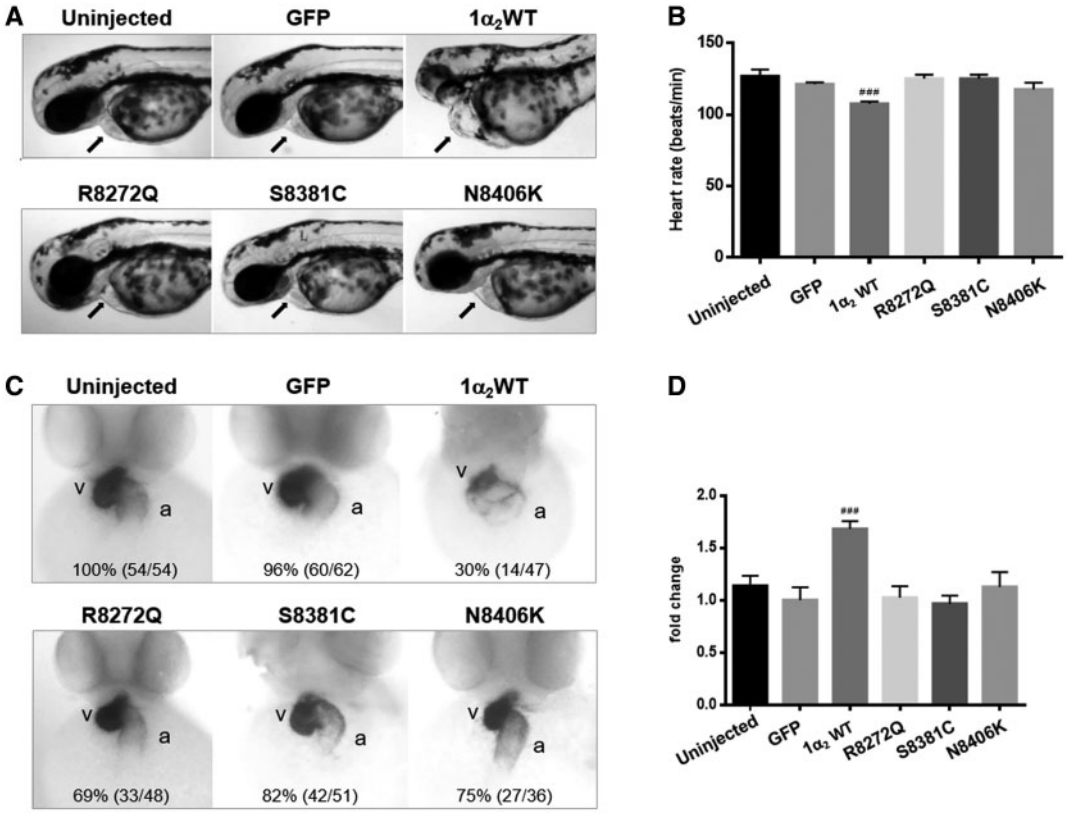


Figure 9. Human nesprin-1α_2 WT induces heart development defects in zebrafish. Lateral views of zebrafish live embryos at 48 hpf. The pericardium (**A**, arrowed) and heart rate are shown for each corresponding mRNA injected (**B**), zebrafish embryos with nesprin1α_2 WT mRNA showed slow heart rate and dilated atrial chambers. Whole-mount *in situ* hybridization (WISH) monitoring expression of the *myl7* gene at 48 hpf (**C**), the numbers (left in brackets) indicate the percentage of embryos displaying the phenotype represented in the picture shown, the numbers (right in brackets) is the total numbers counted of observed embryos. The relative atrium area of embryos for the corresponding mRNA injection was measured and calculated by the area of *myl7* expression using ImageJ (**D**), which was normalised to the atrium area of the embryos injected with GFP mRNA. Embryos are in ventral views with the anterior at the top. About 4–7 embryos for each injection were measured. Means and SEM were obtained from three independent experiments for each treatment. $P < 0.001$ using Student's *t*-tests. a: atrium, v: ventricle.

disrupted nesprin/lamin/emerin/SUN1/2 interactions and nuclear morphology defects (40,41). In the current study, three novel missense mutations (R8272Q, S8381C and N8406K) were identified in the same C-terminal region of nesprin-1 in DCM patients, which affected nuclear morphology and impaired protein–protein interaction with lamin A/C and SUN2. The mutants also augmented ERK activation *in vitro*. Importantly, these mutations, especially mutant R8272Q, caused defects in myoblast differentiation associated with dysregulation of MTFs and disruption of the nesprin-1/KLC-1/2 interaction at the ONM. These findings provide new information on how nesprin-1 performs multi-functional roles in muscle cell development and disease via its connections at both INM and ONM, and also how these mutations and disruption of the LINC complex contribute to muscle dysfunction, and potentially the pathogenesis of DCM.

Nesprin-1 mutations interfere with NE organisation

Mutations in the *LMNA* gene, encoding A-type lamins, cause a number of different tissue specific laminopathies, including DCM (42). The molecular pathogenesis of these diseases is unknown but in some cases may be related to disruption of the LINC complex. Mice lacking A-type lamins display phenotypes that are reminiscent of human muscular dystrophies and cardiomyopathies (43,44). Embryonic fibroblasts derived from *LMNA* KO mice are characterised with grossly misshapen cell nuclei and a structurally weakened NE, and mislocalization of nesprins leading to reduced mechanical stiffness (45). Mutations in both nesprins and SUN1/2 have also been implicated in EDMD-DCM, whereby mutants cause abnormal localisation of the LINC complex proteins including lamin, emerin and SUN, and disrupted nesprin/lamin/emerin/SUN interactions, leading to defects in nuclear morphology and nuclear-cytoskeletal coupling (13–16). Furthermore, the disruption of endogenous LINC complexes by recombinant dominant negative-KASH constructs of nesprins-1, -2 and -3 also causes a significant loss of mechanical stiffness (6,33,46). Interestingly, the three novel missense mutations (R8272Q, S8381C and N8406K) identified in DCM patients in this study reside within the unique AD region at the C-terminus of the nesprin-1 and -2 proteins (25,26). This region is evolutionally highly conserved and overlaps with the lamin and emerin binding regions. It has relatively little secondary structure and is likely to be flexible (26), and potentially able to adapt its conformation to stabilise the associations between nesprin SRs, lamin A/C and emerin at the INM (for nesprin-1α_2) or SUN proteins at the ONM (for nesprin-1α_2 and -1 giant isoforms). The three nesprin-1 mutations (R8272Q, S8381C and N8406K) identified in this study cause changes in the charge or hydrophilic/hydrophobic properties of conserved amino acids and likely affect the structure/flexibility of the AD region of nesprin-1, altering it interactions with lamin A/C and SUN2. These binding changes were most likely due to

Downloaded from https://academic.oup.com/hmg/article-abstract/26/12/2258/3111721
by King's College London user
on 07 December 2017

disruption of the functions of all the endogenous nesprin-1 isoforms containing the KASH domain in the transfected cells (19). Interestingly, the R8272Q mutant was able to bind lamin A at comparable levels to the WT nesprin-1, in contrast to weak binding to lamin C. Our current understanding of the interactions between nesprins and lamin A and lamin C remains incomplete, so this apparent binding difference requires further investigation. We did not observe a defect in binding between nesprin-1 mutants and emerin, which is consistent with the notion that mutations in emerin are primarily associated with EDMD rather than DCM (28,47). The data above support possible involvement of LINC complex disruption in the pathogenesis of DCM. Future studies on structure/flexibility of the SRs that are predominantly present in the muscle-specific nesprin isoforms will be required to confirm this hypothesis.

Several studies on *LMNA* KO and H222P knock-in mice have indicated activation of MAPKs in the development of DCM. Inhibitors of MAPKs could partially rescue the DCM phenotype, implicating ERK in the pathogenesis of lamin A/C cardiomyopathy (48,49). Our data showed that enhanced ERK activity is also observed in heart tissue from the nesprin-1 KASH KO mice, fibroblasts derived from EDMD-DCM patients and nesprin-1 mutant transfected cells, suggesting that nesprin and lamin A/C function through a similar pathway and trigger up-regulation of ERK. Future work will examine how NE proteins regulate ERK activity potentially via influencing interactions between A-type lamins, NE proteins and components of MAPK cascades, as well as nuclear translocation of activated MAPKs (50,51).

Nesprin-1 mutations and dysregulation of MTFs in myoblast differentiation

Nesprin-1α_2 is highly expressed in both skeletal and cardiac muscles as previously shown (7,52,53). Although there were no obvious muscle phenotypes recorded, it is plausible that in the patients presenting with the *SYNE1* mutations the skeletal muscle dysfunction was too subtle or underestimated at clinical examination. Alternatively, in addition to these *SYNE1* mutations, another cardiac disease gene is mutated thus enhancing the phenotype. Therefore, due to restricted accessibility to patient samples, we focused on investigating if these three novel mutants cause muscle dysfunctions by using the C2C12 mouse myoblast differentiation model.

Myogenesis involves a series of sequential steps. Myoblasts originating from the mesoderm are converted to skeletal muscle lineage myoblasts after MyoD expression, enter the cell cycle and proliferate, then withdraw from the cell cycle and initiate differentiation with expression of MTFs such as myogenin (54). Next cell fusion occurs to form multinucleated myotubes and expression of the muscle specific protein MHC. Increasing evidence indicates that multiple cell signalling pathways play critical roles in myoblast fusion, including those involved in cytoskeleton organization, cell adhesion and migration (55) as well as extracellular signalling molecules and components of extracellular matrix (54,56). Recent literature shows that LINC complex components, including nesprins and SUN1/2, mechanically couple the nucleus to the extracellular matrix and play an important role in differentiating muscle. In addition, these proteins have been implicated in regulating chromatin structure and gene expression. For example, C2C12 cells expressing a *LMNA* R453W mutant have reduced capacity to differentiate, yet retain an unaltered morphology (57), suggesting that subtle abnormal changes in lamina structure or composition may impair the anchoring of chromatin to the NE, affecting gene regulation and perturbing myogenesis.

Using retroviral transduction in mouse C2C12 myoblasts in the current study, our data showed myoblasts expressing mutant nesprin-1α_2 R8272Q or dominant negative-1KASH had a significantly lower capacity to differentiate and form multinucleated cells than those expressing 1α_2 WT, although exogenously expressed 1α_2 WT and mutants were observed to be properly localised at the NE. Importantly, the inhibition of multinucleation by dominant negative-1KASH and 1α_2 mutants, especially R8272Q, is potentially linked to the inhibition of myogenin and MHC expression in the transduced C2C12 cells. Our data also showed that nesprin-1α_2 was expressed in the initial stage crucial for converting C2C12 myoblasts into myotubes and promoted myoblast differentiation during the process of myotube formation, whereas the mutants reduced or abolished the effects, suggesting that expression of nesprin-1α_2 mutants does not alter the proliferation of myoblasts, but rather impairs their capacity to express muscle-specific genes (myogenin and MHC). This results in an inability to fuse, especially observed in the R8272Q mutant, which also explains why nesprin-1 mutants affect the expression levels of myogenin more severely than MyoD, because MyoD is already expressed prior to initiation of differentiation at a stage when the expression level of nesprin-1 is still low. Therefore, we propose the following mechanisms whereby nesprin mutants may affect muscle differentiation: regulation of myogenin and expression of MHC are influenced by the LINC complex; nesprin mutants may fail to build a functional scaffold and/or to maintain chromatin compartmentalisation with lamin A/C, leading to an alteration in the amount of heterochromatin formed and/or its localisation. Potentially this causes defects in initiation of the terminal differentiation process resulting in decreased or delayed expression of myogenin and MHC, thus causing a delayed differentiation. This effect may be similar to that observed in C2C12 cells expressing an *LMNA* R453W mutant (57) that showed a reduced capacity to differentiate. However, further experimentation on how the nesprin-1 mutants affect regulation of MTFs is required to elucidate the precise function of nesprin in muscle cell differentiation.

Nesprin-1 mutations disrupt nesprin-1/KLC interaction and myoblast fusion

Proper nuclear positioning and movement is critical in muscle cell differentiation and development. In the nucleus, changes in gene activity that occur during terminal cell differentiation are correlated with gene migration and relocation (58,59). Nuclear movement and positioning are driven by cytoskeletal networks of MTs, actin and/or intermediate filaments and involve a connection between the cytoskeleton and the NE, mediated by the LINC complex (60,61). KO mouse studies have shown that nesprin-1 and SUN1/SUN2 play critical roles in anchoring nuclei in skeletal muscle (62,63). Similarly, mutations identified in *SUN1* and *SUN2* genes associated with EDMD like phenotypes cause defective nuclear positioning when expressed in mouse fibroblasts (15,16). The MT-based kinesin motor, kinesin-1, consisting of two KHCs and two KLCs, is localised at the NE. Binding of the dominant light chain isoform in muscle, KLC-2, to nesprin-2 has been shown to be responsible for nuclear rotations and movement along MTs (27). There is evidence that nuclear position can influence gene expression. For example, nuclei at the neuromuscular junction (NMJ) have a unique

Downloaded from https://academic.oup.com/hmg/article-abstract/26/12/2258/3111721
by King's College London user
on 07 December 2017

transcriptional profile relative to the non-synaptic nuclei (59). Nesprin-1 (*SYNE1*) levels are much higher in synaptic nuclei than extrasynaptic nuclei, and also higher in myotubes than myoblasts in culture and central nuclei during regeneration (52,64). In addition, maintaining proper nuclear positioning is thought to ensure sufficient transcriptional capacity and minimise transport distances between the nuclei and the cytoplasm in highly organised long muscle cells (60,65). Our data confirmed that nesprin-1 binds to KLC-1/2, and nesprin-1 mutants, particularly R8272Q, disrupted this interaction. Furthermore, depletion of KLC-1 resulted in nuclear clustering, whereas depletion of KLC-2, a dominant muscle isoform, caused reduction of MHC levels and the fusion index in myotubes, that was consistent with those observed in the R8272Q mutant. This disruption of nesprin-1/KLC interaction in C2C12 myoblasts may result in defects in nuclear movement along MTs, leading to abnormal nuclear positioning. Further investigations are required to elucidate the precise roles of nesprin-1 and KLC-1 and -2 in myonuclear positioning in muscle cell differentiation.

Expression of nesprin-1α_2 mutants induce less severe heart defects during zebrafish heart development compared to 1α_2 WT

To investigate whether the nesprin mutants affect cardiac structure or function *in vivo*, we generated a zebrafish model by expressing human nesprin-1α_2 WT and mutants (R8272Q, S8381C and N8406K) in zebrafish embryos via injection of the corresponding human SYNE1α_2 (nesprin-1α_2) mRNAs. Our data showed that human nesprin-1α_2 WT causes heart developmental and conduction defects in zebrafish embryos, and all three 1α_2 mutants caused less severe heart developmental defects. Although these results are unexpected, there are some potential explanations. Human nesprin-1α_2 is not expressed in the heart and muscle until the initial stages of muscle cell differentiation (7,52,53). Therefore, injection of human nesprin-1α_2 mRNA into zebrafish larvae at the one cell stage, when the expression level of endogenous nesprin-1 was minimal, caused ectopic expression effects on heart development. The effect of the mutants was less severe potentially because their binding interactions are compromised leading to less disruption. Future studies utilising the zebrafish model with either cardiac (tissue specific)/heat shock protein (timing dependent) promotors or CRISPR/Cas9-mediated knock-in is required to clarify underlying disease mechanism.

In summary, our data support the hypothesis that nesprin-1 plays multi-functional roles at both INM and ONM during muscle cell development and disease (Fig. 10). Although the role of nesprin-1 dysfunction in DCM requires further experimentation, we show that novel nesprin-1 mutants affect diverse functions, including gene expression and myoblast fusion and differentiation. Further investigation is now required to elucidate the complex mechanisms behind this dysregulation especially in the cardiac system.

Materials and Methods

Research subjects

The study cohort consisted of 218 unrelated individuals with DCM and 210 healthy controls, collected from the West China Hospital, Sichuan University, China. All blood materials of the patients and controls included in this study were taken with informed consent for DNA analysis and approval of the local ethics board. The clinical characteristic of the patients and controls were summarized in Supplementary Material, Table S1 and Supplementary material. Most of DCM patients were men and had significantly larger left ventricular (LV) chamber and lower left ventricular ejection fraction (LVEF) when compared with the ethnic and age-control samples.

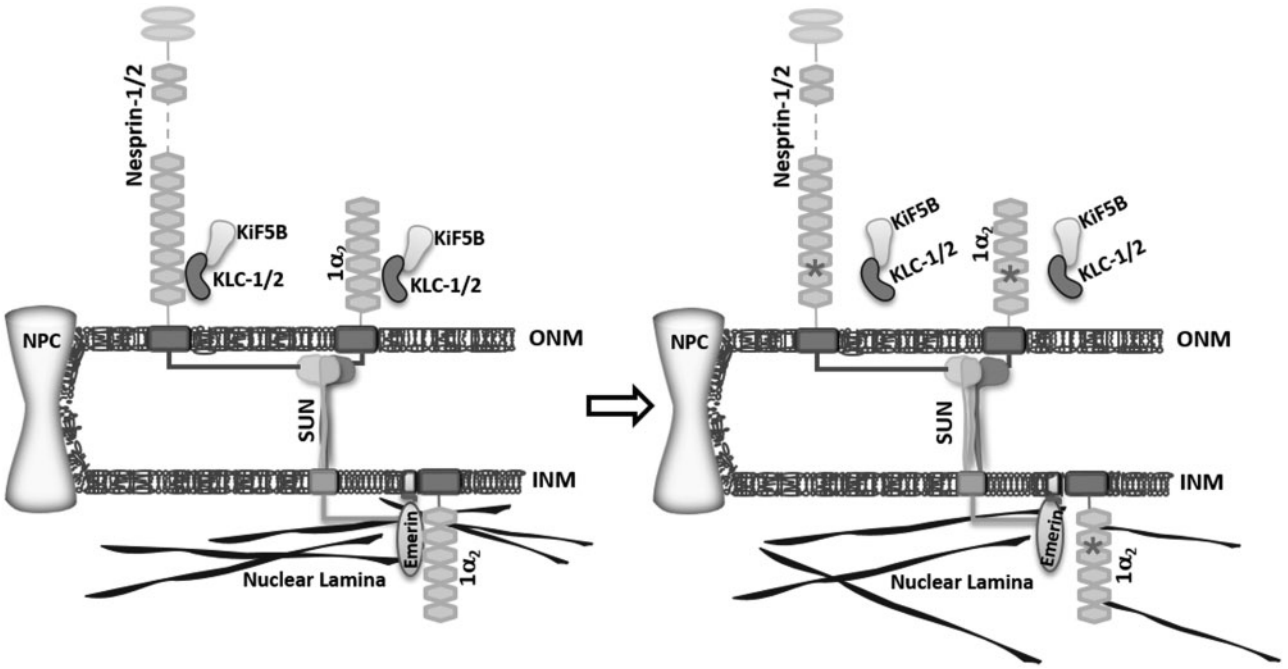


Figure 10. Working model for the role nesprin-1. The schematic figure shows nesprin-1 plays multiple-functions at both INM and ONM, and how mutants can disrupt the NE-LINC complex, contributing to the pathogenesis of muscle disease. *Indicates where the mutants are.

Downloaded from https://academic.oup.com/hmg/article-abstract/26/12/2258/3111721
by King's College London user
on 07 December 2017

Mutation analysis

Primer pairs were designed across the intron/exon boundaries and untranslated regions of nesprin-1α_1 and 1α_2, nesprin-2α_1, 2α_2, 2β, 2ϵ_1 and 2ϵ_2, i.e. the smaller INM localised isoforms of nesprin-1 and nesprin-2 shown to bind emerin and lamin and be either highly or specifically expressed in muscle tissue. 180 oligonucleotide primers from intronic sequences for 88 exons were designed using the program Primer3Input (primer3_www.cgi v 0.2) and used previously (13). Mutation screening was performed using the PCR-based mutation detection technique DHPLC (WAVE 4500B system, Transgenomic). Appropriate DHPLC conditions for running temperatures and buffer gradients were established for each individual exon.

Plasmid constructs/retroviral constructs/site-directed mutagenesis

Human cDNA of nesprin-1α_2 WT constructs (amino acids 1–977, equivalent to nesprin-1 giant 7875–8796) were amplified using a high-fidelity GC-rich PCR kit (Roche) and inserted respectively in-frame into the EcoRI site of the pEGFP-C1 vector (Clontech) for overexpression of GFP-nesprin, and the NotI and EcoRI sites of pcDNA3.1(-) vector (Invitrogen) for *in vitro* synthesis of Flag-tagged nesprin mRNA and microinjection. GST nesprin-1α_2 SR1-6 construct (amino acids 1–837, lacking KASH domain, equivalent to nesprin-1 giant 7875–8662, SR 69–74) and V5-tagged nesprin-1α_2 construct (amino acids 1–977, equivalent to nesprin-1 giant 7875–8796) were amplified from the established pEGFP-C1-nesprin-1α_2 WT construct and inserted into EcoRI and SalI sites of the pGEX-4T-1 vector (Pharmacia) and EcoRI and NotI sites of the MIGplus retroviral vector respectively. The MIGplus vector was a kind gift from Prof. Peter Zammit (66), which was modified from the retroviral (RV) backbone pMSCV-puro (Clontech, Mountain View, CA), in which the puromycin selection gene was replaced with eGFP to create pMSCV–IRES–eGFP, served as the RV control vector and *eGFP* as a reporter for retroviral infection. Retroviruses were then packaged into 293T cells using standard methods as described previously (66). All the constructs of nesprin-1 mutant constructs (R8272Q, S83831C, N8406K) were generated using QuickChange™ XL site-directed mutagenesis kit (Stratagene). Primers for the constructs above are listed in Supplementary Material, Tables S3–S5. Myc-SUN2 has been reported previously (67). CB6-HA-KCL2 WT and mutant N287L were kind gifts from Dr Mark Dodding (King's College London, UK). GST-lamin A (amino acids 356–665) and GST-emerin (amino acids 1–176) were kind gifts from Dr Juliet Ellis (King's College London, UK).

Cell nuclei circularity quantification

'Analyse particles' function in ImageJ was used to measure circularity of cell nuclei, with circularity values given between 0 and 1 (values closer to 1 being more circular in shape) (68).

Antibodies and immunofluorescence

Primary antibodies were sourced as follows: lamin A/C (N-18, sc-6215, Santa Cruz), SUN2 [kind gifts from Dr Didier Hodzic, University of Washington, US and (67)], emerin (NCL-EMERIN, Novacastra), GFP (ab290, ab13970, Abcam), GAPDH (sc-25778, Santa Cruz), β-actin (A5316, Sigma), α-tubulin (ab52866, Abcam), phospho-p44/42 MAPK (pERK1/2) (4370, Cell Signalling Technology), p44/42 MAPK (tERK1/2) (9102, Cell Signalling Technology), V5 (R96025, Invitrogen), nesprin-1 (MANNES1A and MANNES1E (52), generated against the C-terminus of the nesprin-1 giant), myogenin (sc-576, Santa Cruz), myosin (clone A4.1025, against all isoforms expressed by *MYH1*, Alexis Corporation), HA (ab1424, Abcam), KLC-1/2 (63–90, a kind gift from Prof Scott Brady, University of Illinois at Chicago, USA). Alexa fluorophore (488/546/647)-conjugated secondary antibodies were from Invitrogen. HRP-conjugated secondary antibodies were from Amersham. IF staining was performed as described previously (13). In particular, to further define the subcellular localisation for GFP-tagged nesprin-1α_2, the transfected cells were fixed by 4% paraformaldehyde/PBS, then permeabilized using either 0.001% digitonin/PBS or 0.5% NP40/PBS.

Cell culture, transfection and RNAi

HDFs, U2OS, C2C12 myoblasts were cultured at 37 °C/5% CO_2 in Dulbecco's modified Eagle's medium (DMEM) supplemented with 10% fetal calf serum (FCS) and 1% Pen-Strep-Glutamine (PSG). For myoblast differentiation, C2C12 were cultured in low-mitogen medium (DMEM supplemented with 1% PSG and 2% horse serum) as described previously (7). For transient transfection, cells were plated onto glass coverslips or T25 flask at approximately 1.2×10^5 cells/ml and transfected using FuGENE HD™ (Promega) according to the manufacturer's instructions and fixed for IF staining or harvested for Western blotting 24 h after transfection as described previously (7,13). siRNA transfections were also performed by using HiPerFect (Qiagen) according to the manufacturer's instructions. KLC-1/2 siRNA oligomers targeting to the mouse KLC-1/2 were previously described (27) and obtained from Dharmacon, named as KLC-1A and KLC-2A. Additional four KLC-1/2 siRNA oligos obtained from Qiagen (Cat. No: SI01085154, SI01085168, SI01083327 and SI01083341) were renamed as KLC-1B and -1C, KLC-2B and -2C respectively. Allstars negative control siRNA was also supplied from Qiagen.

Neonatal rat cardiomyocytes (NRCs) isolation, culture and transfection

Primary cultures of NRCs were isolated from 1- or 2-day-old neonatal Sprague–Dawley rats. Hearts were collected and atria were removed. Hearts were then washed, excised, minced and enzymatically digested at 37 °C with ADS buffer [116 mmol/L NaCl, 20 mmol/L HEPES, 0.8 mmol/L NaH_2PO_4, 5.6 mmol/L glucose, 5.4 mmol/L KCl, 0.8 mmol/L $MgSO_4$] containing collagenase (57.5 U/mL) and pancreatin (1.5 mg/mL). The suspension was pre-plated to remove contaminating cells, before being cultured on gelatin (Sigma) pre-coated 35 mm petri dishes with a density of 2×10^5 cells/ml. Cells were allowed to adhere for 24 h, and then transfected using Escort III (Sigma) following the manufacturer's instruction as described previously (69).

Retroviral infection and myoblast differentiation

Retroviral constructs, together with an ectopic packaging plasmid, were transiently co-transfected into 293T cells to produce non-replicating retrovirus and the supernatant harvested 48, 60 and 72 h later. Retroviral infection was performed as described previously (66). Briefly, C2C12 cells were plated in T25 flasks. After 24 h, the medium was replaced with a 1:5 dilutions of 293T retroviral supernatant supplemented with 4 μg/ml polybrene and incubated at 37 °C for 4–6 h, and then changed into fresh medium. FACS was performed to purify the infected GFP

Downloaded from https://academic.oup.com/hmg/article-abstract/26/12/2258/3111721
by King's College London user
on 07 December 2017

positive cells in 48 h and these were used to in subsequent myoblast differentiation experiments. To induce differentiation, the medium was replaced with the differentiation medium (DM) containing 2% horse serum and 1% PSG, and cell lysates were collected for further investigation at day 0, 2, 4 and 6.

Co-immunoprecipitation assays

U2OS cells were transfected using GFP-nesprin-1α_2 WT/mutants with HA-KLC-1/2 WT/mutant as well as Myc-SUN2 respectively, harvested about 24 h later and kept in IP buffer [10 mM Tris (PH 7.4), 50 mM NaCl, 5 mM EDTA, 1% Triton X-100] with protease inhibitor cocktail (Sigma) on ice for 30 min, followed by 10 s sonication and centrifugation. About 500 μg of protein was precleaned with Protein A/G sepharose beads (Sigma) for 1 h at 4 °C. Beads were removed by centrifugation and 2.5 μg primary antibody was added to lysates and left rotating at 4 °C for 16 h. Beads were then added to reactions and incubated for 2 h rotating at 4 °C. Samples were centrifuged and supernatant discarded. Pellets were washed and re-suspended in sample buffer, heated at 95 °C for 10 min and analysed by WB as described previously (13).

GST pull-down assays

GST fusion proteins and GST alone were induced from 100 ml of bacterial culture for 4 h by addition of 0.2 mM isopropyl-1-thio-β-D-galactopyranoside. Purification of the proteins was performed according to the Amersham Biosciences protocol using glutathione-Sepharose 4B beads (Amersham Biosciences). Pull-down assays were performed as described previously (70). Briefly, 200 μg extracts from U2OS or C2C12 myoblasts/myotubes were incubated with 50 μl beads with constant rotation for 16 h at 4 °C. Bound proteins were washed and eluted into sample buffer, followed by WB. In particular, to investigate the interaction between nesprin-1 and its NE binding partners, protein lysates from Myc-SUN2 transfected (for SUN binding) and untransfected U2OS cells (for lamin A/C and emerin binding), C2C12 myoblast and myotubes (for KLC-1/2 interaction) were harvested and subjected to pull down using either GST-WT or mutant nesprin-1α_2 SR1-6 beads. To further confirm the bindings, U2OS cells were transfected with either GFP-nesprin-1α_2WT or mutants, protein lysates were harvested and subjected to pull-down using either GST-lamin A (amino acids 356–665) or GST-emerin (amino acids 1–176).

Quantitative RT-PCR (QPCR)

C2C12 Cells were cultured in T25 flasks in proliferation or differentiation medium. Total RNA was extracted using RNA-STAT 60 (Amsbio) according to manufacturer's protocol. Reverse transcription synthesis of cDNA and qPCR was performed as described previously (13). Relative expression of each myogenic transcriptional factor between proliferating and differentiated cells was measured in three replicates in at least three independent experiments. Primers for myogenin, MHC, MyoD, V5 and GFP have been previously described and listed in Supplementary Material, Table S6.

Zebrafish embryos

WT embryos from AB strain were used. Embryos were obtained by natural matings and cultured in embryo medium (71). Staging of the embryos was carried out as described by Kimmel *et al.* (72). Ethical approval was obtained from the Animal Care and Use Committee of Sichuan University.

In vitro synthesis of mRNA and microinjection

Capped GFP and nesprin mRNAs were synthesized using mMESSAGE mMACHINE® Kit (Ambion); Synthetic capped mRNAs were injected into single-cell embryos. Injection dose (60 mg) was an optimised amount received by a single embryo.

Zebrafish whole-mount *in situ* hybridization

Whole-mount *in situ* hybridization was carried out as previously described (73,74). After linearization by appropriate restriction enzymes, antisense RNAs for *in situ* hybridization were synthesized using DIG RNA Labelling Kit (SP6/T7) (Roche) and purified by MEGAclear (Ambion). Signal area of whole-mount *in situ* hybridization was measured by software ImageJ.

Statistical analysis

Cell counts for statistical analysis were performed on $n = 100$–200 cells/$n = 10$ confocal microscope fields (63× magnification) for each control and experimental group, and results were verified in at least three independent experiments. The data were analysed using GraphPad Prism software by the Student's *t*-tests, One way or Two-way analysis of variance (ANOVA) with Dunnett's multiple comparison test for two independent groups or multiple comparisons, respectively. The values are expressed as mean ± standard error of mean (SEM). The *P*-values < 0.05 were considered statistically significant.

Supplementary Material

Supplementary Material is available at *HMG* online.

Acknowledgements

We thank the patients for their participation to the study, Dr Yaniv Hinits (King's College London) for his advice and critical comments on Zebrafish experiments, Dr Andrew Cobb (King's College London) for critical reading of this manuscript, Dr Flavia Autore and Miss Aisling Williams (King's College London) for their help with the artwork.

Conflict of Interest statement. None declared.

Funding

British Heart Foundation (BHF), UK [PG/11/58/29004 to Q.P.Z., RG/11/14/29056 to C.M.S., PG/11/71/29091 to I.H. and G.E.M.]; National Natural Science Foundation of China [81270289 to L.R.]. Funding to pay Open Access publication charges for this article was provided by the BHF.

References

1. Towbin, J.A. and Bowles, N.E. (2002) The failing heart. *Nature*, **415**, 227–233.
2. Hershberger, R.E., Hedges, D.J. and Morales, A. (2013) Dilated cardiomyopathy: the complexity of a diverse genetic architecture. *Nat. Rev. Cardiol.*, **10**, 531–547.

Downloaded from https://academic.oup.com/hmg/article-abstract/26/12/2258/3111721
by King's College London user
on 07 December 2017

3. Capell, B.C. and Collins, F.S. (2006) Human laminopathies: nuclei gone genetically awry. *Nat. Rev. Genet.*, **7**, 940–952.
4. Bonne, G., Di Barletta, M.R., Varnous, S., Becane, H.M., Hammouda, E.H., Merlini, L., Muntoni, F., Greenberg, C.R., Gary, F., Urtizberea, J.A., *et al.* (1999) Mutations in the gene encoding lamin A/C cause autosomal dominant Emery-Dreifuss muscular dystrophy. *Nat. Genet.*, **21**, 285–288.
5. Bione, S., Maestrini, E., Rivella, S., Mancini, M., Regis, S., Romeo, G. and Toniolo, D. (1994) Identification of a novel X-linked gene responsible for Emery-Dreifuss muscular dystrophy. *Nat. Genet.*, **8**, 323–327.
6. Crisp, M., Liu, Q., Roux, K., Rattner, J.B., Shanahan, C., Burke, B., Stahl, P.D. and Hodzic, D. (2006) Coupling of the nucleus and cytoplasm: role of the LINC complex. *J. Cell Biol.*, **172**, 41–53.
7. Zhang, Q., Skepper, J.N., Yang, F., Davies, J.D., Hegyi, L., Roberts, R.G., Weissberg, P.L., Ellis, J. and Shanahan, C.M. (2001) Nesprins: a novel family of spectrin-repeat-containing proteins that localize to the nuclear membrane in multiple tissues. *J. Cell Sci.*, **114**, 4485–4498.
8. Haque, F., Lloyd, D.J., Smallwood, D.T., Dent, C.L., Shanahan, C.M., Fry, A.M., Trembath, R.C. and Shackleton, S. (2006) SUN1 interacts with nuclear lamin A and cytoplasmic nesprins to provide a physical connection between the nuclear lamina and the cytoskeleton. *Mol. Cell. Biol.*, **26**, 3738–3751.
9. Zhang, Q., Ragnauth, C., Greener, M.J., Shanahan, C.M. and Roberts, R.G. (2002) The nesprins are giant actin-binding proteins, orthologous to *Drosophila melanogaster* muscle protein MSP-300. *Genomics*, **80**, 473–481.
10. Lüke, Y., Zaim, H., Karakesisoglou, I., Jaeger, V.M., Sellin, L., Lu, W., Schneider, M., Neumann, S., Beijer, A., Munck, M., *et al.* (2008) Nesprin-2 Giant (NUANCE) maintains nuclear envelope architecture and composition in skin. *J. Cell Sci.*, **121**, 1887–1898.
11. Kim, D.I., Birendra, K.C. and Roux, K.J. (2015) Making the LINC: SUN and KASH protein interactions. *Biol. Chem.*, **396**, 295–310.
12. Cain, N.E. and Starr, D.A. (2015) SUN proteins and nuclear envelope spacing. *Nucleus (Calcutta)*, **6**, 2–7.
13. Zhang, Q., Bethmann, C., Worth, N.F., Davies, J.D., Wasner, C., Feuer, A., Ragnauth, C.D., Yi, Q., Mellad, J., Warren, D.T., *et al.* (2007) Nesprin-1 and -2 are involved in the pathogenesis of Emery Dreifuss muscular dystrophy and are critical for nuclear envelope integrity. *Hum. Mol. Genet.*, **16**, 2816–2833.
14. Puckelwartz, M.J., Kessler, E.J., Kim, G., Dewitt, M.M., Zhang, Y., Earley, J.U., Depreux, F.F., Holaska, J., Mewborn, S.K., Pytel, P., *et al.* (2010) Nesprin-1 mutations in human and murine cardiomyopathy. *J. Mol. Cell. Cardiol.*, **48**, 600–608.
15. Li, P., Meinke, P., Huong le, T.T., Wehnert, M. and Noegel, A.A. (2014) Contribution of SUN1 mutations to the pathomechanism in muscular dystrophies. *Hum. Mutat.*, **35**, 452–461.
16. Meinke, P., Mattioli, E., Haque, F., Antoku, S., Columbaro, M., Straatman, K.R., Worman, H.J., Gundersen, G.G., Lattanzi, G., Wehnert, M., *et al.* (2014) Muscular dystrophy-associated SUN1 and SUN2 variants disrupt nuclear-cytoskeletal connections and myonuclear organization. *PLoS Genet.*, **10**, e1004605.
17. Rajgor, D., Mellad, J.A., Autore, F., Zhang, Q. and Shanahan, C.M. (2012) Multiple novel nesprin-1 and nesprin-2 variants act as versatile tissue-specific intracellular scaffolds. *PLoS One*, **7**, e40098.
18. Zhang, Q., Ragnauth, C.D., Skepper, J.N., Worth, N.F., Warren, D.T., Roberts, R.G., Weissberg, P.L., Ellis, J. and Shanahan, C.M. (2005) Nesprin-2 is a multi-isomeric protein that binds lamin and emerin at the nuclear envelope and forms a subcellular network in skeletal muscle. *J. Cell Sci.*, **118**, 673–687.
19. Duong, N.T., Morris, G.E., Lam le, T., Zhang, Q., Sewry, C.A., Shanahan, C.M. and Holt, I. (2014) Nesprins: tissue-specific expression of epsilon and other short isoforms. *PLoS One*, **9**, 10–1371.
20. Gros-Louis, F., Dupre, N., Dion, P., Fox, M.A., Laurent, S., Verreault, S., Sanes, J.R., Bouchard, J.P. and Rouleau, G.A. (2007) Mutations in SYNE1 lead to a newly discovered form of autosomal recessive cerebellar ataxia. *Nat. Genet.*, **39**, 80–85.
21. Puckelwartz, M.J., Kessler, E., Zhang, Y., Hodzic, D., Randles, K.N., Morris, G., Earley, J.U., Hadhazy, M., Holaska, J.M., Mewborn, S.K., *et al.* (2009) Disruption of nesprin-1 produces an Emery Dreifuss muscular dystrophy-like phenotype in mice. *Hum. Mol. Genet.*, **18**, 607–620.
22. Banerjee, I., Zhang, J., Moore-Morris, T., Pfeiffer, E., Buchholz, K.S., Liu, A., Ouyang, K., Stroud, M.J., Gerace, L., Evans, S.M., *et al.* (2014) Targeted ablation of nesprin 1 and nesprin 2 from murine myocardium results in cardiomyopathy, altered nuclear morphology and inhibition of the biomechanical gene response. *PLoS Genet.*, **10**, e1004114.
23. Brosig, M., Ferralli, J., Gelman, L., Chiquet, M. and Chiquet-Ehrismann, R. (2010) Interfering with the connection between the nucleus and the cytoskeleton affects nuclear rotation, mechanotransduction and myogenesis. *Int. J. Biochem. Cell Biol.*, **42**, 1717–1728.
24. Wilson, M.H. and Holzbaur, E.L. (2012) Opposing microtubule motors drive robust nuclear dynamics in developing muscle cells. *J. Cell Sci.*, **125**, 4158–4169.
25. Simpson, J.G. and Roberts, R.G. (2008) Patterns of evolutionary conservation in the nesprin genes highlight probable functionally important protein domains and isoforms. *Biochem. Soc. Trans.*, **36**, 1359–1367.
26. Zhong, Z., Chaing, S., Kalinowski, A. and Wilson, KaD. KN. (2010) Stabilization of the spectrin-like domains of nesprin-1α by the evolutionarily conserved "adaptive" domain. *Cell. Mol. Bioeng.*, **3**, 139–150.
27. Wilson, M.H. and Holzbaur, E.L. (2015) Nesprins anchor kinesin-1 motors to the nucleus to drive nuclear distribution in muscle cells. *Development*, **142**, 218–228.
28. Mislow, J.M.K., Holaska, J.M., Kim, M.S., Lee, K.K., Segura-Totten, M., Wilson, K.L. and McNally, E.M. (2002) Nesprin-1alpha self-associates and binds directly to emerin and lamin A in vitro. *FEBS Lett.*, **525**, 135–140.
29. Wheeler, M., Davies, J.D., Zhang, Q., Emerson, L.J., Hunt, J., Shanahan, C.M. and Ellis, J. (2007) Distinct functional domains in nesprin-1alpha and nesprin-2beta bind directly to emerin and both interactions are disrupted in X-linked Emery-Dreifuss muscular dystrophy. *Exp. Cell Res.*, **313**, 2845–2857.
30. Libotte, T., Zaim, H., Abraham, S., Padmakumar, V.C., Schneider, M., Lu, W., Munck, M., Hutchison, C., Wehnert, M., Fahrenkrog, B., *et al.* (2005) Lamin A/C-dependent localization of nesprin-2, a giant scaffolder at the nuclear envelope. *Mol. Biol. Cell*, **16**, 3411–3424.
31. Muchir, A., Pavlidis, P., Decostre, V., Herron, A.J., Arimura, T., Bonne, G. and Worman, H.J. (2007) Activation of MAPK pathways links LMNA mutations to cardiomyopathy in Emery-Dreifuss muscular dystrophy. *J. Clin. Invest.*, **117**, 1282–1293.

Downloaded from https://academic.oup.com/hmg/article-abstract/26/12/2258/3111721
by King's College London user
on 07 December 2017

32. Muchir, A., Pavlidis, P., Bonne, G., Hayashi, Y.K. and Worman, H.J. (2007) Activation of MAPK in hearts of EMD null mice: similarities between mouse models of X-linked and autosomal dominant Emery Dreifuss muscular dystrophy. *Hum. Mol. Genet.*, **16**, 1884–1895.
33. Lombardi, M.L., Jaalouk, D.E., Shanahan, C.M., Burke, B., Roux, K.J. and Lammerding, J. (2011) The interaction between nesprins and sun proteins at the nuclear envelope is critical for force transmission between the nucleus and cytoskeleton. *J. Biol. Chem.*, **286**, 26743–26753.
34. Frock, R.L., Kudlow, B.A., Evans, A.M., Jameson, S.A., Hauschka, S.D. and Kennedy, B.K. (2006) Lamin A/C and emerin are critical for skeletal muscle satellite cell differentiation. *Genes Dev.*, **20**, 486–500.
35. Favreau, C., Higuet, D., Courvalin, J.C. and Buendia, B. (2004) Expression of a mutant lamin A that causes Emery-Dreifuss muscular dystrophy inhibits in vitro differentiation of C2C12 myoblasts. *Mol. Cell. Biol.*, **24**, 1481–1492.
36. Perry, R.L. and Rudnick, M.A. (2000) Molecular mechanisms regulating myogenic determination and differentiation. *Front. Biosci.*, **5**, D750–D767.
37. Berkes, C.A. and Tapscott, S.J. (2005) MyoD and the transcriptional control of myogenesis. *Semin. Cell Dev. Biol.*, **16**, 585–595.
38. Chen, Z., Huang, W., Dahme, T., Rottbauer, W., Ackerman, M.J. and Xu, X. (2008) Depletion of zebrafish essential and regulatory myosin light chains reduces cardiac function through distinct mechanisms. *Cardiovasc. Res.*, **79**, 97–108.
39. Hwang, P.M. and Sykes, B.D. (2015) Targeting the sarcomere to correct muscle function. *Nat. Rev. Drug Discov.*, **14**, 313–328.
40. Meinke, P., Nguyen, T.D. and Wehnert, M.S. (2011) The LINC complex and human disease. *Biochem. Soc. Trans.*, **39**, 1693–1697.
41. Meinke, P. and Schirmer, E.C. (2016) The increasing relevance of nuclear envelope myopathies. *Curr. Opin. Neurol.*, **29**, 651–661.
42. Schreiber, K.H. and Kennedy, B.K. (2013) When lamins go bad: nuclear structure and disease. *Cell*, **152**, 1365–1375.
43. Sullivan, T., Escalante-Alcalde, D., Bhatt, H., Anver, M., Bhat, N., Nagashima, K., Stewart, C.L. and Burke, B. (1999) Loss of A-type lamin expression compromises nuclear envelope integrity leading to muscular dystrophy. *J. Cell Biol.*, **147**, 913–920.
44. Stewart, C.L., Kozlov, S., Fong, L.G. and Young, S.G. (2007) Mouse models of the laminopathies. *Exp. Cell Res.*, **313**, 2144–2156.
45. Muchir, A., van Engelen, B.G., Lammens, M., Mislow, J.M., McNally, E., Schwartz, K. and Bonne, G. (2003) Nuclear envelope alterations in fibroblasts from LGMD1B patients carrying nonsense Y259X heterozygous or homozygous mutation in lamin A/C gene. *Exp. Cell Res.*, **291**, 352–362.
46. Stewart-Hutchinson, P.J., Hale, C.M., Wirtz, D. and Hodzic, D. (2008) Structural requirements for the assembly of LINC complexes and their function in cellular mechanical stiffness. *Exp. Cell Res.*, **314**, 1892–1905.
47. Dellefave, L. and McNally, E.M. (2010) The genetics of dilated cardiomyopathy. *Curr. Opin. Cardiol.*, **25**, 198–204.
48. Wu, W., Muchir, A., Shan, J., Bonne, G. and Worman, H.J. (2011) Mitogen-activated protein kinase inhibitors improve heart function and prevent fibrosis in cardiomyopathy caused by mutation in lamin A/C gene. *Circulation*, **123**, 53–61.
49. Muchir, A., Wu, W., Sera, F., Homma, S. and Worman, H.J. (2014) Mitogen-activated protein kinase kinase 1/2 inhibition and angiotensin II converting inhibition in mice with cardiomyopathy caused by lamin A/C gene mutation. *Biochem. Biophys. Res. Commun.*, **452**, 958–961.
50. Gonzalez, J.M., Navarro-Puche, A., Casar, B., Crespo, P. and Andres, V. (2008) Fast regulation of AP-1 activity through interaction of lamin A/C, ERK1/2, and c-Fos at the nuclear envelope. *J. Cell Biol.*, **183**, 653–666.
51. Rodriguez, J., Calvo, F., Gonzalez, J.M., Casar, B., Andres, V. and Crespo, P. (2010) ERK1/2 MAP kinases promote cell cycle entry by rapid, kinase-independent disruption of retinoblastoma-lamin A complexes. *J. Cell Biol.*, **191**, 967–979.
52. Randles, K.N., Lam, L.T., Sewry, C., Puckelwartz, M., Furling, D., Wehnert, M., McNally, E.M. and Morris, G.E. (2010) Nesprins, but not sun proteins, switch isoforms at the nuclear envelope during muscle development. *Dev. Dyn.*, **239**, 998–1009.
53. Holt, I., Duong, N.T., Zhang, Q., Lam le, T., Sewry, C.A., Mamchaoui, K., Shanahan, C.M. and Morris, G.E. (2016) Specific localization of nesprin-1-alpha2, the short isoform of nesprin-1 with a KASH domain, in developing, fetal and regenerating muscle, using a new monoclonal antibody. *BMC Cell Biol.*, **17**, 26.
54. Yun, K. and Wold, B. (1996) Skeletal muscle determination and differentiation: story of a core regulatory network and its context. *Curr. Opin. Cell Biol.*, **8**, 877–889.
55. Hindi, S.M., Tajrishi, M.M. and Kumar, A. (2013) Signaling mechanisms in mammalian myoblast fusion. *Sci. Signal.*, **6**, re2.
56. Krauss, R.S., Cole, F., Gaio, U., Takaesu, G., Zhang, W. and Kang, J.S. (2005) Close encounters: regulation of vertebrate skeletal myogenesis by cell-cell contact. *J. Cell Sci.*, **118**, 2355–2362.
57. Favreau, C., Delbarre, E., Courvalin, J.C. and Buendia, B. (2008) Differentiation of C2C12 myoblasts expressing lamin A mutated at a site responsible for Emery-Dreifuss muscular dystrophy is improved by inhibition of the MEK-ERK pathway and stimulation of the PI3-kinase pathway. *Exp. Cell Res.*, **314**, 1392–1405.
58. Kosak, S.T., Skok, J.A., Medina, K.L., Riblet, R., Le Beau, M.M., Fisher, A.G. and Singh, H. (2002) Subnuclear compartmentalization of immunoglobulin loci during lymphocyte development. *Science*, **296**, 158–162.
59. Jevsek, M. and Burden, S.J. (2006) Microarray screen for synaptic genes in the neuromuscular junction. *J. Mol. Neurosci.*, **30**, 29–30.
60. Gundersen, G.G. and Worman, H.J. (2013) Nuclear positioning. *Cell*, **152**, 1376–1389.
61. Chang, W., Antoku, S., Ostlund, C., Worman, H.J. and Gundersen, G.G. (2015) Linker of nucleoskeleton and cytoskeleton (LINC) complex-mediated actin-dependent nuclear positioning orients centrosomes in migrating myoblasts. *Nucleus (Calcutta)*, **6**, 77–88.
62. Zhang, J., Felder, A., Liu, Y., Guo, L.T., Lange, S., Dalton, N.D., Gu, Y., Peterson, K.L., Mizisin, A.P., Shelton, G.D., *et al.* (2010) Nesprin 1 is critical for nuclear positioning and anchorage. *Hum. Mol. Genet.*, **19**, 329–341.
63. Lei, K., Zhang, X., Ding, X., Guo, X., Chen, M., Zhu, B., Xu, T., Zhuang, Y., Xu, R. and Han, M. (2009) SUN1 and SUN2 play critical but partially redundant roles in anchoring nuclei in skeletal muscle cells in mice. *Proc. Natl. Acad. Sci. U. S. A.*, **106**, 10207–10212.

Downloaded from https://academic.oup.com/hmg/article-abstract/26/12/2258/3111721
by King's College London user
on 07 December 2017

64. Apel, E.D., Lewis, R.M., Grady, R.M. and Sanes, J.R. (2000) Syne-1, a dystrophin- and Klarsicht-related protein associated with synaptic nuclei at the neuromuscular junction. *J. Biol. Chem.*, **275**, 31986–31995.
65. Bruusgaard, J.C., Liestol, K., Ekmark, M., Kollstad, K. and Gundersen, K. (2003) Number and spatial distribution of nuclei in the muscle fibres of normal mice studied in vivo. *J. Physiol.*, **551**, 467–478.
66. Scharner, J., Brown, C.A., Bower, M., Iannaccone, S.T., Khatri, I.A., Escolar, D., Gordon, E., Felice, K., Crowe, C.A., Grosmann, C., *et al.* (2011) Novel LMNA mutations in patients with Emery-Dreifuss muscular dystrophy and functional characterization of four LMNA mutations. *Hum. Mutat.*, **32**, 152–167.
67. Haque, F., Mazzeo, D., Patel, J.T., Smallwood, D.T., Ellis, J.A., Shanahan, C.M. and Shackleton, S. (2010) Mammalian SUN protein interaction networks at the inner nuclear membrane and their role in laminopathy disease processes. *J. Biol. Chem.*, **285**, 3487–3498.
68. Cobb, A.M., Larrieu, D., Warren, D.T., Liu, Y., Srivastava, S., Smith, A.J., Bowater, R.P., Jackson, S.P. and Shanahan, C.M. (2016) Prelamin A impairs 53BP1 nuclear entry by mislocalizing NUP153 and disrupting the Ran gradient. *Aging Cell*, **15**, 1039–1050.
69. Wheeler, M.A., Warley, A., Roberts, R.G., Ehler, E. and Ellis, J.A. (2010) Identification of an emerin-beta-catenin complex in the heart important for intercalated disc architecture and beta-catenin localisation. *Cell. Mol. Life Sci.*, **67**, 781–796.
70. Warren, D.T., Tajsic, T., Mellad, J., Searles, R., Zhang, Q. and Shanahan, C.M. (2010) Novel nuclear nesprin-2 variants tether active extracellular signal-regulated MAPK1 and MAPK2 at promyelocytic leukemia protein nuclear bodies and act to regulate smooth muscle cell proliferation. *J. Biol. Chem.*, **285**, 1311–1320.
71. Westerfield, M. (2000) *The Zebrafish Book. A Guide for the Laboratory Use of Zebrafish (Danio rerio)*. University of Oregon Press, Eugene.
72. Kimmel, C.B., Ballard, W.W., Kimmel, S.R., Ullmann, B. and Schilling, T.F. (1995) Stages of embryonic development of the zebrafish. *Dev. Dyn.*, **203**, 253–310.
73. Thisse, C. and Thisse, B. (2008) High-resolution in situ hybridization to whole-mount zebrafish embryos. *Nat. Protoc.*, **3**, 59–69.
74. Sun, H., Li, D., Chen, S., Liu, Y., Liao, X., Deng, W., Li, N., Zeng, M., Tao, D. and Ma, Y. (2010) Zili inhibits transforming growth factor-beta signaling by interacting with Smad4. *J. Biol. Chem.*, **285**, 4243–4250.

Downloaded from https://academic.oup.com/hmg/article-abstract/26/12/2258/3111721
by King's College London user
on 07 December 2017

Appendix VI: N-terminal nesprin-2 variants regulate β-catenin signalling

Experimental Cell Research 345 (2016) 168–179

Contents lists available at ScienceDirect

Experimental Cell Research

journal homepage: www.elsevier.com/locate/yexcr

Research Article

N-terminal nesprin-2 variants regulate β-catenin signalling

Qiuping Zhang, Rose-Marie Minaisah, Elisa Ferraro, Chen Li, Lauren J. Porter, Can Zhou, Fang Gao, Junyi Zhang, Dipen Rajgor, Flavia Autore, Catherine M. Shanahan, Derek T. Warren *

British Heart Foundation Centre of Research Excellence, Cardiovascular Division, King's College, SE5 9NU London, UK

ARTICLE INFO

Article history:
Received 19 October 2015
Received in revised form
13 June 2016
Accepted 14 June 2016
Available online 16 June 2016

Keywords:
Nesprin-2
B-catenin
Cell-cell junctions
Scaffold protein

ABSTRACT

The spatial compartmentalisation of biochemical signalling pathways is essential for cell function. Nesprins are a multi-isomeric family of proteins that have emerged as signalling scaffolds, herein, we investigate the localisation and function of novel nesprin-2 N-terminal variants. We show that these nesprin-2 variants display cell specific distribution and reside in both the cytoplasm and nucleus. Immunofluorescence microscopy revealed that nesprin-2 N-terminal variants colocalised with β-catenin at cell-cell junctions in U2OS cells. Calcium switch assays demonstrated that nesprin-2 and β-catenin are lost from cell-cell junctions in low calcium conditions whereas emerin localisation at the NE remained unaltered, furthermore, an N-terminal fragment of nesprin-2 was sufficient for cell-cell junction localisation and interacted with β-catenin. Disruption of these N-terminal nesprin-2 variants, using siRNA depletion resulted in loss of β-catenin from cell-cell junctions, nuclear accumulation of active β-catenin and augmented β-catenin transcriptional activity. Importantly, we show that U2OS cells lack nesprin-2 giant, suggesting that the N-terminal nesprin-2 variants regulate β-catenin signalling independently of the NE. Together, these data identify N-terminal nesprin-2 variants as novel regulators of β-catenin signalling that tether β-catenin to cell-cell contacts to inhibit β-catenin transcriptional activity.

© 2016 The Authors. Published by Elsevier Inc. This is an open access article under the CC BY license (http://creativecommons.org/licenses/by/4.0/).

1. Introduction

Nesprins are a family of spectrin repeat containing proteins that are encoded by four genes (*SYNE1-4*) [1–4]. Nesprins-1 and -2 are highly complex and multiple variants arise due to alternative initiation and termination of the genes [5]. The giant nesprin-1 and -2 variants consist of an N-terminal paired calponin homology domain (CHD) that has been shown to bind filamentous actin (F-actin), a central rod region composed of numerous spectrin repeats and a C-terminal Klarsicht, ANC-1, SYNE Homology (KASH) domain that is required for the nuclear envelope (NE) localisation of these proteins [4,6,7]. To date, the best studied function of these proteins is at the NE, where smaller variants function to organise the inner nuclear membrane (INM) via interactions with lamins A/C and emerin [6,8], whereas the nesprin giant variants reside on the outer nuclear membrane (ONM) and are components of the LInker of Nucleoskeleton to Cytoskeleton (LINC) complex. The LINC complex physically couples the ONM to the INM via interactions between the KASH domain of nesprins and the SUN domain of SUN1/2 in the perinuclear space [9,10]. SUN1/2 span the INM and interact with lamins A/C [11,12], thus forming a continuous biophysical network between the cytoskeleton and nucleoskeleton [10–12]. In addition to the giant nesprin-1 and -2 isoforms, nesprin variants that lack the KASH domain have been shown to localise to the cytoplasm and nucleoplasm [5,13–15]. Although the functions of these KASH-less variants remain to be fully defined, they show tissue and cell specific expression patterns, suggesting nesprins are tailored for specific cellular functions.

Nesprins are comprised of multiple spectrin repeats that are proposed to mediate protein-protein interactions, however, our knowledge of nesprin binding partners remains limited [16]. At the INM, nesprin variants interact with lamins A/C, SUN1/2 and emerin [6,12]. Mutations in these nesprin variants result in emerin mislocalisation, nuclear morphology defects and are associated with Emery–Dreifuss muscular dystrophy (EDMD), suggesting that nesprins perform a scaffolding role at the NE [1]. KASH-less variants also perform a scaffolding role in the nuclear interior and we have previously identified nesprin-2 as a nuclear ERK scaffold that

Abbreviations: NE, nuclear envelope; ONM, outer nuclear membrane; INM, inner nuclear membrane; F-actin, filamentous actin; EDMD, Emery–Dreifuss muscular dystrophy; CHD, calponin homology domain; SR, spectrin repeat; LINC, Linker of nucleoskeleton and cytoskeleton; WB, Western blot; IF, immunofluorescence microscopy; IP, immunoprecipitation; ESC, embryonic stem cells; VSMC, human vascular smooth muscle cell; HDF, human dermal fibroblast cell; HUVEC, human umbilical vein endothelial cells

* Correspondence to: Kings College London, Division of Cardiovascular Medicine, James Black Centre, 125 Coldharbour Lane, London SE5 9NU, UK.
E-mail address: derek.warren@kcl.ac.uk (D.T. Warren).

http://dx.doi.org/10.1016/j.yexcr.2016.06.008
0014-4827/© 2016 The Authors. Published by Elsevier Inc. This is an open access article under the CC BY license (http://creativecommons.org/licenses/by/4.0/).

tethers ERK1/2 at promyelocytic leukaemia nuclear bodies to regulate proliferation [14]. Importantly, several cytoplasmic binding partners have also been identified for nesprin-1 and -2 including the RNA binding proteins Dcp1a, Rck and Ago2, and meckelin, respectively [13,17]. Moreover, nesprin-1 and -2 KASH-less variants localise to focal adhesions and actin/microtubule filaments, suggesting that the cytoplasmic KASH-less variants may perform a similar scaffolding role [5,13]. Nesprin-2 has also been implicated in the WNT pathway that transfers signals from the plasma membrane to the nucleus via nuclear translocation of the transcription factor β-catenin [18–21]. Both α- and β-catenin interact with spectrin repeats (SRs) toward the C-terminus of nesprin-2 giant to attenuate β-catenin signalling [22]. In addition to this direct interaction, nesprin-2 may also indirectly associate with β-catenin at the INM, where the nesprin-2 binding protein emerin interacts with β-catenin to facilitate its nuclear export [23].

In this study we investigate the role of recently identified N-terminal nesprin-2 variants that retain the CHD but lack the KASH domain. We show that these variants are novel components of cell-cell junctions, where they colocalise and interact with β-catenin. Importantly, these nesprin-2 variants anchor β-catenin to cell-cell junctions to negatively regulate β-catenin mediated transcriptional activity.

2. Materials and methods

2.1. Cell culture

Human bone osteosarcoma epithelial (U2OS), human umbilical vein endothelial cells (HUVEC), mouse C2C12 myoblast, human dermal fibroblast and human vascular smooth muscle cells were cultured as described previously [24,25]. The following nesprin-2 siRNA oligomers targeting the N-terminus of the giant variant were used in this study: siN2CH2 (5′ AGGAAGACACCCAGAAGUU 3′), siN2CH3 (5′ CUUCAGAAUUGCAGAACAAUU 3′), siN2CH5 (5′ GCCUUCACGUGCUGGAUAAUU 3′), p220CH^{Nesp2} 3′UTR1 (5′ GAGAAUAGUCUGUGGAGAAUU 3′), p220CH^{Nesp2} 3′UTR2 (5′ GGAACGUAGUGGAGGAUAUU 3′), p380CH^{Nesp2} 3′UTR1 (5′ AUCGAAAGCCAGAGAGUAAUU 3′) and p380CH^{Nesp2} 3′UTR2 (5′ AGUCAGAGGUCAACAACAAUU 3′) (Dharmacon). C-terminal nesprin-2 siRNA designed to a region close to the KASH domain (siN2KASH) have been described previously [14]. Emerin smart pool siRNA oligomers from Dharmacon were used in this study. Transfection of siRNA was performed using HiPerfect (Qiagen), as per manufacturer's instructions. DNA transfections of were performed with Fugene (Promega) as per manufacturer's instructions.

2.2. PCR and 3′UTR amplification

PCR for N-terminal nesprin-2 3′UTRs were performed using 3′ UTR specific primer sets as described previously [5].

2.3. Nesprin constructs

The following N-terminal nesprin-2 fragments were cloned into pEGFP-C1 vector (Clontech): ABDN2 (amino acids 1-531). The CHDN2 (amino acids 1-278) fragment was cloned into the pCMV-Tag vector (Agilent Technologies). The SR 1-3 region (amino acids 279-531) was cloned into the pGEX4T-1 (Amersham) and pCMV-Tag (Agilent Technologies) vectors.

2.4. Calcium switch assay

Cells were grown to 80–100% confluency and serum starved overnight. Next day, cells were incubated with 4 mM EGTA in calcium free media for 1 h to promote cadherin mediated cell-cell junction disassembly. Junction re-assembly was promoted by incubating cells in media containing 1.8 mM calcium for 1 h. Cells were fixed and processed for immunofluorescence microscopy.

2.5. Western blot analysis, antibodies and immunofluorescence microscopy

Cell lysates were run on 5% or 8% polyacrylamide gels and subjected to Western blotting as described previously [6]. Antibodies used for Western blot, confocal immunofluorescence microscopy (IF) and immunoprecipitation were; GFP (ab290), GFP-Sepharose (ab69314) (Abcam), Vinculin (Sigma), Emerin (VP-E602) (Vector Labs), lamin A/C (sc-6215) (Santa Cruz), total β-catenin, active β-catenin clone 8E7 (05-665) (Millipore), nesprin-2 CH3 and nesprin-2 N3 (Immune Systems). N2CH3 peptide blocking experiments were performed as described previously using the peptide KRDLDELKDHLQL (Immune Systems) [6]. Filamentous actin was observed by IF using Rhodamine phalloidin (Invitrogen). Secondary antibodies for WB were horseradish peroxidase-conjugated anti mouse (NA931) or anti rabbit (NA94V) antibodies from GE Healthcare. ECL chemiluminescent kit (RPN2132, GE Healthcare) was used for detection according to manufacturer's instructions. Invitrogen anti-mouse Alexa fluor 568 (A11031) and anti-rabbit Alexa fluor 488 (A11034) were used as IF secondary antibodies. For IF cells were cultured on cover slips, fixed in 4% paraformaldehyde (Sigma), permeabilised in 0.5% NP-40 (Sigma) and processed as described previously [6]. All images were captured at 63 × magnifications using a Leica SP5 laser scanning confocal microscope.

2.6. Immunoprecipitation, GST pull-downs and subcellular fractionations

Subcellular fractionations were performed as described previously [14]. GST expression, purification and pull-down assays were performed as described previously [14]. For immunoprecipitation (IP), U2OS cells were transfected with either GFP or GFP-ABDN2 and incubated overnight. Cells were processed for IP as described previously [14]. GFP was immunoprecipitated by incubating with anti-GFP coated Sepharose beads for 2 h at 4 °C. Beads were washed three times in IP buffer before bound proteins were eluted in sample buffer, as described previously [14]. Coomassie staining was performed using the Bio-Safe™ Coomassie stain (BIORAD) as per manufacturer's instructions.

2.7. Luciferase assays

U2OS cells were seeded onto a 6 well plate at a density of 2.5×10^5 cells per well. Next day cells were transfected with mixtures of 1 μg TOP-FLASH or FOP-FLASH, 0.1 μg TK Renilla and 1 μg of GFP, GFP-ABDN2, FLAG or FLAG-SR 1-3 using Fugene (Promega). Cells were incubated overnight. For analysis of siRNA on transcriptional activity the TOP-FLASH or FOP-FLASH and TK Renilla mix was added directly to siRNA transfection mixture containing HiPerfect (Qiagen). Cells were incubated for 48 h. Luciferase and Renilla activities were assayed using the Dual-Glo® Luciferase assay system (Promega) as per manufacturer's instructions. Control Luciferase activities were assigned a value of 1.

2.8. Statistical analysis

Results are presented as mean +/− SEM. For comparison of siRNA knockdown groups paired Student's *t*-tests or one way ANOVA with Bonferroni's post-test were performed.

3. Results

3.1. Cell specific distribution of nesprin-2 variants

Recently, 3′UTRs encoding KASH-less N-terminal nesprin-2 variants (p220CH^{Nesp2} and p380CH^{Nesp2}) were identified by EST data base searches (Fig. 1A). These 3′UTRs display tissue specific expression patterns [5]. To describe the cell specificity of these 3′ UTRs, we performed PCR analysis and we show that p220CH^{Nesp2} is abundant in human bone osteosarcoma epithelial (U2OS) and

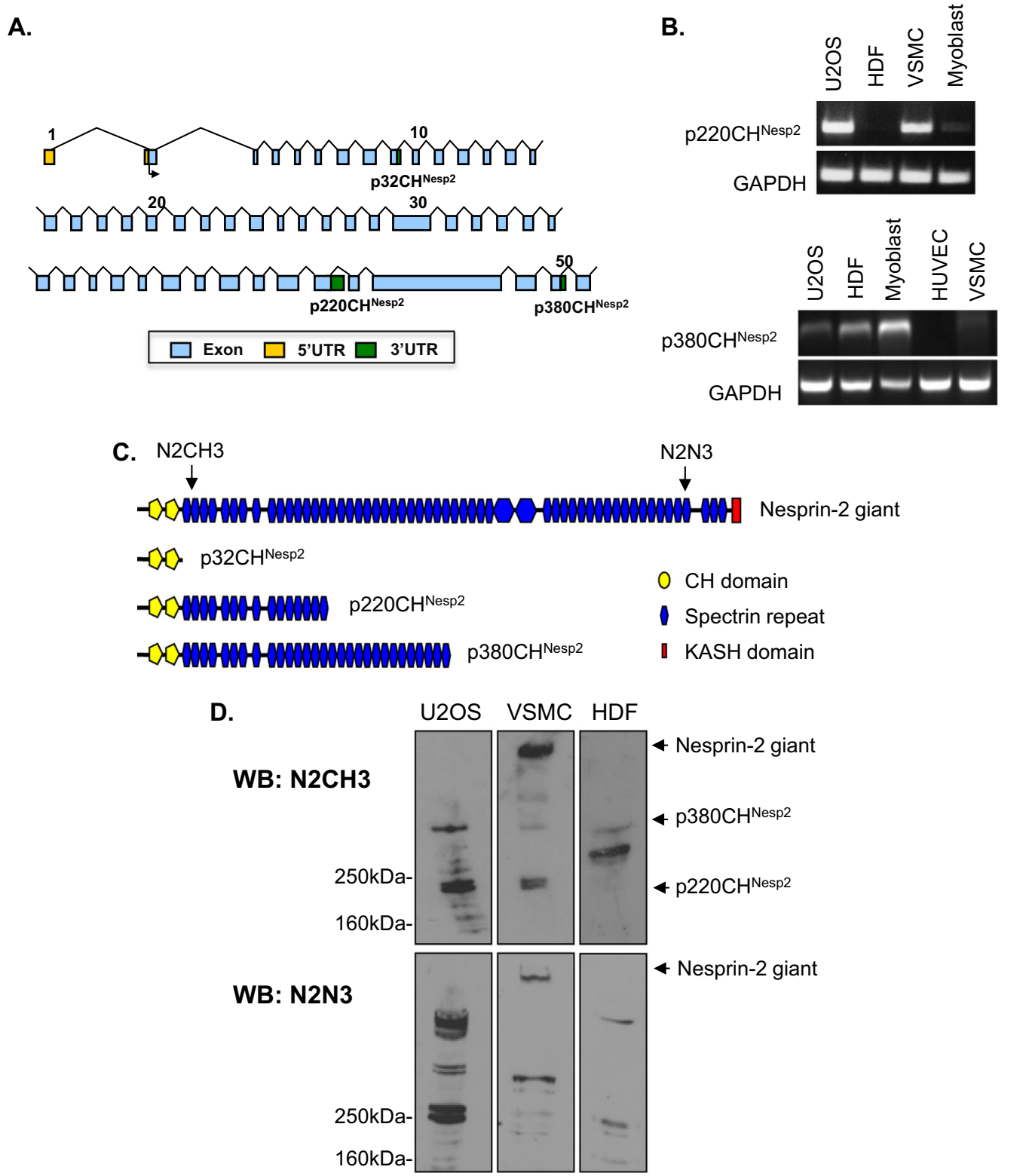


Fig. 1. Cell type specific expression of N-terminal nesprin-2 variants. A) Schematic representation of the genomic organisation of 5′ and 3′ UTRs encoding the N-terminal variants of nesprin-2 N-terminus. B) PCR analysis of cDNA derived from U2OS, dermal fibroblast (HDF), vascular smooth muscle (VSMC), C2C12 myoblast and human umbilical vein endothelial (HUVEC) cells for p220CH^{Nesp2} and p380CH^{Nesp2} 3′UTRs. C) Schematic representation of nesprin-2 N-terminal variant structure and N-terminal (N2CH3) and C-terminal (N2N3) nesprin-2 antibody epitope regions. D) WB of U2OS, VSMC and HDF whole cell lysates separated on 5% polyacrylamide gels.

vascular smooth muscle cells (VSMC) but absent in human dermal fibroblast (HDF) and mouse C2C12 myoblast cells. The p380CH^{Nesp2} variant was abundant in U2OS, HDF and myoblast cells, but lacking in human umbilical vein endothelial cells (HUVEC) and VSMCs (Fig. 1B). Western blot analysis (WB) was performed on whole cell lysates using an antibody raised to the N-terminus of the nesprin-2 giant (N2CH3) (Fig. 1C). To confirm the specificity of the N2CH3 antibody we performed peptide blocking experiments and show that the activity of the antibody is efficiently blocked by the target sequence on WB (Supplementary Fig. 1A). In agreement with the PCR data, we show that U2OS cells possess both the p220CH^{Nesp2} and p380CH^{Nesp2} variants whereas VSMCs and HDFs possess either the p220CH^{Nesp2} or p380CH^{Nesp2} variant, respectively (Fig. 1D). Importantly, using the N2CH3 antibody and a C-terminal nesprin-2 antibody (N2N3) we show that the nesprin-2 giant is highly abundant in VSMCs but was not detectable in U2OS and HDF cells tested (Fig. 1C and D). As previous studies have shown that the nesprin-2 giant is present in HDF cells at low levels, we performed subcellular fractionation experiments to concentrate the nuclear proteins [26]. WB revealed that nesprin-2 giant was weakly present in HDF nuclear fractions. Importantly, nesprin-2 giant was not detected in U2OS nuclear fractions, further confirming that U2OS cells lack nesprin-2 giant (Supplementary Fig. 1B).

Subcellular fractionation of U2OS cells demonstrated that p220CH^{Nesp2} and p380CH^{Nesp2} reside in both the cytoplasmic and nuclear fractions (Fig. 2A). In addition, smaller unknown nesprin-2 bands were observed in the cytoplasmic (55 kDa) and nuclear (60 and 70 kDa) fractions (Fig. 2A). The p220CH^{Nesp2} variant was also detected in both nuclear and cytoplasmic fractions in VSMCs (Fig. 2B), however, the p380CH^{Nesp2} variant was nuclear in HDF cells (Fig. 2C). In all cell types tested, unknown variants were detected, suggesting that our knowledge of nesprin-2 variants remains incomplete (Fig. 2A–C).

3.2. *Nesprin-2 variants localise to cell-cell junctions and interact with β-catenin*

Next, we employed confocal fluorescence microscopy (IF) to investigate the cellular localisations of these variants. IF demonstrated that the nesprin-2 antibody raised to the N-terminus of nesprin-2 giant (N2CH3) diffusely stained within the nucleus and at the sites of cell-cell contact at the cell periphery, where nesprin-2 colocalised with active β-catenin in U2OS cells (Fig. 3A and B). In contrast, no colocalisation with β-catenin was observed in HDF cells (Supplementary Fig. 2). To investigate the significance of nesprin-2 localisation at cell-cell contacts further, U2OS cells were grown in high or low calcium conditions to promote or inhibit cadherin mediated cell junction formation respectively. IF revealed that, U2OS cells in the presence of high calcium, displayed colocalisation of nesprin-2 and active β-catenin at cell-cell junctions, however, localisation of both nesprin-2 and β-catenin is rapidly lost from the plasma membrane when cells were switched to low calcium conditions to promote cadherin disassembly (Fig. 3B). Localisation of nesprin-2 and β-catenin at cell-cell contacts was rescued by replenishing calcium levels (Fig. 3B).

To further interrogate the localisation of nesprin-2 variants that retain the CHD but lack the KASH domain, we employed an overexpression strategy using an N-terminal nesprin-2 construct that possessed the CHD and the antibody binding region (amino acids 1-531) (Fig. 3A). IF demonstrated that the N-terminal fragment (GFP-ABDN2) colocalised efficiently with active β-catenin at cell-cell junctions in U2OS (Fig. 3C, left panel) and HDFs (Fig. 3C, right panel). Importantly a similar fragment of nesprin-1 failed to localise to cell-cell junctions and was predominantly nuclear, suggesting that cell-cell junction localisation is specific for nesprin-2 (Supplementary Fig. 3). To further define the requirements for cell-cell junction localisation, we next expressed the CHD region (amino acids 1-279) of nesprin-2. IF revealed that the CHD localised to cell-cell junctions, although some stress fibre staining was also observed (Fig. 3C).

Next, we investigated whether nesprin-2 interacted with β-catenin by performing immunoprecipitation experiments. WB revealed that β-catenin was precipitated by the GFP-ABDN2 fragment but not GFP-alone (Fig. 4A and B). Conversely, the GFP-ABDN2 fragment was efficiently precipitated by β-catenin IP, confirming the nesprin-2 is a novel β-catenin interacting protein (Fig. 4C). Next, we mapped the β-catenin binding site by fusing the SR region of the ABDN2 construct (SR 1-3 containing amino acids 278-531) to GST (Fig. 4A). GST pull down assays confirmed that β-catenin was precipitated by GST-SR 1-3, but not GST alone (Fig. 4D), confirming that this spectrin repeat region interacts with β-catenin.

3.3. *Nesprin-2 disruption induces cell-cell junction disassembly and augments β-catenin transcriptional activity*

We next investigated the impact of nesprin-2 disruption on β-catenin localisation by utilising a siRNA mediated knockdown

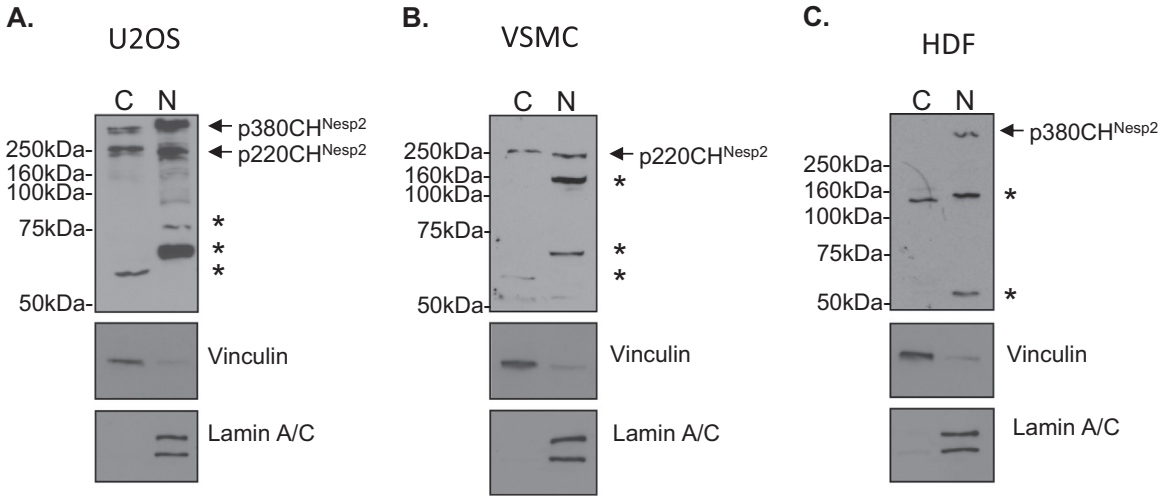


Fig. 2. N-terminal nesprin-2 variants reside in the cytoplasm and nucleus. WB of U2OS, VSMC and HDF of cytoplasmic (C) and nuclear (N) fractions separated on 8% polyacrylamide gels. * mark unidentified nesprin variant bands.

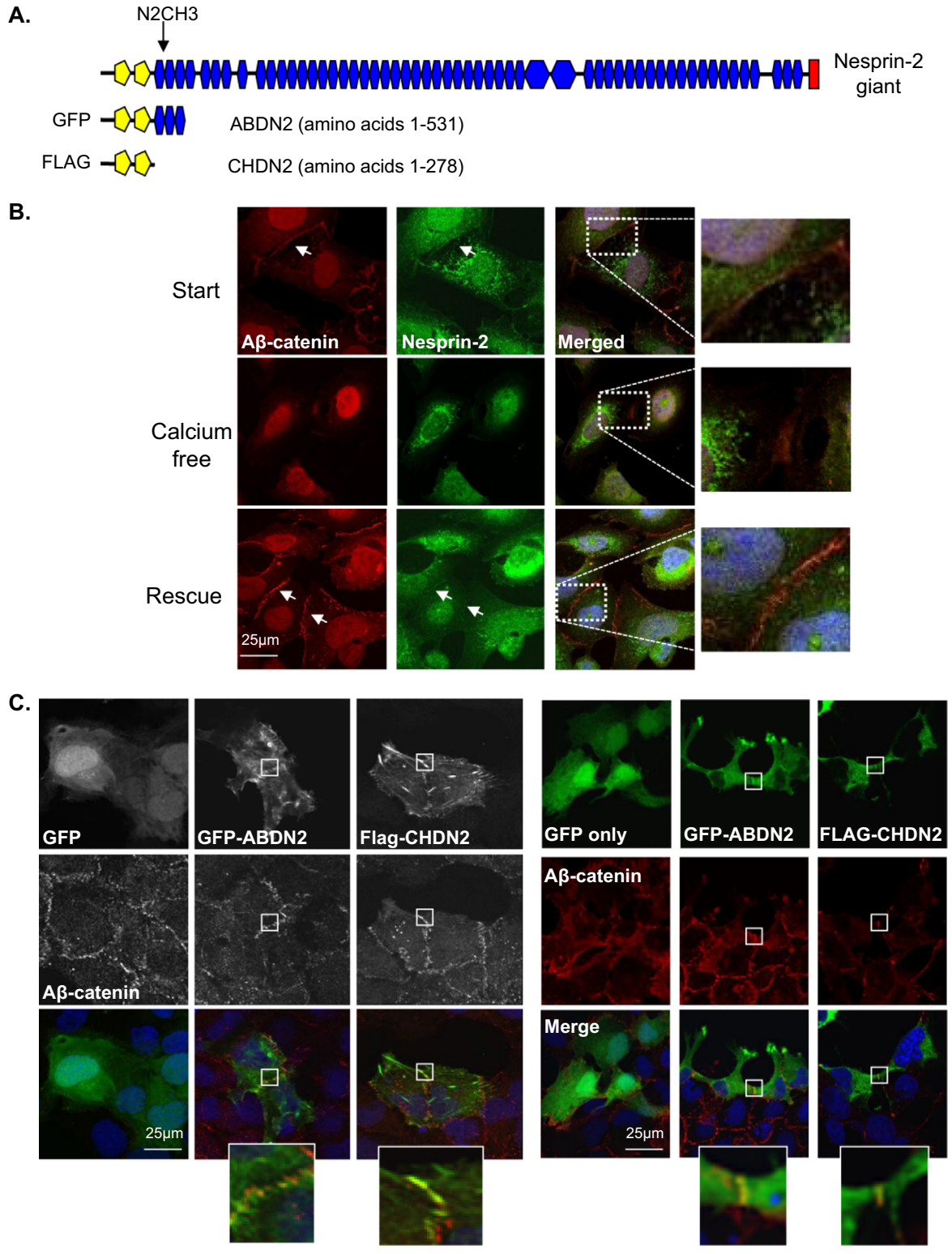


Fig. 3. N-terminal nesprin-2 variants colocalise with β-catenin at cell-cell junctions. A) Schematic representation of nesprin-2 CH3 antibody epitope position and nesprin-2 constructs used. B) IF of nesprin-2 (CH3) (green), active β-catenin (Aβ-catenin) (red) and DAPI (blue) localisation in U2OS cells before, during and after calcium depletion. C) IF of GFP-ABDN2, Flag-CHDN2 (green) and active β-catenin (Aβ-catenin) (red) in U2OS (left panel) and fibroblast cells (right panel). Scale bar = 25 μm.

strategy that targeted nesprin-2 variants containing the CHDs. U2OS cells were transfected with either control or nesprin-2 specific siRNA that targeted the N-terminus of p220CH^{Neps2} and p380CH^{Nesp2} (Fig. 5A). WB analysis confirmed knockdown of p220CH^{Nesp2} using 3 independent nesprin-2 specific siRNAs (Fig. 5B and C). Levels of the p380CH^{Nesp2} variant remained unaltered by our siRNA strategy (Fig. 5B and D), suggesting that p380CH^{Nesp2} is more stable than p220CH^{Nesp2}. WB also revealed that protein levels of C-terminal variants that lack the siRNA target sequence remain unaltered (Fig. 5B). Importantly, levels of active β-catenin and total β-catenin remained unaltered by our nesprin-2 depletion strategy (Fig. 5B). To specifically target the p220CH^{Nesp2}

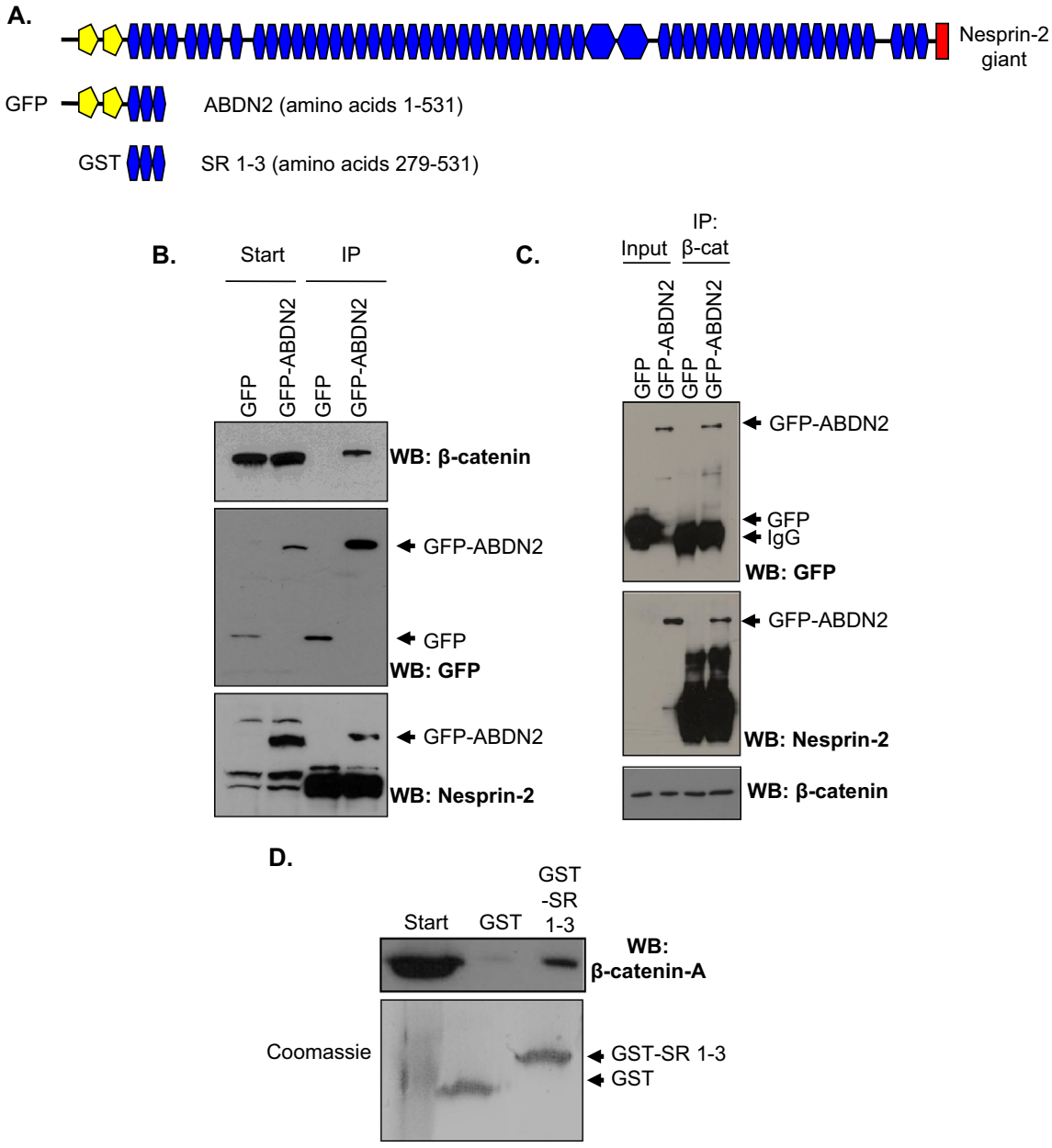


Fig. 4. The N-terminus of nesprin-2 interacts with β-catenin. A) Schematic representation of the nesprin-2 constructs used. B) WB of GFP/GFP-ABDN2 immunoprecipitation. C) WB of β-catenin IP. D) WB of GST-alone and GST-SR 1-3 construct pull downs. GST-loading was shown by coomassie stain.

and p380CH^{Nesp2} variants we designed siRNAs targeting the unique 3′UTRs, however, WB revealed that this strategy was unsuccessful and failed to deplete the p220CH^{Nesp2} and p380CH^{Nesp2} variants (Supplementary Fig. 4).

IF was performed to observe whether nesprin-2 depletion altered β-catenin organisation in U2OS cells and revealed that nesprin-2 depleted cells displayed reduced staining of active β-catenin at cell-cell junctions compared to control cells (Fig. 6A and B and Supplementary Fig. 5A), suggesting that the p220CH^{Nesp2} variant tethers active β-catenin to the sites of cell-cell contact. Importantly, subcellular fractionation revealed that nesprin-2 depleted cells displayed increased levels of nuclear active β-catenin (Fig. 6C) and TOP-FLASH/FOP-FLASH luciferase assays confirmed that nesprin-2 depleted cells possessed augmented β-catenin transcriptional activity compared to control cells (Fig. 6D). In contrast, siRNAs targeting the C-terminus of nesprin-2 giant that the p380CH^{Nesp2} and p220CH^{Nesp2} variants lack, failed to alter luciferase activity (Fig. 6A and D), supporting the notion that N-terminal variants are responsible for localising β-catenin to cell-cell junctions. Next, we assessed the impact of overexpression of the β-catenin binding fragments of the N-terminal nesprin-2 variants on β-catenin signalling. However, TOP-FLASH/FOP-FLASH luciferase assays revealed that the β-catenin binding fragments had no impact on β-catenin transcriptional activity (Supplementary Fig. 5B).

3.4. *β-catenin localisation at cell-cell junctions is independent of emerin*

Previous studies have shown that nesprin disruption triggers nuclear morphology defects, so we next performed IF to observe if our siRNA strategy altered nuclear morphology. Analysis revealed that control cells contained spherical nuclei, however, nesprin-2 depleted nuclei possessed a more convoluted morphology (Fig. 7A and B). Next, we performed IF to observe the localisation of the nesprin-2 interacting protein emerin and show that nesprin-2

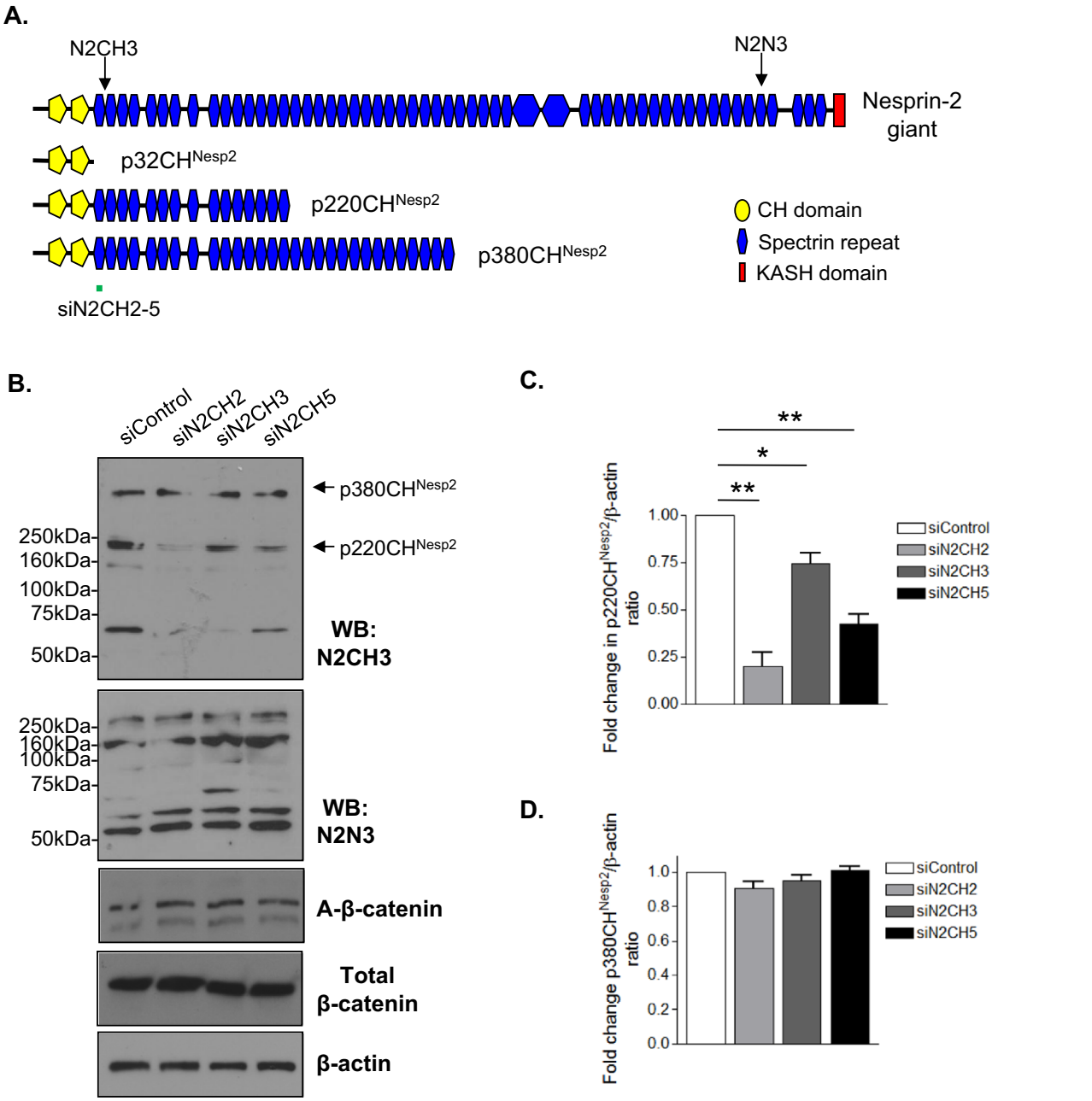


Fig. 5. Validation of nesprin-2 depletion strategy. A) Schematic representation of nesprin-2 CH3 and N3 antibody epitopes and the region targeted by siRNA siN2CH2–5. B) WB of N-terminal (N2CH3) and C-terminal (N2N3) variants after control and nesprin-2 (siN2CH2/CH3/CH4) siRNA knockdown. Samples were separated on 8% polyacrylamide gels. Graphs show relative level of C) p220CH^{Nesp2} and D) p380CH^{Nesp2}. Graphs represent combined data from 3 independent siRNA experiments for fold change in densitometry ratio ($^{*}p = < 0.05$, $^{**}p = < 0.001$).

depleted cells display normal NE emerin staining (Fig. 7C). As emerin has previously been implicated in β-catenin signalling, we further investigated whether changes in β-catenin signalling were due to impaired emerin function by performing emerin knockdown experiments. WB confirmed efficient emerin depletion in U2OS cells (Fig. 8A), however, β-catenin organisation and transcriptional activity remained unaltered in emerin depleted cells (Fig. 8B and C).

4. Discussion

Nesprins have emerged as signalling scaffold proteins that localise to multiple subcellular compartments, including the NE, cytoplasm and nucleoplasm [5,6]. In this current study, we show that nesprin-2 N-terminal variants colocalise with β-catenin at cell-cell junctions. We show that a fragment containing the CHD and SR 1-3 region (ABDN2) was sufficient for both β-catenin binding and cell-cell junction localisation. Further mapping identified the N-terminal SRs 1-3 of nesprin-2 as a novel β-catenin binding region, although we did not rule out the possibility that the CHD and β-catenin also interact. We propose that the N-terminal nesprin-2 KASH-less variants tether β-catenin at cell-cell junctions and inhibit β-catenin transcriptional activity. In support of this notion, nesprin-2 depleted U2OS cells displayed loss of β-catenin from cell-cell contacts, accumulation of active β-catenin in the nucleus and augmented β-catenin transcriptional activity. Importantly, levels of active β-catenin remained

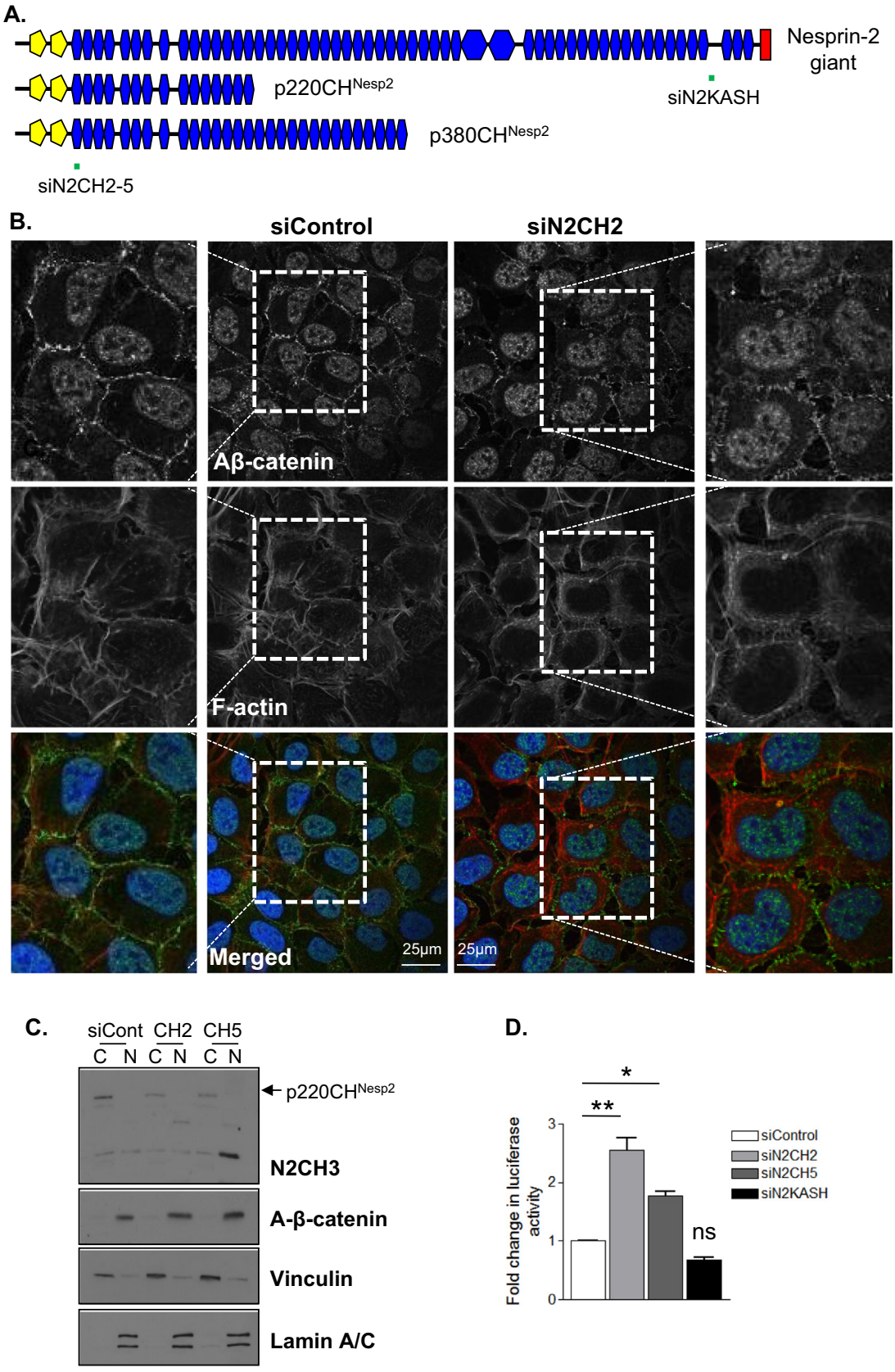


Fig. 6. Nesprin-2 is required for β-catenin localisation at cell-cell junctions and negatively regulates β-catenin transcriptional activity. A) Schematic representation of siN2CH2/siN2CH5 and siN2KASH target regions. B) IF of active β-catenin (Aβ-catenin) (green), F-actin (red) and DAPI (blue) in control and nesprin-2 (siN2CH2) depleted U2OS cells. Scale bar=25 μm. C) WB of control, siN2CH2 and siN2CH5 cytoplasmic (C) and nuclear (N) fractions. D) TOP/FOP Luciferase assay of control, siN2CH2, siN2CH5 and siN2KASH depleted cells. Graph shows combined data from 3 independent experiments repeated in triplicate ($^{*}p = < 0.05$, $^{**}p < 0.001$).

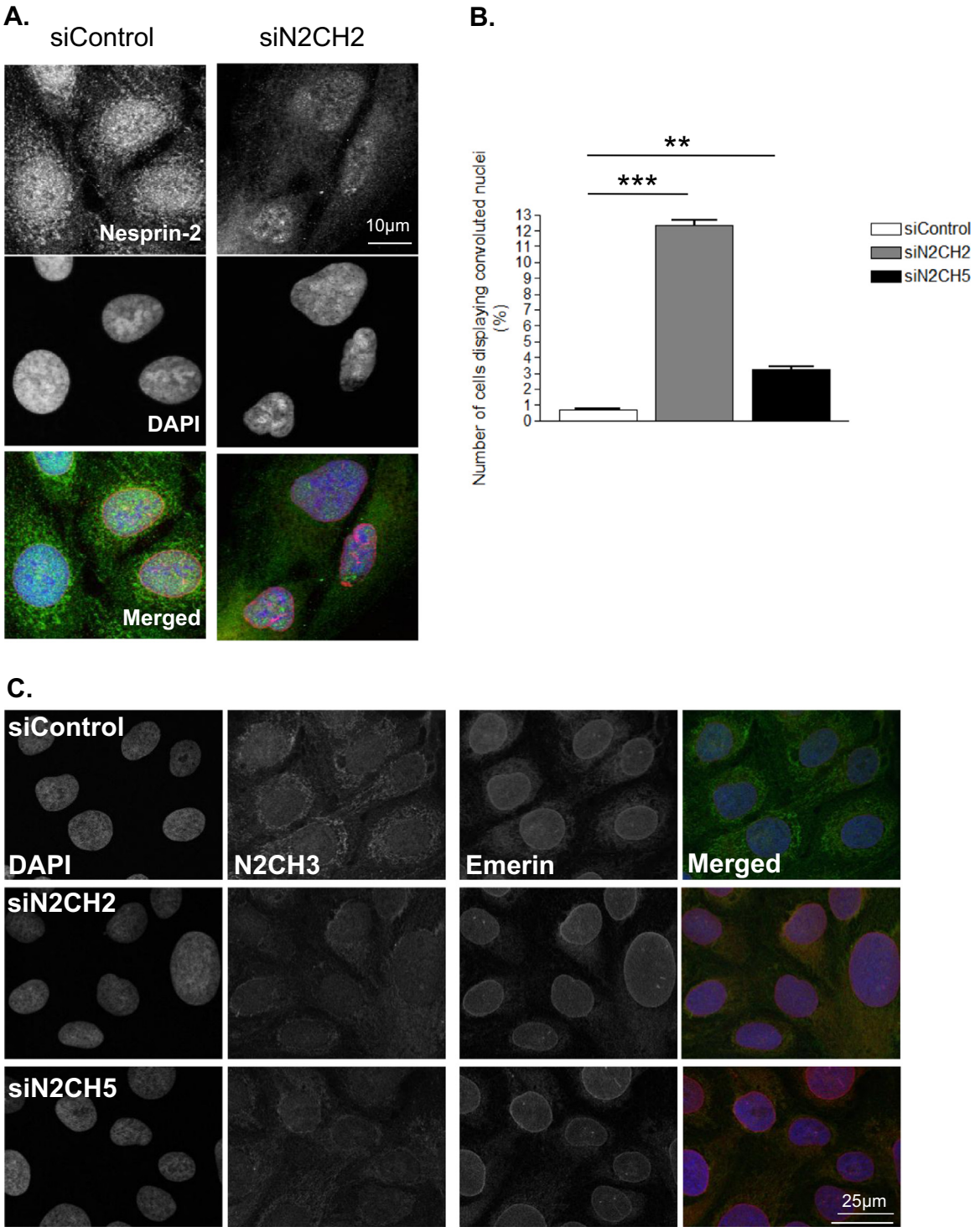


Fig. 7. Nesprin-2 disruption alters nuclear morphology but not emerin localisation. A) IF of nesprin-2 (green), emerin (red), and DAPI (blue) staining of control and nesprin-2 depleted cells. Scale bar = 10 μm. B) Quantification of number of control and nesprin-2 depleted (siN2CH2 and siN2CH5) cells displaying convoluted nuclei. Graph show combined data from 3 independent experiments counting 300 cells per group (**$p = < 0.001$ and ***$p = < 0.0001$). C) IF staining of DAPI (blue), N2CH3 (green) and emerin (red) in control and nesprin-2 depleted U2OS cells. Scale bar = 25 μm.

unchanged in nesprin-2 depleted U2OS cells, suggesting that nesprin-2 depletion triggers redistribution of active β-catenin from cell-cell contacts to the nucleus. Our overexpression experiments show that N-terminal CHD containing nesprin-2 fragments localise to cell-cell contacts, colocalise with active β-catenin but did not alter β-catenin transcriptional activity. N-terminal nesprin-2 fragments that lack the CHD but retain the β-catenin binding site also failed to alter β-catenin transcriptional activity. This suggests that the association between active β-catenin and the N-terminal nesprin-2 variants at cell-cell contacts is stable, further experimentation is required to elucidate the functions/dynamics of these N-terminal nesprin-2 variants at cell-cell contacts.

We also demonstrate that the p220CH^{Nesp2} and p380CH^{Nesp2} variants, that contain the β-catenin binding domain, reside in both

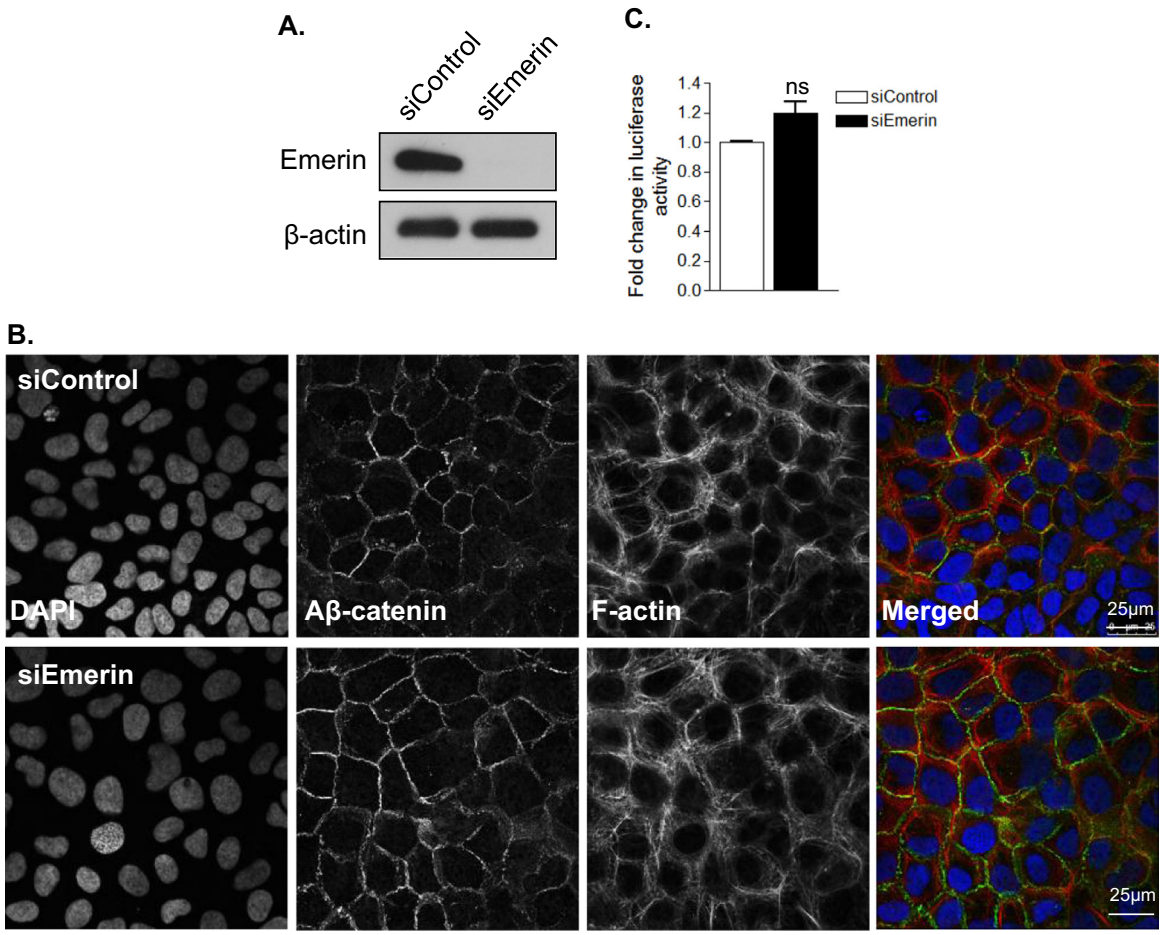


Fig. 8. Emerin disruption does not impact on β-catenin localisation. A) WB confirming emerin knockdown. B) IF of active β-catenin (Aβ-catenin) (green), F-actin (red) and DAPI (blue) in control and emerin depleted U2OS cells. Scale bar = 25 μm. C) TOP/FOP luciferase assay of control and emerin depleted cells. Graph shows combined data from 3 independent experiments repeated in triplicate.

the nucleus and cytoplasm, raising the intriguing possibility that these KASH-less variants may shuttle between these compartments. However, further investigation is now required to clarify whether KASH-less nesprin-2 variants associate with and organise other components of the β-catenin pathway, as well as to identify the exact nesprin-2 variant. Our knockdown strategy efficiently depleted p220CH^{Nesp2} but not p380CH^{Nesp2} and presumably these two variants display differences in protein turnover as both contain the target sequence. This suggests that p220CH^{Nesp2} is potentially a good candidate for future investigation however, our siRNA strategy targeted multiple nesprin-2 variants so the possibility remains that an unidentified variant may localise to cell-cell contacts and regulate β-catenin signalling.

4.1. N-terminal nesprin-2 variants regulate β-catenin signalling independently of the NE

Nesprin-2 variants organise the NE and several recent studies have identified the NE as a novel regulator of β-catenin signalling [22,23,30]. Firstly, β-catenin interacts with the C-terminus of the nesprin-2 giant to positively regulate β-catenin signalling [22]. In addition, the nesprin-1/2 orthologue ANC1 regulates β-catenin signalling during neuronal development in *Caenorhabditis elegans* [30]. Due to the sequence identity between nesprin-2 variants, our knockdown strategy potentially targeted both KASH-less N-terminal and the KASH-containing nesprin-2 giant variants [5]. Importantly, we show that U2OS cells lack nesprin-2 giant and β-catenin transcriptional activity was enhanced by N-terminal nesprin-2 depletion in U2OS cells. These data suggest that the N-terminal nesprin-2 variants negatively regulate β-catenin transcriptional activity in U2OS cells and highlight the complexity of nesprin-2 function in regulating β-catenin signalling. Previous studies have also demonstrated that emerin interacts with both the C-terminal nesprin-2 variants and β-catenin at the INM to negatively regulate β-catenin mediated transcription [23]. KASH-containing nesprin-2 variants are essential for emerin organisation at the NE [6], however, emerin organisation was unaltered by depletion of N-terminal nesprin-2 variants in U2OS cells, suggesting that changes in β-catenin signalling induced by our siRNA strategy were NE independent. Furthermore, emerin depletion in U2OS cells failed to displace β-catenin from cell-cell junctions or alter β-catenin transcriptional activity, further suggesting that the N-terminal nesprin-2 variants regulate β-catenin signalling independently of the NE.

Despite our evidence showing that nuclear envelope function is not disrupted by our nesprin-2 siRNA strategy, nuclear morphology was altered by our approach. Previous studies have demonstrated that actomyosin, cell morphology and adhesion all contribute to defining nuclear morphology and potentially, in addition to disrupting cell-cell contacts, our nesprin-2 depletion strategy induced cytoskeletal reorganisation that altered nuclear morphology [27,28]. However, the potential role of the nesprin-2 N-terminal variants in cytoskeletal organisation remains untested.

4.2. Nesprin-2 variants fine tune β-catenin signalling for cell specific functions?

Nesprin variants demonstrate complex tissue and cell-specific distributions [5,29]. Nesprin giant variant expression is abundant in the majority of human tissues, except cardiac and skeletal muscle, which are enriched in shorter isoforms [29]. In addition, the nesprin-2 epsilon-1 and epsilon-2 variants are highly expressed in embryonic stem cells (ESC) and heart respectively [29]. Here, we confirm that the p220CH^{Nesp2} and p380CH^{Nesp2} variants display cell-specific expression, suggesting that nesprin function is tailored to specific cellular functions. In support of this, up regulation of nesprin variants and nesprin variant switching is observed in ESC, mesenchymal stem cell and skeletal muscle differentiation [26,30,31]. Nesprins have emerged as signalling scaffolds for the ERK and β-catenin pathways and these pathways exist in multiple cell types. Furthermore, recent evidence demonstrates the importance of the signalling scaffolding functions of the nesprin family during development, where the nesprin-1/2 orthologue ANC1 regulates β-catenin signalling during neuronal development in *C. elegans* [32]. However, we show that the nesprin-2 giant is not detectable in U2OS cells and potentially adaptation of nesprin variant expression may fine tune these pathways and facilitate cell-specific signalling. In support of this, we show that U2OS cells display high levels of the p220CH^{Nesp2}, whereas fibroblasts lack the p220CH^{Nesp2} variant. In addition to changes in nesprin-2 variant expression, the p380CH^{Nesp2} variant displayed differential compartmentalisation between U2OS and HDF cells, therefore, differential nesprin variant expression/compartmentalisation may contribute to cell specific functions for nesprin-2 in β-catenin signalling. Further investigation is now required to clarify the cell-specific functions of nesprin variants in regulating β-catenin signalling.

Conflicts of interest

The authors declare that no conflicts of interest exist.

Sources of funding

This work was funded by a British Heart Foundation, United Kingdom (BHF) program grant to CMS (program Grant number RG/11/14/29056), a BHF IBSRF awarded to DTW (FS/11/53/29020) and a BHF project grant to QPZ (PG/11/58/29004).

Appendix A. Supplementary material

Supplementary data associated with this article can be found in the online version at http://dx.doi.org/10.1016/j.yexcr.2016.06.008.

References

[1] Q. Zhang, C. Bethmann, N.F. Worth, J.D. Davies, C. Wasner, A. Feuer, C. D. Ragnauth, Q. Yi, J.A. Mellad, D.T. Warren, M.A. Wheeler, J.A. Ellis, J. N. Skepper, M. Vorgerd, B. Schlotter-Weigel, P.L. Weissberg, R.G. Roberts, M. Wehnert, C.M. Shanahan, Nesprin-1 and -2 are involved in the pathogenesis of Emery Dreifuss muscular dystrophy and are critical for nuclear envelope integrity, Hum. Mol. Genet. 16 (2007) 2816–2833.
[2] M. Ketema, A. Sonnenberg, Nesprin-3: a versatile connector between the nucleus and the cytoskeleton, Biochem. Soc. Trans. 39 (2011) 1719–1724.
[3] K.J. Roux, M.L. Crisp, Q. Liu, D. Kim, S. Kozlov, C.L. Stewart, B. Burke, Nesprin 4 is an outer nuclear membrane protein that can induce kinesin-mediated cell polarization, Proc. Natl. Acad. Sci. USA 106 (2009) 2194–2199.
[4] Y. Luke, H. Zaim, I. Karakesisoglou, V.M. Jaeger, L. Sellin, W. Lu, M. Schneider, S. Neumann, A. Beijer, M. Munck, V.C. Padmakumar, J. Gloy, G. Walz, A. A. Noegel, Nesprin-2 Giant (NUANCE) maintains nuclear envelope architecture and composition in skin, J. Cell Sci. 121 (2008) 1887–1898.
[5] D. Rajgor, J.A. Mellad, F. Autore, Q. Zhang, C.M. Shanahan, Multiple novel nesprin-1 and nesprin-2 variants act as versatile tissue-specific intracellular scaffolds, PLoS One 7 (2012) e40098.
[6] Q. Zhang, C.D. Ragnauth, J.N. Skepper, N.F. Worth, D.T. Warren, R.G. Roberts, P. L. Weissberg, J.A. Ellis, C.M. Shanahan, Nesprin-2 is a multi-isomeric protein that binds lamin and emerin at the nuclear envelope and forms a subcellular network in skeletal muscle, J. Cell Sci. 118 (2005) 673–687.
[7] V.C. Padmakumar, S. Abraham, S. Braune, A.A. Noegel, B. Tunggal, I. Karakesisoglou, E. Korenbaum, Enaptin, a giant actin-binding protein, is an element of the nuclear membrane and the actin cytoskeleton, Exp. Cell Res. 295 (2004) 330–339.
[8] M.A. Wheeler, J.D. Davies, Q. Zhang, L.J. Emerson, J. Hunt, C.M. Shanahan, J. A. Ellis, Distinct functional domains in nesprin-1alpha and nesprin-2beta bind directly to emerin and both interactions are disrupted in X-linked Emery-Dreifuss muscular dystrophy, Exp. Cell Res. 313 (2007) 2845–2857.
[9] W. Wang, Z. Shi, S. Jiao, C. Chen, H. Wang, G. Liu, Q. Wang, Y. Zhao, M.I. Greene, Z. Zhou, Structural insights into SUN-KASH complexes across the nuclear envelope, Cell Res. 22 (2012) 1440–1452.
[10] M. Crisp, Q. Liu, K. Roux, J.B. Rattner, C. Shanahan, B. Burke, P.D. Stahl, D. Hodzic, Coupling of the nucleus and cytoplasm: role of the LINC complex, J. Cell Biol. 172 (2006) 41–53.
[11] F. Haque, D.J. Lloyd, D.T. Smallwood, C.L. Dent, C.M. Shanahan, A.M. Fry, R. C. Trembath, S. Shackleton, SUN1 interacts with nuclear lamin A and cytoplasmic nesprins to provide a physical connection between the nuclear lamina and the cytoskeleton, Mol. Cell Biol. 26 (2006) 3738–3751.
[12] F. Haque, D. Mazzeo, J.T. Patel, D.T. Smallwood, J.A. Ellis, C.M. Shanahan, S. Shackleton, Mammalian SUN protein interaction networks at the inner nuclear membrane and their role in laminopathy disease processes, J. Biol. Chem. 285 (2010) 3487–3498.
[13] D. Rajgor, J.A. Mellad, D. Soong, J.B. Rattner, M.J. Fritzler, C.M. Shanahan, Mammalian microtubule P-body dynamics are mediated by nesprin-1, J. Cell Biol. 205 (2014) 457–475.
[14] D.T. Warren, T. Tajsic, J.A. Mellad, R. Searles, Q. Zhang, C.M. Shanahan, Novel nuclear nesprin-2 variants tether active extracellular signal-regulated MAPK1 and MAPK2 at promyelocytic leukemia protein nuclear bodies and act to regulate smooth muscle cell proliferation, J. Biol. Chem. 285 (2010) 1311–1320.
[15] T. Lam le, S.V. Bohm, R.G. Roberts, G.E. Morris, Nesprin-2 epsilon: a novel nesprin isoform expressed in human ovary and Ntera-2 cells, Biochem. Biophys. Res. Commun. 412 (2011) 291–295.
[16] F. Autore, M. Pfuhl, X. Quan, A. Williams, R.G. Roberts, C.M. Shanahan, F. Fraternali, Large-scale modelling of the divergent spectrin repeats in nesprins: giant modular proteins, PLoS One 8 (2013) e63633.
[17] H.R. Dawe, M. Adams, G. Wheway, K. Szymanska, C.V. Logan, A.A. Noegel, K. Gull, C.A. Johnson, Nesprin-2 interacts with meckelin and mediates ciliogenesis via remodelling of the actin cytoskeleton, J. Cell Sci. 122 (2009) 2716–2726.
[18] F. Cong, L. Schweizer, H. Varmus, Wnt signals across the plasma membrane to activate the beta-catenin pathway by forming oligomers containing its receptors, Frizzled and LRP, Development 131 (2004) 5103–5115.
[19] F. Cong, H. Varmus, Nuclear-cytoplasmic shuttling of Axin regulates subcellular localization of beta-catenin, Proc. Natl. Acad. Sci. USA 101 (2004) 2882–2887.
[20] N. Wiechens, K. Heinle, L. Englmeier, A. Schohl, F. Fagotto, Nucleo-cytoplasmic shuttling of Axin, a negative regulator of the Wnt-beta-catenin Pathway, J. Biol. Chem. 279 (2004) 5263–5267.
[21] M. Sharma, C. Jamieson, C. Lui, B.R. Henderson, The hydrophobic rich N- and C-terminal tails of beta-catenin facilitate nuclear import of beta-catenin, J. Biol. Chem. (2014).
[22] S. Neumann, M. Schneider, R.L. Daugherty, C.J. Gottardi, S.A. Eming, A. Beijer, A.A. Noegel, I. Karakesisoglou, Nesprin-2 interacts with {alpha}-catenin and regulates Wnt signaling at the nuclear envelope, J. Biol. Chem. 285 (2010) 34932–34938.
[23] E. Markiewicz, K. Tilgner, N. Barker, M. van de Wetering, H. Clevers, M. Dorobek, I. Hausmanowa-Petrusewicz, F.C. Ramaekers, J.L. Broers, W. M. Blankesteijn, G. Salpingidou, R.G. Wilson, J.A. Ellis, C.J. Hutchison, The inner nuclear membrane protein emerin regulates beta-catenin activity by restricting its accumulation in the nucleus, EMBO J. 25 (2006) 3275–3285.
[24] Q. Zhang, J.N. Skepper, F. Yang, J.D. Davies, L. Hegyi, R.G. Roberts, P. L. Weissberg, J.A. Ellis, C.M. Shanahan, Nesprins: a novel family of spectrin-repeat-containing proteins that localize to the nuclear membrane in multiple tissues, J. Cell Sci. 114 (2001) 4485–4498.
[25] C.D. Ragnauth, D.T. Warren, Y. Liu, R. McNair, T. Tajsic, N. Figg, R. Shroff, J. Skepper, C.M. Shanahan, Prelamin A acts to accelerate smooth muscle cell senescence and is a novel biomarker of human vascular aging, Circulation 121 (2010) 2200–2210.
[26] K.N. Randles, T. Lam le, C.A. Sewry, M. Puckelwartz, D. Furling, M. Wehnert, E. M. McNally, G.E. Morris, Nesprins, but not sun proteins, switch isoforms at the nuclear envelope during muscle development, Dev. Dyn. 239 (2010) 998–1009.
[27] B. Chen, C. Co, C.C. Ho, Cell shape dependent regulation of nuclear morphology, Biomaterials 67 (2015) 129–136.
[28] M. Versaevel, T. Grevesse, S. Gabriele, Spatial coordination between cell and nuclear shape within micropatterned endothelial cells, Nat. Commun. 3 (2012) 671.

[29] N.T. Duong, G.E. Morris, T. Lam le, Q. Zhang, C.A. Sewry, C.M. Shanahan, I. Holt, Nesprins: tissue-specific expression of epsilon and other short isoforms, PLoS One 9 (2014) e94380.
[30] E.R. Smith, X.Y. Zhang, C.D. Capo-Chichi, X. Chen, X.X. Xu, Increased expression of Syne1/nesprin-1 facilitates nuclear envelope structure changes in embryonic stem cell differentiation, Dev. Dyn. 240 (2011) 2245–2255.
[31] W. Yang, H. Zheng, Y. Wang, F. Lian, Z. Hu, S. Xue, Nesprin-1 has key roles in the process of mesenchymal stem cell differentiation into cardiomyocyte-like cells in vivo and in vitro, Mol. Med. Rep. 11 (2015) 133–142.
[32] E.D. Tulgren, S.M. Turgeon, K.J. Opperman, B. Grill, The Nesprin family member ANC-1 regulates synapse formation and axon termination by functioning in a pathway with RPM-1 and beta-Catenin, PLoS Genet. 10 (2014) e1004481.